RESILIENCE OF COUPLED URBAN SOCIO-PHYSICAL SYSTEMS TO DISASTERS: DATA-DRIVEN MODELING APPROACH

by

Takahiro Yabe

A Dissertation

Submitted to the Faculty of Purdue University

In Partial Fulfillment of the Requirements for the degree of

Doctor of Philosophy

Lyles School of Civil Engineering

West Lafayette, Indiana

August 2021

THE PURDUE UNIVERSITY GRADUATE SCHOOL
STATEMENT OF COMMITTEE APPROVAL

Dr. Satish V. Ukkusuri, Chair

Lyles School of Civil Engineering

Dr. Seungyoon Lee, Co-Chair

School of Communication

Dr. P. Suresh C. Rao

Lyles School of Civil Engineering and Department of Agronomy

Dr. David R. Johnson

School of Industrial Engineering and Department of Political Science

Approved by:

Dr. Dulcy M. Abraham

Graduate Chair, Lyles School of Civil Engineering

To my loving parents, sister, grandparents, Maple, and my wife.

ACKNOWLEDGMENTS

I would like to first express my deepest gratitude to my advisor and mentor, Dr. Satish V. Ukkusuri for his expert supervision, guidance, and support during my 4 years at Purdue. Your technical depth in networks, modeling, and data, and also the breadth in knowledge about societal issues were always an inspiration for me to keep on learning. I will remember not only the fun discussions and hot debates, but also your warm support during my tough moments in life. *"Focus on the process and the journey, and the results will follow"* is an advice I will treasure forever.

I would like to express my appreciation to my Ph.D. advisory committee: Dr. P. Suresh C. Rao, Dr. Seungyoon Lee, and Dr. David R. Johnson. I would like to especially thank Dr. Rao for being my second academic mentor. I truly enjoyed our exciting research collaborations, discussions which were a tremendous source of ideas, and inspiring conversations over a pint of beer. I was extremely privileged to have had 2 excellent mentors guiding me through my Ph.D. journey.

Many thanks to my former and current lab mates at the UMNI Lab - Dr. Xinwu Qian, Dr. Tho V. Le, Dr. Wenbo Zhang, Dr. Hemant Gehlot, Dr. Dheeraj Kumar, Fasil Sagir, Zengxiang Lei, Jiawei Xue, Lu Ling, Sangung Park, Rajat Verma, Xiaowei Chen, Omar Faruqe Hamim, Eunhan Ka, and Shagun Mittal - for their help, support, and the exciting group meetings.

My interdisciplinary research would not have been possible without the support of my collaborators. Many thanks to the CRISP Project team members at Purdue and The University of North Texas. I would like to also thank Dr. Kota Tsubouchi and Mr. Toru Shimizu at Yahoo Japan Corporation, Mr. Nicholas Jones at The World Bank, Dr. K. E. Seetharam at the Asian Development Bank Institute, Dr. Yoshihide Sekimoto at The University of Tokyo, and Dr. Naoya Fujiwara at Tohoku University.

Finally, my deepest gratitude goes to my family, who always offered me warm support and encouragement. I must thank my wife, who initially pushed my back to pursue a Ph.D. in the USA, and continuously supported me for 4 years from across the Pacific Ocean with many long late-night video calls. What a journey it has been!

Funding for my Ph.D. study was provided through the NSF CRISP Grant (CMMI-1638311) and the Doctoral Systems Fellowship from Purdue Systems Collaboratory (between 2018 Fall and 2020 Summer). The financial support is gratefully acknowledged.

TABLE OF CONTENTS

LIST OF TABLES . . . 8

LIST OF FIGURES . . . 9

ABSTRACT . . . 11

1 INTRODUCTION . . . 13
- 1.1 Background and Motivations . . . 13
  - 1.1.1 Rising Frequency and Intensity of Shocks . . . 13
  - 1.1.2 Rapid Urbanization . . . 16
  - 1.1.3 Complexity of Cities . . . 18
- 1.2 Literature Review . . . 20
  - 1.2.1 Resilience Concepts . . . 20
  - 1.2.2 Disaster Recovery and Community Resilience . . . 24
  - 1.2.3 Novel Data Sources in Urban Analytics . . . 26
  - 1.2.4 Application of Mobile Phone Data in Disaster Management . . . 30
  - 1.2.5 Literature Summary and Research Gaps . . . 37
- 1.3 Overarching Goal and Objectives . . . 38
- 1.4 Organization of Dissertation: a Synthesis Approach . . . 40

2 DISASTER RECOVERY TRAJECTORIES . . . 43
- 2.1 Universal Recovery Patterns . . . 45
- 2.2 Spatial Heterogeneity . . . 50
- 2.3 Social and Physical Network Effects . . . 56
  - 2.3.1 Node-level Network Statistics . . . 57
  - 2.3.2 Spatial Regression Models . . . 62

3 INTRA-REGIONAL INEQUALITY . . . 68
- 3.1 Income Inequality in Post-Disaster Mobility . . . 68
  - 3.1.1 Case Study of Miami-Dade after Hurricane Irma . . . 70

3.1.2 Effects of Income Inequality on Evacuation and Reentry 74
3.1.3 Temporal Variation of Spatial Income Segregation 78
3.2 Region and Sector Inequality in Business Impacts 82
3.2.1 Bayesian structural time series model 86
3.2.2 Estimation Results of Disaster Impacts 90
3.2.3 Unraveling the Recovery Sequence of Industries 99

4 SOCIO-PHYSICAL SYSTEM INTERDEPENDENCIES 105
4.1 Modeling Interdependent Socio-Physical Systems 107
4.1.1 Observations of Social and Physical Recovery 107
4.1.2 Socio-Physical Systems Dynamics Model 110
4.1.3 Urban Scale and Socio-Physical Interdependencies 115
4.2 Interdependencies and Resilience 118

5 TOWARDS INTER-REGIONAL TRANSFERABILITY 125
5.1 Inter-Regional Translation of Places 125
5.1.1 Methodology: Unsupervised machine translation of places 128
5.1.2 Experimental Validation 130
5.1.3 Results 134
5.2 Overcoming City Size Imbalance via Hierarchical Anchoring 141
5.2.1 Methodology: Hierarchical Anchoring 143
5.2.2 Experiment Settings 148
5.2.3 Results of Domain Imbalance Urban Translation 151

6 KNOWLEDGE SYNTHESIS 160
6.1 Summary of Contributions on Urban Resilience Research 160
6.2 From "Data-Driven Modeling" to "Data-Driven Dynamical Systems Modeling" . . 162
6.3 Linking "Data-Driven Systems Modeling" and "Management" 165
6.3.1 Opportunities 166
6.3.2 Challenges in Linking Data, Systems Modeling, and Policy 169
6.4 Future Research Directions 173

REFERENCES 178

PUBLICATIONS 212

VITA 215

LIST OF TABLES

1.1 Novel datasets, their descriptions and applications 26

1.2 Types of mobile phone location data 28

2.1 Statistics of GPS data 46

2.2 Descriptions, variable transformations, and sources of socio-economic data 53

2.3 Distance metrics x that were used as edge weights to build inter-city network $\mathscr{N}_x$ . . . 58

2.4 Correlation between edge weights based on distance metrics $\mathscr{N}_x$ 60

2.5 Node-level statistics of node i given inter-city network $\mathscr{N}_x$ 61

2.6 Statistics of independent and objective variables 63

2.7 Ordinary Least Squares Regression Results with $W(\mathscr{N}_F)$ as network metric 65

2.8 Spatial dependence tests 65

2.9 Regression Results of Spatial Error Model 66

3.1 Income inequality and hurricane damage 73

3.2 Model validation results of two experimental settings. 91

3.3 Estimated parameter values and goodness of fit 102

4.1 Socio-demographic, -economic, and hurricane damage statistics 109

5.1 Data statistics for the two cities 131

5.2 Statistics showing the varying scales of the cities 148

5.3 Quality of generated place embeddings measured by land use classification accuracy. . 151

LIST OF FIGURES

1.1 Number of disaster events by year 14
1.2 Rapid growth of urban areas in Shenzhen, China 17
1.3 Socio-physical interdependencies in disaster recovery 19
1.4 Number of research articles on human mobility using mobile phone data 27
1.5 Mobility reduction in Tokyo during COVID-19 31
1.6 Population displacement after the Puebla Earthquake in Mexico City. 32
1.7 Predicting COVID-19 outbreaks with web search data 37
1.8 Organization of research gaps 39
1.9 Organization of dissertation. 42
2.1 Locations and disaster events of study. 47
2.2 Similarity of macroscopic population recovery patterns across the five disasters. . . . 48
2.3 Relationship between displacement distance and duration after disasters 51
2.4 Explaining the spatial heterogeneity in population recovery 52
2.5 Connectedness to neighboring cities as a key factor to recovery. 56
2.6 Visualization of distance weights of each network metric. 59
2.7 Results of OLS with network factors 65
3.1 Comparison of census data and mobile phone data 71
3.2 Hurricane Irma trajectory, median income, and hurricane evacuation zones 72
3.3 Out-of-county and out-of-state evacuation rates 75
3.4 Out-of-county evacuation rates of residents in mandatory evacuation zones 76
3.5 Inequity in evacuation destinations 78
3.6 Dynamic income distribution of Miami residents 79
3.7 Quantifying spatial segregation after disasters 80
3.8 Overview of causal inference method 84
3.9 Business types and locations in Puerto Rico 85
3.10 Bayesian structural time series model 88
3.11 Disaster impact analysis example 92
3.12 Disaster impacts across different categories and locations 94

3.13 Cumulative disaster impacts across different categories and regions 96
3.14 Posterior estimates of model parameters 97
3.15 Partition results of counties in Puerto Rico 99
3.16 Inter-regional heterogeneity in POI recovery dynamics 101
3.17 Inter-regional heterogeneity in recovery dynamics of visits to all POIs 103
3.18 Inter-regional and inter-POI heterogeneity in recovery speed of visits to POIs 104
4.1 Fusion of large-scale data and dynamical model 106
4.2 Estimation of regional socio-physical recovery dynamics 113
4.3 Location and categories of POIs in Puerto Rico used in the analysis. 115
4.4 Social and physical recovery dynamics for different POI types 116
4.5 Regional differences in system dynamics model parameters 117
4.6 Resilience implications of socio-physical interdependencies 120
4.7 Effects of physical robustness on resilience 124
5.1 Illustration of the inter-city place translation problem 127
5.2 The overview of the LSTM RNN decoder/autoencoder 132
5.3 Intra-city translation validation results 135
5.4 Inter-city translation results from Kumamoto to Okayama City 136
5.5 Qualitative inspection of translated place representations 137
5.6 Sensitivity to training pairs 139
5.7 Illustration of the *domain imbalance problem* setting 143
5.8 Universal hierarchical structure of cities 144
5.9 Illustration of hierarchical anchoring 146
5.10 Translation performance of various anchoring methods 152
5.11 Pairwise translation accuracy 153
5.12 Sensitivity of translation accuracy to hierarchical levels 155
5.13 Case study of translating Tsukiji Fish Market 156
6.1 Data-driven dynamical systems modeling (D3S) approach 164
6.2 Analysis of population density in Mexico City 168
6.3 Flowchart of the disaster mobility analytics toolkit 169

ABSTRACT

Cities face significant challenges in developing urban infrastructure systems in an inclusive, resilient, and sustainable manner, with rapid urbanization and increasing frequency of shocks (e.g., climate hazards, epidemics). The complex and dynamic interdependencies among urban social, technical, institutional, and natural components could cause disruptions to cascade across systems, and lead to heterogeneous recovery outcomes across communities and regions. Large scale data collected from mobile devices, including mobile phone GPS data, web search data, and social media data, allow us to observe urban dynamics before, during, and after disaster events in an unprecedented spatial-temporal granularity and scale. Despite these opportunities, we lack data-driven methods to understand the underlying mechanisms that govern the recovery and resilience of cities to shocks. Such dynamical models, in contrast to static index based metrics of resilience, will allow us to test the effects of policies on the heterogeneous post-disaster recovery trajectories across space and time.

In this dissertation, I studied the recovery dynamics and resilience of urban systems to disasters using a large-scale human-centered data-driven modeling approach, with particular emphasis on the complex interdependencies among social, economic, and infrastructure systems. First, statistical analysis of large-scale human mobility data collected from over 1 million mobile phone devices in five major disaster events across the globe, revealed universal population recovery processes across regions and disasters, including disproportionate disaster effects based on income inequalities and urban-rural divide. Second, human mobility data are used to infer the recovery of various socio-economic systems after disasters. Using Bayesian causal inference models, regional and business sectoral inequalities in disaster recovery are quantified. Finally, the analysis on social, economic, and physical recovery were integrated into a dynamical model of coupled urban systems, which captures the bi-directional interdependencies among socio-economic and physical infrastructure systems during disaster recovery. Using the model and data collected from Puerto Rico during Hurricane Maria, a trade-off relationship in urban development is revealed, where developed cities with robust centralized infrastructure systems have higher recovery efficiency of critical services, however, have socio-economic networks with lower self-reliance during

crises, which lead to loss of community resilience. Managing and balancing the socio-economic self-reliance alongside physical infrastructure robustness is key to resilience.

The proposed models and results presented in this dissertation lay the scientific foundations of urban complexity and resilience, encouraging us to move towards dynamical and complex systems modeling approaches, from conventional static index-based resilience metrics. Big data-driven, dynamical complex systems modeling approaches enable quantitative understanding of the underlying disaster recovery process (e.g., interdependencies, feedbacks, cascading effects) across large spatial and temporal time scales. The approach is capable of proposing community-based policies for urban resilience via cross-regional comparisons and counterfactual scenario testing of various policy levers.

1. INTRODUCTION

1.1 Background and Motivations

1.1.1 Rising Frequency and Intensity of Shocks

Natural hazards are increasing both in terms of intensity and frequency across the globe in recent years, due to effects of climate change [1]–[3]. Figure 1.1 shows the number of disaster events by year, collected from EM-DAT. EM-DAT is a global database on natural and technological disasters, containing data on the occurrence of more than 21,000 disasters in the world, from 1900 to present. EM-DAT contains all disasters from 1900 until the present where more than one of the following criteria are conformed: 1) 10 or more people dead, 2) 100 or more people affected, 3) declaration of a state of emergency is issued, or 4) a call for international assistance is issued (https://www.emdat.be/). The number of disaster events are increasing over time, especially floods and extreme weather events, which are caused by climate change. A recent paper by the United Nations Office for Disaster Risk Reduction reported that climate-related and geophysical disasters have caused 1.3 million deaths and left a further 4.4 billion injured, homeless, displaced or in need of emergency assistance between 1998 and 2017 [4]. While the majority of fatalities were due to geophysical events, mostly earthquakes and tsunamis, 91% of all disasters were caused by floods, storms, droughts, heatwaves and other extreme weather events. In addition to human losses, disaster affected countries experienced direct economic losses valued at US$ 2.9 trillion. This is a significant increase from the preceding 20 year period, with an increase by 151% in reported losses from extreme weather events. A study using decades of empirical data and statistical methods has shown that the estimated upward trend of disaster intensity and frequency is indeed responsible for an increase in economic damages across the globe [5], [6].

Given these increasing threats of natural hazards, reducing people's vulnerability and improving the resilience of communities has become a more prioritized policy item among governments and multilateral development agencies [7]. Recently there have been many major international conferences and target frameworks to address these policy needs, including the Third United Nations World Conference on Disaster Risk Reduction, the United Nations Sustainable Development Goals (SDGs), and the Paris Agreement for Climate Change. The Third United Nations World Conference on Disaster Risk Reduction, which was held in Sendai, Japan, led to the adoption of the Sendai Declaration and the Sendai Framework for Disaster Risk Reduction 2015 – 2030. The Sendai Framework targets "substantial reduction of disaster risk and losses in lives, livelihoods and health and in the economic, physical, social, cultural and environmental assets of persons, businesses, communities and countries." The SDGs include several goals that are closely tied with disaster risk reduction and urban resilience, including Goal 1 "No Poverty", especially Target 1.5 that focuses on "building the resilience of the poor and those in vulnerable situations and reduce their exposure and vulnerability to climate-related extreme events and other economic, social and environmental shocks and disasters", and Goals 9 "Industry, Innovation and Infrastructure", 11 "Sustainable Cities and Communities", and 13 "Climate Action". The Paris Agreement also supports more resilient development by reducing the vulnerability to future climate change scenarios. The agreement includes priority areas such as early warning systems, emergency preparedness, comprehensive risk assessment and management, and risk insurance facilities, climate risk pooling, and other insurance solutions [8]. While disaster recovery efforts often focus on repairing infrastructure services to pre-disaster conditions, the concept of "build back better" is also gaining attention among the international community [9]. Build back better aims to take advantage of that opportunity to build the social and physical systems to even more robust levels than before to decrease vulnerability to future hazards [10]. Such strategies include improved preparedness,

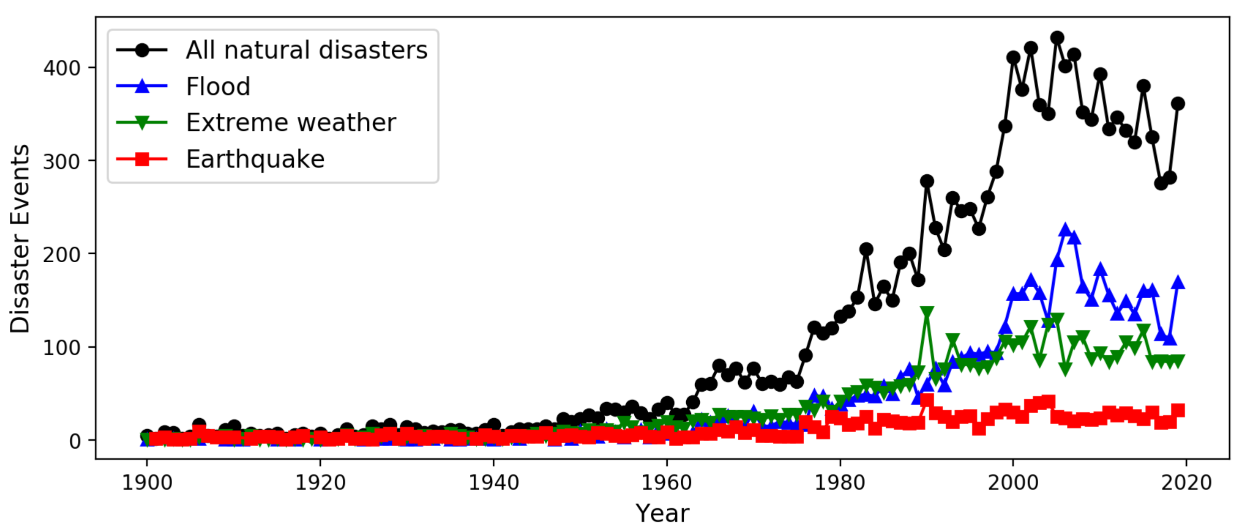

Figure 1.1. Number of disaster events by year. Figure produced by author using data provided by EM-DAT (https://www.emdat.be/).

innovations in rebuilding (e.g. decentralized) infrastructure [11], empowering local organizations [12]–[15] and various other ways to amplify existing social connectivity and adaptive capacity.

Improving the resilience to natural hazards and various other forms of shocks, are complementary with efforts to reduce poverty [16], [17]. Numerous studies have shown that disaster events disproportionately affect the poor and underprivileged, increasing the socio-economic inequality among the population. For example, a study that examined the effects of Typhoon Milenyo in rural Philippines showed that while the poor suffered from sharp drops in the price of fish, which are their main source of income, the richer experienced positive net welfare gains and also were able to cope better with the typhoon, with better protection with insurance [18]. Similar disproportionate effects were observed in various other regional disaster contexts, including Haiti [19], Myanmar [20], Senegal [21], and the United States [22]. Such disproportionate effects could further pull down the poor while enabling the rich to stay as rich, resulting in significant gaps among society. In addition to economic inequality, disasters are known to disproportionately affect populations based on gender [23] and disabilities [24]. The recent coronavirus pandemic (a different form of shock) highlighted this inequality as well. Many studies have reported that the COVID-19 pandemic affected the poor populations more, because of their inability to work remotely from home, lack of healthcare, and social protection [25]–[28]. Therefore, improving the resilience of cities to various shocks is essential in order to eradicate poverty and boost shared prosperity [29].

"Shocks", in this dissertation, refers to not only acute events (e.g., earthquakes, floods, hurricanes), but also includes various types of chronic stresses that are less severe in intensity but are more persistent. In the context of urban systems, chronic stresses are low-intensity but frequent or persistent shocks that degrade the system performance but not to the extent of complete malfunction on its own, including traffic jams, pipe bursts, and power outages. Chronic stresses also include social system characteristics, such as poverty, fragility and violence. Such chronic stresses also disproportionately affect the poor and informal populations, as shown in a study in Rio de Janerio [30]. Both empirical and theoretical results indicate that such chronic shocks could exacerbate the impacts of rare but high-intensity acute shocks, and could contribute to the loss of resilience of urban systems [31]. This raises a need for a holistic framework that can analyze the resilience of cities to compound impacts of both acute and chronic shocks along the time horizon.

The rising frequency and intensity of shocks due to accelerating climate change poses a pressing need for policy makers, academics, and communities to find solutions to improve the resilience of cities. Despite the increasing attention to disaster risk, recovery, and resilience from the international community, widening socio-economic inequality and the persistence of socio-economic and political chronic stresses that exacerbate the impacts of acute disaster events pose significant challenges. An additional factor that urges us to act immediately to address these issues is the rapid progression of urbanization in cities across many low- and medium-income countries.

1.1.2 Rapid Urbanization

According to a report by the World Bank, over 4 billion people around the world, which is more than half the global population, live in cities [32]. Cities have been the central drivers of economic and cultural productivity with its dense social networks of knowledge and labor igniting innovations and new ideas. A recent study reported that the ten most innovative cities in the United States account for 23% of the national population, but for 48% of its patents and 33% of its gross domestic product [33]. The economic productivity concentrated in urban areas leads to an increase in better labor opportunities in cities, attracting people to relocate to urban areas. This reinforcing feedback cycle is propelling the urbanization process in many cities around the world, and by 2050, nearly 7 of 10 people in the world is projected to be living in cities. Figure 1.2 shows the rapid growth of urban areas in Shenzhen over a twenty year time horizon, between 1992 and 2013, using calibrated satellite images (DMSP-OLS) [34].

This trend of rapid urbanization could lead to further acceleration of innovations and productivity if managed well. However, the scale and speed of urbanization poses a wide range of challenges for government agencies to build resilient, sustainable, and inclusive urban systems. In many cities, we have witnessed a failure of urban management, where unplanned urban sprawl have resulted in an increase in informal settlements with insufficient physical infrastructure services and connectivity (e.g., case study of Brazil [35]). In such scenarios, existing infrastructure systems and governance agencies are overwhelmed by increasing demands, and lack of required financial and technological resources to maintain and build required infrastructure. Communities living in informal settlements (20-30% of urban population) are not connected to centralized in-

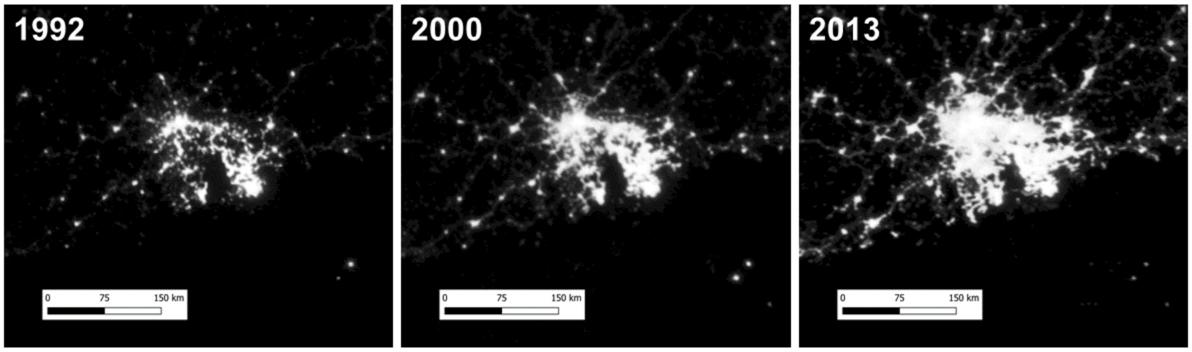

Figure 1.2. Rapid growth of urban areas in Shenzhen, China, observed using night light data from satellite images (DMSP-OLS). Figure produced by author using data provided by Li et al. [34].

frastructure and/or to governance institutions. These communities do not receive adequate critical services, and cope with chronic shortages of power [36], accessibility to water supplies [37], and have less accessibility to various education and job opportunities [38], [39]. These communities are further marginalized by not having a political ”voice” and participation in management and decision processes [40].

In addition to such challenges in managing rapid urbanization with sufficient public services, rapid urbanization increases the exposure and vulnerability of residents to climate risks and shocks. According to the World Bank, almost half a billion urban residents live in coastal areas (defined as 100km inland from the coast), and in the 136 biggest coastal cities, there are 100 million people (20% of their population) and $4.7 trillion in assets exposed to coastal floods, according a global study by Hallegatte et al. [41]. Around 90% of urban expansion in developing countries is near hazard-prone areas and built through informal and unplanned settlements [32]. In particular, informal settlements are equipped with housing structures and water irrigation infrastructure with low standards. Such areas could face much substantial impacts due to climate shocks, such as flooding, including loss of housing and assets, inundation, and casualties [42]. Combined with lack of access to public health services and adequate infrastructure systems, informal settlements are prone to spread of diseases [43].

As a result of the increasing vulnerability to hazards, past events have shown that disasters trigger mass population movements across regions, including evacuation to safer locations [44], displacement due to difficulties in living in original locations [45], long term migration to other regions [46], and returning back to original locations after the region has recovered [47]. For example, Hurricane Irma which made landfall in September 2017 caused one of the largest mass evacuation events in the history of the country, where over 6 million people were ordered to evacuate in Florida [48]. Understanding the mass movement dynamics of people affected by disasters is crucial for making various policy decisions, including allocation strategies of relief resources, optimal investment to repair damaged physical infrastructure, and providing subsidies for damaged local businesses for quick recovery to support the demand of disaster affected residents. Mass population movement triggered by disaster events could have various consequences on spatial distributions of population groups, economic activities, and demand for public infrastructure services, which could have significant implications on urban policy making. At the same time, various policies on post-disaster repairing of physical infrastructure systems, land use planning, and public incentive schemes for businesses and households could alter the outcomes of the post-disaster population dynamics. This bi-directional dependency between social systems, comprised of households, businesses, and local organizations, and physical infrastructure systems managed by public agencies and decision makers, is one example of the complex processes that governs the dynamics of cities.

1.1.3 Complexity of Cities

During the past couple of decades, cities have been treated as complex systems, which are composed of networks of heterogeneous components with dynamic interactions and interdependencies [49], [50]. With the help of various novel sensor data, various empirical analysis has been conducted to understand the properties of cities. Empirical observations have revealed "scaling relationships in cities", where on average, various urban quantities (e.g., gross domestic product, total road mileage) grow super-linearly with the population of the city [51]. Such scaling relationships, or fractal properties, have also been discovered in the functionality of urban infrastructure networks, such as water pipe networks [52], road networks [53], human settlement with respect to river networks [54], and urban heat island topology [55]. Cities are composed of *social systems*, including networks of households, business firms, local organization, and public agencies, *physi-*

cal infrastructure systems composed of various critical services, such as power grids, water pipe networks, and transportation systems, and *natural systems*, such as river networks and terrains.

Recent disaster events have revealed the complexity and uncertainty in recovery dynamics after disasters, resulting in drastically heterogeneous outcomes across communities and regions [56]–[58]. Various functional interdependencies that exist between the social, physical, institutional, and natural components in urban systems complicate the recovery process. For instance, the recovery of service of physical infrastructure systems (e.g., power networks) are dependent on the repairing capacity of institutional systems, and on the other hand, the operation capacity of institutional systems are dependent on the performances of the physical systems. Social systems (e.g., households and business firms) depend on the physical systems to provide critical services, and on public agencies to provide stability, safety, and recovery assistance after disasters. Population movements of residents, including evacuation, migration, and returning decisions, are also affected by the states of both physical and institutional systems, as well as the capacity (social capital) and decisions of the peer members in their community [57]. Moreover, such mobility decisions of people in one region could affect the mobility decisions of people in neighboring cities, as the influx of populations would increase the demand for public services and cause competition of resources in destination cities (inter-regional dependencies). Such complex intra-regional interdependencies across social and physical systems, as well as the inter-regional effects contribute to the complexity of post-disaster recovery dynamics 1.3.

Understanding the interplay between the physical infrastructure systems and social systems, and their impacts on population movement (displacement and return) and to the overall recovery of

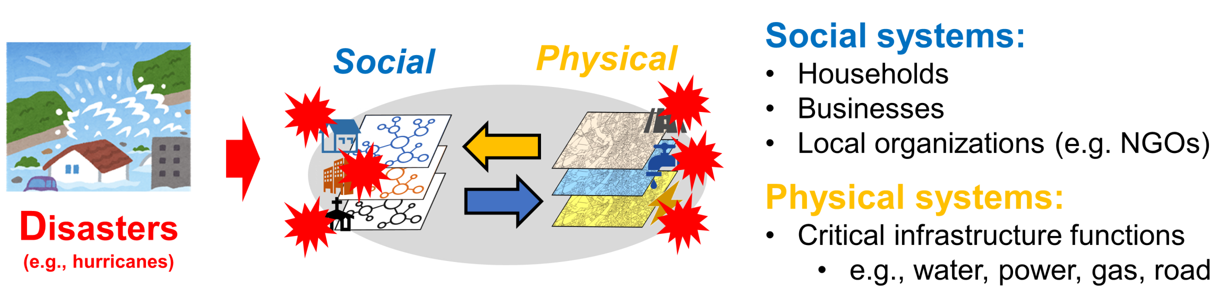

Figure 1.3. Disaster disruptions could cascade across social, economic, and physical infrastructure systems.

the urban systems after large-scale disasters is essential for developing policies that could enhance effective population recovery in communities, and foster sustainable development in hazard prone areas [59].

Taken together, this dissertation is motivated by the *increasing societal importance and urgency of improving the resilience of urban systems to the intensifying external shocks*, and the *scientific ambition to unravel how the complexity of urban systems characterize their resilience*. In this dissertation, we present novel approaches that improve our understanding of the underlying complex dynamics of coupled urban socio-physical systems after shocks, which can be used to inform decision making for designing more resilient cities.

1.2 Literature Review

Understanding the resilience of systems have been studied in many disciplines, ranging from ecological, engineered, to social systems. This dissertation aims to understand the resilience of coupled urban socio-physical systems in a dynamic and quantitative manner, building upon the concepts and theories of resilience, community resilience theories, and data-driven modeling techniques. This Section reviews these topics and provides a holistic review and evaluation of the related literature to provide a basis for my dissertation work. Section 1.2.1 reviews the concepts and theories related to resilience, starting from the ecological sciences, socio-ecological resilience, and towards network and engineered resilience. Section 1.2.2 discusses the current literature in disaster recovery and community resilience, both from qualitative and quantitative approaches. Section 1.2.3 surveys the novel data sources that are available and are being used for analyzing disaster recovery, and their applications are discussed in Section 1.2.4.

1.2.1 Resilience Concepts

Socio-Ecological Resilience

The concept of resilience emerged from the field of ecology in the 1960s through the analysis of interacting population groups and their stability [60]. In his seminal paper, Holling introduced resilience as “the persistence of relationships within a system and is a measure of the ability of these systems to absorb changes of state variables, driving variables, and parameters, and still persist" [61]. Studies on ecological resilience, using shallow lakes, tropical forests, and biological systems as examples, illustrated the concepts of multiple basins of attractions, and how disruptions could tip the system over a critical threshold ("tipping points") to an alternative stable equilibrium state (causing a "regime shift") [62]–[64]. Such concepts have been mathematically studied using nonlinear dynamics and chaos theory [65], leading to a better understanding of how and why critical slowing down [66]–[68], rising variance [69], and changing skewness [70] could be used as early warning signals for regime shifts [71]. Ecological systems are known to follow the "adaptive cycle" process which follows the four phases: growth, conservation, collapse, and reorganization, which is important in understanding the resilience of ecological (and other types of) systems. The growth phase (often referred to as the foreloop) is a slow process that allows system components to connect and accumulate capital (e.g., nutrients and biomass in ecosystems, assets and social capital in social systems), and the destruction phase (the backloop) is a rapid process that leads to reorganization and renewal of the system. Moreover, this adaptive cycle exists in multiple scales – from microscopic and quick to macroscopic and slow – and are connected via vertical feedback loops. This hierarchical organization of adaptive cycles is known as the panarchy framework [72], and helps us to understand the resilience of ecological systems and, more recently, social-ecological systems.

The concept of resilience has been further adopted in other domains including social systems, and the nexus of social and ecological systems [73]. Social dynamics, including collapse of society [74] and opinion dynamics [75] have been studied using resilience concepts including regime shifts. Instead of studying social systems and ecological systems in isolation, socio-ecological systems modeling attempts to understand the interdependencies (feedback effects) that exist between social systems and ecological systems due to actions and disturbances such as resource management, exploitation, and changing environmental conditions. Biggs et al. proposed seven key principles for building resilience in social-ecological systems, including "maintaining diversity and redundancy, managing connectivity, managing slow variables and feedbacks, fostering complex adaptive systems thinking, encouraging learning, broadening participation, and promoting polycentric governance systems" [76]. Adaptive capacity of social systems allow socio-ecological systems to reconfigure and adapt to changing environments without significant disruptions in resource supply or degradation in natural and ecological services [77]. In socio-ecological systems and other coupled social systems, adaptive capacity is constituted by the ability of organizations, institutions, and more broadly, social networks to accumulate knowledge and experience, and to develop problem solving capacities to navigate through environmental changes for transitions to favorable states [78].

Theories of Network Resilience

Social systems, ecological systems, and socio-ecological systems all can be perceived as components (e.g., households, lakes, institutions) that are connected together through bi-directional dependencies, forming dynamical networks. Motivated by such views of systems, the resilience of networks have been studied extensively in the physics community, under the field of network science [79], [80]. The resilience of internet networks with power-law degree distributions ([81]) to random breakdowns [82] and intentional and targeted attacks [83] have been studied using analytical and percolation approaches, and have revealed that internet networks are robust against random breakdowns, but are sensitive to intentional attacks. Studies have investigated methods in which to mitigate such attacks by re-configuring the network structures [84]. Moreover, recently an analytical framework that systematically separates the roles of the system's dynamics and network topology and collapses the behaviour of different networks onto a single universal resilience function was proposed [85]. A more thorough literature review on this area can be found in [86].

In addition to single networks, there are extensive literature on the robustness [87] and resilience of interdependent networks. Theoretical results show that catastrophic cascades of failures that could occur on interdependent networks, using the case study from the power outage in Italy [88]. Another study shows that reducing the coupling strength between the interdependent networks leads to a change from a first to second order percolation transition [89]. Given such theoretical foundations of the resilience of interdependent networks, studies have proposed analytical solutions to stop failure cascades [90]. Furthermore, a more complex, network composed of interdependent networks [91] and their robustness [92] have been studied. While there is a rich literature on the theoretical understandings of complex networks and their resilience to various shocks, many of the studies are based on strong assumptions. Including realistic features such as the properties of the coupling between networks, the dynamical nature of networks, and various spatial properties of networks remain as critical challenges when applying these theories to real world problems, such as the disaster resilience of urban systems [93].

Resilience of Engineered Systems

In engineering, resilience has often been referred to differently from ecological systems, as the efficient stability of a system state, which is more close to the concept of risk and robustness [94]. For example in the context of transportation systems, "resilience" has been measured using various indices including vulnerability, robustness, rapidity of recovery, and flexibility (for a review, see [95]). Other studies apply a percolation based method to analyze the resilience of transportation systems [96]. However, more recently, this definition has been revised towards the original definition proposed in ecology, as "an emergent property of what an engineering system does, rather than a static property the system has" [97], [98]. Recent views on engineering resilience point out that physical infrastructure systems are not capable of recovering and transforming on their own, and that the interdependencies between social systems are crucial for physical systems to recover [99]. Moreover, studies have pointed out the various types of complex interdependencies that critical physical infrastructure have across eachother [100]. Therefore, resilience of engineered systems i) need to be analyzed at the systems level instead of inspecting each infrastructure component individually, ii) needs to take into consideration the interdependencies with social systems that manage physical systems, and iii) needs to be studied in a dynamic manner, by observing the dynamic system states, making controls based on predictions, learning from past events, and adapting to new environmental scenarios.

In this dissertation, we adopt this notion of engineering resilience to study the resilience of social and physical coupled systems to external shocks. Using novel datasets, the complex interdependencies between dynamical socio-economic and physical infrastructure systems, and their effects on resilience (potential regime shifts) will be modeled and analyzed. In the next section, we review the vast literature on the resilience of social systems (i.e., cities and communities) to disasters, and identify key research gaps that we will bridge in this dissertation.

1.2.2 Disaster Recovery and Community Resilience

Index-based Approaches

The recovery process and resilience of cities to disasters have been studied from multiple perspectives and disciplines. The disaster resilience of place (DROP) model provides a conceptual framework that outlines the components and processes that need to be considered to model the resilience of cities and communities [101]. The DROP model frames disaster resilience as a continuous process dependent on antecedent conditions, where effects of disaster events accumulate over time, and communities respond and adapt to such shocks by repetitive mitigation and preparation. The study listed the key variables that are theoretically validated to affect disaster resilience, from dimensions of ecological, social, economic, institutional, infrastructure, and community competence. Following the DROP model, numerous studies have attempted to measure disaster resilience of communities using various indexes and metrics. For example, a study in Nepal quantified the resilience of communities by using 22 variables as indicators of social, economic, community, infrastructure, and environmental resilience [102]. A study reviewed twenty seven different resilience assessment tools, indices, and scorecards across the world, and evaluated them using four different parameters: focus, spatial orientation, methodology, and domain area [103]. Common factors used in the index-based community resilience measures include social, economic, institutional, infrastructure, community capital, and environmental factors. Such measurement index tools can quantify the resilience of communities to disasters and provide directions for future development, it models disaster resilience as a static measure and neglects the dynamic feedbacks and complexities of urban systems resilience. Moreover, using static metrics, we are not able to understand the existence of tipping points, which are critical thresholds where systems experience regime shifts in the performances of urban systems (as shown in [63]). An alternative approach to this index-based quantification of resilience is to develop dynamical models of urban recovery, and to evaluate resilience using simulations.

Dynamical Modeling Approaches

To overcome such drawbacks of index-based measures, several dynamic models have been proposed for understanding community resilience. Studies have modeled the interdependent dynamics in physical systems [104]. On the social systems side, studies have used household surveys and interviews to understand post-disaster evacuation behavior for the past several decades (e.g., [44], [105], [106]). Various characteristics including hazard characteristics, ethnicity, gender and race [107], as well as storm intensity [108], risk perception [109], information dissemination methods [110], past disaster experiences [111], and social network effects [112], [113] have been understood to affect evacuation decisions of individuals and households. By leveraging such empirical insights, there has been numerous efforts to build agent based models for simulating post-disaster mobility patterns [44], [114].

However, such studies treat social and physical systems in isolation, neglecting any complex interdependencies which might exist in the recovery process. Several studies have modeled the interactions between social and physical (structural) systems. For example, Dong et al. constructed an agent based modeling framework to simulate the resilience of healthcare facilities during flooding events [115]. Grinberger et al. investigate the welfare effects of disaster recovery after an earthquake in Jerusalem using an agent based simulation [116]. The COPEWELL framework is a system dynamics model for predicting community functioning and resilience after disasters [117]. Several interdisciplinary system dynamics models that model the housing recovery after disasters are presented [118], [119]. The agent based simulation by Kanno et al. is a human-centered modeling framework of urban systems to capture various types of interdependency underlying urban sociotechnical and socioeconomic systems [120]. Despite such advancements, they lack empirical testing using large-scale real world data from past disaster events. Without such empirical testing from various events and regions, it is difficult to obtain generalizable insights on the resilience of urban systems to disasters. To bridge this research gap, we leverage novel large scale data sources in this dissertation. In the next section, we review the various types of novel data sources, their properties, and their applications.

Table 1.1. Brief descriptions and applications of the four novel types of data: mobile phone location data, social media data, web search query data, and satellite imagery night time light data.

Data type	Data Description	Applications
Mobile phone location data	Location information and timestamps collected from individual mobile/smart phones. Typically are either call detail records (CDRs), which record the locations of cell phone towers, or GPS signals.	Monitor and analyze human mobility patterns at the urban scale for various applications ranging from population mapping, epidemic modeling, traffic analysis, disaster management.
Social media data	Content of social media posts (text, images), online social network structures of users, and occasionally geo-locations.	Sentiment analysis, topic modeling, text mining for understanding social dynamics during political/disaster events.
Web search query data	Query words that individual users have searched in browsers. Rarely used compared to social media and mobile phone location data.	Modeling the online information seeking behavior of individuals, analyzing the needs of the users during disaster events.
Nightime light data	Satellite image data; DMSP-OLS (1993-2017) and VIIRS DNB (2012-2020) are commonly used to capture nighttime lights.	Modeling the online information seeking behavior of individuals, analyzing the needs of the users.

1.2.3 Novel Data Sources in Urban Analytics

With the ubiquitousness of mobile devices and low cost sensors, we are now capable of collecting various types of data from individual users at an unprecedented scale. In this section, we will review mainly four types of novel data sources that have become increasingly popular in the past decade, their pros and cons, and applications in tackling urban challenges. Brief descriptions of the four types of data: mobile phone location data, social media data, web search query data, and satellite imagery data, are listed in Table 1.1.

Mobile Phone Location Data

The recent spread in mobile devices allow us to observe and analyze the individual mobility patterns of people at an unprecedented granularity and scale [121], [122]. During the last decade,

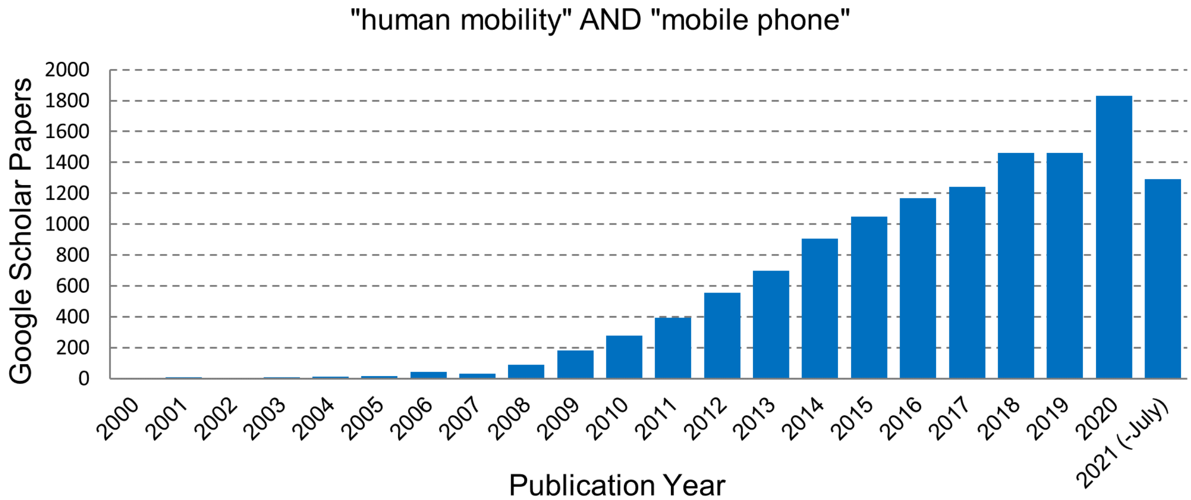

Figure 1.4. Number of research articles returned by searching "human mobility" and "mobile phone" in Google Scholar by year. Research has substantially increased over the years and was further spurred in 2020 due to the COVID-19 pandemic. The count for 2021 was computed on July 12th, 2021.

mobile phone location data, also known as call detail records (CDR), have become one of the primary data sources for analyzing human mobility patterns on the urban scale [123] (see Figure 1.4 for number of publications on human mobility and mobile phone data). Mobile phone location data can be classified into three main categories: mobile phone call detail records (CDR), smartphone GPS location data collected by location intelligence companies, and smartphone GPS location data collected and processed by major tech companies. Table 1.2 organizes how they are collected, the pros, cons, and examples of providers for each dataset.

Mobile Phone Call Detail Records (CDR)

During the last decade, mobile phone call detail records (CDR) have become one of the primary data sources for analyzing human mobility patterns on the urban scale [123]. Call detail records typically contain the unique ID of the user, timestamp, and location information of the observed cell phone tower. Note that unlike smartphone GPS data introduced later, the location information of CDRs are not the actual location of the user, thus contains typically around couple 100 meters to several kilometers in the rural areas where cell phone towers are sparsely located. Using large-

Table 1.2. Brief descriptions and applications of the four novel types of data: mobile phone location data, social media data, web search query data, and satellite imagery night time light data.

Data type	Description	Pros and Cons	Providers (e.g.)
Mobile phone call detail records (CDR)	Location information of cell phone towers when users make calls or text messages	(+) substantial coverage of the population (-) Low spatial and temporal resolution compared to GPS datasets	NCell, Orange, Vodafone, Turkcell
Smartphone GPS location data (Location Intelligence firms)	GPS data collected and aggregated from several third party smartphone applications	(+) precise location information of users (-) No transparency in data generation process; covers a small sample of population compared to CDR; available for fewer countries	Cuebiq, Veraset, Safegraph, Unacast
Smartphone GPS location data (Major Tech firms)	GPS data collected and aggregated from their own platforms	(+) Available in standardized formats across multiple countries and across time (-) Outputs restricted to selected metrics produced by the tech firms	Google, Facebook, Apple, Yahoo Japan

scale datasets of CDR data, a seminal paper by Gonzalez et al. unraveled the basic laws of human mobility patterns [124]. Several more papers have used CDR data to understand spatio-temporal patterns of urban human mobility, routine behavior, and their predictability (e.g., [125], [126]). Moreover, human activity patterns and land use patterns have been studied using CDR data (e.g., [127]). In addition to understanding human behavioral laws, such data has enabled us to obtain dynamic and spatially detailed estimations of population distributions (e.g., [128]), social integration and segregation of mobility (e.g., [129]), and macroscopic migration patterns (e.g., [130]). Moreover, these datasets have been applied to solve various urban problems such as preventing disease spread [131]–[133], estimating traffic flow (e.g., [134], [135]), and estimating socioeconomic statistics (e.g., [136]) and impacts of shocks [137] (for a full review, see [121], [122]).

Smartphone GPS Location Data from Location Intelligence Firms

More recently, we have seen an increase in the availability of mobile phone GPS location datasets collected by location intelligence companies, such as Cuebiq (https://www.cuebiq.com/), Unacast (https://www.unacast.com/), and Safegraph (https://www.safegraph.com/). Location intelligence companies collect location data (e.g., GPS data) from third-party data partners such as mobile location-based application developers. GPS data have been previously collected from taxis (for example, see [138]) to understand traffic patterns. Typically for each data point, a user identifier, timestamp of observation, and the longitude and latitude information are included in the dataset. More recently, these firms have started provided more aggregate (e.g., aggregated for each point-of-interest) data to preserve the privacy of the users. Compared to CDR, GPS logs have higher spatial preciseness, and moreover, higher observation frequency, allowing us to understand mobility patterns in more detail. However, often the specific sources of the location data nor the process in which the data are collected and combined from several application services are undisclosed to the users. Therefore, using such data requires a rigorous analysis of checking the representativeness of the mobile phone location dataset.

Smartphone Location Data from Major Tech Firms

Similar to the smartphone GPS location data collected by location intelligence firms, major tech firms such as Facebook, Google, and Apple, also collect GPS location data from their users. The major difference in the data generative process is that these major tech firms use data collected from their own platform, not by third party services. Often, these data are provided in a pre-processed form, aggregated by both time and space. Facebook, through its "Data for Good" program, provides various types of location information products to researchers, agencies, and non-profits (https://dataforgood.fb.com). In particular, the "Facebook Disaster Maps" provides detailed density maps of the population density and movement patterns before, during, and after disaster events. The data is temporally aggregated (usually every 24 hours), spatially aggregated (usually into 360,000 square meter tiles), and spatially smoothed, to anonymize and protect the users' privacy [139], [140]. The Maps have been utilized by many significant nonprofit organizations and international agencies in disaster response, including the International Federation of the

Red Cross, the World Food Programme, the United Nations Children's Fund (UNICEF), NetHope, Direct Relief, and others.

The availability of such high-frequency, high-resolution data has become more common with the coronavirus pandemic in 2020/2021. During the current COVID-19 crisis, researchers from academia, industry, and government agencies have utilized large-scale mobility datasets to estimate the effectiveness of control measures in various countries including China, Germany, France, Italy, Spain, Sweden, United Kingdom and the United States [141]–[152]. We have made several contributions to the scientific literature during the COVID-19 pandemic, including understanding the effects of non-compulsory lockdown orders on mobility restrictions in Tokyo (Figure 1.5) [152], the income inequality in mobility reductions in the United States [28], and a policy brief with the Asian Development Bank Institute on the importance of balancing out economic recovery and pandemic suppression, and the usage of large-scale mobility data [25]. Data sharing platforms such as the PlaceKey community (https://www.placekey.io/) has contributed to this effort by providing a semi-open platform where researchers can freely access aggregated mobile phone location data for analysis. I have summarized the efforts on using such novel data for development in Section 6.3.1.

1.2.4 Application of Mobile Phone Data in Disaster Management

Recently, mobile phone data has been utilized in many applications for disaster response and recovery, given its high spatial and temporal granularity, scalability to analyze millions of individuals' mobility, and increasing availability. In this section, the studies using mobile phone data for natural hazard response and recovery are categorized into 3 categories of applications: population displacement and evacuation modeling, longer-term recovery analysis, and inverse inference of damages to the built environment. The required inputs, methodologies, obtained outputs, and case studies are presented for each application.

Population Displacement and Evacuation Modeling

The most widely studied applications of mobile phone location data in disaster response and recovery is to estimate the population displacement and evacuation dynamics after disasters. In

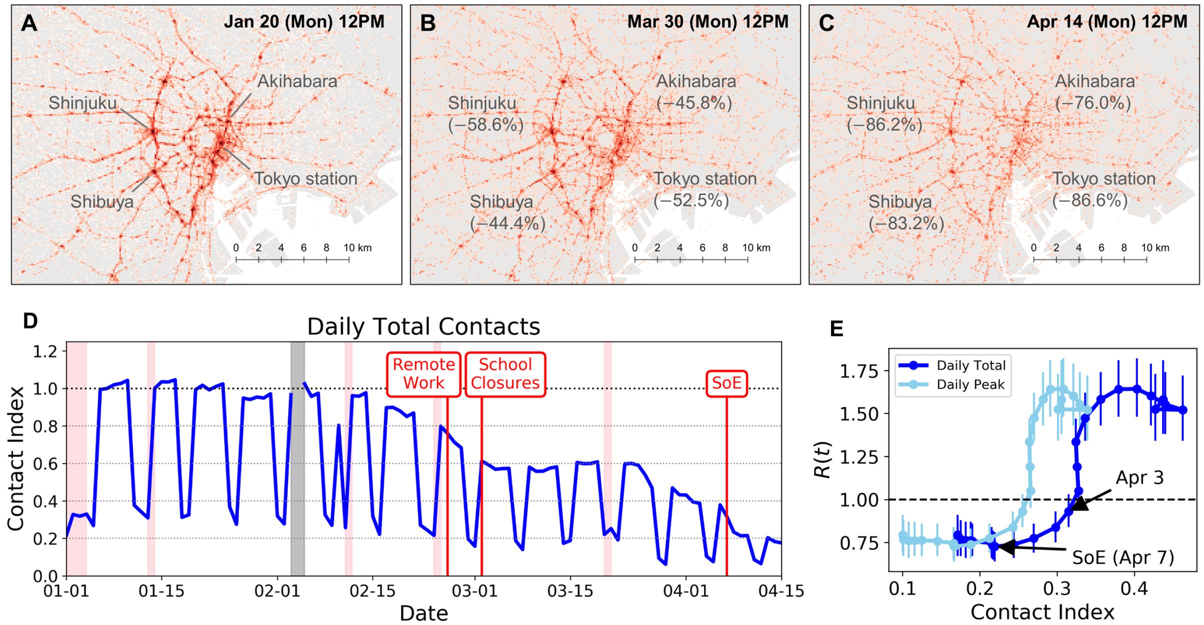

Figure 1.5. (A-C) Population distribution estimated from mobile phone GPS location data, on 3 different dates at same times (12PM), each on the same day of week (Mondays) in Tokyo during the COVID-19 pandemic. Substantial decrease in the population density at stations and cities along the Yamanote-line (ring railway) can be observed. (D) shows the amount of contacts an individual potentially encounters outside home for each time period. (E) shows the non-linear relationship between the mobility metrics and $R(t)$. (Yabe et al., 2020 [152])

their seminal paper, Lu et al. used CDR to study the predictability of displacement mobility patterns after the Haiti Earthquake in 2010 [45]. Using data collected from 1.9 million mobile phone users during the period from 42 days before to 341 days after the shock, the study estimated that 23% of the population in Port-au-Prince had been displaced due to the earthquake. Despite the substantial displacement, they also found that the destinations of the displaced people were highly correlated with their pre-earthquake mobility patterns. This finding shed light on the possibility of predicting post-disaster mobility patterns, and had significant implications on relief operations including the pre-positioning of distribution centers [153] and evacuation shelters. Another seminal disaster event that highlighted the use of mobile phone location data was the Gorkha Earthquake (intensity of 7.8Mw) which struck Nepal in 2015 [154]. Wilson et al. rapidly analyzed the displacement movements of 12 million de-identified mobile phone users after the earthquake within nine days from the event [155]. It was estimated that over 390,000 people left the Kathmandu

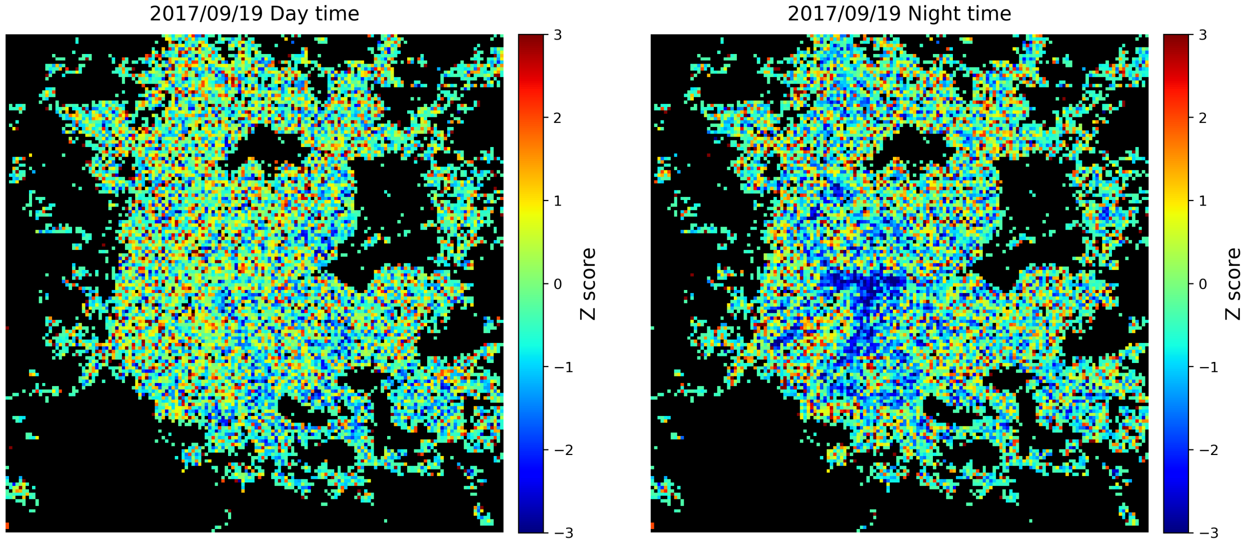

Figure 1.6. Population displacement after the Puebla Earthquake in Mexico City. Anomaly score (z score; number of standard deviations more/less than the pre-earthquake mean) of population density during the day (left) and night (right) on September 19th, 2017 in Mexico City. Significant displacement is observed during the night time of the day of the earthquake (Source: [157])

Valley after the earthquake. These results were released as a report with the United Nations Office for the Coordination of Humanitarian Affairs (UN OCHA) and a range of relief agencies. This effort by Flowminder, a non-profit foundation for analyzing mobile phone location datasets, was the first significant practical use-case of large scale mobile phone location data in disaster relief and response [156].

Following the aforementioned two seminal works after the Haiti Earthquake and Gorkha Earthquake, several studies have developed methods to estimate population displacement and post-disaster evacuation patterns using mobile phone location data. A general framework for the spatio-temporal detection of behavioral anomalies using mobile phone data was proposed by Dobra et al. [158]. Using smartphone location data from before and after disasters, population displacement can be quantified by measuring the anomaly score (z-score; the number of standard deviations more or less from the mean population on a typical day) of the daytime and nighttime population in highly granular (1km x 1km) grid cells, as shown in Figure 1.6 [157]. During the night time after the earthquake, blue-colored clusters with z scores below -2, indicating a likelihood of less than 1% on a typical day, can be observed in central Mexico City, showing significant decrease in nighttime population. Yabe et al. used smartphone GPS location data collected by Yahoo Japan Corporation to analyze the evacuation rates after five earthquake events in Japan [159]. Cross-comparative analysis of five earthquakes and over 100 affected communities revealed similar relationships between evacuation rates and seismic intensity levels, where evacuation rates significantly increased in communities that experienced magnitudes above 5.5. Several computational frameworks have been proposed to estimate the spatial patterns of evacuation destinations and hotspot locations using anomaly detection techniques on large-scale mobility data [160]. Just after the Kumamoto Earthquake in April 2016, population distribution and evacuation hotspot maps were produced jointly by researchers at the University of Tokyo and Yahoo Japan Research, and were delivered to city governments for relief and response [161]. Duan et al. studied the evacuation patterns after a train collision incident in China using mobile phone location data, identifying a two-stage evacuation process, and also behavioral changes in commuters' travel route choices [162]. Ghurye et al. study the displacement patterns after the Rwanda Flood in 2012 using Markov Chain models and CDR [163]. The study compares the observed human behavior during a disaster with the behavior expected under normal circumstances to understand the causal effects of the disaster event. Yin et al. combined mobile phone location data with agent based simulations (which are widely used in evacuation analysis; e.g., [114]) to improve the estimation accuracy of evacuation movement, proposing a hybrid approach [164].

More computational approaches using data assimilation techniques have been explored for online, near real-time predictions of post-disaster mobility patterns. Song et al. proposed a mobility prediction model based on a Hidden Markov Modeling framework, and tested its validity using data collected from 1.6 million mobile phone users in Japan before, during, and after the Great East Japan Earthquake in 2011 [165]. Sudo et al. developed a Bayesian data assimilation framework by combining the particle filter and Earth Mover's Distance algorithms, that updates the urban-scale agent based mobility simulation in an online manner using spatially aggregate mobile phone location data provided in real time [166], [167]. Several online algorithms have been proposed since these seminal works, including CityMomentum [168] that uses a mixture of multiple random Markov chains, CityCoupling [169] that aims to perform cross-city predictions, and inverse reinforcement learning approaches that attempt to learn the behavioral patterns of human mobility during disasters from large scale data [170], [171]. Although these computational, online approaches are shown to be effective in experimental and post-hoc settings, none have been utilized in real-time after real-world disaster events.

Longer-term Analysis: Migration and Recovery

One advantage of mobile phone location data is the ability to track the movements of users over a long period of time (several months $\sim$ year) with high frequency (e.g., hourly $\sim$ daily), which are extremely difficult to perform using household survey data. Therefore, in the normal setting, there have been attempts to use mobile phone location data to estimate population migration dynamics [130], [172], [173]. In the disaster setting, Lu et al. studied the migration patterns in regions stressed by climate shocks in Bangladesh using CDR [174]. In addition to analyzing the short term human mobility patterns after Cyclone events (hours $\sim$ weeks), the study quantifies the incidence, direction, duration and seasonality of migration in Bangladesh. Acosta et al. quantified the migration dynamics from Puerto Rico after Hurricane maria using mobile phone, showing a shift from rural to urban areas after the disaster [175]. Marzuoli et al. used mobile phone data to analyze the recovery dynamics of residents in South Texas after Hurricane Harvey [176]. The study provided detailed statistics of population movement and origin destination patterns for different zipcodes in Texas. In addition, the role of social networks [113], [177], hedonic behavior [178], and post-disaster spatial segregation [179] have been tested using mobile phone location data after disasters. Although mobile phone location data provide significant advantages in analyzing longer-term phenomena (e.g., migration and recovery after disaster events) compared to household survey data, most studies focus on shorter term displacement and evacuation analysis, leaving substantial room for research in understanding the long term recovery and resilience of urban and rural areas to disasters.

Inverse Inference of Damage to the Built Environment

The studies introduced in the previous two subsections studied the anomalies in human mobility patterns disrupted by shocks (e.g., hurricanes, earthquakes, tsunami) inflicted to the built environment. However, several studies have approached the problem in an inverse manner, by using anomalies observed in the mobile phone location data and human mobility dynamics to inversely estimate the damage to and recovery of the built environment, which have traditionally been estimated using hazard simulations and structural mechanics (e.g., [180]). Andrade et al. propose a novel metric "reach score" that quantifies the amount of movement of mobile phone users, and finds that the reach score has significant correlation with the damage inflicted to infrastructure systems by the earthquake at the canton level in Ecuador [181]. Pastor-Escuredo et al. show that by analyzing the anomalous patterns in mobile phone communications, we are able to conduct infrastructure impact assessment due to flooding events, using retrospective data collected from a flood in Mexico [182]. Finally, Yabe et al. propose a machine learning algorithm that combines mobile phone location data with terrain information to conduct a rapid and accurate estimate of the inundated areas during a flood event [183]. These studies show the potential of using mobile phone location data to infer the abnormal states of the built environment. Mobile phone location data has several advantages compared to conventional methods in data quality, including satellite imagery which are often observed sparse in time (e.g., once a day at most), and social media data which are more sparsely observed. While the application potential of these studies are promising, we lack comprehensive analysis of its real-time feasibility and accuracy under different types of events.

Despite the increasing number of studies using large scale mobility data sources for human mobility analysis, there is still little work that utilizes such novel mobile phone location datasets to fully understand the longitudinal dynamics of recovery after disasters. This dissertation contributes to this area of research by developing methods and models to further utilize large-scale mobile phone location data collected before/during/after disasters, to reveal the complex dynamics of disaster recovery.

Social Media Data

Mobile phone location datasets are relatively new to the research field, however, there are other data sources that have been used more extensively in urban science and disaster recovery research. Social media data, mainly data collected from Twitter, allows us to observe individual users' views and opinions on various topics, as well as their mood and sentiment, at an extremely large scale (scale of millions of users). Due to this advantage in scale and temporal granularity compared to conventional surveys, Twitter data has been a popular source for analyzing social dynamics across disciplines, including public health [184], [185], analysis of political discourse and election predictions [186], [187], and disaster management [188]. In particular, studies have used Twitter data to understand communication patterns before, during, and after disaster events [189]–[191], disruptions in mobility behavior during disasters using Twitter geotag data [192], [193], earthquake event detection [194], and rapid assessment of disaster impacts [195]. We have made several contributions in this literature, on understanding emergency needs of disaster affected users via text analysis and machine learning [196], and predicting evacuation and return behavior of users by using sentiment analysis and machine learning [197]. Social media data are similar to mobile phone location data in the sense that the data are disaggregated to individuals, however, the percentage of tweets that contain location information (geotags) are extremely sparse (around 0.1% of all tweets), and is difficult to use for mobility analytics [198].

Web Search Data

Another type of data that are more recently used, are the web search query data of individual users [199]. Studies have used aggregate web search query counts to predict various phenomena, including epidemics and disease spread [200], [201]. Others have used web search data to predict users' demographics [202], to understand consumer behavior [203] and to improve click through rates [204], mainly for commercial applications. More recently, web search query datasets of individual users have become available for analysis. To analyze web search queries, a popular approach is to produce word embeddings using methods such as `word2vec` [205], `FastText` [206], `GloVe` [207], and `Query2Vec` [208]. We used individual web search data and developed a bi-level long short term memory (LSTM) model to predict the evacuation mobility behavior of individuals [209].

During the COVID-19 pandemic, many studies have utilized web search query data to understand information seeking behavior and the occurrence of infodemics [211]–[213]. Others have used such data to detect the increase in COVID-19 symptoms (e.g. loss of smell) [214], [215], and also for predicting outbreaks [216], [217]. With the availability of open datasets [218], there is great potential in further using web search query data for pandemic response and prevention.

Our study used web search data and GPS location data, which are linked with common user IDs, to predict outbreak hotspot locations [210]. Validation using data from Tokyo, Japan showed that compared to previously proposed metrics, the high risk social contact index is capable of predicting the timing of outbreaks 1-2 weeks beforehand in a microscopic (125 meters) spatial scale (Figure 1.7). Web search data, despite its infancy, has great potential in understanding and predicting social dynamics, along with mobile phone location data and social media data.

1.2.5 Literature Summary and Research Gaps

In this section, we have reviewed the literature on three broad topics: 1) resilience concepts, 2) disaster recovery and community resilience, and 3) novel data sources. The literature can be organized using two axes: complexity of the modeling approach, and the characteristics of the data used for analysis. As summarized in Figure 1.8, the current literature are focused in three out of the

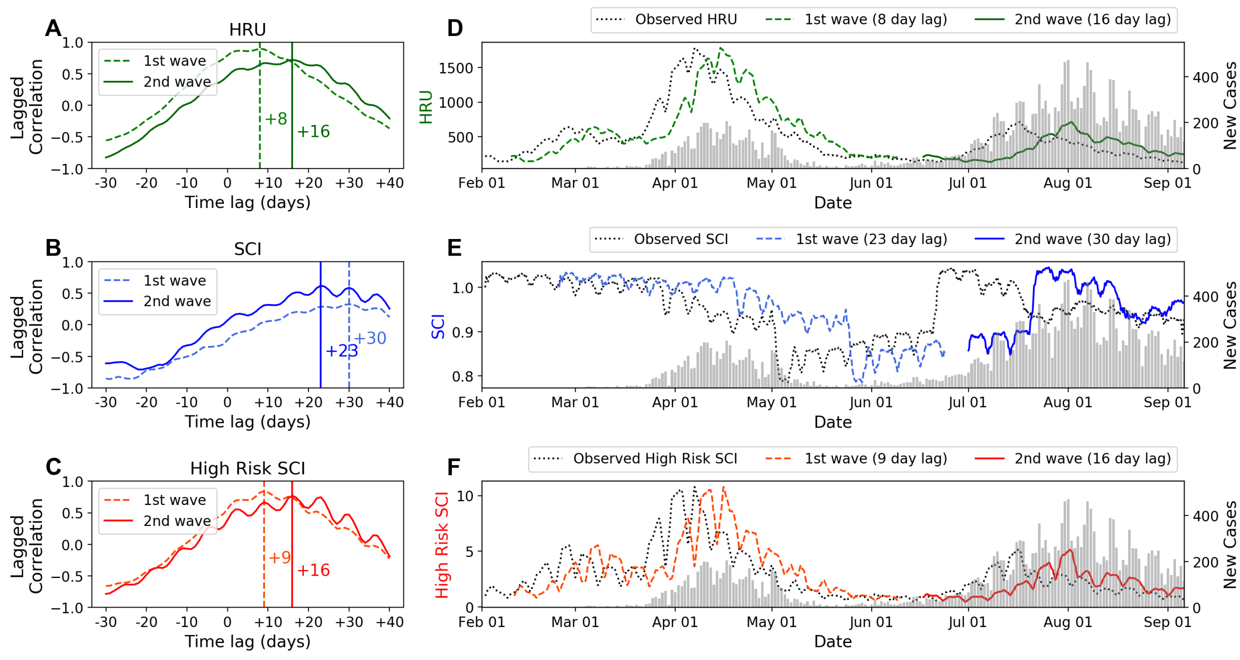

Figure 1.7. Predicting COVID-19 outbreaks with web search data. Time lagged cross correlation analysis of the high risk users, social contact index, and high risk social contact index metrics against the daily number of new cases. Web search-driven metrics preceded the daily cases trend by 8-9 days during the first wave, and by 16 days during the second wave. (Yabe et al., 2020 [210])

four quadrants in this space. Component-level analysis, for example of social behavior modeling of evacuation analysis, have been performed using both conventional (e.g., household surveys) and novel datasets (e.g., mobile phone location data; introduced in Section 1.2.3). While there has been several studies on the analysis and modeling of interdependent systems using agent based models and system dynamics, such studies have been based on conventional survey data. This dissertation attempts to make contributions in the top right quadrant, to model the interdependent systems dynamics using novel datasets. In summary, the literature review has identified several key research gaps in the field of disaster resilience modeling:

- Despite the vast literature on disaster resilience, there is limited work that investigate the dynamical interdependencies across social, economic, and physical infrastructure systems, and their effects on the resilience to shocks of the overall urban system.
- In addition to the above gap, existing work on disaster recovery and resilience simulations lack rigorous empirical validation using large-scale novel datasets from various disasters and regions, despite their availability.
- Many studies across various disciplines have used novel large-scale datasets for post-disaster analysis, however, we lack methods to leverage such data to understand the complex recovery dynamics of coupled systems.

1.3 Overarching Goal and Objectives

The overarching goal of the dissertation is to address the aforementioned key challenges in the resilience literature, by **developing data-driven dynamical systems methods to understand the post-disaster recovery dynamics of coupled socio-physical systems**. A series of novel data-driven, computational methods will be developed with a multi-disciplinary approach, integrating methods and theories from machine learning, Bayesian statistics, social network analysis, ecological resilience and system dynamics. To achieve the overarching goal of the dissertation, the following five major objectives are proposed in this dissertation:

1. To develop a data-driven generalizable model of post-disaster recovery dynamics using large scale empirical data collected from various disaster events.

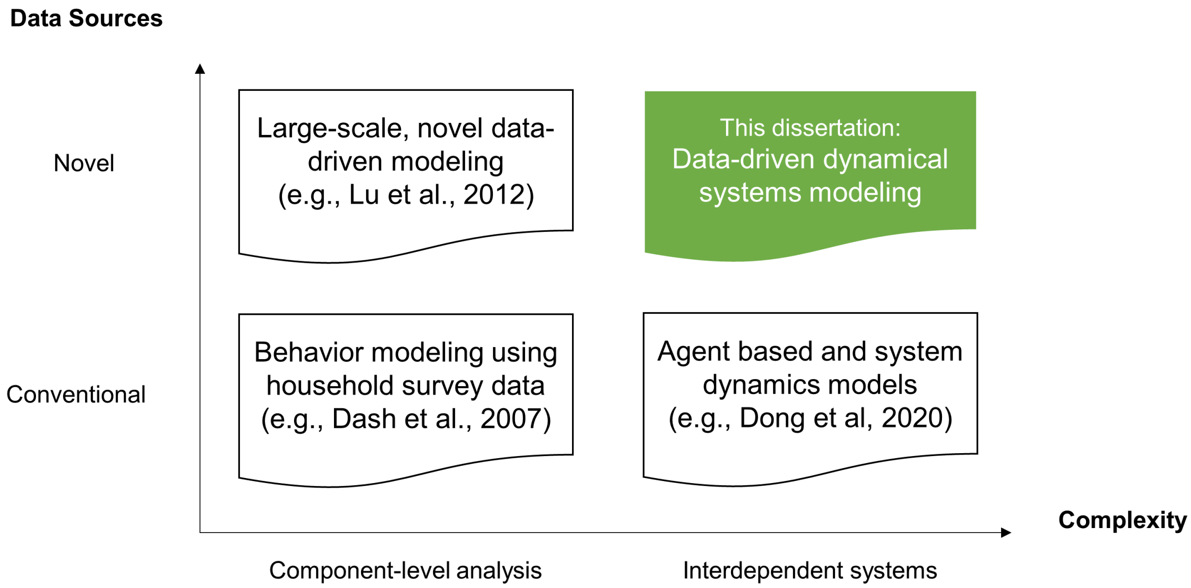

Figure 1.8. Research gap in data-driven dynamical systems modeling that this dissertation attempts to bridge.

2. To unravel intra-regional, intra-sectoral socio-economic inequalities that exist in the recovery of heterogeneous social systems.

3. To develop a data-driven system dynamics model of coupled urban socio-physical systems exposed to external shocks to predict post-disaster recovery dynamics.

4. To apply the developed system dynamics model for evaluating the resilience of urban systems to hypothetical future climate scenarios.

5. To develop artificial intelligence methods that identifies functional similarities across cities, to transfer knowledge from past disasters across cities.

To fulfill these objectives, novel data-driven models, algorithms, and theories are developed in Sections 2, 3, 4, and 5. While each Section focuses on a particular set of research questions and attempts to answer a set of hypotheses on the corresponding topics, the overarching hypotheses of the dissertation on the recovery and resilience of coupled urban systems are as follows:

H1. Similar to usual human mobility behavior (as shown in [124]), the recovery patterns of human mobility and population movement after shocks can be characterized by a universal function in the form of truncated power law distributions.

H2. The recovery speed of social systems after shocks vary across regions and industry categories, however the recovery sequences of business categories are similar across regions.

H3. Urban systems are composed of interdependent socio-economic and physical infrastructure systems, however, the degree of interdependency varies across regions depending on the urban-ness of the region, which affects the resilience of coupled systems.

1.4 Organization of Dissertation: a Synthesis Approach

The dissertation aims to develop data-driven computational models that improve our understanding of the disaster recovery dynamics of coupled socio-physical systems, and to provide methods and case studies that can assist future decision makings in improving the resilience of cities to future disasters. The overall structure of the dissertation is shown in Figure 1.9. The contents of the dissertation are organized to collectively address the aforementioned objectives and research questions. Although each chapter may be read independently of each other, analyses and modeling in some of the chapters depend on models and insights from the preceding chapter(s). For example, the insights from disaster recovery trajectories and intra-regional inequalities in Chapters 2 and 3, respectively, are key components used in the system dynamics modeling in Chapter 4.

Chapter 2 of the dissertation focuses on developing methods and models to extract theoretical insights of post-disaster population recovery dynamics from large-scale mobility data (e.g. mobile phone GPS data). Section 2.1 uses large-scale mobility data collected from five heterogeneous disasters (e.g. tsunami, hurricane, earthquake, flood) across the US and Japan to generate universal insights on population recovery patterns. In addition to discovering the universal patterns, the observed heterogeneity in recovery model parameters across communities are explained using a set of key factors in Section 2.2. Furthermore, the significance of social and physical network effects are investigated in Section 2.3 using spatial econometric models.

Chapter 3 further investigates the intra-regional heterogeneity and inequalities in post-disaster recovery patterns. Using Miami-Dade after Hurricane Irma as a case study, methods based on information theory are proposed to quantify the inequity in post-disaster evacuation and return movements in Section 3.1. Section 3.2 proposes and tests a Bayesian structural time series model to quantify the causal impact of a disaster on local businesses using foot traffic data observed via mobile phone location data. The model is tested on data collected from Hurricane Maria in Puerto Rico to estimate the inequality in disasters impacts on different business categories and business locations. Section 3.3 further characterizes the sequence of disaster recovery of business sectors across regions.

Chapter 4 integrates the insights and models from Chapters 2 and 3 to develop a system dynamics model of coupled socio-physical systems after disasters. Section 4.1 focuses on developing the formulation and analysis of the system dynamics model, by extending socio-physical system dynamics models developed in the socio-ecological domains. Section 4.2 integrates the model with empirical data from Hurricane Maria in Puerto Rico to unravel the effects of interdependencies on resilience, and critical trade-offs between infrastructure efficiency and socio-economic self-reliance. Section 4.3 further proposes a network diffusion model that characterizes the inter-city spillover effects of disaster recovery, using insights obtained from Section 2.3.

Chapter 5 proposes a new stream of work, on developing deep-learning based techniques to transfer insights across different cities using a data-driven approach. Section 5.1 introduces an unsupervised machine translation approach that translates the functionality of places that are produced via LSTM-based representation models. Section 5.2 presents a methodology that utilizes the urban hierarchical structures to overcome the difficulties in translating the functionalities of places across cities of different sizes (i.e. domain imbalance problem).

Chapter 6 will synthesize the key contributions of the dissertation, present transitions from data-driven modeling to data-driven dynamical systems approach, and also discuss the important future research directions.

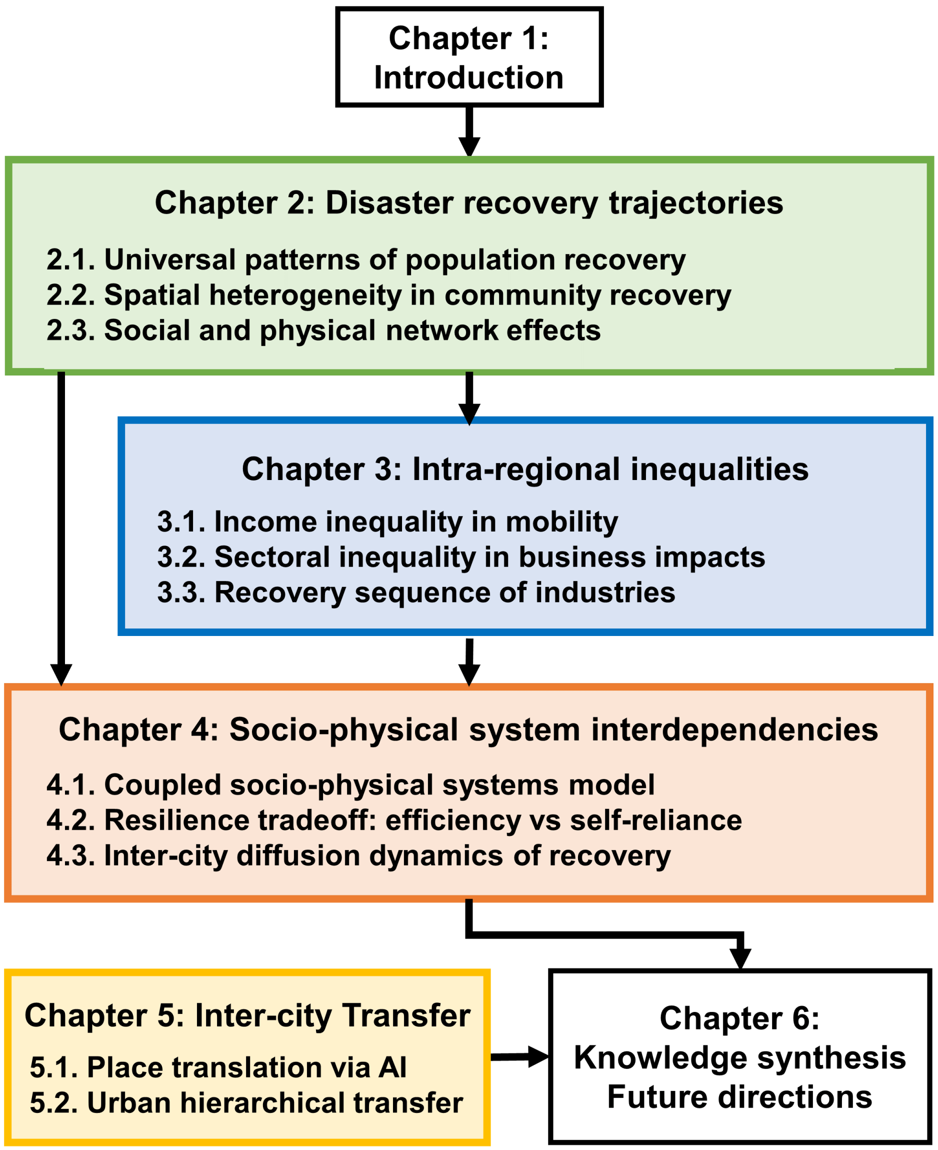

Figure 1.9. Organization of dissertation.

2. DISASTER RECOVERY TRAJECTORIES

In this chapter, aim to understand how cities recovery after shocks through the lens of human mobility dynamics. As introduced in Section 1, human mobility patterns are known to follow a universal law – a truncated power law distribution – in the usual setting (normal, daily lives) [124]. Truncated power law distributions are products of substantial variance in behavioral patterns and limits in space and time of observation. We hypothesize that even after shocks (e.g., floods, earthquakes, hurricanes, tsunami), human mobility behavior exhibit universal patterns, similar to a truncated power law distribution (Hypothesis 1). To answer this question, we use large mobile phone location data collected from five large scale disasters across the US and Japan.

Household surveys and interviews have been the primary data sources to understand post-disaster evacuation behavior for the past several decades [105]. Surveys conducted after various disasters and events have revealed the high complexity of evacuation decision making processes [106]. Previous works have studied the effects of various factors on the evacuation process (for a review on this topic, see [44]). Although findings vary across disaster events due to the differences in social context and the hazard characteristics, personal and household characteristics such as ethnicity, gender and race [107], as well as storm intensity [108] have been understood to affect evacuation decisions. Moreover, risk perception [109] and past disaster experiences [111] affect how individuals and households react to disasters. In addition to such individual-level characteristics, how evacuation orders are delivered to households during evacuation [219] and also the type of sources the information is disseminated through are also known to be important factors [110]. Also, recent studies have revealed the significant effect of social influences [220] through connected peers in their social networks [112]. A study in rural Indiana showed the importance of social capital, personal networks, and emergency responders in evacuation decision making [113]. Studies have also used survey data to understand evacuation activities after no notice disasters [221]. In terms of Hurricane Irma, a study analyzed survey data collected from surveys to show the importance of social connections on evacuation behavior [222]. Similar to evacuation behavior, the effect of various features on reentry behavior has been analyzed using data collected via household surveys [47]. Another study analyzed the evacuation behavior after Hurricane Irma using discrete choice models based on data collected from surveys, with 645 respondents [223].

Despite the various advantages of survey data (e.g. qualitative details on individual experiences), such data have several drawbacks that limit our analysis on the evacuation behavior of the affected individuals. The main limitations are the number of samples (number of respondents were 645 in [223]) and the coarse spatio-temporal granularity in which we are able to track the movements of people.

In the context of disasters, studies have used mobile phone location data to analyze population displacement patterns [155], [174]. Lu et al. [45] revealed the predictability of displacement destinations from pre-disaster behavioral patterns in Haiti. Other studies have used a more online machine learning approach to predict the population flow after disasters using real time location data in an online manner [165], [166]. Despite the increasing number of studies using large scale mobility data sources for human mobility analysis, none of the existing studies have used mobility data to model the longitudinal post-disaster population dynamics.

Summary of key challenges related to disaster recovery trajectories: Based on the literature review, the key challenges in modeling post-disaster population dynamics in urban systems can be summarized as the following:

1. There is a lack of understanding of how the complex and dynamic coupling between social, physical and institutional systems effect inter-city population dynamics after disasters.

2. Many of the studies on the analysis of disaster recovery and resilience lack sufficient empirical testing, often due to the limitations of data collected via household surveys.

3. Despite the availability of large-scale mobility data collected from various disaster events, we lack computational methods to leverage such data to model and predict post-disaster population dynamics.

Key hypotheses to be tested in this chapter:

H2-1. Similar to usual human mobility behavior (as shown in [124]), the recovery patterns of human mobility and population movement after shocks can be characterized by a universal function in the form of truncated power law distributions.

H2-2. Heterogeneity in recovery parameters (speed, initial displacement rate, long term displacement rate) can be explained by a set of key socio-economic parameters.

H2-3. Topological organizations of cities and the structures of the inter-city networks (characterized by both physical distance and social mobility flow) affect recovery outcomes.

2.1 Universal Recovery Patterns

In order to bridge the gaps in the current literature, we analyzed large scale mobile phone GPS datasets collected before and after multiple disasters across different counties. We collaborated with 3 different companies across the US and Japan that collect GPS location data from mobile phones, and studied the movements of more than 1.9 million mobile phones of affected individuals over a six-month period. We studied the recovery patterns after Hurricane Maria (Puerto Rico, USA, 2017), Hurricane Irma (Florida, USA, 2017), Tohoku Tsunami (Tohoku area, Japan, 2011), Kumamoto Earthquake (Kyushu area, 2016), and Kinugawa Flood (Ibaraki area, Japan, 2015), shown in Figure 1a. These five disasters, in total, destroyed more than 1.5 million residential buildings, caused power outages in more than 8 million households, and caused more than $350 billion in economic loss. The five disasters were diverse in various aspects including the type of disaster (tsunami, earthquake, hurricane, flood), location of occurrence (Puerto Rico, Florida, Tohoku, Kumamoto), and the socio-economic characteristics of the affected regions.

For each disaster, we analyzed the longitudinal population recovery patterns in the affected areas (Table 2.1). The affected areas were defined as the set of local government units (LGUs), which experienced damages to residential buildings due to the hazard. LGUs correspond to counties in Florida and Puerto Rico, and "shichoson (cities/wards)" in Japan in this study. There are mainly 3 reasons to why we perform our analysis on the LGU scale. Firstly, due to the limitation in the number of mobile phone user samples, analysis at a further finer scale would yield statistically insignificant results especially in rural areas. Second, the LGU scale is the finest scale in which we can obtain socio-economic data in Japan, unlike the US where data is available on the census tract level through the American Community Survey. Third, government agencies often make policy decisions on the LGU scale, thus insights on that spatial scale would provide decision makers with relevant and useful insights.

Housing damage data collected from official sources are used to understand the spatial extent of damage inflicted to each of the communities. For disasters in the US, the "housing damage

Table 2.1. Statistics of GPS data for all disasters. For all disasters, GPS location data of affected individuals were observed for approximately 6 months, including days before and after the disaster. All datasets had more than 30 datapoints per day for each individual on average, allowing us to accurately track where each individual stayed every night after the disaster.

Disaster	Main Study Area	Observed Period	Users (affected)	Observations (/day/user)
Hurricane Maria	Puerto Rico	2017/9/1-2018/3/15	53,511 (53,511)	82.8
Hurricane Irma	Florida, USA	2017/9/1-2018/3/1	1,730,326 (1,599,370)	97.0
Tohoku Tsunami	Tohoku, Japan	2011/3/1-2011/9/1	68,416 (10,697)	33.4
Kumamoto Earthquake	Kumamoto, Japan	2016/4/1-2016/10/1	80,933 (5,944)	40.7
Kinugawa Flood	Ibaraki, Japan	2015/9/1-2016/3/1	2,580 (437)	46.0

rate" of a given LGU refers to the rate of houses approved for the Individuals and Households Program of FEMA in each LGU [224]. For disasters in Japan, it refers to the rate of residential buildings classified as "totally destroyed" or "half destroyed" by the Cabinet Office of Japan (COJ) in each LGU [225]. Both datasets are publicly accessible. 78 LGUs in Puerto Rico, 49 LGUs in Florida, 30 LGUs in Tohoku, 33 LGUs in Kumamoto, and 10 LGUs in Kinugawa were classified as affected areas with housing damages, and were included in the analysis. Figure 2.1 shows the LGUs that were included in the analysis along with the housing damage rates in red color.

Mobile phone location data for the five disasters were provided by 3 different companies in Japan and the US. Location data were collected by Yahoo Japan Corporation (https://www.yahoo.co.jp/) for Kumamoto Earthquake and Kinugawa Flood, by Zenrin Data Com (http://www.zenrin-datacom.net/toppage) for Tohoku Tsunami and Earthquake, and Safegraph (https://www.safegraph.com/) for Hurricanes Irma and Maria. All companies obtained the location information (time, longitude, latitude) of mobile phones from users who agreed to provide their location data for research purposes, and all information were anonymized to protect the security of users. Each mobile phone user's home location was estimated by performing a weighted mean-shift clustering

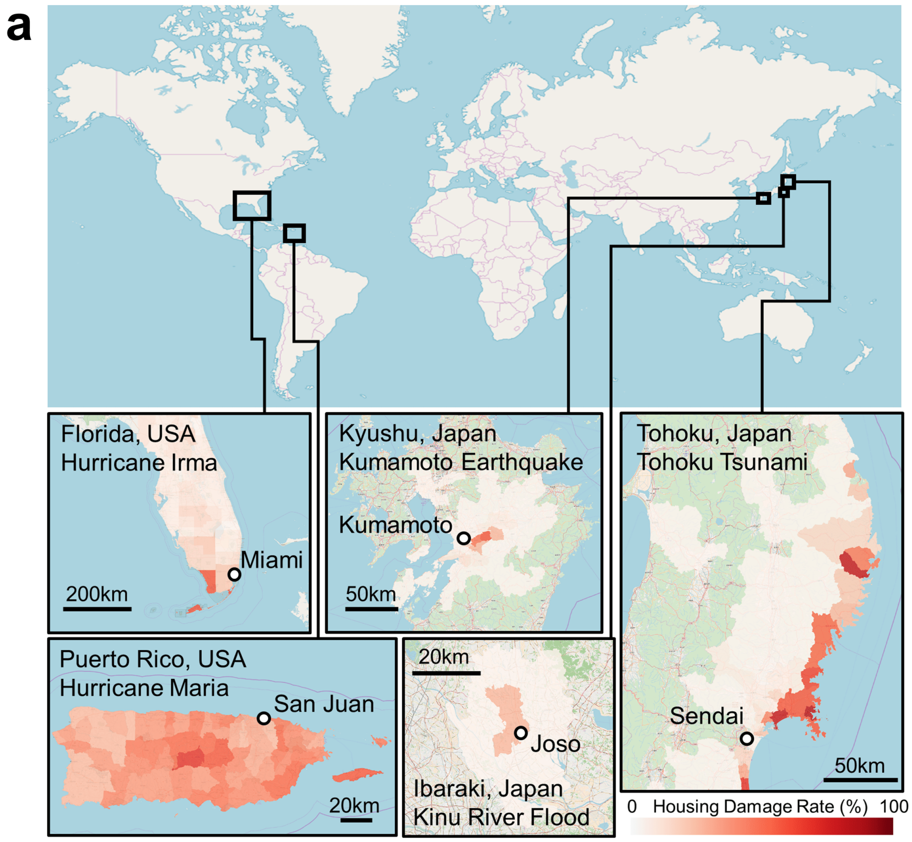

Figure 2.1. Locations and disaster events of study. Location, spatial scale, and severity of disasters that were studied. Red colors indicate the percentages of houses that were severely damaged in each community.

on the GPS location points observed during nighttime prior to the disaster date [226], [227]. As a result, a total of 1.9 million individual users were identified to be living in the affected areas before the disaster. We refer to these users as "affected users". Correlations (both Pearson and Spearman rank correlations) between the number of affected mobile phone users in each LGU and the census population data were very high in all datasets. Thus, we assume that distribution of mobile phone users have little spatial bias, and that they are representative of the entire population in the macroscopic spatial scale, which is also shown in previous works using other mobile phone datasets [45], [128], [159]. The mobility trajectories of each user were tracked during and after the disaster, and were used to quantify the longitudinal population recovery patterns. The rate of displacement on a given day was defined as the rate of affected users who stayed outside their

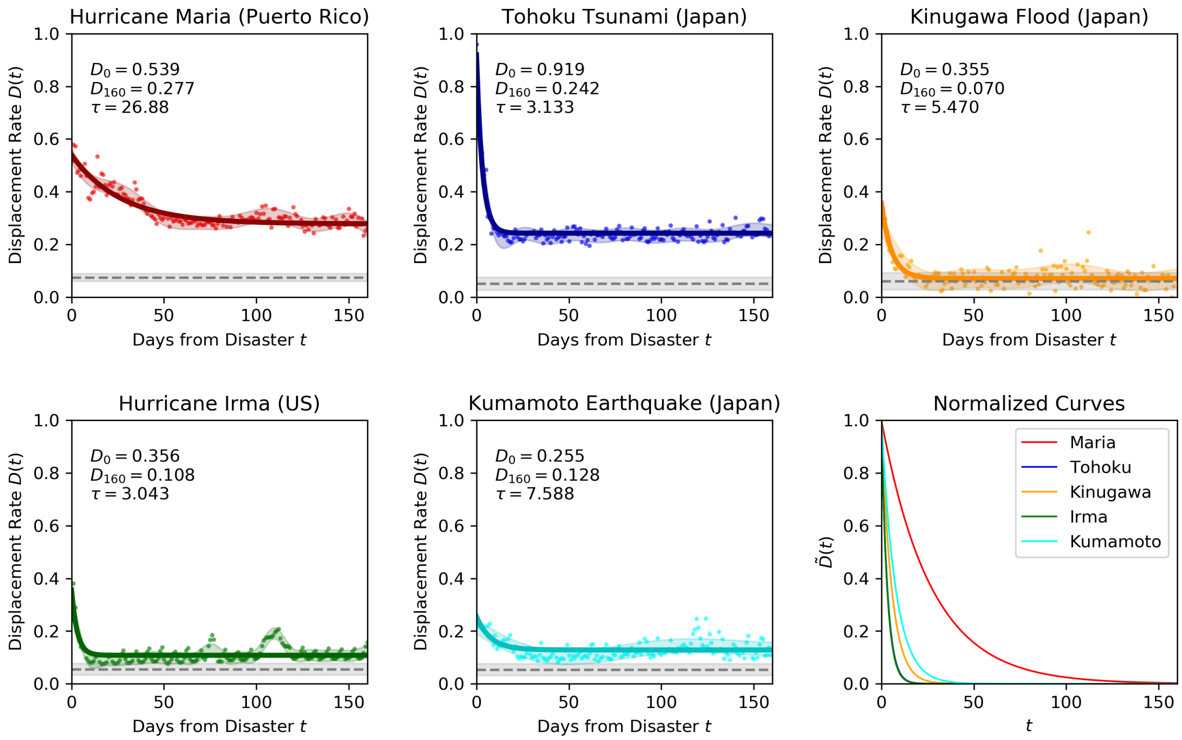

Figure 2.2. Macroscopic population recovery patterns after each disaster. Raw observations of displacement rates were fitted with a negative exponential function. D_0, D_{160} and τ denote the displacement rates on day 0, day 160, and recovery time parameter of each fitted negative exponential function. Black horizontal dashed line shows average displacement rates observed before the disaster.

home LGU out of all affected users on that day. To capture the short term fluctuations in the population recovery patterns, the raw observations of displacement rates were denoised using Gaussian Process Regression, which is a non-parametric probabilistic model for denoising and regression [228]. To capture the general trend of population recovery, the raw observations were fitted using a negative exponential function $D(t) = (D_{160} - D_0)\exp\left(-\frac{t}{\tau}\right) + D_{160}$, where D_0, D_{160}, and τ denote the displacement rates on day 0, day 160, and recovery time parameter, respectively. Further, the fitted negative exponential functions were normalized $\tilde{D}(t) = \frac{D(t)-D_{160}}{D_0-D_{160}} = e^{\frac{-t}{\tau}}$ to compare the speed of population recovery across different disasters.

Despite the differences in the disaster types and the heterogeneity in socio-economic characteristics among the affected regions, the recovery of displacement rates after the five disasters were all approximated well by a negative exponential function $D(t) = (D_0 - D_{160})\exp(-\frac{t}{\tau}) + D_{160}$, where D_0 and D_{160} denote the displacement rates on day 0 and day 160, respectively, and τ are the recovery time parameters. Figures 2.2 show the observed daily displacement rates, smoothed trend estimated using Gaussian Process Regression, and the fitted exponential functions for each disaster. Goodness of fit measures were computed to show that the exponential functional form fits the data well, and that the estimation of parameters are robust. The observations were cut off on day 160 due to data limitation. Minor anomalies observed in the recovery patterns were due to national holidays such as Christmas (around day 100 of Hurricane Maria and day 110 of Hurricane Irma), Thanksgiving Holidays (around day 80 of Hurricane Irma), and "Obon Breaks", which is a national holiday in Japan (around day 120 of Kumamoto Earthquake). The baseline (pre-disaster) displacement rates are shown in Figures 2.2 in horizontal gray dotted lines (mean) and the gray shaded region (standard deviation) to compare the post-disaster displacement rates with the "usual" displacement rates that are caused by activities such as travelling. In extreme disasters such as Hurricane Maria and Tohoku Tsunami, we observe a high long term displacement even after 150 days from the disaster. We can infer that this population segment could have migrated out of the disaster affected areas to other locations. Figure 2.2 shows the normalized displacement rate observations $\tilde{D}(t)$ for each disaster in colors, along with the negative exponential function ($\tilde{D}(t) = \mathrm{e}^{\frac{-t}{\tau}}$) shown in black. The closeness between the standard negative exponential function and the normalized population recovery patterns show that for all disasters, population recovery curves can be well approximated by a negative exponential function.

The negative exponential functional form of the population recovery patterns across the five disasters imply that the majority of users returned quickly within a couple of weeks from the disaster, but the rest of the users gradually returned over a longer time period. The exponential decay also indicates that for each day, a constant rate $\frac{1}{\tau}$ of the remaining displaced population decides to return to their original home location. This variance in recovery timings can be explained by observing the relationship between the temporal duration and spatial distance of individual displacement mobility patterns. Figure 2.3a shows that the average evacuation duration increases with evacuation distance. Figure 2.3b shows the probability density plots of the maximum distance traveled from his/her estimated home location on a usual day before the disaster (gray), on the day of the disaster (brown), 10 days after the disaster (red), and 1 month after the disaster (orange). More people stayed further away ($> 10^3$m) from their home locations after disasters compared to before the disaster due to evacuation activities. The distribution of evacuation distances is long tailed after all disasters at various time points, which indicates the majority of people evacuate short distances (thus short duration) and a small fraction evacuation extremely long distances (thus long duration). This explains why we observe the negative exponential function in population recovery patterns after all disasters. The recovery times after disasters that occurred in Japan and Florida were relatively short ($3 < \tau < 8$), but very long $\tau = 26.8$ after Hurricane Maria. The differences in recovery time parameter values τ across disasters can be explained by the differences in the speed of infrastructure recovery in each of the affected regions. In Japan and Florida, power was restored in over 90% of the households (that were not destroyed) within 10 days from the disaster, while it took more than 200 days for Puerto Rico.

Revealing the negative exponential function common across different disasters and locations could significantly contribute to the efforts in modeling and simulating human mobility patterns after disasters [114]. Further analysis using the individual evacuation mobility patterns showed that these patterns emerge because of the combined effect of long-tailed distributions in evacuation distances and positive correlation between evacuation distance and duration. The long tailed distributions of evacuation distance had been observed in previous studies using other datasets from Haiti [45] and Japan [159], however, the latter relationship had not been shown in previous studies.

2.2 Spatial Heterogeneity

We now downscale our analysis to LGUs (counties in the US, cities/wards in Japan) within each affected area to understand the spatial heterogeneity in population recovery patterns. Since only one a few number of LGUs (10) were affected by the Kinugawa Flood, with most of them (9) having little housing damage (less than 1% housing damage rates), the Kinugawa Flood was not included in the LGU-scale analysis. The LGU-scale analysis was performed on the four major disasters (Hurricanes Maria and Irma, Tohoku Tsunami, and Kumamoto Earthquake). In total, there are 200 LGUs with large diversity in socio-economic characteristics that were affected by

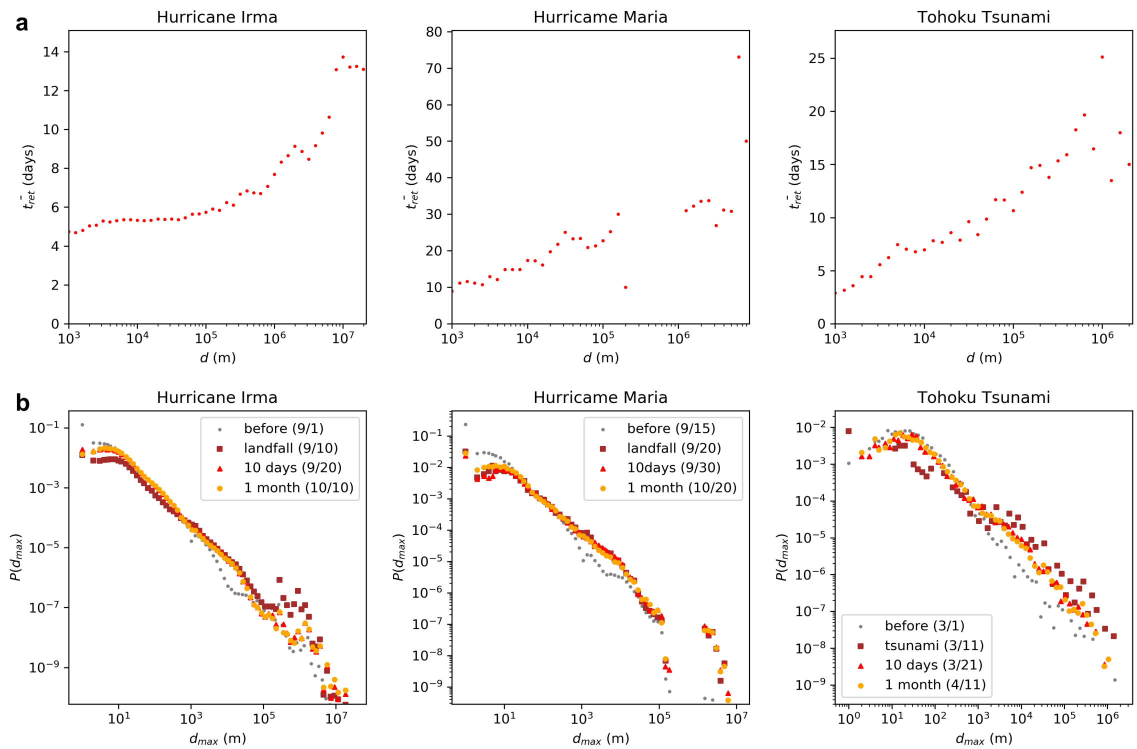

Figure 2.3. Relationship between displacement distance and duration after disasters. **a.** The longer the evacuation distance, the longer the average evacuation duration. **b.** Probability densities of maximum distance from home on a usual day (gray) and at various timings after the disaster day (brown: day of occurrence, red: 10 days after, orange: 1 month after) are all long-tailed. The long tailed distribution of evacuation distances and the relationship between displacement distance and duration were common across disasters. The majority of people evacuating short distances (thus short duration) and a small fraction of the people evacuating extremely long distances (thus long duration) explains why similar negative exponential functions were observed after the disasters.

the four disasters. The inset in Figure 3a shows the large heterogeneity in recovery patterns across LGUs, even within each disaster. Figure 2.4a shows moderate level of correlation ($R = 0.612$) between D_0 and D_{160} for all LGUs.

To understand the effect of the independent variables on the displacement rates and the speed of recovery, we apply a generalized linear regression modeling framework. Because the displacement rates are probabilities, $0 < D(t) < 1$ holds for any t. Therefore, we apply a logit link function to the displacement rates in the regression model. Similarly, because the recovery times take only positive values ($0 < \tau$), we apply a log link function to the speed parameter. Equations (3) and

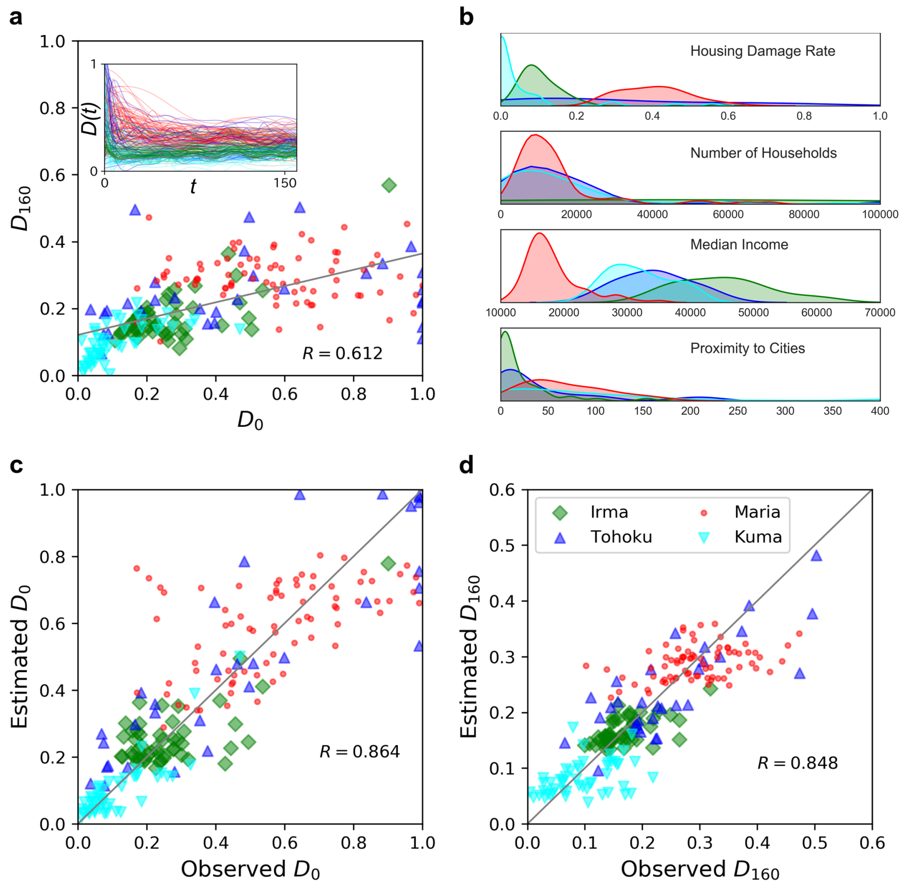

Figure 2.4. Explaining the spatial heterogeneity in population recovery using key common factors. **a.** D_0 and D_{160} of all LGUs. Each trajectory corresponds to an LGU, and colors represent the disaster. D_0 and D_{160} have a moderate correlation of $R = 0.612$. The inset shows the high spatial heterogeneity of recovery trajectories. **b.** Density plots of the four features of the affected LGUs, showing the heterogeneity in socio-economic characteristics. **c.** Observed and estimated D_0 for all LGUs in all disasters had high correlation $R = 0.864$. **d.** Observed and estimated D_{160} values had high correlation $R = 0.848$.

(4) show the generalized linear regression model where β are the regression coefficients, x are the independent variables explained in the next section, and $\varepsilon \sim \mathcal{N}(0, \sigma^2)$ is the error term. The model parameters are estimated via maximum likelihood estimation.

$$\log\left(\frac{D(t)}{1-D(t)}\right) = \beta^T x + \varepsilon \tag{2.1}$$

Table 2.2. Descriptions, variable transformations, and sources of socio-economic data

Variable	Description	Trans.	Data Source
Households	Number of households in LGU	log	Statistics Bureau (Japan) ACS* (USA)
Median income	Median household income in LGU	log	Statistics Bureau (Japan) ACS* (USA)
Housing damage	Rate of households damaged in LGU	-	Cabinet Office (Japan) FEMA (USA)
Proximity to large cities	$\frac{\sum_{\mathrm{j}\in S(\mathrm{i})} N_{\mathrm{j}}}{N_{\mathrm{i}}}$ N_{i}: households in LGU i $S(\mathrm{i})$: nearby cities from i	-	-
Proximity to wealthy cities	$\frac{\sum_{\mathrm{j}\in S(\mathrm{i})} (MI)_{\mathrm{j}}}{(MI)_{\mathrm{i}}}$ $(MI)_{\mathrm{i}}$: income in LGU i $S(\mathrm{i})$: nearby cities from i	-	-
Infrastructure recovery	Days until power recovery in LGU	-	Local government reports

*ACS: American Communty Survey

$$\log(\tau) = \beta^T x + \varepsilon \tag{2.2}$$

In the regression models of population recovery, socio-economic data (population, median income, housing damage rates, power outage recovery time, connectedness to surrounding cities) were used as independent variables (Table 2.2). In addition to housing damage rates which directly quantify the magnitude of the disaster effect on each LGU, socio-economic variables (population and income) of LGUs were included in the model to seek any inequality between the urban and rural, and the rich and poor on the disaster recovery performances. Infrastructure recovery (power outage duration) was included in the model to assess the importance of the local agency's capacity to respond to extreme events. Moreover, we test whether the geographical configurations and accessibility between LGUs are important for post disaster recovery, by including variables related to the proximity to large and wealthy cities. For Florida and Puerto Rico, population data were obtained from the US National Census (https://www.census.gov/), and median income data were obtained from the American Community Survey (https://www.census.gov/programs-surveys/acs). Similarly, for Japanese LGUs, population and income data were obtained from the Statistics Bureau (https://www.stat.go.jp/) of the Ministry of Internal Affairs and Communications of Japan. Power outage data of LGUs in Puerto Rico were collected from the website StatusPR (http://status.pr/), which is a government operated website that showed the recovery status of Puerto Rico after the Hurricane. Power outage data of Hurricane Irma were collected from the Florida Division of Disaster Management (https://www.floridadisaster.org/). Power outage information in the Japanese disasters were collected from the utility companies. The connectedness to surrounding cities were calculated by $d_p(\mathrm{i}) = \frac{\sum_{\mathrm{j} \in S(\mathrm{i})} N_\mathrm{j}}{N_\mathrm{i}}$, where N_i is the number of households in city i, and $S(\mathrm{i})$ is the set of cities that can be reached within 1 hour by vehicles from city i. d_p would be large for small cities that have large cities around it, and small for more isolated cities. For cities with similar population levels, d_p would be proportional to the total population of surrounding cities. Similarly, we propose the proximity to wealthy cities by using the median income value instead of the household number in the previous equation. This value would be large if the origin city has a relatively low income and it is surrounded by wealthier cities nearby. Note that these two complex variables capture not only the characteristics of the origin city, but that of the receptor cities. Correlations among variables in all disasters were not significantly high, thus we included them in the regression analysis. Power outage recovery time was excluded in the models for estimating D_0, since this information would not be available on day 0. The probability densities of the four attributes in each disaster are shown in Figure 2.4b. Housing damage rates and median income levels significantly differ across the four disasters, however the number of households and the connectedness of cities have more similar distributions. The set of independent variables for the best model for each disaster was chosen based on the lowest AIC value and statistical significance ($p < 0.1$). Figure 2.4c plots the observed values and estimated D_0. Although we use only key variables in our model, the estimated values had high correlation with observed values ($R = 0.864$). For LGUs in Japan (Tohoku Tsunami and Kumamoto Earthquake) and Florida (Hurricane Irma), housing damage rates were good estimators of D_0. On the other hand, housing damage rates had low and insignificant correlation with $\log\left(\frac{D_0}{1-D_0}\right)$ in Puerto Rico after Hurricane Maria. Rather, median income levels and number of households for each community had significant and stronger correlations with initial displacement rates. Median income and the proximity to wealthy cities had negative correlations with initial displacement rates, indicating that communities with lower incomes in isolated areas had higher initial displacement rates. Figure 2.4d shows that D_{160}

values were predicted by the five variables with high accuracy ($R = 0.848$). Median income and housing damage rates had positive effects on long term displacement, implying that people with more income were able to evacuate from the affected regions. In addition to such socio-economic variables, infrastructure recovery speed had a significant effect on long term displacement rates. Recovery speed $\log(\tau)$ had the lowest predictability out of all objective variables. The significant variables varied across different disasters, however, the connectedness to large cities and wealthy cities was a common variable with significant impact on recovery speed across three disasters. The negative coefficient implies that if a city is surrounded by larger or wealthier cities, it has a shorter time needed for recovery. To check the temporal robustness of these findings, we performed the regression analysis on various timepoints $(D_{10}, D_{20}, D_{30}, D_{60}, D_{90}, D_{120})$, and found that the set of important variables generally stay similar for all disasters across different timepoints. However, as time progresses, infrastructure recovery variables become more significant while the significance of housing damage rates gradually decrease.

Previous studies on individual case studies have noted the relationship between such variables and population recovery (reentry) decisions. For example, studies on Hurricanes Katrina and Rita show that the rate of disadvantaged populations (characterized by variables including household income), density of the built environment, and housing damage contribute to migration and displacement [229]. This work contributes to the literature in disaster resilience and population migration by testing the insights obtained from individual case studies with multiple disasters in different locations.

Figure 2.5 shows pairwise comparisons after Hurricane Maria and Tohoku Tsunami where a pair of similar LGUs with different levels of connectedness to neighboring cities have distinct recovery outcomes, even though other socio-economic characteristics such as population, housing damage rates and income levels are similar. This contradicts previous findings on non-disaster human mobility patterns (e.g. commuting), where out-migration increases with amount of opportunities available in surrounding cities [230]. This finding shows that after disasters, the existence of neighboring cities act as catalysts that enhance recovery rather than attractors that drain population from damaged cities. This extends the theories on the importance of social capital and social support [57], [113] to an intercity-scale. One example of such effect is how Tono City, an inland city close to the Tohoku area towns that were affected by the tsunami, acted as a recovery support

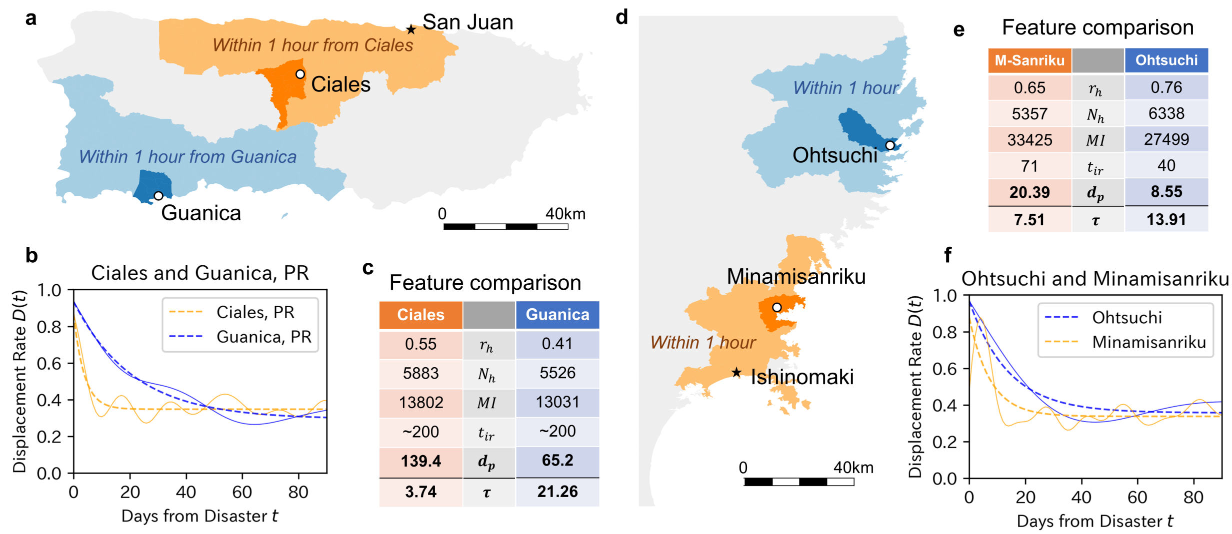

Figure 2.5. Connectedness to neighboring cities as a key factor to recovery. **a.** Map of Ciales and Guanica, Puerto Rico. Light colored areas show the area that can be reached from each city within one hour of driving time. **b.** Recovery patterns of both communities, showing the faster recovery of Ciales. **c.** Comparison of factors for both cities. Factors other than connectedness to other large cities (e.g. San Juan) were similar between the two communities. **d-f.** Similar phenomenon was seen after Tohoku Tsunami in Japan. Minamisanriku city and Ohtsuchi city shared similar characteristics except for the connectedness to large cities (e.g. Ishinomaki), resulting in differences in recovery patterns.

hub after the Tohoku Tsunami [231]. The coastal cities were provided humanitarian, informational, and material support from surrounding nearby cities such as Tono City which experienced less damage due to the tsunami/earthquake. The effect of inter-city connectivity on community recovery is understudied in the urban resilience literature, and could have significant implications on the planning of inter-city networks to enhance the resilience of communities.

2.3 Social and Physical Network Effects

In this section, we further investigate how inter-city dependencies in both physical as well as social forms contribute to the recovery of cities after disasters. We investigate this problem through a case study of the population recovery patterns of 78 Puerto Rican counties after Hurricane Maria. We analyze mobile phone location datasets, which include the GPS location data of more than 50,000 unique users from over 6 months before and after the Hurricane. Various metrics from the spatial networks literature are used to quantify the node-level characteristics of Puerto Rican counties on social and physical inter-city networks to understand the types of inter-city dependencies that play an important role for effective post-disaster recovery. We find that inter-city *social* connectivity, which is measured using pre-disaster mobility patterns, is crucial for quicker recovery after Hurricane Maria. More specifically, counties that had more influx and outflux of people prior to the hurricane were able to recover faster. Our findings highlight the importance of fostering the social connectivity between cities as well as strengthening the physical infrastructure, to prepare effectively for future disasters. This paper introduces a new perspective in the community resilience literature, where we take into account the inter-city dependencies in the recovery process rather than analyzing each community as independent entities.

2.3.1 Node-level Network Statistics

Distance Metrics for Edge Weights

To investigate the effect of various types of inter-city dependencies on post-disaster recovery, we construct multiple networks based on various edge weights between nodes (78 counties in Puerto Rico). Table 2.3 lists the 5 distance metrics that were used as edge weights to build the inter-city network $\mathscr{N}$ in this study. Given a distance metric x, we denote the network built using distance metric x as $\mathscr{N}_x$. The distance metrics (edge weights) are Euclidean distance e, travel time TT, road distance RD, mobility flow F, and the number of overnight stays S. Euclidean distance is an undirected metric, calculated by $\mathrm{e_{ij}} = \sqrt{(x_\mathrm{i} - x_\mathrm{j})^2 + (y_\mathrm{j} - y_\mathrm{j})^2}$ given center points of two counties $(x_\mathrm{i}, y_\mathrm{i})$ and $(x_\mathrm{j}, y_\mathrm{j})$. Travel time and road distance between counties i and j were calculated using `Google Maps API`[1] in the usual conditions (prior to the disaster). Although these metrics are almost symmetrical, there are differences in travel times and fastest routes depending on the direction of travel, thus would produce directed networks. The two social distance metrics are mobility flow F and the number of overnight stays S, which are both observed using mobile phone data from prior to the disaster. Mobility flow F_ij is defined as the inverse of the average number of travelers from node i to node j in the usual state (prior to disaster). The number of overnight stays

[1] ↑https://developers.google.com/maps/documentation/

Table 2.3. Distance metrics x that were used as edge weights to build inter-city network $\mathcal{N}_x$

Distance Metric x	**Notation**	**Directed?**	**Category**	**Description**
Euclidean distance	e_{ij}	Undirected	Physical	Euclidean distance between center of counties i and j
Travel time	TT_{ij}	Directed	Physical	Driving time from i to j in usual state (`GoogleMaps API`)
Road distance	RD_{ij}	Directed	Physical	Road distance on quickest route from i to j in usual state (`GoogleMaps API`)
Mobility flow	F_{ij}	Directed	Social	Inverse of the # of travelers from i to j in usual state (from mobile phones)
# of overnight stays	S_{ij}	Directed	Social	Inverse of the # of visitors from county i who stay overnight in county j in usual state (from mobile phones)

S_{ij} is similar to mobility flow, and is defined as the inverse of the average number of visitors from node i who stay overnight at node j in the usual state (prior to disaster).

Figure 2.6 visualizes the networks built using the 5 distance metrics. Node sizes are proportional to the pre-disaster population of each county prior to the disaster. All of these metrics can be defined for all origin-destination pairs, however for clarity of the figures, we only show the edges with the 500 highest edge weights. The weight of each edge is shown as the width of each edge. For the direct networks (**B-E**), sum of the weights on both directions are visualized. From visual inspection, we can see a large difference in the structure of networks built based on physical (**A-C**) and social metrics (**D,E**). In particular, in **D)** and **E)**, we can see that some cities on the coast have large direct weights between San Juan, which mean that despite the large physical distance, there are many people who travel and/or stay overnight between these cities.

Table 2.4 shows the element-wise Pearson correlation between edge weights based on different distance metrics. We can see that Euclidean distance $\mathcal{N}_{\mathrm{e}}$ has high correlations with road distance $\mathcal{N}_{RD}$ and travel times $\mathcal{N}_{TT}$, thus we exclude Euclidean distance from our analysis, and focus on networks constructed by the four remaining distance metrics.

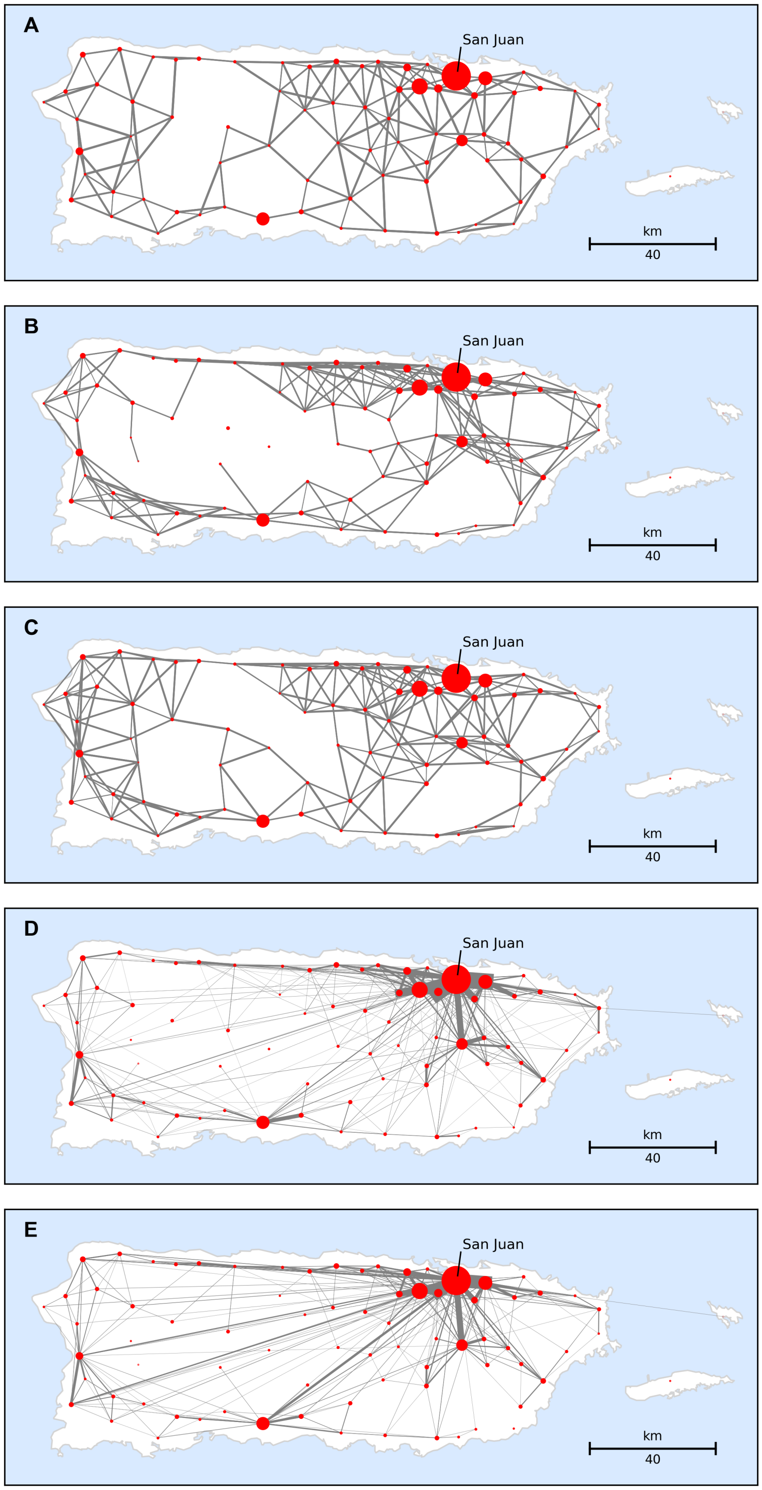

Figure 2.6. Visualization of distance weights of each network metric.

Table 2.4. Correlation between edge weights based on distance metrics $\mathscr{N}_x$

	$\mathscr{N}_{\mathrm{e}}$	$\mathscr{N}_{TT}$	$\mathscr{N}_{RD}$	$\mathscr{N}_F$	$\mathscr{N}_S$
($\mathscr{N}_{\mathrm{e}}$)	1.000	0.605	0.933	0.271	0.293
$\mathscr{N}_{TT}$		1.000	0.923	0.357	0.341
$\mathscr{N}_{RD}$			1.000	0.307	0.304
$\mathscr{N}_F$				1.000	0.509
$\mathscr{N}_S$					1.000

Network Statistics

Using the four different networks built from physical and social distance metrics defined above, we attempt to understand what type of network statistic on these networks can explain the time until recovery well in Puerto Rico. Identifying the most highly correlated network statistic and distance metric could provide insights into the underlying process that dictates the recovery of counties after disasters. In a similar manner as the distance metrics, we test various node-level statistics to compute the importance of each node in each network. Table 2.5 lists the node-level statistics that we will test on the four different networks $\mathscr{N}_x$. The six network statistics for node i in network $\mathscr{N}_x$ are: weighted in, out, and total degrees ($WI(\mathscr{N}_x)_{\mathrm{i}}$, $WO(\mathscr{N}_x)_{\mathrm{i}}$, and $W(\mathscr{N}_x)_{\mathrm{i}}$, respectively), weighted clustering coefficient $CC(\mathscr{N}_x)_{\mathrm{i}}$, direct distance from the source of recovery (San Juan in the case of Puerto Rico) $DSJ(\mathscr{N}_x)_{\mathrm{i}}$, and shortest path distance from the source of recovery $SPSJ(\mathscr{N}_x)_{\mathrm{i}}$.

Such network statistic measures were proposed in the literature of weighted directed and spatial networks to quantify the characteristics of each node [232]–[236]. Such metrics are applied in various domains to assess the importance of nodes in weighted networks, including urban networks [237], urban traffic networks [238], airport networks [239], and metabolic processes [240].

A weighted network $\mathscr{N}_x$ can be described with a $N \times N$ adjacency matrix W, where w_{ij} denotes the (i.j)-th element and the weight assigned to edge i to j. The weighted in, out, total degrees, weighted clustering coefficient, and weighted betweenness centrality of node i were calculated for each weighted network $\mathscr{N}_x$. The weighted in-degree of node i is calculated by $WI(\mathscr{N}_x)_{\mathrm{i}} = \sum_{\mathrm{j}\in\mathscr{V}(\mathrm{i})} w_{\mathrm{ji}}$, where $\mathscr{V}(\mathrm{i})$ is the set of nodes connected to node i. Similarly, the weighted out-degree of node i is calculated by $WO(\mathscr{N}_x)_{\mathrm{i}} = \sum_{\mathrm{j}\in\mathscr{V}(\mathrm{i})} w_{\mathrm{ij}}$. The weighted total degree of node i is the sum of in and out degrees $W(\mathscr{N}_x)_{\mathrm{i}} = WI(\mathscr{N}_x)_{\mathrm{i}} + WO(\mathscr{N}_x)_{\mathrm{i}}$. The weighted clustering coefficient

Table 2.5. Node-level statistics of node i given inter-city network $\mathcal{N}_x$

Network statistic	**Notation**	**Description**
Weighted in-degree	$WI(\mathcal{N}_x)_\mathrm{i}$	Total weighted in-degree of i on $\mathcal{N}_x$
Weighted out-degree	$WO(\mathcal{N}_x)_\mathrm{i}$	Total weighted out-degree of i on $\mathcal{N}_x$
Weighted total degree	$W(\mathcal{N}_x)_\mathrm{i}$	Total weighted degree of i on $\mathcal{N}_x$
Weighted clustering coefficient	$CC(\mathcal{N}_x)_\mathrm{i}$	Weighted clustering coefficient of i on $\mathcal{N}_x$
Direct distance from San Juan	$DSJ(\mathcal{N}_x)_\mathrm{i}$	Direct distance to i from San Juan on $\mathcal{N}_x$
Shortest path distance from San Juan	$SPSJ(\mathcal{N}_x)_\mathrm{i}$	Distance of shortest path to i from San Juan on $\mathcal{N}_x$

measures the statistical level of cohesiveness around node i. In general, this value decays with respect to degrees, shown in both airplane network and authors network [234]. This is because low degree nodes are connected to highly connected communities, while large degree nodes are connected to many nodes that are not directly connected. It is computed by $CC(\mathcal{N}_x)_\mathrm{i} = \frac{(\hat{W}+\hat{W}^T)^3_{\mathrm{ii}}}{2T^D_\mathrm{i}}$, where $\hat{W} = \{w_{\mathrm{ij}}^{\frac{1}{3}}\}$ and $T^D_\mathrm{i} = d^{tot}_\mathrm{i}(d^{tot}_\mathrm{i} - 1) - 2d^{\leftrightarrow}_\mathrm{i}$, $d^{\leftrightarrow}_\mathrm{i} = W^2_{\mathrm{ii}}$. The direct distance from San Juan of node i is the simply the distance metric between node i and San Juan. San Juan is chosen as the destination because it was the major source of recovery after Hurricane Maria in Puerto Rico. Similarly, we also measure the shortest path distance from San Juan on network $\mathcal{N}_x$.

Thus, in summary, we construct networks based on four different distance metrics, and define six node-level statistics for each defined network. This gives us 24 different network metrics that each quantify the physical and/or social characteristics of each node from different aspects. In the next section, we test whether these network metrics can explain the variance in recovery speed across counties in Puerto Rico after Hurricane Maria.

2.3.2 Spatial Regression Models

First, ordinary least squares (OLS) method is used to estimate the parameters of the general regression model specified below.

$$\boldsymbol{y} = \boldsymbol{x}\boldsymbol{\beta} + \varepsilon \tag{2.3}$$

where, $\boldsymbol{y}$ is an $n \times 1$ vector representing the objective variable (recovery time), $\boldsymbol{x}$ is an $n \times k$ matrix of the independent variables, and $\boldsymbol{\beta}$ is a $k \times 1$ vector of the coefficients. Here, the error term $\boldsymbol{\varepsilon}$ is assumed to be an i.i.d. normal. When there is spatial dependence in the error term, the i.i.d. normal assumption is violated. Two approaches are taken to deal with spatial correlation [241]. First is the spatial lag model, where the error term is decomposed into a spatially lagged term for the dependent variable and an independent error term, $\varepsilon = \rho W y + \mathrm{e}$, where W is the matrix that reflects the spatial proximity between areas which is commonly defined by encoding the k-nearest neighbors. This gives us the spatial lag model, described by the following equation:

$$\boldsymbol{y} = \rho \boldsymbol{W}\boldsymbol{y} + \boldsymbol{x}\boldsymbol{\beta} + \varepsilon \tag{2.4}$$

where $\varepsilon \sim N(0, \sigma^2 I)$. The parameters can be estimated using maximum likelihood estimation.

The other approach is to assume that the error is spatially correlated, instead of the objective variables affecting the objective variables of neighboring areas. We can write the spatial error model as follows:

$$\boldsymbol{y} = \boldsymbol{x}\boldsymbol{\beta} + \lambda \boldsymbol{W}\boldsymbol{\xi} + \varepsilon \tag{2.5}$$

where $\varepsilon \sim N(0, \sigma^2 I)$. In the following regression analysis, we first test the general regression model and also test for significance in spatial lag ρ and spatial error λ terms. Then, we apply the appropriate spatial regression analysis accordingly.

Estimation Results

Table 2.6 shows the statistics of the independent and objective variables. In the regression models, recovery time T_{i} is set as the objective variable. The variables in the second block (county population, median income, and housing damage rate) and one variable from the third block (net-

Table 2.6. Statistics of independent and objective variables

Variable	Min.	Max.	Med.	Mean	Std. Dev.	Corr. with T_i
Recovery time T_i (days)	1	243	74	80.2	58.2	–
County population	1,818	395,326	34,154	46,862	53,884	-0.476***
Median income ($)	11528	35074	17054.5	18152	4466	-0.489***
Housing damage rate	0.138	0.657	0.339	0.349	0.119	0.384***
$WI(\mathcal{N}_{TD})$	0	1.0	0.183	0.232	0.197	0.054
$WI(\mathcal{N}_{TT})$	0	1.0	0.585	0.581	0.152	0.105
$WI(\mathcal{N}_{F})$	0	1.0	0.356	0.386	0.208	-0.55***
$WI(\mathcal{N}_{S})$	0	1.0	0.396	0.404	0.201	-0.43***
$WO(\mathcal{N}_{TD})$	0	1.0	0.184	0.232	0.198	0.054
$WO(\mathcal{N}_{TT})$	0	1.0	0.578	0.580	0.151	0.084
$WO(\mathcal{N}_{F})$	0	1.0	0.310	0.352	0.205	-0.564***
$WO(\mathcal{N}_{S})$	0	1.0	0.341	0.350	0.204	-0.498***
$W(\mathcal{N}_{TD})$	0	1.0	0.184	0.232	0.198	0.054
$W(\mathcal{N}_{TT})$	0	1.0	0.582	0.580	0.151	0.094
$W(\mathcal{N}_{F})$	0	1.0	0.349	0.400	0.217	-0.602***
$W(\mathcal{N}_{S})$	0	1.0	0.359	0.382	0.220	-0.511***
$CC(\mathcal{N}_{TD})$	0	1.0	0.182	0.221	0.185	0.098
$CC(\mathcal{N}_{TT})$	0	1.0	0.832	0.811	0.151	0.011
$CC(\mathcal{N}_{F})$	0	1.0	0.361	0.373	0.150	0.533***
$CC(\mathcal{N}_{S})$	0	1.0	0.509	0.509	0.176	0.570***
$DSJ(\mathcal{N}_{TD})$	0	1.0	0.367	0.451	0.279	0.092
$DSJ(\mathcal{N}_{TT})$	0	1.0	0.431	0.487	0.272	0.187*
$DSJ(\mathcal{N}_{F})$	0	1.0	0.084	0.185	0.243	0.282**
$DSJ(\mathcal{N}_{S})$	0	1.0	0.185	0.288	0.263	0.397***
$SPSJ(\mathcal{N}_{TD})$	0	1.0	0.036	0.064	0.154	0.198*
$SPSJ(\mathcal{N}_{TT})$	0	1.0	0.367	0.451	0.279	0.092
$SPSJ(\mathcal{N}_{F})$	0	1.0	0.117	0.143	0.144	0.326***
$SPSJ(\mathcal{N}_{S})$	0	1.0	0.173	0.205	0.179	0.482***

work statistics) are used as independent variables for each of the regression models. The network statistic variables are normalized by the following equation:

$$\hat{x} = \frac{x - \min(x)}{\max(x) - \min(x)} \tag{2.6}$$

where $\max(x)$ and $\min(x)$ are maximum and minimum values of variable x.

The Pearson correlations between recovery time and each independent variable are shown in the right column of Table 2.6. We observe that all socio-demographic variables (county population, median income, and housing damage rate) have moderate correlations with recovery time, as shown in past studies [242]. Among the network statistic variables, all of the node-level statistics of the mobility flow based network and overnight stay network had significant correlations with recovery time, indicating the significant effect of inter-city social connectivity on post-disaster recovery. In contrast to social connectivity, node-level statistics computed from physical networks were less significantly correlated with recovery time in Puerto Rico. To examine the collinearity effect of these network statistics, we test the regression models using each node-level network statistics. Figure 2.7 shows the Akaike Information Criterion (AIC) and adjusted R^2 of each regression model. We observe that the regression model using the weighted total degree of the mobility flow network ($W(\mathcal{N}_F)$) has the lowest AIC and adjusted R^2 value. Table 2.7 shows the detailed regression results of the two regression models with and without the $W(\mathcal{N}_F)$ variable. The estimated regression coefficients and their significance levels are shown in stars. Using the network statistic, both the AIC and adjusted R^2 improve significantly, and we observe that the population variable becomes insignificant when considering the inter-city network variable. Moreover, the results show that the network metric variable negatively affects recovery time, meaning that the more the influx and outflux mobility flow before the disaster, the quicker the recovery.

The spatial dependence of recovery time is tested using various metrics in Table 2.8. All metrics including the Moran's I, the lag Lagrange multiplier ρ, and the error Lagrange multiplier λ are significant, showing significant spatial dependence. Robust tests of both Lagrange multipliers show that the error Lagrange multiplier λ is more significant. Thus, we test the Spatial Error Model and compare the results with the OLS Model in Table 2.9. Results show that the AIC is lower in the Spatial Error Model, indicating that spatial dependence in the error term explains the heterogeneity in recovery time across the counties in Puerto Rico. In both models, income levels and the network metric ($W(\mathcal{N}_F)$) have significant effects on the recovery time. Housing damage rates, however, become insignificant under the spatial error model.

Our analyses based on observational data from Puerto Rico after Hurricane Maria confirmed that inter-city network metrics, namely the pre-disaster mobility flow, has a significant positive influence on the speed of recovery. The results imply that the more socially connected an area is

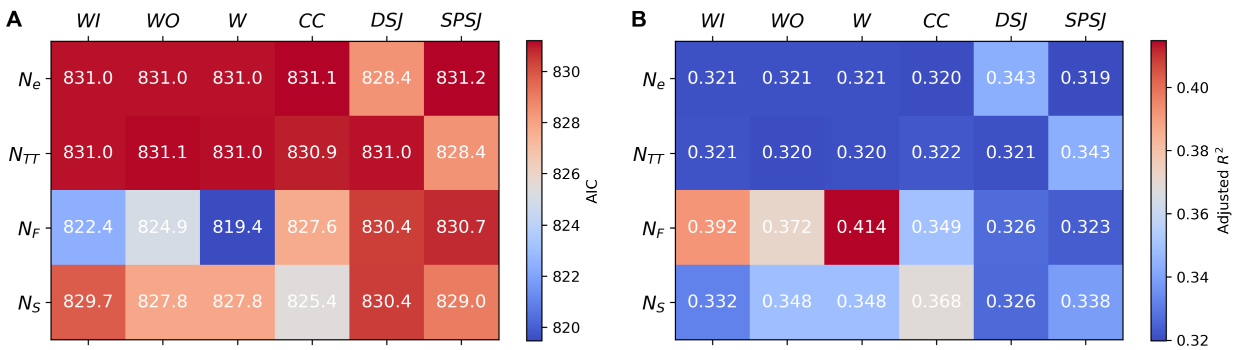

Figure 2.7. (A) AIC and (B) adjusted R^2 of ordinary least squared regression models using different node level network statistics.

Table 2.7. Ordinary Least Squares Regression Results with $W(\mathscr{N}_F)$ as network metric

	Socio-demographic Only	Socio-demographic + Network Metric
Constant	297.21***	22.48
ln(Population)	-19.18**	10.54
Income	-4.06***	-2.78**
Housing Damage	140.6**	140.1**
Network Metric	–	-145.5***
Adjusted R^2	0.329	0.416
AIC	829.21	819.48

*** $p < 0.01$, ** $p < 0.05$

Table 2.8. Spatial dependence tests

Moran's I	7.433***
Lag Multiplier ρ	24.82***
Error Multiplier λ	31.60***
Robust Lag Multiplier ρ	0.747
Robust Error Multiplier λ	7.53***

*** $p < 0.01$

to other counties, the more easier it is for people living in those communities to receive support and to recovery quickly. This paper introduces a new perspective in the community resilience literature, where we take into account the inter-city dependencies in the recovery process rather than analyzing each community as independent entities. These insights encourage communities to prepare for future hazards by not only preparing its physical infrastructure (e.g. roads), but also

Table 2.9. Regression Results of Spatial Error Model

	Non-Spatial	Spatial Error Model
Constant	22.48	78.40
ln(Population)	10.54	12.31
Income	-2.78**	-3.17**
Housing Damage	140.1**	10.86
Network Metric	-145.5***	-155.49***
λ	–	0.78***
AIC	819.48	796.84

*** $p < 0.01$, ** $p < 0.05$

by strengthening their social connectivity with other cities, to have greater chances of receiving support in case of emergencies.

Now, we discuss future research opportunities that this study enables. First, Puerto Rico is a unique case study because of its island geography. It is valuable to examine whether the same rules apply to other regions with different geographical characteristics. We will start collecting additional data from other disaster events to test the generalizability of our method between different disaster events. The Haiti Earthquake is an example where a large disaster struck a low-income island region. Another example where we observe severe damage is the Tohoku Tsunami (Japan) in 2011, where the coastal cities of the east coast of the Tohoku region are still struggling to recovery from the disaster. Comparing the analysis presented in this study across different disaster instances would be an interesting topic for future research.

Second, modeling the underlying process of recovery was not in the scope of this study. This work was limited to testing the statistical significance of network metrics using econometric models. To better understand, predict and control the recovery of communities after disasters, there is a need to model the underlying process that dictates the population recovery. Developing agent based models and system dynamics models for predicting community recovery based on the insights obtained from this study will be the next steps in our research.

Thirdly, the reliability of the results in this study could improve if we could increase the diversity of datasets to quantify the social connectivity between counties. One candidate would be Twitter data, where we can use text-mining to determine counties that have frequent contacts via messaging or retweeting. Also, call records of mobile phones would be a good data source to quantify social connections between two counties. In Puerto Rico, social connectivity measured by the mobility of people was shown to explain recovery times. It would be valuable to investigate whether the social measures used in this study would apply to other regions with different social norms, such as Japan or mainland US. Using more datasets to investigate such questions on the inter-city dependencies in the recovery process would be the focus of future studies.

Finally, the analysis presented in this chapter were conducted on community level (e.g., counties, census tracts, census blocks) aggregation to obtain recovery insights that can be used for regional policy making. However, mobile phone location data has significant potential in revealing how individuals behave and react to disaster events. More specifically, we are able to understand the types and sequences of points-of-interests that each individual visits after disasters while evacuating and returning to their original communities. This avenue of research opens up a wide array of research questions on the detailed movement patterns of individuals after disasters (e.g., whether they frequently check back to their damaged homes before permanent return) and their socio-demographic and -economic determinants.

Using large scale mobile phone data collected from Puerto Rico, we revealed the importance of inter-city social connectivity on disaster recovery after Hurricane Maria. More specifically, we showed that observing the mobility patterns between counties prior to the disaster can increase the predictability of time until recovery of communities. These insights highlight the importance of communities and policy makers to invest more into developing the social networks across counties or nearby cities through the interaction of people prior to the disaster to prepare for future disasters, as well as investing into the physical infrastructure networks. In the next section, we further downscale the analysis to investigate the inequalities that exist within communities, businesses, and regions, during disaster recovery.

3. INTRA-REGIONAL INEQUALITY

Among the various dimensions of disaster management, social equity [243] is understood to be an important concept that needs to be addressed for effective disaster relief and recovery [244]. Social equity during a disaster is defined as the state where all affected people are given equal access to resources and opportunities that enable them to meet their needs for safe evacuation and recovery [245]. In the context of social equity in disaster evacuation and reentry, it is essential to quantify and understand the effects of inequality that exist between socio-economic groups using observations from past disasters. More specifically, quantifying how the evacuation rates and destination characteristics differ across different income groups is crucial for addressing policies that enhance social equity. Studies have used data from household surveys collected after disasters to understand the effect of household socio-economic characteristics on evacuation behavior [106]. Although findings differ across disasters, in general, past studies have used survey data collected after disasters to show that higher income households are able to evacuate more and further away compared to low income households [108]. Such effects of inequality on evacuation behavior could allow higher income households to evacuate to safer locations compared to lower income households, which would increase the social inequity across population groups after disasters, leading to depletion of social resilience of communities [246]. A quantitative understanding of the effects of socio-economic inequality on evacuation and reentry behavior are needed, however, such efforts have been hindered by the low spatio-temporal resolution and limited scale of data collected from household surveys.

3.1 Income Inequality in Post-Disaster Mobility

Social equity is an important concept in disaster management that addresses the fair treatment of all individuals in the face of disaster situations [245]. It is now understood that social equity plays an important role in the social resilience of communities after disasters [246]. [106] found that higher income households were able to evacuate with a higher rate after disasters, and [247] found that households with higher income were able to evacuate further distances after Hurricane Katrina. Moreover, income segregation and fractionalization are known to have negative impacts on the economic performance of cities and communities [248]. As a result, many efforts have been allocated to promote integration and diversity within communities. Recent studies have quantified income segregation in cities and communities on usual days, by combining large scale mobility data (e.g. mobile phone data) with income information obtained from economic census [249]. In the disaster context, studies have assessed the effect of natural hazards on the dynamics of income distributions [250], and a cross-comparative study on disasters across 73 countries for a period of 22 years showed that higher income inequality leads to more deaths due to disasters on the national scale [251]. To overcome the issues regarding social equity during evacuation after disasters, studies have focused on the evacuation of disadvantaged population groups such as older people [252]. Studies have been conducted in the transportation engineering domain to assess the effectiveness of carsharing [253], [254] and bus-based evacuation [255] as potential solutions to issues in social equity after disasters [256]. To assess the impact of such solutions for disaster social equity, a quantitative understanding of the effects of income inequality on evacuation and reentry behavior is needed.

While there are various socio-economic characteristics that affect social equity, we focus on the effects of income inequality in this study. In this study, we aim to overcome the aforementioned research gaps by answering the following research questions using large scale mobility data of affected individuals observed before, during, and after a severe disaster.

1. Do the dynamic patterns of evacuation and reentry rates differ across income groups? If so, by how much?
2. Do the effects of income inequality hold under various settings, including evacuation from inside and outside mandatory evacuation zones?
3. How do the effects of income inequality on evacuation behavior result in macroscopic spatial segregation of income groups over time after the disaster?
4. Are there differences in evacuation destination characteristics across income groups?

To answer these research questions, we analyze mobility data collected from more than 1.7 million mobile phone users in Florida affected by Hurricane Irma. The income level of each mobile phone user is estimated by spatially overlaying census-block level median income information obtained from national census with the estimated home locations of mobile phone users. The spatio-temporal movement trajectories of individual mobile phone users attributed with estimated income values are tracked over a 3 month period from the landfall of the hurricane.

3.1.1 Case Study of Miami-Dade after Hurricane Irma

Mobile Phone Location Data

Mobile phone location data used in this study were provided by Safegraph, a data company that aggregates anonymized location data from numerous applications in order to provide insights about physical places. To enhance privacy, SafeGraph excludes census block group information if fewer than five devices visited an establishment in a month from a given census block group. Each observation in the dataset contains the user ID, timestamp, longitude, latitude of mobile phones measured via the Global Positioning Satellite (GPS) system, with the agreement of individuals to provide their location data for research purposes. All user IDs were anonymized and other demographic information were not collected to protect the privacy of the users. In total, mobile phone data of 1,730,326 unique users who were observed in Florida at least once with in the period between 10 days before the landfall of Hurricane Irma (August 31st) and landfall (September 10th) were collected. The location data of these users were collected from 2 weeks before the landfall of Hurricane Irma, until 3 months after the landfall date. Each user was observed at high frequency with 97 observations on average per day, which is temporally granular enough to capture the date the users evacuated from their home locations, where they evacuated to, how long they were evacuated for, and where they stayed the night each day.

The mobile phone data contains several limitations. The first limitation is that the data does not include the exact demographic characteristics of the individual users. Such demographic characteristics include information such as age, gender, and occupation. This is a disadvantage compared to survey based data, however, we use mobile phone data for this study because of the advantages in the number of samples (over 1.7 million versus several hundreds), and also because such demographic data are not required for our objective of the study. The second limitation is the potential bias in the user samples. People who do not own mobile phones are more likely to have a lower income, which could skew the income distribution upwards. The third limitation is that we are not able to completely exclude the non-residents (e.g. tourists and transients) from the dataset. We

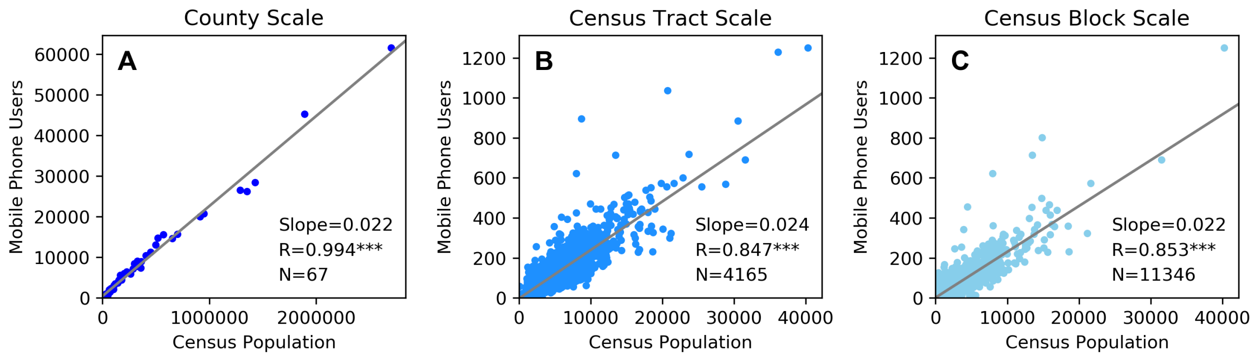

Figure 3.1. Comparison between census population and mobile phone users in (A) county scale, (B) census tract scale, and (C) census block scale.

find that the estimated number of mobile phone users in each census block agrees well with actual census population data (shown in Figure 3.1).

Hurricane Damage Data

Hurricane Irma made landfall on Florida on September 10th as a category 4 hurricane and traversed through the Florida peninsula, spawning storm surge and causing major inland flooding. Especially in the Florida Keys, 25 percent of the homes were destroyed and 65 percent were damaged. Many homes and businesses suffered damage or destruction, with more than 65,000 structures damaged to some degree in West Central and Southwest Florida alone. The hurricane caused more than 7.7 million homes and businesses to be out of power in the entire state of Florida, and at least 134 fatalities were confirmed [48]. The total economic losses caused by the hurricane is estimated to be $50 billion [257].

To understand the spatial distribution of hurricane damage, we use the housing damage rates in each zip code. The housing damage rate of a given zip code area refers to the rate of houses approved for the Individuals and Households Program of FEMA in each zip code. This dataset is publicly accessible from the FEMA website [224]. Figure 3.2A shows the housing damage rates in all zip codes in Florida. Out of all the counties, 6 of them experienced extensive damage, with housing damage rates of more than 10%. In particular, Miami-Dade County experienced the largest number of affected households (179,069), which was 25% of all of the affected households (Table 3.1). In addition to the housing damage rate data, we also used the power outage data

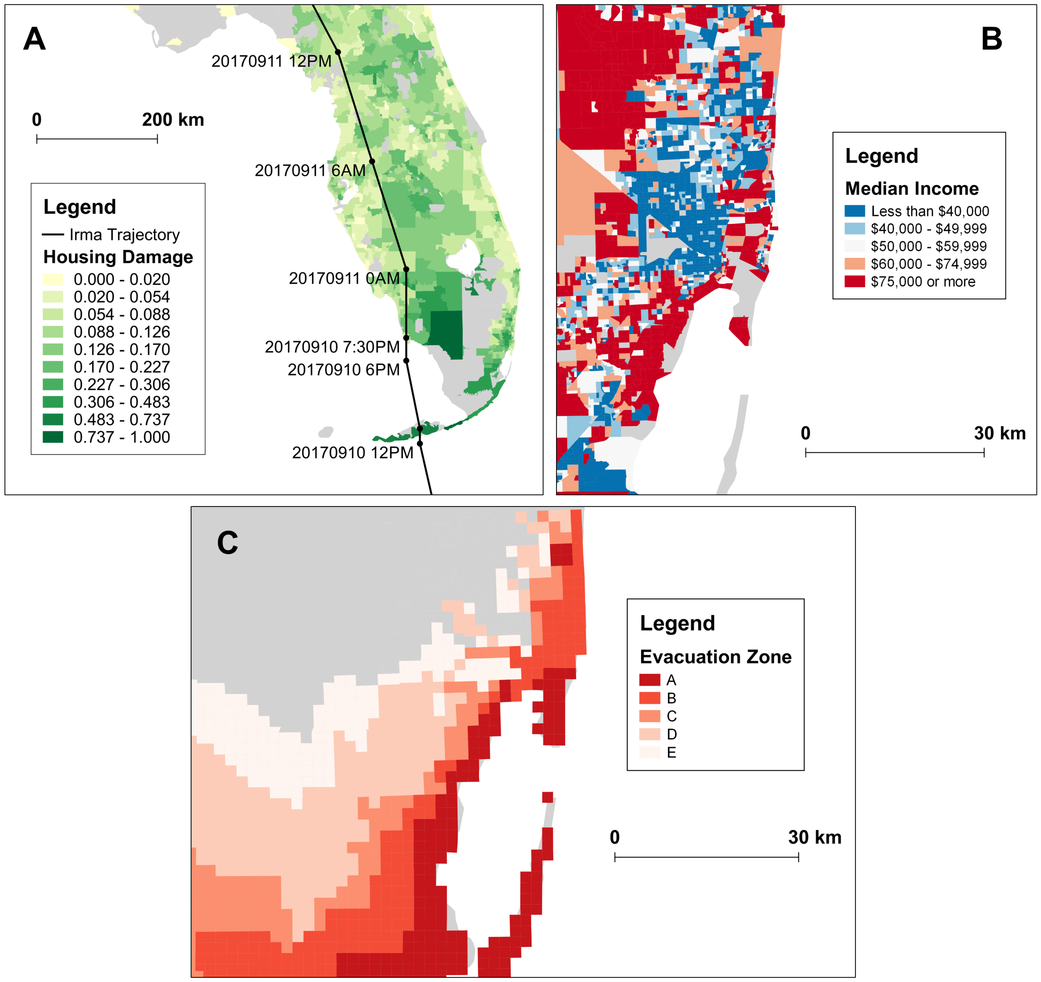

Figure 3.2. (A) Trajectory of Hurricane Irma and housing damage rates in each zip code. (B) Median income of all census blocks in Miami-Dade County. Miami-Dade County has the largest income inequality among all counties in Florida State. (C) Hurricane evacuation zones in Miami-Dade County.

provided by the Florida Division of Emergency Management. This data contains the percentage of power outages in each county every six hours between September 9th and 28th. The floodzone map of Miami-Dade County (Figure 3.2C) was obtained from the Open Data Hub of Miami-Dade County [258]. In Miami-Dade County, mandatory evacuation orders were issued to residents in evacuation zones A and a portion of B that covers barrier islands between Biscayne Bay and the ocean on September 6th at around 6AM, and were expanded to zones A, B, and C on September 7th at around 2:15PM.

Table 3.1. Miami-Dade county had largest hurricane damage and income inequality in Florida.

Rank in State	Households affected by Hurricane Irma			Income inequality	
	County	Number of Households	Percentage	County	Gini Index
1	**Miami-Dade**	179,069	25.0%	**Miami-Dade**	0.5256
2	Broward	86,811	12.1%	Lafayette	0.5248
3	Pinellas	44,603	6.2%	Collier	0.5237
4	Orange	43,685	6.1%	Martin	0.5219
5	Lee	39,423	5.5%	Palm Beach	0.5197
	(State Total)	715,679	100.0%	(State Average)	0.4858

Socio-Economic Data

Out of all the counties in Florida, Miami-Dade County has the largest Gini Index, meaning that the income inequality is highest among all counties (Table 3.1). The Gini index, or Gini coefficient, is a metric that quantifies the degree of inequality in a distribution [259]. Given a set of values x_{i} $(\mathrm{i}=1,\ldots,n)$, the Gini index G is calculated as:

$$G = \frac{\sum_{\mathrm{i}=1}^{n}\sum_{\mathrm{j}=1}^{n}|x_{\mathrm{i}} - x_{\mathrm{j}}|}{2n^2\bar{x}} \tag{3.1}$$

where $\bar{x} = \frac{1}{n}\sum_{\mathrm{i}=1}^{n} x_{\mathrm{i}}$. The Gini Index takes a value between 0 and 1, where 0 indicates perfect equality and 1 indicates maximal inequality where one individual owns all income and all others own nothing. Considering that Miami-Dade County also had the largest number of affected households due to Hurricane Irma (Table 3.1), we focus our analysis on the residents of Miami-Dade County in this study. Population data, median income data, and Gini Index data on the census block, census tract, and county level were all obtained from the American Community Survey [260]. Income ranges used commonly by the United States Census Bureau (less than \$40,000, \$40,000 to \$49,999, \$50,000 to \$59,999, \$60,000 to \$74,999, more than \$75,000) were used in the analysis [261]. To perform spatial analysis including geographical extraction and labeling, we used the Shapefile data of Florida provided by the National Census [262].

3.1.2 Effects of Income Inequality on Evacuation and Reentry

We first quantify the evacuation and reentry rates of Miami-Dade County residents on each day during the observation period. Figure 3.3 shows the net evacuation rates of the Miami-Dade County residents on each day before, during and after Hurricane Irma. The upper panel (A) shows the rate of evacuees who evacuated outside Miami-Dade County, and the lower panel (B) shows the rate of evacuees who went outside the State of Florida. The net evacuation rates of different income groups are shown in color in each panel. The Thanksgiving Holidays (around November 23rd to 26th) are highlighted as unusual periods. Several observations can be made from the analysis results. First, we observe a sharp increase in the net evacuation rates in both panels until September 10th, which is the date of hurricane landfall. The daily differences of the net evacuation rates show that most evacuation occurred on September 8th (+12.3% for all income groups aggregated together), which was a day after the evacuation orders were issued. We also observe a large portion of evacuation on September 10th, which was the day of the landfall (+9.0% for all income groups aggregated together). After September 10th, the evacuation rates gradually decrease and by around September 18th, the rates stabilize. Most evacuees returned and reentered Miami-Dade County on September 11th and 12th, shortly after the hurricane struck the peninsula. Second, we observe a significant difference in evacuation rates across income groups, where higher income population groups had higher evacuation rates, both in terms of out-of-county evacuation and out-of-state evacuation rates. This difference was verified to be statistically significant ($p < 0.01$) in most days (shaded in gray) using a Chi-Squared test. 38.6% of high income ($75,000 or more) residents were able to evacuate from Miami-Dade County, compared to 21.7% of low income residents ($40,000 or less). The differences between income groups are larger in out-of-state evacuation rates, indicating that higher income groups were more likely to travel further away from Miami-Dade when evacuating. Third, the evacuation rates stayed significantly larger than pre-disaster (August 31st to September 5th) levels for a long duration after the hurricane (around 10% for high income groups on November 15th). Similar to short term evacuation rates, the high income population groups had higher long term evacuation rates, indicating that these people were able to find places to stay for long durations outside Miami-Dade County. Fourth, we see weekly fluctuations in evacuation rates after the hurricane in both panels, where evacuation rates are higher on Fridays and Saturdays compared

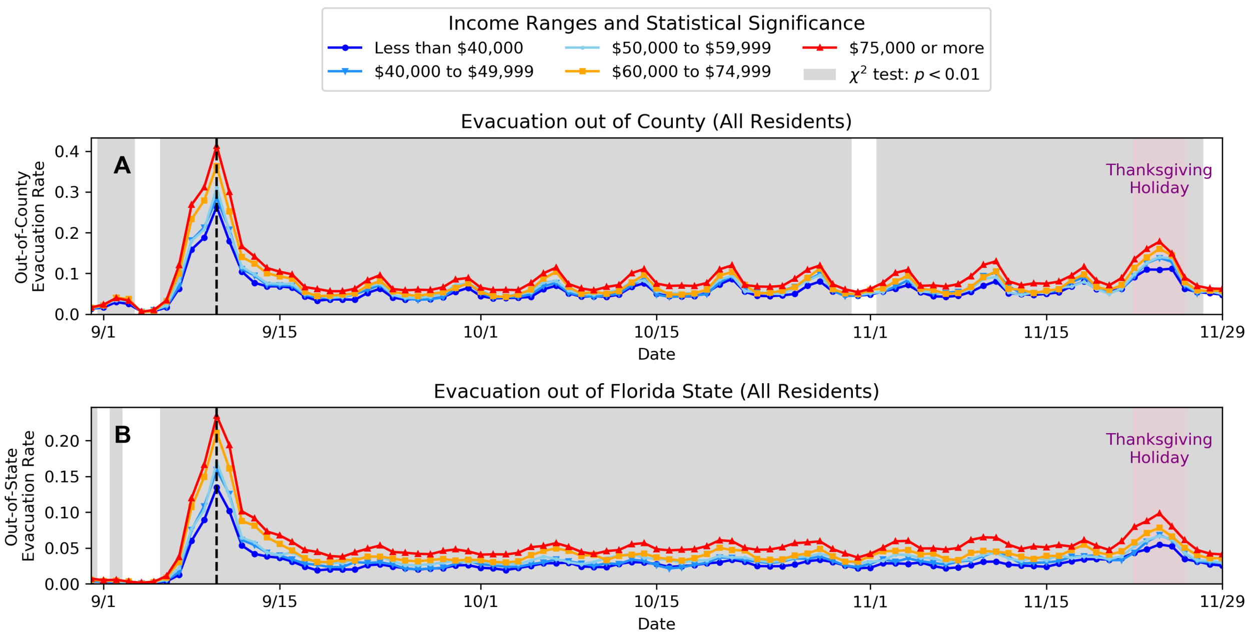

Figure 3.3. Out-of-county and out-of-state evacuation rates of Miami-Dade residents. Higher income residents were more likely to evacuate than low income residents, and were also able to stay away from the affected areas for a longer duration. Gray shades indicate days where differences in evacuation rates were statistically significant between income groups.

to weekdays. This pattern indicates that a fraction of the people traveled outside the county or state on weekends. This weekly increase in evacuation rates may be due to actual evacuation, or it may contain non-evacuation trips going outside of the county or state since we are not capable of identifying trip purposes from mobile phone trajectories, which is one limitation of our analysis.

The analysis presented in the previous section shows the rates of evacuation from all residential areas. In the following results (Figure 3.4, we group the mobile phone users into residents of areas inside the mandatory evacuation zones (zones A, B, C in Figure 3.2C), and residents outside the mandatory evacuation zones. Distinguishing between these two population groups is important from the viewpoint of disaster management officials, since they need to develop policies for future disasters based on how the residents in the designated flood zones complied with the evacuation orders, and also by how much of the residents outside those regions evacuated ("shadow evacuation") despite receiving no evacuation orders.

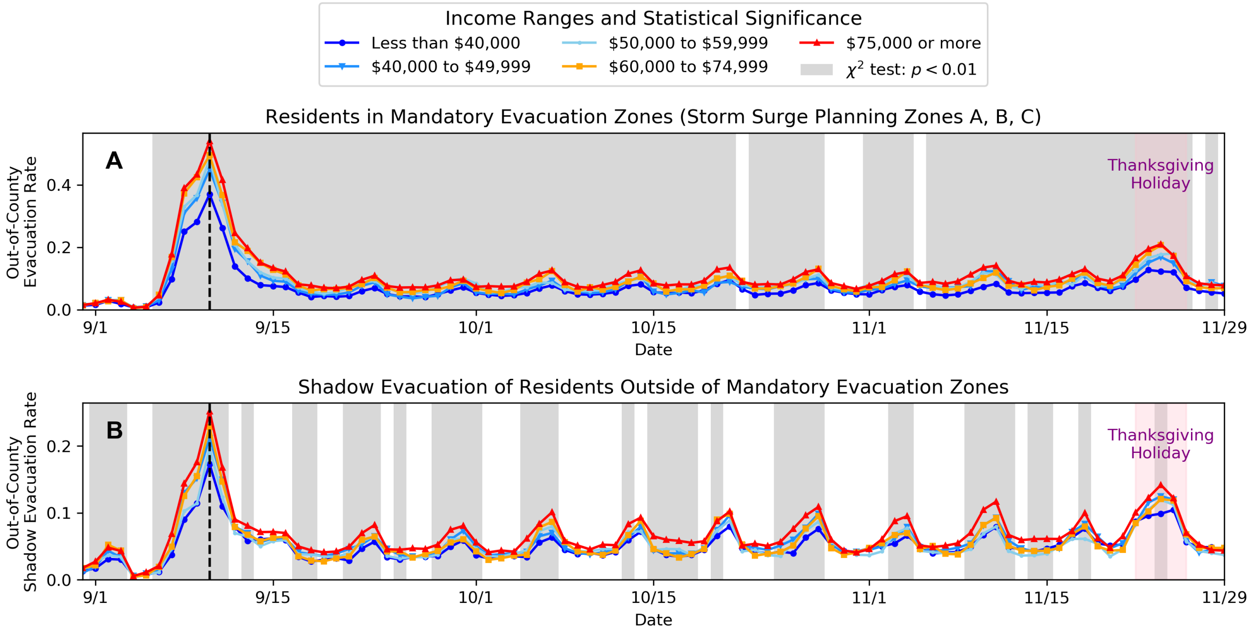

Figure 3.4. Out-of-county evacuation rates of residents (A) living inside mandatory evacuation zones (zones A, B, C), and (B) living outside mandatory zones (shadow evacuation rates), across different income groups.

Figure 3.4 shows the (A) out-of-county net evacuation rates of residents in the mandatory evacuation zones (zones A, B, C) and (B) shadow net evacuation rates for residents outside the mandatory zones. We observe that the peak evacuation rate from the mandatory zones (47.5%) was around double of the shadow evacuation rates (21.3%). The effects of income inequality in evacuation rates for both zone types were strikingly similar, where we observe significant differences in both short term and long term evacuation rates across income groups. This difference was also verified to be statistically significant ($p < 0.01$) in most of the days (shaded in gray) using a Chi-Squared test. During the reentry phase, effects of income inequality were larger inside mandatory evacuation zones, where for example on September 15th, the evacuation rates of high income residents were around double (13.3%) compared to low income residents (7.5%). On the other hand, reentry patterns were similar across income groups outside of the mandatory evacuation zones, with less days with statistical significant differences across income groups.

In addition to quantifying the effects of income inequality on evacuation and reentry rates and spatial segregation after the hurricane, we further analyze the characteristics of evacuation destinations across different income groups. The box plots in the two panels (each consisting of 4 sub-panels) in Figure 3.5 show the various characteristics of evacuation destinations of evacuees belonging to each of the 5 income groups (shown in blue to red colors). In each sub-panel, the horizontal line in each whisker plot shows the median value, and the white marker shows the mean value of each population group.

The left panel (Figure 3.5(a)) shows the results for September 10th, which is the day of the landfall. The top left sub-panel shows the the distributions of evacuation distances of the five population groups. In addition to Figures 3.3 and 3.4 where it was shown that people with higher income evacuate at a higher rate, it is shown here that people with higher income tend to evacuation longer distances. Since the mean distance is significantly greater than the median distance in low income groups, we can infer that the majority of the low-income evacuees traveled short distances (less than 10km). Similar to how we estimated the income of evacuees based on their residential census block, we estimated the income level of the destination area of each individual using census block level income data. The top right sub-panel shows that people with higher income were more likely to evacuate to locations of high income. Moreover, using the power outage data, the distributions of the power outage rate of the destination locations were estimated for each income group. The bottom left sub-panel shows that the high-income evacuees were able to reach areas with less power outage rates compared to low income evacuees. Similarly, the bottom right sub-panel shows that high income evacuees were able to reach locations with lower housing damage rates compared to low income evacuees. These latter two results which indicate that higher income residents were able to reach safer locations than lower income residents, highlight the inequity in evacuation destinations across income groups. To test the statistical significance of these differences, Kolmogorov-Smirnov tests (KS-tests) were performed on the neighboring pairs of data in each of the panels in Figure 3.5. The p-values of the KS-tests for the pair of data distributions of neighboring income groups are shown in the figures. For most neighboring pairs of income groups, the differences in the data distributions were significant with $p < 0.1$, often even with $p < 0.01$. The instances with no significant differences are observed mainly between the second group (\$40K$\sim$\$50K) and third group (\$50K$\sim$\$60K). However, in many of the income group pairs, significant differences in evacuation destination characteristics were observed. In summary, the more high income population groups were able to reach safer locations with less power outages and housing damages, whereas the lower income population groups had to stay in areas with

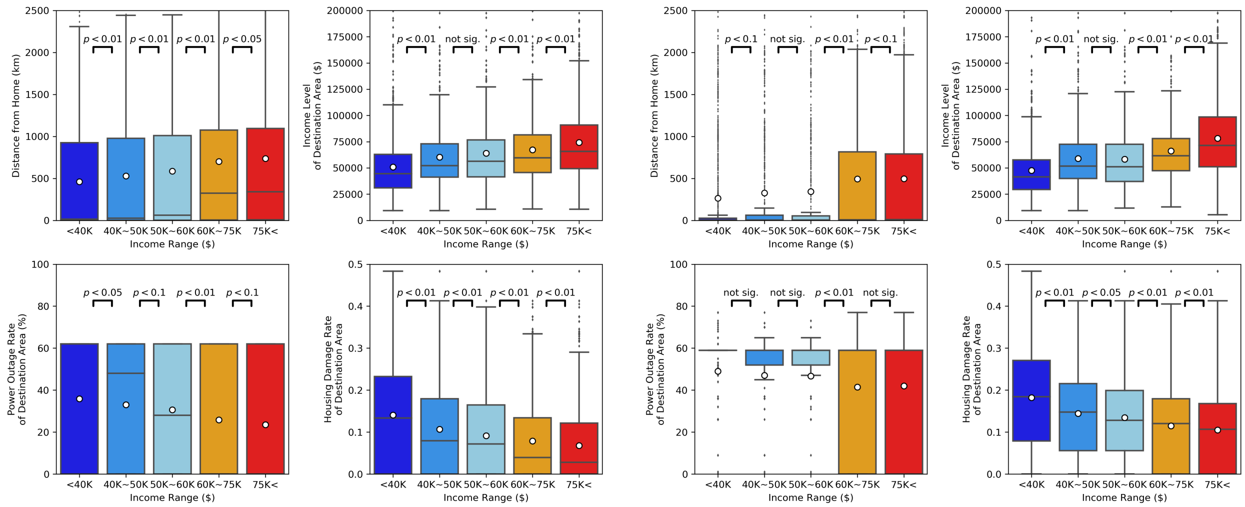

(a) Results for September 10th

(b) Results for September 12th

Figure 3.5. Evacuees with higher income levels were able to evacuate further, to locations of higher income, lower power outages, and less housing damages due to the hurricane compared to lower income evacuees.

more damage. These analyses were performed for all days after the hurricane, and these findings were found to be consistent over days after the hurricane until the end of September. Results for September 12th are shown in the right panel Figure 3.5(b).

3.1.3 Temporal Variation of Spatial Income Segregation

As a result of the effects of income inequality on evacuation and reentry mobility patterns, we observe high spatial income segregation between people who stayed inside Miami-Dade County and people who moved to outside Miami-Dade County after the disaster. Figure 3.6 shows the histograms of mobile phone users' income values for the two population groups: users who stayed inside Miami-Dade (gray color) and users who evacuated out of the county (green color), for each day between September 4th and 15th. Since previous studies have empirically shown that the income values of the majority (97% $\sim$ 99%) of the population are distributed log-normally [263], we fit the income values of the two groups with log normal distributions. The probability density function of the (2-parameter) log-normal distribution is

$$f(x) = \frac{1}{xs\sqrt{2\pi}} \exp\Big\{ -\frac{\big(\ln\big(\frac{x}{m}\big)\big)^2}{2s^2} \Big\} \tag{3.2}$$

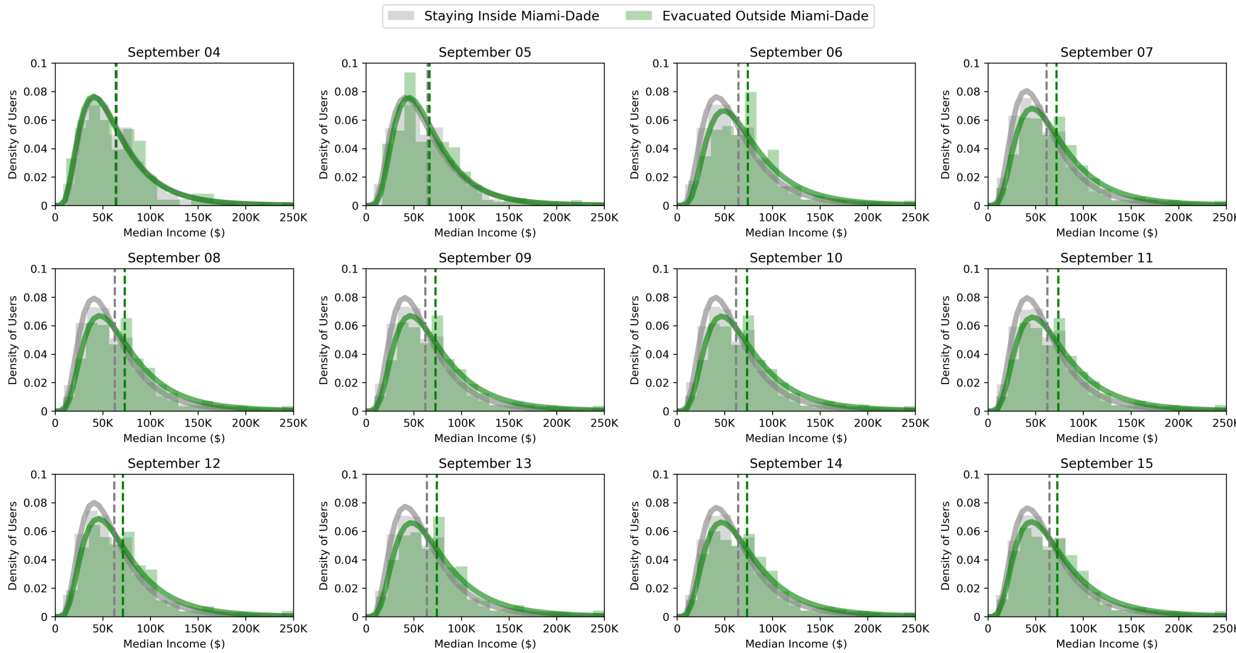

Figure 3.6. Income distributions and fitted lognormal density functions of residents staying inside Miami-Dade County (in gray) and residents who evacuated outside Miami-Dade (in green) for all days between September 4th and 15th. Vertical dotted lines show the mean income values of the two population groups.

where s is the shape parameter (and also is the standard deviation of the log of the distribution) and m is the scale parameter (which is also the median of the distribution). We may also have location parameter θ in the formulation, however this parameter does not appear in our formulation because we restrict this to $\theta = 0$. We assume that an income value of a resident who is *IN*side (or *OUT*side) Miami-Dade County on day t, which is denoted as x_t^{IN} (or x_t^{OUT}) comes from a lognormal distribution with parameters (s_t^{IN}, m_t^{IN}) (or (s_t^{OUT}, m_t^{OUT})). All parameters for both IN and OUT, for all days t, are estimated using maximum likelihood estimation:

$$\hat{m}_t^{IN} = \exp\left\{\hat{\mu}_t^{IN}\right\} \tag{3.3}$$

$$\hat{s}_t^{IN} = \sqrt{\frac{\sum_{\mathrm{i}=1}^{N}\left(\ln(x_t^{IN})_{\mathrm{i}} - \hat{\mu}_t^{IN}\right)^2}{N}} \tag{3.4}$$

$$\text{where,} \qquad \hat{\mu}_t^{IN} = \frac{\sum_{\mathrm{i}=1}^{N}\ln(x_t^{IN})_{\mathrm{i}}}{N} \tag{3.5}$$

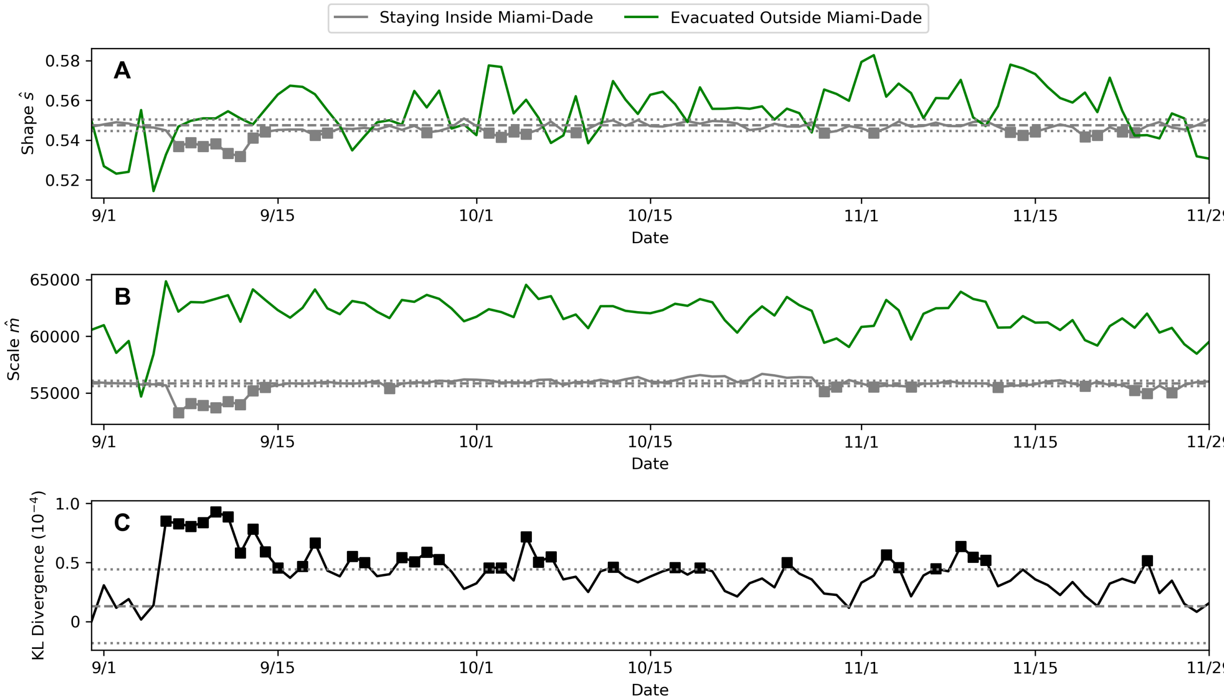

Figure 3.7. Quantifying spatial segregation after disasters. (A) Shape parameter and (B) scale parameter estimates of income distributions of the 2 population groups over time. (C) Kullback-Leibler Divergence between the income distributions of the two population groups over time.

The above equations are applied to estimate parameters for all days of observation t and for both user groups inside (IN) and outside (OUT) Miami-Dade County. Figure 3.6 shows the income distributions and fitted lognormal density functions of residents staying inside Miami-Dade County (in gray) and residents who evacuated outside Miami-Dade (in green) for all days between September 4th and 15th. Vertical dotted lines show the mean income values of the two population groups. We visually observe that the income distributions are very similar before the hurricane on September 4th and 5th. However, the the distributions of evacuated users diverge to the right, indicating that a larger fraction of the high income populations evacuated to outside the county, causing spatial income segregation.

The estimated parameter values of the lognormal distributions are shown in Figure 3.7A (shape parameter s_t) and 3.7B. In Figure 3.7A, the estimated $\hat{s}_t^{IN}$ and $\hat{s}_t^{OUT}$ are plotted in gray and green colors, respectively. The gray square scatter plots show the shape parameter values that are anomalous compared to usual values. Anomalies were detected using the 3-standard deviations rule.

More specifically, the horizontal dashed gray line is the mean value of $\hat{s}_t^{IN}$ before the evacuation starts ($t \leq 6$), which is calculated by $\mu_s^{IN} = \frac{1}{6}\sum_{t=1}^{6} \hat{s}_t^{IN}$. The standard deviation of $\hat{s}_t^{IN}$ before the evacuation starts ($t \leq 6$), can be calculated by $\sigma_s^{IN} = \sqrt{\frac{1}{6}\sum_{t=1}^{6}(\hat{s}_t^{IN} - \mu_s^{IN})^2}$. The dotted lines above and below the mean horizontal line are $\mu_s^{IN} + 3\sigma_s^{IN}$ and $\mu_s^{IN} - 3\sigma_s^{IN}$, respectively. Similarly, in Figure 3.7B, anomalous scale parameters were plotted with gray squares. We observe that in both panels A and B, the estimated parameters of the users inside Miami-Dade significantly (anomalously) decrease between September 7th and September 14th. Decrease in both of the parameters indicate that the income distribution shifts to the left (towards lower income), and that the distribution has less variance. On the other hand, both the shape and scale parameters of users who have evacuated outside of Miami-Dade County increase, indicating that the distribution shifts to the right and that the variance also increases. The shifts of the two distributions in sum indicate that the distributions are shifting away from each other, implying an increase in spatial income segregation.

Further, we quantify the magnitude of segregation by calculating the Kullback-Leibler Divergence (KL divergence) between the two income distribution functions. The KL divergence between 2 functions $P(x)$ and $Q(x)$ is formulated by the following equation:

$$D_{KL}(P||Q) = \int_{-\infty}^{\infty} P(x) \log\left\{\frac{Q(x)}{P(x)}\right\} dx \tag{3.6}$$

Figure 3.7C plots the daily KL divergence between the income distributions of the two population groups (inside and outside Miami-Dade County). Similar to the previous analyses, the dashed and 2 dotted horizontal lines mark the mean, mean plus 3 standard deviations, mean minus 3 standard deviations, respectively, of the KL divergence values before the evacuation started on September 7th. The black square plots show the anomalous values of KL divergence, indicating that spatial segregation is occurring with statistical significance ($p < 0.01$). We observe significant spatial segregation in most of the days in September, and over a long period of time after the landfall even during November (2 months after landfall). To summarize, the analysis presented in this section using mobility data and income information shows that spatial income segregation does occur after disasters due to the effects of income inequality in post-disaster mobility patterns, and that it persists for a long period of time after the hurricane landfall.

The presented results should be considered in the light of some limitations. For example, the income values of the individual mobile phone users were estimated by using the median income values of census blocks. This approximation neglects the variance that exists within census blocks and could cause the income inequality and segregation effects to shrink compared to the true effects. One method to overcome this issue would be to use a Monte Carlo approach where we stochastically draw income values of each user from the income distribution.

3.2 Region and Sector Inequality in Business Impacts

The ability of businesses to rebuild after disasters is a critical factor that significantly contributes to the economic recovery of cities. Previous studies have analyzed the post-disaster recovery of businesses through the means of surveys and interviews. Such studies have identified factors such as pre-disaster size of the business and category of business that partly explain the reopening and demise of businesses after disasters including Hurricanes Katrina [264], [265], Andrew [266], and more recently, Harvey [267]. Although these studies provide a general understanding of the effect of various characteristics of businesses that affect the post-disaster recovery performances, they suffer from two critical drawbacks. First, observations are limited to discrete measurements at a few number of timings, failing to give a quantifiable, continuous and longitudinal understanding of the recovery process of businesses. Second, the applied methods fail to model the causal effect of the disaster, which require a statistical framework that predicts the performances of businesses if the disaster did not occur.

With the emergence of novel and often large-scale data collected from mobile sensors and online social platforms, we are now capable of observing and analyzing the dynamics of people, goods, and information at an unprecedented spatio-temporal granularity [268]. In particular, location data collected from mobile phones (e.g. call detail records, GPS trajectories) have enabled us to observe individual mobility patterns at an unprecedented high spatio-temporal granularity [121], [124]. Despite such progress, none of the previous studies have used large scale mobility data to analyze the recovery of businesses after disasters. A recent study using mobile phone GPS data (same data used in this study) revealed the impact of the recent policy regarding the usage of bathrooms in Starbucks on the visit behavior of people to the cafe chain [269]. They validated that the spatio-temporal granularity of the mobile phone GPS data is of sufficient detail to analyze the store level visit behavior. In this study we apply a similar approach, and estimate the visit behavior of people to stores and businesses using mobile phone GPS data. Recent advances in statistical models, in particular Bayesian structural time series (BSTS) models, allow flexible predictions of time series data, which can be used to estimate the causal impact [270]. BSTS has several advantages over conventional difference in differences models [271], including its flexibility to model the causal impact over a longitudinal time horizon rather that across 2 time points. A recent study using website click-through data applied BSTS models to quantify the causal impact of an online advertisement [272]. We take advantage of this recently proposed methodology to quantify the causal impact of hurricanes on businesses in Puerto Rico.

This study makes several contributions to overcome the aforementioned drawbacks in the previous studies on business recovery after disasters. First, this is the first work to utilize large scale mobility data collected from mobile phones to estimate the popularity of businesses before, during and after a disaster. Second, a Bayesian structural time series model combined with an inter-city matching scheme is proposed to infer the causal impact of the disaster on businesses. Third, the proposed methodology is applied on mobile phone data collected from Puerto Rico to quantify the resilience of businesses after Hurricane Maria. Figure 3.8 illustrates the overview of the study. The causal inference procedure is composed of 3 steps. i) To measure the causal impact of the disaster on business i, we first identify a similar business j in another region which was not affected by the disaster. ii) We then predict the counterfactual (*"what-if the disaster did not occur?"*) visit count of i after the disaster timing using observed data from j, via a Bayesian structural time series model. iii) As a result, we can quantify the causal impact of the disaster by taking the difference between the predicted and observed visit counts in i.

Establishment-level visit data are provided by Safegraph[1], a data company that aggregates anonymized location data collected from smartphone applications to provide insights about physical places. Safegraph's location dataset covers around 10% of all smartphones in the United States, and each observation is consisted of a unique (but anonymized) user ID, longitude, latitude, and timestamp information. The longitude and latitude information are accurate to within a few meters, allowing us to analyze the visit counts to each establishment. To detect a user visiting an

[1]↑https://www.safegraph.com/

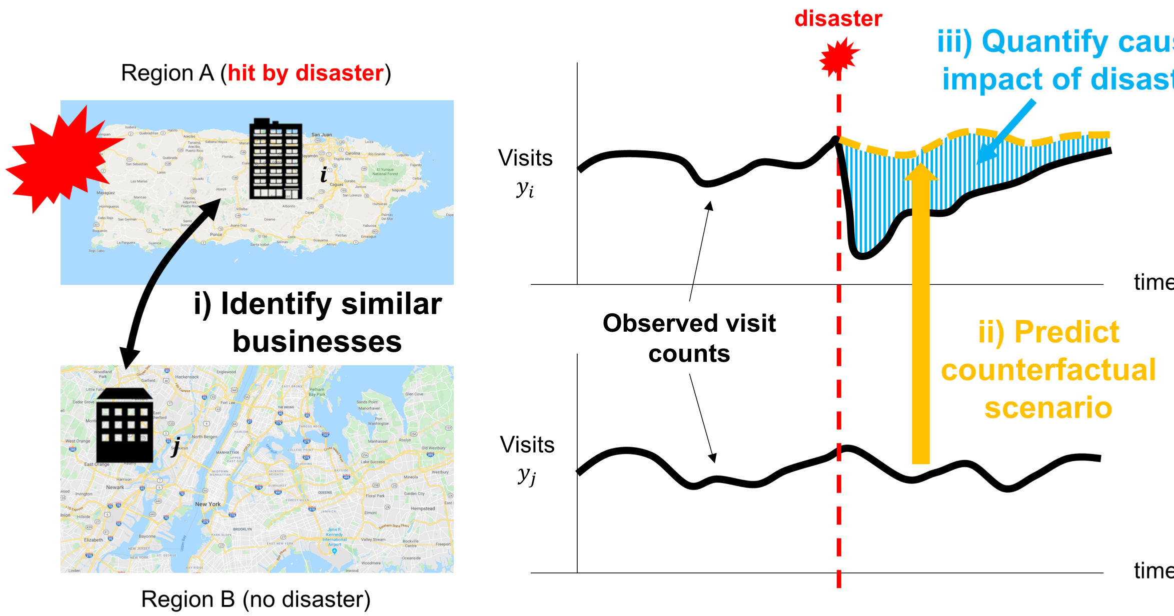

Figure 3.8. Our causal inference procedure is composed of 3 steps. i) To measure the causal impact of the disaster on business i, we first identify a similar business j in another region which was not affected by the disaster. ii) We then predict the counterfactual ("what-if the disaster did not occur?") visit count of i after the disaster timing using observed data from j. iii) We can quantify the causal impact of the disaster by taking the difference between the predicted and observed visit counts in i.

establishment, the location data are first cleaned by removing GPS signal drifts and jumpy observations using a spatial threshold, then clustered into a staypoint using a spatio-temporal DBSCAN algorithm. Then, the visited establishment is predicted from establishments nearby the clustered staypoint by using a machine learning algorithm that takes into account various features such as distances from establishment to the cluster centroid, time of day, and North American Industry Classification System (NAICS) code. Performing this procedure for all days in the dataset produces a time series data of daily visit counts for each establishment.

We use daily visit data of establishments located in Puerto Rico and the State of New York between January 2017 and March 2018 to quantify the causal impact of the hurricane on business resilience. Daily visit data of businesses in New York are used since these businesses constitute a reasonable control group which were not affected by the disruptions caused by Hurricane Maria.

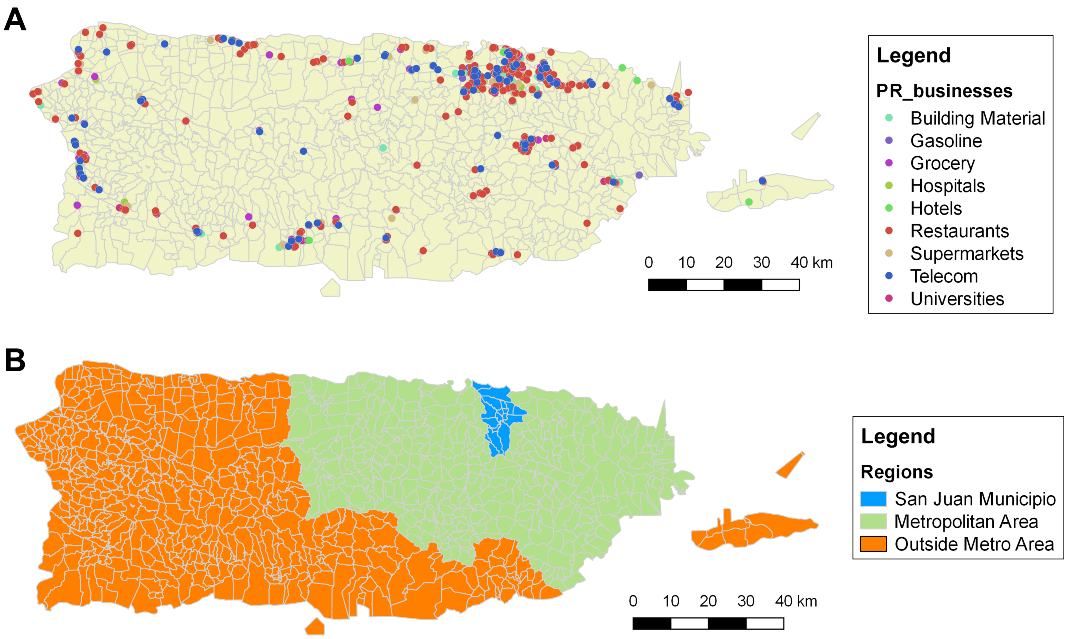

Figure 3.9. Characteristics of businesses in Puerto Rico. (A) Business locations and categories in Puerto Rico. (B) 3 regions of Puerto Rico used in this study.

How we use the visit data from the control group in the causal inference model is explained in the Methods section. We limit the analysis to business categories that sell products or services directly to the customers, since we will approximate business performances from the number of visits per day, observed from mobile phone data. We also limit the analysis to medium or large sized businesses with more than 100 customers per day on average (before the disaster), since we are not able to observe visit patterns below that level using mobile phone data.

Socio-economic data

In this study, population and income data of each county were used for later analysis. Population data were obtained from the US National Census[2], and median income data were obtained from the American Community Survey[3].

[2]↑https://www.census.gov/
[3]↑https://www.census.gov/programs-surveys/acs

Spatial distribution of housing damages due to Hurricane Maria

Physical damage caused by the hurricane are measured by the housing damage rates in each county, which was provided through the "Housing Assistance Data" provided by the Federal Emergency Management Agency (FEMA). The raw data can be found through the link[4]. We defined "housing damage rate" for each county as the total number of houses that were inspected to have had more than $ 10,000 worth of damage due to the target hurricane, divided by the number of households in that county. Many of the counties in Puerto Rico experienced high housing damage rates, between 20% and 60%.

3.2.1 Bayesian structural time series model

Compared with the classical DiD model [271], [273], a structural time series model promisingly relaxes the parallel trends assumption and captures the variations of time-varying local trends and seasonality for time-correlated response variables [270], [274]. In addition, structural time series models encompass a flexible model structure that enables us to analyze the dynamic effects of the outcome of interest during a time period [275]. Due to a large number of predictors in structural time series models, a Bayesian approach was introduced to sparse the estimation of coefficients. Scott and Varian [276], [277] proposed a spike-and-slab prior to the regression coefficients in a Google search query study, which significantly reduces the size of the problem. Nakajima and West [278] elicited a dynamic spike-and-slab prior that sparsified the estimation of time-varying parameters for a Bayesian macroeconomic time series model. The most recent Google study for causal inference of a market intervention [272] slightly revised the dynamic version of pike-and-slab prior [278] with a weakly informative prior. In addition, the Bayesian structural time series models (BSTS) have been constructed to strengthen causal inference for time series data (Figure 3.10). To address the fundamental problem in causal inference [279], pre-treatment observations are trained and tested via BSTS and consequently the fitted BSTS can simulate the counterfactual as the synthetic post-treatment controls via posterior predictive samples. This method is extensively applied in causal inference throughout various fields, such as socio-economics [280], [281], political science [282], [283], environmental studies [284], [285].

[4]↑https://www.fema.gov/media-library/assets/documents/34758

The basic structural time series model is defined as the following:

$$\begin{cases} y_{t,\mathrm{i}} = \mu_{t,\mathrm{i}} + \tau_{t,\mathrm{i}} + \beta x_{t,\mathrm{i}} + \varepsilon_{t,\mathrm{i}} \quad \forall t \\ \varepsilon_{t,\mathrm{i}} \sim \mathcal{N}(0, \sigma_y^2) \\ \sigma_y \sim Cauchy(0, 2.5) \end{cases} \tag{3.7}$$

where $y_{t,\mathrm{i}}$ is the observed daily visits to business i on day t in the target region (in our case, Puerto Rico). $y_{t,\mathrm{i}}t$ is predicted by state components $\mu_{t,\mathrm{i}}$, $\tau_{t,\mathrm{i}}$ and $\beta x_{t,\mathrm{i}}$ that capture critical features of the time-series data [272]. A weakly informative prior is elicited for each state component.

Local Level Trend: The local level model represents local variations of the time series data. To simplify the model structure, we assume the mean of the trend is a random walk with the initialization of μ_1:

$$\begin{cases} \mu_{t+1,\mathrm{i}} = \mu_{t,\mathrm{i}} + \eta_{1,t,\mathrm{i}} \quad \forall t > 1 \\ \mu_{1,\mathrm{i}} \sim \mathcal{N}(\mu_0, \sigma_0^2) \\ \eta_{1,t,\mathrm{i}} \sim \mathcal{N}(0, \sigma_\mu^2) \\ \sigma_0, \mu_0, \sigma_\mu \sim Cauchy(0, 2.5) \end{cases} \tag{3.8}$$

Seasonality: Let S denote the total number of seasons. The sum of seasonal effects over S time periods is assumed to be zero. In this study, weekly seasonality is taken into account ($S = 7$) with the initialization of $\tau_{1,\mathrm{i}}$, $\tau_{2,\mathrm{i}}$, $\tau_{3,\mathrm{i}}$, $\tau_{4,\mathrm{i}}$, $\tau_{5,\mathrm{i}}$, and $\tau_{6,\mathrm{i}}$:

$$\begin{cases} \tau_{t+1,\mathrm{i}} = -\sum_{s=1}^{S} \tau_{t-s,\mathrm{i}} + \eta_{2,t} \quad \forall t > 1 \\ \tau_{1,\mathrm{i}}, \tau_{2,\mathrm{i}}, \tau_{3,\mathrm{i}}, \tau_{4,\mathrm{i}}, \tau_{5,\mathrm{i}}, \tau_{6,\mathrm{i}} \sim \mathcal{N}(\mu_{\tau_0}, \sigma_{\tau_0}^2) \\ \eta_{2,t} \sim \mathcal{N}(0, \sigma_\tau^2) \\ \mu_{\tau_0}, \sigma_{\tau_0}, \sigma_\tau \sim Cauchy(0, 2.5) \end{cases} \tag{3.9}$$

Choice of Covariates: Apart from the local level model and seasonality, there are other unobserved effects such as impacts of holidays and sport events that may contaminate the estimation of the $y_{t,\mathrm{i}}$. To capture the unobserved heterogeneity, $x_{t,\mathrm{i}}$ in Equation (1) is used as the simultaneous daily visits to a similar business type at time t in a different region that was not affected by the disaster (in our case, New York). $x_{t,\mathrm{i}}$ accounts for the shared variance of the time series data from

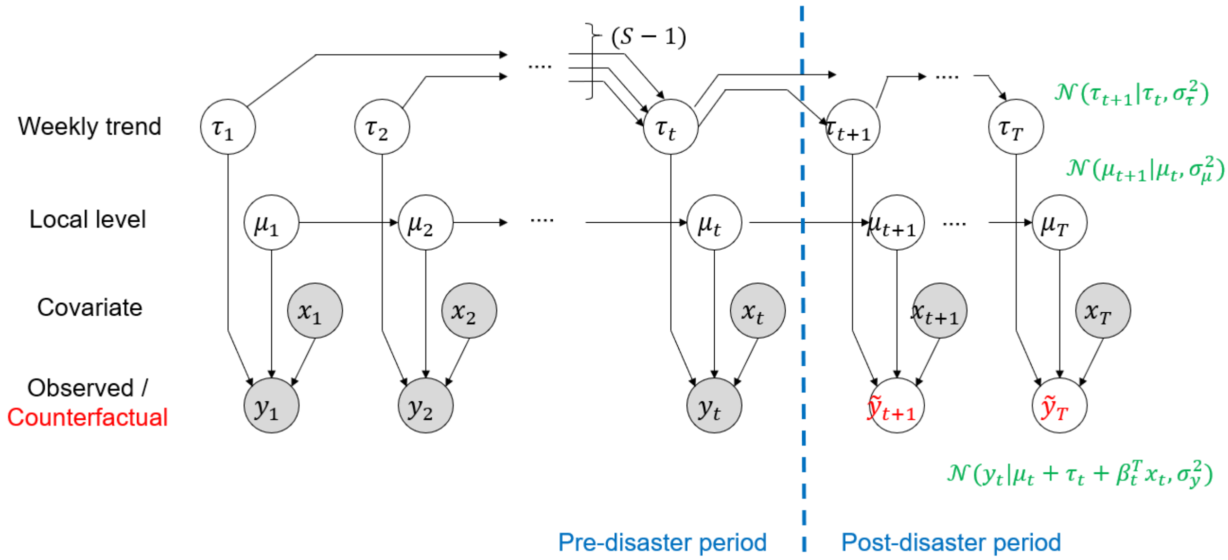

Figure 3.10. Graphical representation of the Bayesian structural time series model.

two different regions. The static coefficient β represents the relationship between daily visits to a specific business type from Puerto Rico and New York. In this study, we test three methods for the choice of covariates, which we will test in the experiments Section: (i) no covariate, (ii) use the average daily visit trends of the same brand businesses in the other city as covariate (e.g. if y_{i} was a Starbucks, we would use the average daily visit counts of all Starbucks in New York as the covariate), which we denote as $x_{category}$, and (iii) use the daily visit count of a specific business which has the highest correlation with the target business, which we denote as $x_{specific}$. For (iii), we compute the Pearson's correlation between the daily visit count data of the target business with that of all same category businesses in New York, and use the business with the highest Pearson R.

Estimating causal impact of disasters on businesses: Let N denote the total number of days observed. We first fit the BSTS model with pre-disaster data (n = 150) from New York and Puerto Rico. For each business with index i, posterior predictive samples can be simulated to develop a counterfactual as the synthetic control group ($t = n+1, ..., N$) from Equation (4).

$$\hat{y_{t,\mathrm{i}}} \sim p(\hat{y_{t,\mathrm{i}}}|y_{t,\mathrm{i}}) \quad t \geq n \tag{3.10}$$

Let $m \in [n, N]$ denote the the day when the Hurricane Maria struck Puerto Rico. Point-wise comparisons estimate the impacts of hurricane on daily visits to a target business type between treatment and control groups.

$$\phi_{t,\mathrm{i}} = \frac{y_{t,\mathrm{i}} - \hat{y_{t,\mathrm{i}}}}{\bar{y}_{\mathrm{i}}} \qquad t = m+1, ..., N \tag{3.11}$$

where, $\bar{y}_{\mathrm{i}}$ denotes the mean visit count to the visits prior to the disaster $(t < n)$. The impact $\phi_{t,\mathrm{i}}$ is a normalized measure of the disaster impact to the business. $\phi_{t,\mathrm{i}}$ measures the number of business-as-usual days worth of impact (damage) the disaster inflicted on the business.

Moreover, We hope to estimate the cumulative causal effects of hurricane on a target business type over time, which represents the resilience of business after hurricane. The cumulative sum of causal increments is a practical quantity when the response variable $y_{t,\mathrm{i}}$ is measured over time. We calculate the total impact of the disaster to business i by the following equation.

$$\phi_{\mathrm{i}} = \sum_{t=m}^{N} \phi_{t,\mathrm{i}} \tag{3.12}$$

Daily visits to businesses in Puerto Rico and New York from January 2017 to March 2018 (400 days) are analyzed. As explained in the Methods Section, we will test three methods of selecting the covariate: no covariate, $x_{category}$, and $x_{specific}$. To verify the which type of covariate improves the prediction accuracy the most, two different model settings will be explored:

- Setting 1 (Inter-State prediction): Pre-disaster data will be used from Puerto Rico and New York. The model will be fitted using data until day 150, and tested using data between days 151 and 200.

- Setting 2 (Intra-State prediction): To test the accuracy of long-term predictions, data from businesses in Manhattan will be used to predict the visit counts of businesses in Up-State New York, using the whole observation period (train: 0-150, test: 151-400).

Evaluation Metrics

The prediction tasks will be evaluated using 2 different metrics: i) Pearson's R, which captures the correlation between the predicted and true time series values, and ii) mean absolute percentage error (MAPE), which captures the relative magnitude of the absolute error between the predicted and true time series values. MAPE is calculated by the following equation:

$$MAPE_{\mathrm{i}} = \frac{1}{n}\sum_{t=1}^{n}\left|\frac{y_{t,\mathrm{i}} - \hat{y_{t,\mathrm{i}}}}{y_{t,\mathrm{i}}}\right| \tag{3.13}$$

We measure the performance of the methods using these two distinct metrics, where Pearson's R measures the relative correlation between the two sequences, while MAPE measures the absolute magnitude of discrepancy between the two vectors.

3.2.2 Estimation Results of Disaster Impacts

The performances of the BSTS models with three types of covariates, were tested on the aforementioned two experimental settings, using Pearson's correlation and MAPE as evaluation metrics. Table 3.2 shows the performances of the three BSTS models on both settings. Surprisingly, although the model with business-category covariates perform the best on average in both experimental settings, the predictive performances of the three methods are quite similar. Using extra covariates do not always improve the prediction model, and we see that over 34% of the businesses in experiment setting 1 had best performances when not using extra covariates (similarly, over 40% of businesses in experimental setting 2). Extra covariates, which are aimed to capture the long term trends and anomalies (e.g. New Years, Christmas), are not effective when making predictions of businesses that have less long-term variation and a relatively stable periodicity in visit counts. From experiment 1, we determine the best performing model out of the three for each business, and we use that business to predict the counterfactual daily visit counts after the disaster period.

Figure 3.11 shows an example of how the the disaster impact is quantified. As shown in panel (A), we first predict the counterfactual daily visit counts after the disaster (blue plot) using the best performing model identified in the model validation experiment. Then, as shown in (B), we calculate the point-wise disaster impact $\phi_{t,\mathrm{i}}$, by subtracting the observed daily visit count sequence from the predicted sequence and normalizing it by the pre-disaster mean daily visits. The cumulative disaster impact ϕ_{i} can be calculated by aggregating the point-wise disaster impacts over time.

Table 3.2. Model validation results of two experimental settings.

		Evaluation Metric	Use of Covariates		
			No Covariates	$x_{category}$	$x_{specific}$
Setting 1	Train	MAPE	12.35 (±16.67)	10.50 (±14.03)	10.66 (±14.46)
		Pearson R	0.539 (±0.222)	0.696 (±0.169)	0.626 (±0.136)
	Test	MAPE	8.568 (±14.37)	8.518 (±15.85)	8.888 (±15.30)
		Pearson R	0.351 (±0.238)	0.354 (±0.239)	0.295 (±0.257)
	Selected (%)		34.9	40.4	24.7
Setting 2	Train	MAPE	0.229 (±0.257)	0.249 (±0.251)	0.257 (±0.252)
		Pearson R	0.855 (±0.144)	0.742 (±0.145)	0.744 (±0.115)
	Test	MAPE	0.704 (±0.811)	0.475 (±0.612)	0.477 (±0.538)
		Pearson R	0.420 (±0.189)	0.512 (±0.181)	0.466 (±0.183)
	Selected (%)		40.3	25.1	34.6

Panel (C) shows the cumulative disaster impact over time from the time of the landfall of the hurricane. In this particular business, we observe a significant negative impact until around day 300 with around $\phi_i = -25$, meaning that by day 300, this business lost a 25 business-as-usual days worth of customers due to the hurricane. We actually see positive impacts of the hurricane before the 2 hurricanes, however the positive impacts are significantly negated by the negative impacts. Gradually after 1 month from the hurricane landfall, we see an increase in visits compared to pre-disaster levels, which decrease the negative disaster impact. As a result of the BSTS modeling, we are able to obtain the quantified disaster impact for each of the businesses in Puerto Rico over time. In the next section, we analyze the obtained results to further understand which business categories in which locations suffered disaster impact in Puerto Rico after Hurricane Maria.

Now, using the BSTS method for predicting the counterfactual business performances, we quantitatively analyze the resilience of businesses after Hurricane Maria and answer the following questions:

1. How does the disaster impact evolve over time, and do the temporal patterns vary across business categories and locations?

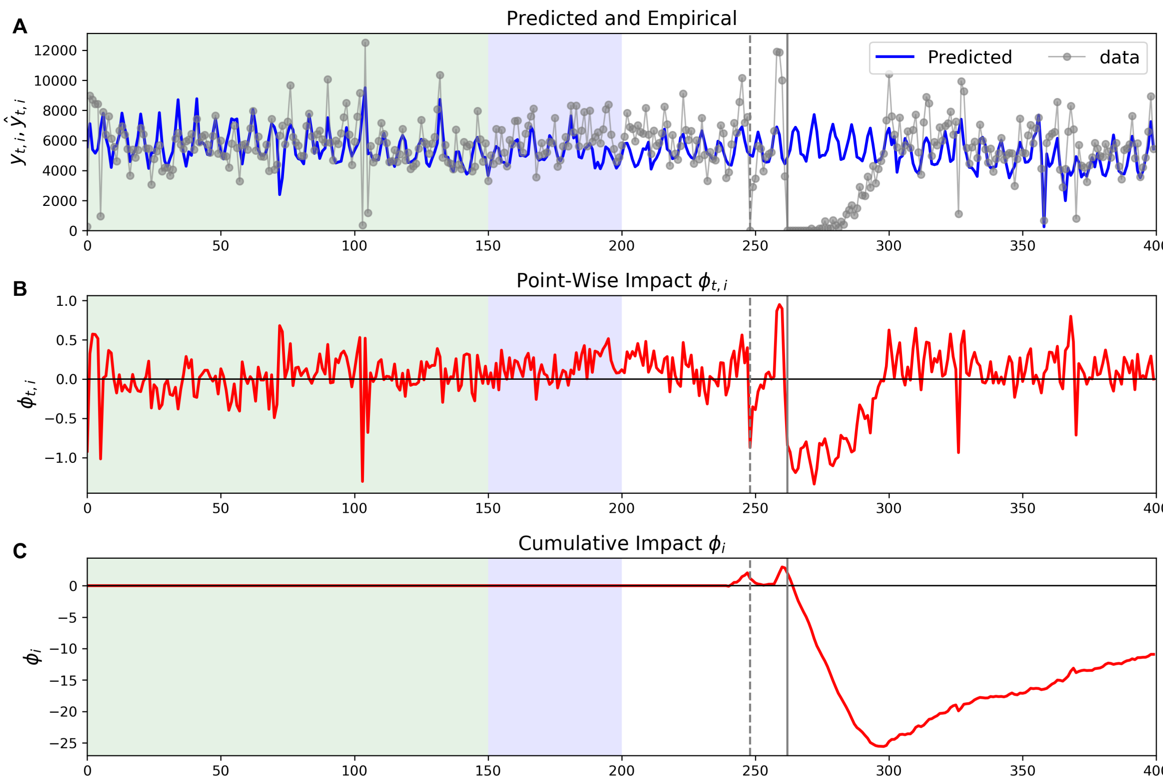

Figure 3.11. Example of how the disaster impact is quantified. (A) Predicted and actual observed daily visit patterns for a randomly selected business. (B) Point-wise impact $\phi_{t,\mathrm{i}}$, and (C) cumulative impact ϕ_i of the disaster.

2. Can we explain why we observe such heterogeneity in disaster impacts across businesses in Puerto Rico?

Since it was revealed that the optimal prediction models varied across different businesses in the Model Validation Section, we use the best performing model out of the three (either no covariate, average NY trend as covariate, or specific NY business trend as covariate) to predict the counterfactual visit time series for each of the businesses in Puerto Rico.

Quantifying disaster impact patterns to businesses

To answer the first research question, we aggregate the disaster impacts over the time horizon by business category and business location (San Juan Municipio, Metropolitan Area, Rural Area, shown in Figure 3.9B). Figure 3.12 shows the longitudinal point-wise disaster impact, which is the difference between the actual and the predicted business performances across time ($\phi_t = y_t - \hat{y}_t$) for all nine business categories. Negative values of ϕ_t would mean that the disaster had a negative impact on businesses, resulting in loss of customers, while a positive ϕ_t would mean that the number of customers increased due to the impact of the disaster. In each panel, the disaster impacts to businesses in the three regions are separately shown in blue (San Juan Municipio), green (Metropolitan Area), and red (rural area). The vertical lines show the timings of the two hurricanes (dotted: Hurricane Irma, solid: Hurricane Maria).

Several interesting observations can be made from these visualizations. First, we observe common trend across several business categories, where all three regions experience negative impact right after Hurricane Maria, and then the businesses in the urban areas recover quicker compared to those in rural areas. This intuitive trend can be observed in various business categories including building materials, supermarkets, restaurants, telecommunications, and grocery stores. Second, we see a significant increase in gasoline stations in metropolitan areas (green) after Hurricane Maria. This reflects the high travel demand from the rural areas towards the metropolitan areas in the island due to evacuation mobility [177]. Third, in some business categories such as hospitals and hotels, we see an increase in visits after the hurricanes compared to before, especially in the San Juan region (blue). An increase in hospital visits reflect the large number of injuries and casualties caused by the flooding and severe winds caused by the hurricane. Significant increase in visits to hotels in San Juan reflect the large number of residents who evacuated from the rural areas in Puerto Rico to the capital city, which agrees with previous studies that observe the influx of population movements in San Juan from the suburban and rural areas of the island [177]. Minor details are captured in the figures as well, for example, how weekly fluctuations are estimated more vividly in universities (students do not attend classes on weekends) compared to other business types, and also how the impacts of Hurricane Irma, although minimal compared to Hurricane Maria, are captured in the time series data.

To further understand the impact of Hurricane Maria on the businesses, we computed the cumulative disaster impact ($\phi = \sum_t \phi_t$) for each business in each region. The cumulative disaster impacts are shown in Figure 3.13 for three different aggregation time thresholds, including (A) landfall to 1 month from landfall, (B) until 2 months from landfall, and (C) until 4 months from landfall. For each business category, the cumulative disaster impacts are aggregated by regions, with the same

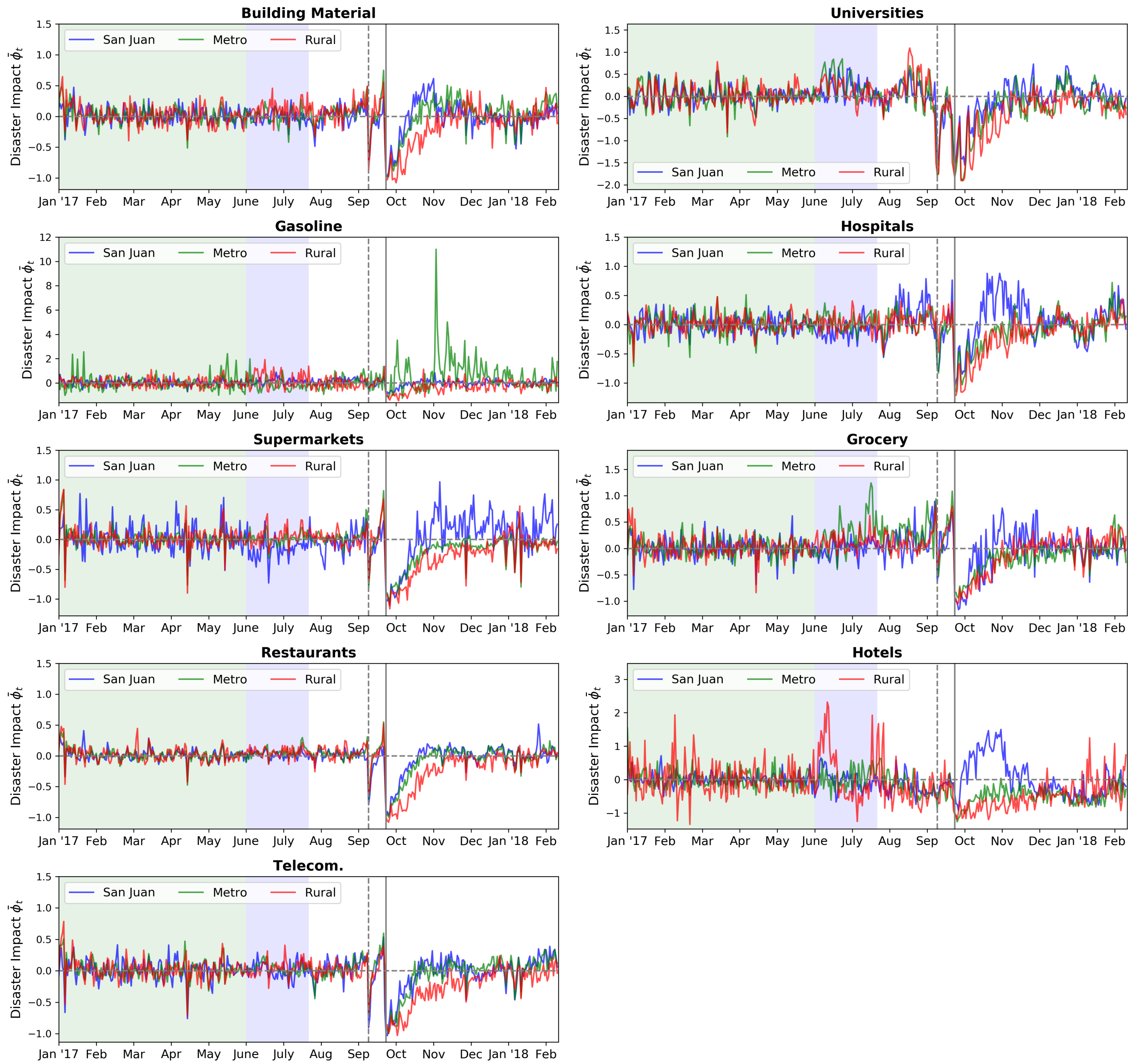

Figure 3.12. Point-wise disaster impacts across different business categories and business locations.

color coding as Figure 3.12. The numbers of ϕ_i should be interpreted as "the number of business-as-usual days worth of impact". For example, building material businesses in San Juan experienced a median disaster impact of $\phi = -10$ during the first month. This indicates that the building material businesses in San Juan lost 10 days worth of customers who were supposed to visit if the disaster did not occur. Most of the regions and business categories experience a negative impact in the first month, except for hotels in San Juan. We also clearly observe the urban-rural disparity in disaster impacts across many of the business categories across all three temporal thresholds. However, the urban-rural gap gradually closes down as time passes, and in many of the industries we observe little differences by 4 months from landfall (e.g. building material, grocery stores, restaurants, and telecommunications).

Although the general patterns show consistent insights such as the urban-rural disparity, larger impact right after the landfall, and differences in disaster impacts across business categories, we are not able to delineate the effects of each characteristic on disaster impacts. In the next section, we attempt to reveal the impacts of business characteristics on the observed disaster impacts, by applying a hierarchical Bayesian modeling techniques.

Although the results shown in the previous section revealed various patterns and correlations, the quantified disaster impacts were all conditioned on various features including the business characteristics (e.g. business category and location) and disaster characteristics. To delineate such effects and to understand the resilience of different business types, we apply a hierarchical Bayesian model approach. Hierarchical Bayesian models (HBMs) allow us to flexibly model the group-level effects on the estimand by introducing hyper prior distributions on the model parameters. This is a significant difference from regular linear regression models which can only either i) assign one global parameter for all groups, or ii) estimate parameters separately for each group. For further details on the advantages of HBMs, readers should refer to [286].

To estimate the cumulative disaster impact of all businesses, we construct the HBM as the following:

$$\begin{cases} \phi_{\mathrm{i}} \sim N(\beta X_{\mathrm{i}} + \delta_{r(\mathrm{i})} + \gamma_{c(\mathrm{i})}, \sigma^2) \\ \delta_{r(\mathrm{i})} \sim N(0, \tau_\delta^2), \quad \forall r \in \{0,1,2\} \quad \#region \\ \gamma_{c(\mathrm{i})} \sim N(0, \tau_\gamma^2), \quad \forall c \in \{0,1,2,3,4,5,6,7,8\} \quad \#category \\ \beta, \sigma, \tau_\delta, \tau_\gamma \sim Cauchy(0, 2.5) \end{cases} \tag{3.14}$$

where, $r(\mathrm{i}) \in \{0,1,2\}$ and $c(\mathrm{i}) \in \{0,1,2,3,4,5,6,7,8\}$ denote the region index and category index for business i. We assume that the cumulative disaster impact on business i, denoted by ϕ_{i}, can be modeled as a linear sum of the effects of exogenous features X_{i} (which include pre-disaster business mean visits, housing damages caused by the disaster), regional effects δ_r, and business categorical

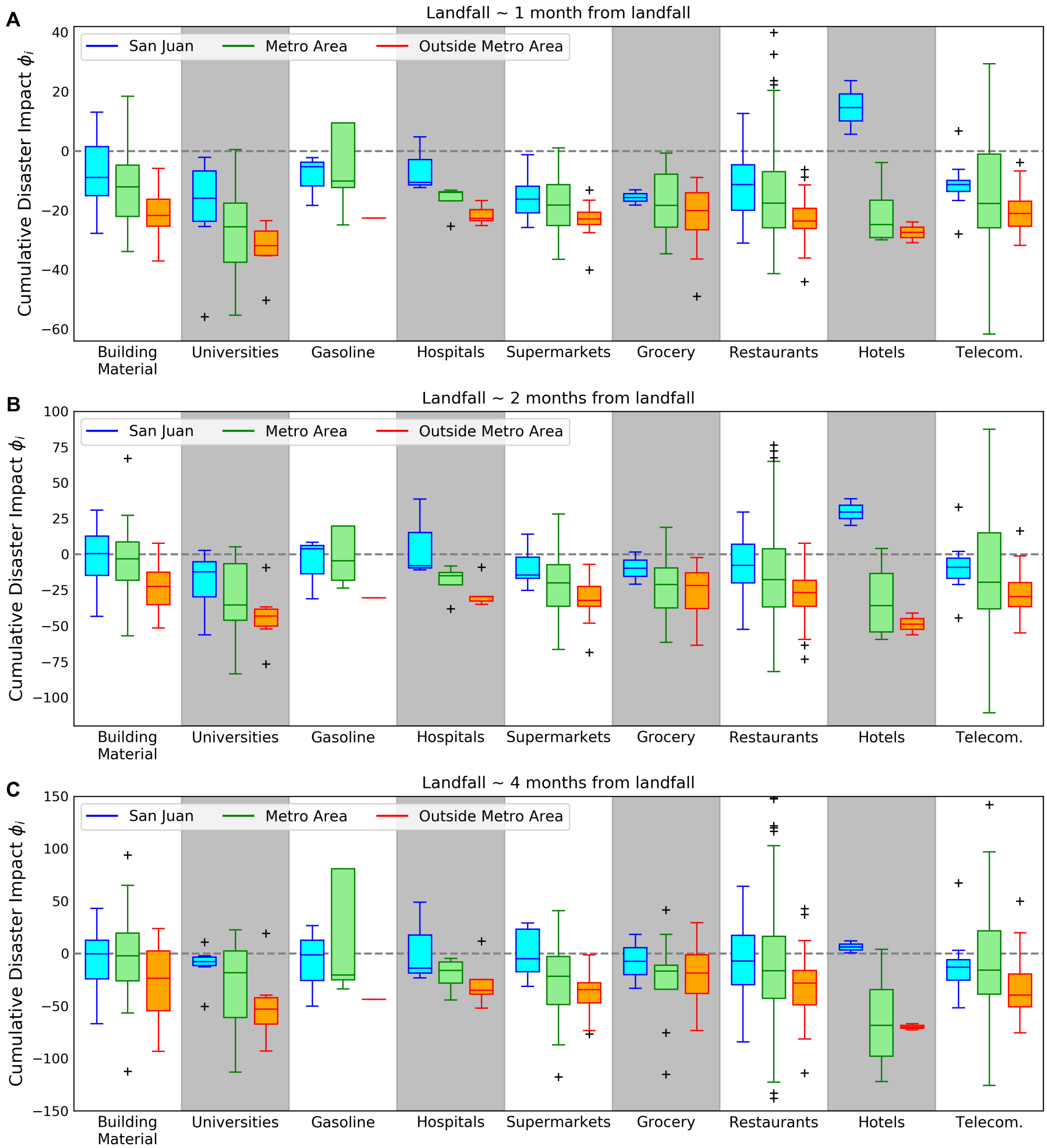

Figure 3.13. Cumulative disaster impacts across different business categories and regions. Results are shown for different aggregation time thresholds, including (A) landfall to 1 month from landfall, (B) until 2 months from landfall, and (C) until 4 months from landfall.

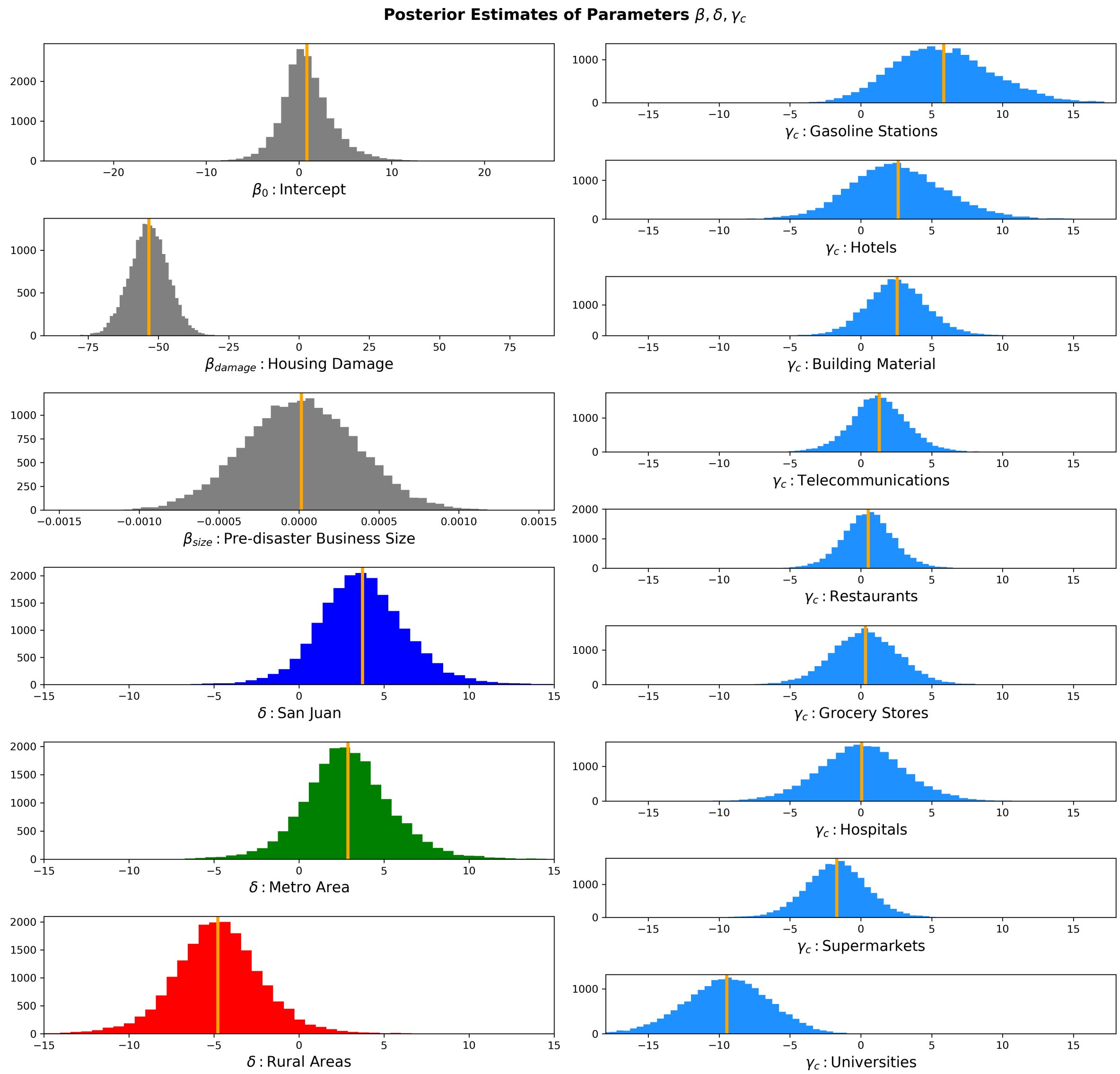

Figure 3.14. Posterior estimates of model parameters of the hierarchical Bayesian model. Using the model, we are able to understand the business impacts that each business category experiences conditioned on other factors such as housing damage rates, pre-disaster business sizes, and locations.

effects γ_c. The model is Bayesian in the sense that the model parameters (β, δ, γ) all have priors, and the model is also hierarchical since the hyper-parameters in the prior distributions $(\tau_\delta, \tau_\gamma)$ come from another higher level distribution. We assume that the hyper-parameters are drawn from weakly informative priors (Cauchy distribution). The hierarchical prior distributions allow us to model the dependencies across different groups (regional groups and categorical groups).

The model was implemented using `stan`, which performs sampling using Hamiltonian Monte Carlo method, and was coded on the `Pystan` package. Sampling was performed for 20,000 iterations with the first 1,000 used as warm-up. Thus, in total 19,000 samples were drawn for each parameter. The sampling was ran on a regular laptop computer with an Intel i7 processor with 3.30GHz, and 8GB of RAM. The sampling took less than 5 minutes in total, which was much faster than the BSTS model due to the small number of parameters. The mixing of the sampling was effective, where $\hat{R}$ values were extremely close to 1.0000 ($\pm$0.0001) for all parameters. Effective sample sizes were all significantly large, where the least was 5143.

Figure 3.14 shows the posterior estimates of the model parameters in the hierarchical Bayesian model (β, δ, γ). The housing damage observed in the county of the business location had a significantly negative effect on the cumulative disaster impact, which was very intuitive. On the other hand, the intercept as well as the pre-disaster business size, which was measured by the mean visits to each business in the first 150 days of the observation (Hurricanes Irma and Maria struck on days 248 and 262), had no effect on the disaster impact. This contradicted previous studies which claim that business sizes have significant impact on the recovery of businesses [265]. However, the study did not have detailed information on the category of the business (only whether or not the business was in the service sector). The effect of the business category may have negated the effect of pre-disaster business size. The estimated location effect agreed with our previous analyses (Figures 3.12 and 3.13), showing that urban businesses had less negative disaster impact than rural ones. By delineating all of these effects, we are able to estimate the business impacts that each business category experiences, conditioned on other factors such as housing damage rates, pre-disaster business sizes, and locations. The estimated effects (γ parameter estimates) are shown in the right column of Figure 3.14. This shows that gasoline stations, hotels, building material, and telecommunications had positive disaster impacts, meaning that people visited these locations after the disaster more than before. This agrees with various news articles and studies that raise evidence of people rushing to purchase gas [287] and evacuating and staying in hotels [288]. This also reflects the household recovery process, where people purchase building materials for rebuilding homes and visits telecommunication companies to fix their mobile devices for internet connectivity. On the other hand, universities and supermarkets had a significant negative disaster effect. Again, this

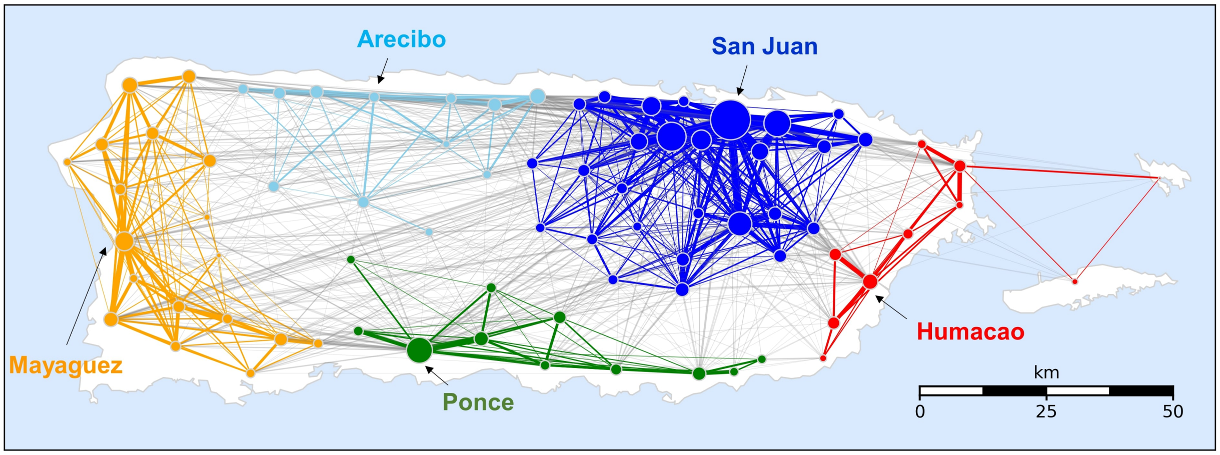

Figure 3.15. Partition results of counties in Puerto Rico based on pre-disaster human mobility flow dynamics network. Each sub-network is labeled by the major cities, respectively. These subnetworks describe the regional clusters that have significant intra-regional mobility flow. The sizes of the nodes correspond to the population in each county, and the width of the links connecting each node represent the amount of mobility flow during normal times (before the hurricane). The links connecting nodes from the same subnetworks are colored with the color of the subnetwork, otherwise colored in gray.

agrees with closures of universities in Puerto Rico after Hurricane Maria [289] and news articles pointing out under-supply in supermarkets after the disaster [290].

3.2.3 Unraveling the Recovery Sequence of Industries

Network Partition of Regional Mobility Flow

First, to conduct analysis on the regional heterogeneity in social and economic recovery trajectories, the entire island is partitioned into appropriate geographical regions. Such geographical regions should reflect the spatial boundaries of daily livelihood and activity patterns of the residents. An ideal partitioned sub-network would include a set of counties with a large amount of internal mobility flow among them (e.g. core city and periphery cities) in the same regional cluster, but separate counties that have small amount of mobility flow among them. More formally, given a directed bi-directional network of mobility flow patterns (from mobile phone movement data), we attempt to find an optimal way to partition the network into subnetworks so that we achieve high network modularity. Various computational algorithms have been proposed to tackle this problem in the context of community detection in networks (or graphs) [291]. Among the variety of network partitioning algorithms, the `infomap` algorithm is shown to be an effective and computationally efficient method [292], and has been applied to network community detection tasks in various domains, including human mobility modeling [293]. `infomap` is an information-theoretic graph partitioning method, which uses the flows of random walkers to find groups of dynamically related nodes in directed, weighted network. The algorithm was implemented on Python, using the `igraph` package for implementation ( ).

The scatter plots and the solid lines in Figure 3.16 show the recovery dynamics of aggregated visits to all points-of-interest (POIs) in each of the five regions based on mobile phone data. The recovery observations, despite the differences in speed, all resemble a logistic growth, which can be modeled with the following equation:

$$g(t) = \frac{L}{1 + \exp\left(-k(t - t_0)\right)}$$

The foot traffic values start at a low value close to 0, and gradually recover to a stable value near L with decreasing growth rate as the value approaches the stable value in the long term. The steepness (rate) of the curve is characterized by parameter k, and the midpoint timing (timing when recovery reaches $0.5L$) is characterized by parameter t_0. The solid lines in Figure 3.16 show the logistic curves fitted to the data. The estimated parameters of the logistic growth function and the Pearson correlation between the data and fitted curves r_{soc} are shown in Table 3.3. We observe significant heterogeneity in recovery curves after Hurricane Maria across the five regions. The San Juan region recovers the fastest after Hurricane Maria in all of the POI types, followed by Arecibo, Mayaguez, Ponce, and Humacao. In particular, Humacao has slowest recovery and by the end of the year 2017, the foot traffic only recovers to up to 50% of the original value.

By dis-aggregating the foot traffic data to various POI types, we observe significant increase in visits to all of the POIs in all regions just before the landfall of Hurricane Maria, and also before Hurricane Irma for medical and construction POI types (Figure 3.17). This implies significant pre-disaster preparation behavior (e.g. shopping for goods), which agrees with insights from past human behavior modeling studies [294]. Also, a decrease in visits to POIs just before Hurricane

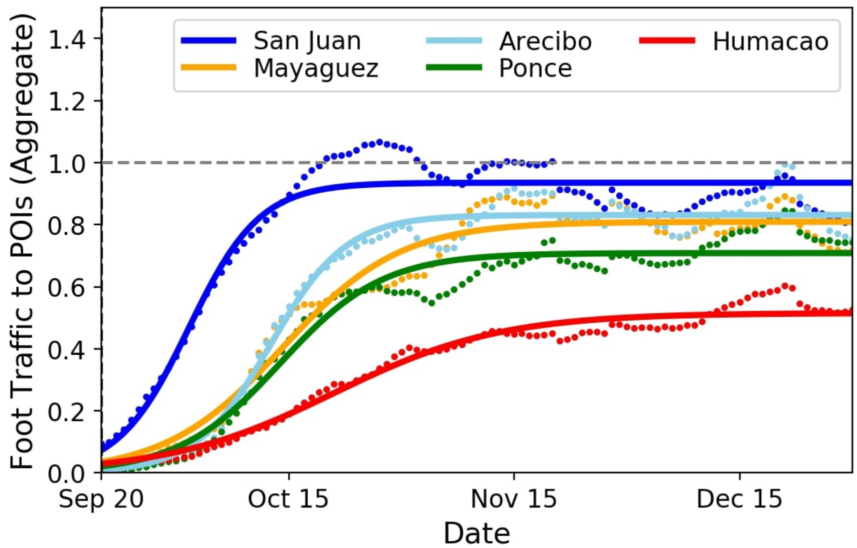

Figure 3.16. Inter-regional heterogeneity in recovery dynamics of visits to various points-of-interest (POIs) in Puerto Rico after Hurricane Maria. The data can be fit well to a logistic growth function $g(t) = \frac{L}{1+\exp(-k(t-t_0))}$, shown in solid curves. Note: Aggregated foot traffic of 1 indicates pre-hurricane standards.

Irma can also be observed; however they are shown to be less severe compared to Hurricane Maria. Further analysis of the spatial heterogeneity and differences across POI types in disaster impacts has been presented in recent studies using the same dataset [295]. Not all POI types in the five regions recovered back to the original (pre-hurricane) states. For example, grocery stores and construction stores in Humacao recovered only to up to 50% of the pre-hurricane visit count, while all three POI types in San Juan recovered to pre-hurricane levels, and even experienced an increase in demand around 1 month after the landfall (in particular for construction material in San Juan on end of October).

Analyzing the fitted parameters of the logistic growth function further reveals how the affected residents coped with the disaster. Figure 3.18 shows the estimated parameter values (k, t_0, L) of each type of POI in each region. The numbers between 1 and 6, annotated above the barplots indicate the rank among the six POI categories within each region. From these results, we infer that, in four regions except Humacao, foot traffic to automobile stores (which includes gas stations and repair) recovered the quickest (largest steepness of curve k and shortest midpoint t_0). This suggests that people first visited gas stations and automotive repair stores to obtain a mode of transport,

Table 3.3. Estimated parameter values and goodness of fit of social and physical recovery models.

Region	τ	r_{phys}	k	t_0	L	r_{soc}
San Juan	0.061	0.914	0.215	11.5	0.925	0.951
Mayaguez	0.031	0.950	0.131	23.9	0.800	0.976
Arecibo	0.031	0.958	0.203	22.5	0.824	0.984
Ponce	0.037	0.945	0.147	23.8	0.707	0.979
Humacao	0.030	0.949	0.091	30.8	0.513	0.986

to begin their recovery and rebuilding processes. Then medical, construction, and grocery POIs were visited for recovery. Education POIs, on the other hand, recovered the slowest in most of the regions, indicating that such educational services recover only after all essential recovery has progressed. POIs in Humacao had different recovery trajectories, where construction POIs recovered the quickest (highest steepness and shortest midpoint time), reflecting the high housing damage rates in Humacao region compared to the other regions within the island. While parameters k (Figure 3.18A) and t_0 (Figure 3.18B) represent the speed of recovery, parameter L (Figure 3.18C) shows how each POI recovers in the longitudinal time horizon compared to pre-disaster standards. We observe that despite the slow speed, educational facilities were able to recover to relatively high standards (ranks 2nd, 1st, 1st, 1st, 3rd, and 1st).

The results observed from different data sources provide several insights on community recovery and resilience. They highlight the disproportionate effects of the hurricane on different regions within the island of Puerto Rico, both in terms of physical (through water service deficit) and social (through the recovery of various essential POI types) systems. We observe that San Juan, the capital city of Puerto Rico, recovers much faster than other regions both physically and socially, while Humacao and Mayaguez fail to recover back to their original states. In addition to such correlations, these relationships of recovery speed suggest the existence of interdependencies among the social and physical systems during the post-disaster recovery period. In the next Section, we further investigate into the recovery dynamics of coupled social and physical systems, and how such interdependent relationships affect the resilience of the overall system.

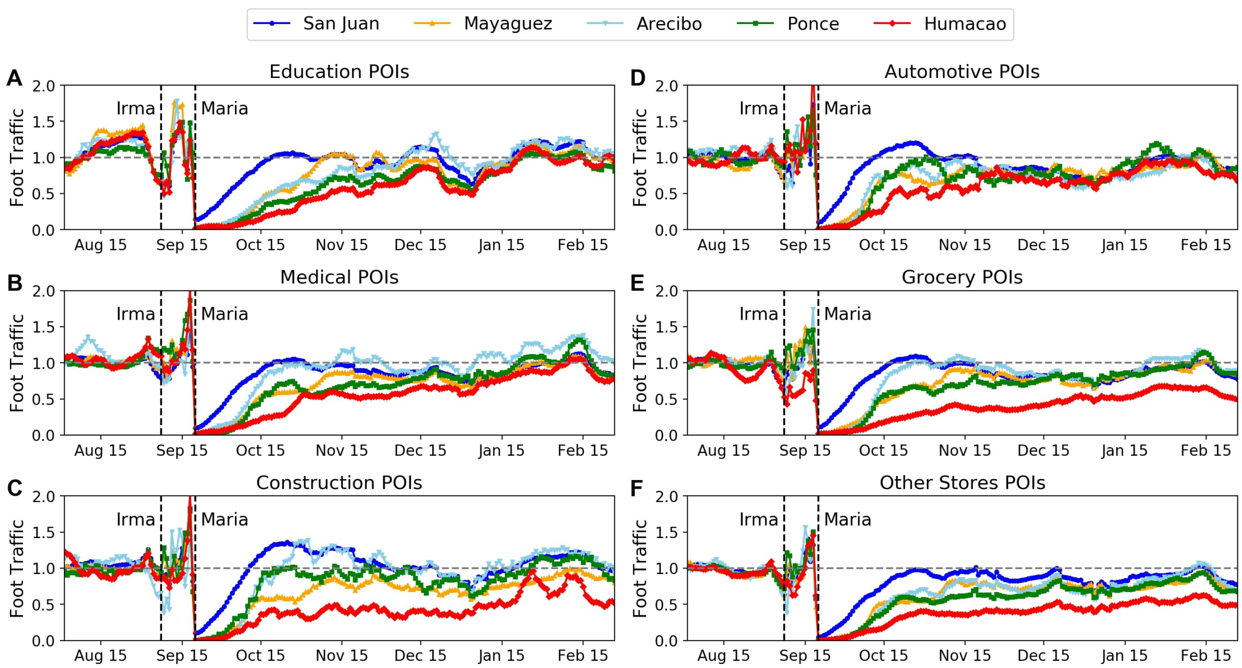

Figure 3.17. Inter-regional heterogeneity in recovery dynamics of visits to POIs in Puerto Rico after Hurricane Maria. Normalized visit counts with respect to pre-disaster (before August 31st, 2017) mean visits are shown on the vertical axis, and dates are shown on the horizontal axis. Colors of the curves correspond to the regions in Figure 3.15. The two dotted vertical lines correspond to the landfall of Hurricanes Irma and Maria.

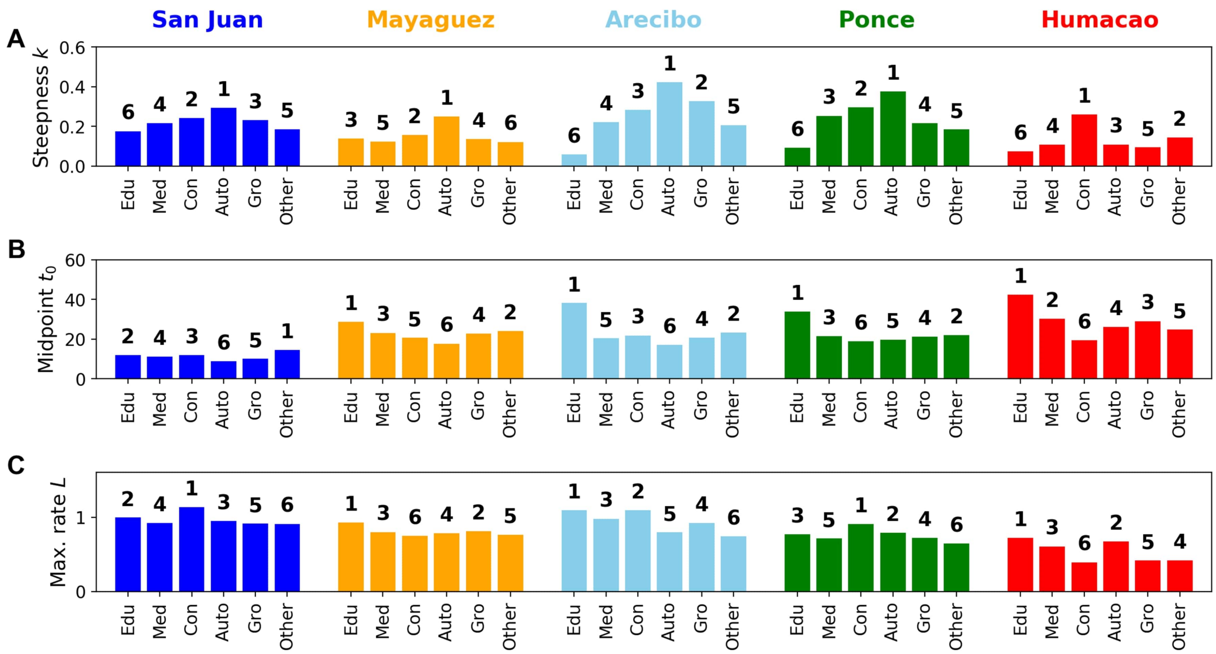

Figure 3.18. Inter-regional and inter-POI heterogeneity in recovery speed of visits to POIs in Puerto Rico after Hurricane Maria. Panels A, B, and C show the estimated parameters k, t_0, L of the logistic functions, respectively. Numbers ($1 \sim 6$) annotated above the bars show the rank among the six POI categories within each region.

4. SOCIO-PHYSICAL SYSTEM INTERDEPENDENCIES

Urban communities depend on reliable provision of multiple critical services supplied through infrastructure networks, which are centrally managed by public and private utilities. In this study, we categorize components of cities into social and physical systems. Social systems include community-based entities at all spatial scales, such as households, non-government organizations, faith-based groups, and businesses. On the other hand, physical systems denote the structural infrastructure systems that serve urban agglomerations, including water pipe networks, road networks, sewage pipe networks, and power grids. These social and physical systems are binded together with complex interdependent relationships embedded within and among urban systems, and its complexity is increasing due to rapid urban growth and expansion in many cities around the world [296]. On the other hand, with the rising intensity and frequency of natural hazards globally, there is an increasing need for agencies to enhance the resilience of urban systems to future shocks [297]. Because of the strong and complex socio-physical coupling, shocks caused by natural hazards may cascade across urban systems, amplifying the disruptions caused by the disaster. This poses significant challenges in understanding, modeling and predicting the recovery of cities from future shocks, and identifying operational mechanisms in social and physical networks that enhance the resilience of cities [298], [299].

The complexity of interdependencies between social and physical systems vary with urban scales. Larger cities have bigger social capital to build and manage critical physical infrastructure, and to acquire necessary natural resources (e.g., water, energy, food), and also have access to external technical and financial assistance (subsidy), not readily available to smaller cities. Typically, small cities rely on their extant social networks and social capacity inherent in the community. During a disaster, due to lack of quick infrastructure recovery, people draw upon their social networks and these are further strengthened [300], [301]. However, in large cities, due to larger infusions of resources on physical infrastructure, these networks recover quickly [302]. The recovery of physical networks is primarily based on resources from a central actor (e.g. government) whereas social networks and the resulting social capital is primarily decentralized. As many smaller cities face urban growth, how could these cities, along the rural – urban growth trajectory, manage the interdependent relationships between social and physical systems for resilient recovery from disasters?

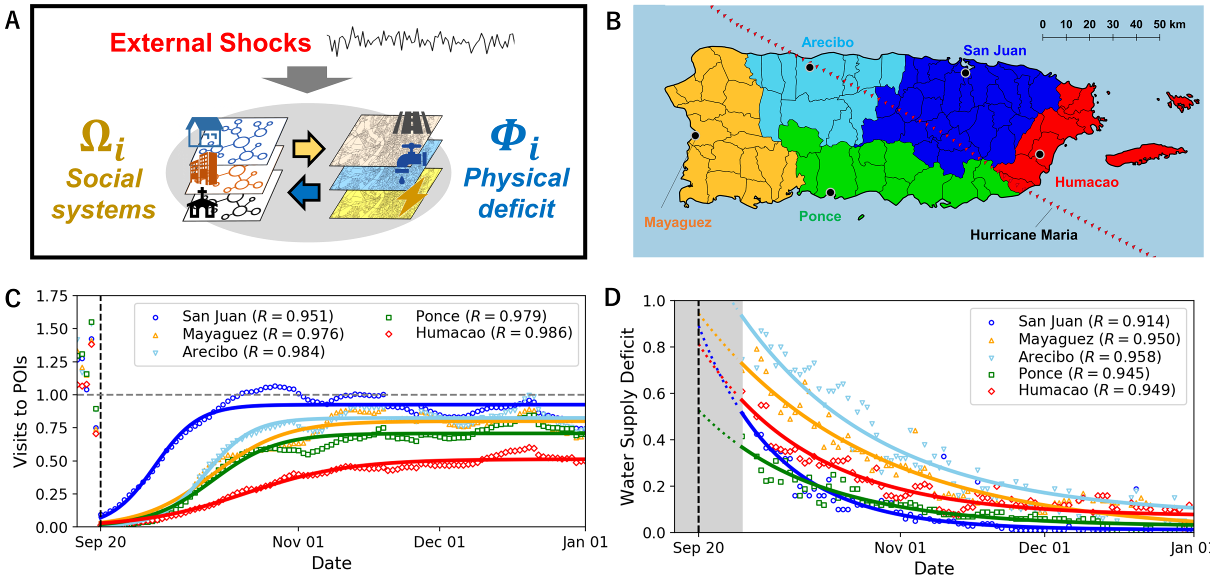

Figure 4.1. Fusion of large-scale data and dynamical model for unraveling socio-physical interdependencies. **A.** Schematic showing the overview of the study. We are interested in how coupled urban socio-physical systems respond to a series of external shocks. Resilience of a CUSPS is quantified using data, system dynamics models, and simulations. **B.** Puerto Rico was divided into five regions based on the modularity of human mobility flow patterns. **C.** Recovery of social systems were measured by visits to various places-of-interest (POIs) using mobile phone location data. **D.** Regional differences in recovery of water service deficit after Hurricane Maria in Puerto Rico. Data were available after September 29th 2017, thus observations for initial service deficits between September 20th and September 29th are missing. Negative exponential functions ($f(t) \propto \exp(-\tau t)$; solid curves) approximate the recovery dynamics well.

A key task is to identify the right amount of self-reliance of social systems despite the existence of robust centralized physical infrastructure, that leads to better recovery outcomes for cities based on their size, location and demographics [303]. Although studies have explored the role of social and physical networks on urban resilience and recovery in isolation (e.g., social [58], [113], [304], [305], physical [100], [104], [306], [307], economic [308]), the interdependencies between socio-physical systems and its implications on urban resilience have been largely neglected in existing studies.

We examine the recovery dynamics of five regions in Puerto Rico island after the devastating damage from the Category 5 Hurricane Maria, to (1) quantitatively assess the temporal trajectories of social and physical recovery, (2) evaluate regional differences in degrees of interdependencies between social and physical systems, and (3) understand the implications of managing such socio-physical interdependencies on urban resilience. To achieve these research goals, a data-driven system dynamics modeling approach is applied to estimate the coupled dynamics between social and physical systems during the disaster recovery process (Figure 4.1A). Empirical data from five regions in Puerto Rico (Figure 4.1B) after Hurricane Maria, including large-scale mobility data collected from mobile phones and recovery data of water infrastructure systems, were used to calibrate and test the dynamics model of coupled socio-physical systems. We also extend this model-data analysis to examine the resilience of urban socio-physical systems in the longer time horizon, exposed to a sequence of shocks. We close with a discussion on strategies on managing the degree of social-physical interdependencies, to design resilient cities as many of them face rapid urban growth in the near future.

4.1 Modeling Interdependent Socio-Physical Systems

4.1.1 Observations of Social and Physical Recovery

Physical Recovery Data

Data for service deficit of physical infrastructure systems after Hurricane Maria in Puerto Rico were publicly posted on the `StatusPR` website, which was active until August 2018, which was the following year from the landfall of Hurricane Maria. The `StatusPR` website served as a web dashboard that curates physical infrastructure service data from multiple public utility companies in Puerto Rico including gas, water, power, and mobile phone tower connectivity. Despite the availability of various physical infrastructure service deficit data, only the water service deficit rates were provided in the regional level; others were all aggregate measures for the entire island. The water service deficit rates were provided for five regions in the island (metro, north, south, west and east). Significant spatial co-location of various physical infrastructure networks with water service networks imply that deficit of water infrastructure systems could serve as an adequate approximation for the aggregated physical infrastructure systems recovery [309]. Therefore, in this study, we use water service deficit recovery data to represent the recovery dynamics of physical infrastructure systems. The recovery dynamics of water service deficit in the five regions are shown in Figure 1D.

Mobile Phone Location Data

The point of interest (POI) visit dataset was provided by Safegraph Inc (https://www.safegraph.com/), a company that aggregates anonymized location data collected from smartphone applications to provide insights about physical places. Safegraph Inc. collects GPS location information from an approximately 10% sample out of all mobile phones and smartphones in the United States through various apps. Each GPS data point consists of an anonymized unique user identifier, the longitude, latitude, and timestamp of the observation. The longitude and latitude information have high spatial accuracy (typically within 10 meters), thus allows us to analyze visit movements to each POI. Users' consent to collect and use their location data were obtained by Safegraph.

The number of daily visits to each POI were estimated using the mobile phone location data. To avoid errors in the estimation, spatial noise in the location data were cleaned by removing jumpy observations where the velocity of the movement was unrealistically high ($>$ 150 kilometers per hour). The cleaned data points were then spatially clustered to detect "stay points"using the DBSCAN algorithm [310]. From the estimated stay points, the visited POI is estimated using a machine learning algorithm that uses various features including: the distance from POI to the stay point, time of day, and likelihood of visits to POI categories (using the North American Industry Classification System code also provided by Safegraph Inc.). This data-processing procedure produces a time series data of daily visit counts to each POI. The POIs in the dataset were categorized into 6 major POI types: education, medical, construction, automobile, grocery, and other department stores. Table S2 shows the number of POIs in each region, in each category.

Regional Socio-Demographic, -Economic, and Hurricane Damage Data

Social and economic data of the 78 counties in Puerto Rico were collected from publicly available sources. For example, the county population and median income data were retrieved from the American Community Survey (https://www.census.gov/programs-surveys/acs). Housing damage

Table 4.1. Socio-demographic, -economic, and hurricane damage statistics of the five regions in Puerto Rico island.

Region	Households	Mean Income ($)	Damaged housing (%)
San Juan	658,457	23,823	36.2
Mayaguez	199,355	15,614	31.4
Arecibo	143,795	16,492	38.9
Ponce	152,153	16,505	40.8
Humacao	83,420	19,047	45.1

percentages in each county represent the percentage of housing structures that were approved for the Individuals and Households Program of FEMA [311].

Figure 4.1C shows the normalized visits to various points-of-interest (POIs) in the five regions observed from mobile phone location data, which increasingly have been used to understand urban dynamics [121], [124]. Several important observations can be made from the time series plotted in Figure 4.1C. First, we observe significant differences in the speed of recovery across the regions after Hurricane Maria. San Juan region experienced the quickest recovery, followed by the Arecibo, Ponce, Mayaguez, and Humacao regions. Socio-demographic, -economic, and hurricane damage characteristics of the five regions are shown in Table 4.1. The recovery trajectories, despite the differences in rates, can be well approximated using a logistic curve starting from around zero (complete failure), and asymptotically converging to one (full recovery) over the long term, which corresponds to the pre-hurricane chronic baseline. We also observe significant increase in visits in all regions just before the landfall of Hurricanes Irma and Maria. This indicates substantial preparation activities of the residents before the hurricane (e.g. shopping for grocery and goods), which was also identified in previous studies [294]. Decreases in visits just before Hurricane Irma are much less compared to Hurricane Maria, reflecting the difference in the severity of the hurricanes. Further analysis of the disaster impact differences in the region and category of the POIs has been studied in a past study using the same dataset [295].

Figure 4.1D shows the time series data of water service deficit rates in the five regions after Hurricane Maria [312]. Negative exponential functions ($f(t) \propto \exp(-\tau t)$), shown in solid curves, are shown to fit the recovery of physical service deficit well with Pearson correlation higher than $R = 0.9$. This trend agrees with previous observations from other disasters including Hurricane

Irma in Florida, Tohoku Tsunami in Japan, and Kumamoto Earthquake in Kyushu, Japan [313]. The recovery rate coefficient τ is significantly different among the five regions, with San Juan being the quickest and Mayaguez having the slowest recovery. The initial value of water supply deficit, which varies among regions but are all below 1, is indicative of estimated initial deficit that was caused by Hurricane Irma.

4.1.2 Socio-Physical Systems Dynamics Model

Klammler et al. [31] proposed a unique approach for modeling the resilience dynamics of socio-physical (or "technological-social") systems. The dynamics of the social and physical systems are characterized by coupled differential equations based on modeling insights from the social and ecological sciences. The adaptive capacity of social systems $\Omega(t)$ and service deficit of physical systems $\Phi(t)$ are described using the following differential equations in the original model:

$$\frac{d\Phi}{dt} = (1-\Phi)b - w\Phi\Omega + \xi \tag{4.1}$$

$$\frac{d\Omega}{dt} = (1-c_1\Phi)\Omega(1-\Omega) - r\frac{\Omega^n}{\Omega^n+\beta^n} - c_2\xi \tag{4.2}$$

where, b, r, β and n are model parameters that characterize the functionality of the systems, c_1 and w are parameters that describe the strength of coupling between the social and physical systems, and ξ represent the external shocks (i.e., natural hazards) that affect the system. c_2 controls how much the social systems are affected by the external shocks. Each of the equations are composed of three components: replenishment (or improvement), depletion (or degradation), and external shock. The equation of physical systems dynamics Φ is characterized by an exponential growth term of degradation (parameterized by b), exponential recovery which depends on the social system state and parameter w, and an external shock ξ. The equation of social capacity dynamics Ω is characterized by a logistic replenishment function term, which depends on the physical deficit state by parameter c_1, a Hill type function representing the depletion of social capacity parameterized by r, n and β, and an external shock multiplied by the impact factor c_2. Simulation results using synthetic data showed that even without external shocks with severe intensity, a series of small but repetitive shocks may tip the system over to a stable undesirable state [31]. While this model was limited to the theoretical discussion of the model and lacked empirical validation, [314] applied the model to the context of water systems, and evaluated the resilience of water systems of various cities around the world. The model parameters were assigned for each city based on a capital portfolio approach that quantifies various urban characteristics [315].

In this study, we modify this model by relaxing the assumption that physical recovery is deterministically dependent on social systems recovery, and to allow the socio-physical system to have no functional coupling. To adjust the model to meet our objective, we reformulate the model by introducing an additional model parameter q, that represents physical system recovery which is independent of social system recovery. Moreover, to fit the dynamics model to data from Hurricane Maria, we remove the repetitive shock sequences ξ, and represent the shock impact using the initial disruption values of Φ and Ω, denoted as Φ_0 and Ω_0, respectively. To simplify the dynamics of the model, and to obtain better convergence probabilities in the estimation of model parameters, we fix $n = 1$. Moreover, we study the socio-physical recovery dynamics for each region $\mathrm{i} = \{1, 2, \ldots, I\}$. Thus, the full model in this study is as follows:

$$\frac{d\Phi_{\mathrm{i}}}{dt} = (1-\Phi_{\mathrm{i}})b_{\mathrm{i}} - (w_{\mathrm{i}}\Omega_{\mathrm{i}} + q_{\mathrm{i}})\Phi_{\mathrm{i}} \tag{4.3}$$

$$\frac{d\Omega_{\mathrm{i}}}{dt} = (1-c_{\mathrm{i}}\Phi_{\mathrm{i}})\Omega_{\mathrm{i}}(1-\Omega_{\mathrm{i}}) - r_{\mathrm{i}}\frac{\Omega_{\mathrm{i}}}{\Omega_{\mathrm{i}}+\beta_{\mathrm{i}}} \tag{4.4}$$

$$\mathrm{i} = 1, 2, 3, ..., I \tag{4.5}$$

where, initial conditions are given by $\Phi_{\mathrm{i}}(0) = \Phi_0^{\mathrm{i}}$, and $\Omega_{\mathrm{i}}(0) = \Omega_0^{\mathrm{i}}$, which are also model parameters. Using this formulation, we are able to estimate and analyze the regional heterogeneity in the system dynamics and model parameters. The social dynamics in each region will be analyzed for multiple POI categories $c = \{1, 2, \ldots, C\}$ as well, to understand the intra-regional heterogeneity in the model parameters. The descriptions of the model parameters are summarized in Table S3. It is important to note that when $c_{\mathrm{i}} = 0$, recovery of social systems are independent of physical deficit states, and when $w_{\mathrm{i}} = 0$, physical recovery occurs independently of social system states. A system where $c_{\mathrm{i}} = w_{\mathrm{i}} = 0$ denotes a completely decoupled system, which serves as our null hypothesis model.

Estimation of Model Parameters

To estimate the model parameters $\Theta_\mathrm{i} = \{\Omega_0^\mathrm{i}, \Phi_0^\mathrm{i}, c_\mathrm{i}, r_\mathrm{i}, \beta_\mathrm{i}, w_\mathrm{i}, b_\mathrm{i}, q_\mathrm{i}\}$, we apply a Hamiltonian Monte Carlo (HMC) sampling approach and obtain the maximum a posteriori (MAP) estimate using empirical observations of social and physical systems collected during the recovery phase after Hurricane Maria. Given the discrete time series data of social and physical systems in region i, ω_t^i and ϕ_t^i, respectively, and the simulated trajectories of social and physical systems of region i, $\Omega(\Theta_\mathrm{i})$ and $\Phi(\Theta_\mathrm{i})$, respectively, the likelihood is computed using a Gaussian distribution:

$$p(\Omega_t(\Theta_\mathrm{i})) \sim \mathcal{N}(\omega_t^\mathrm{i}, \sigma_\mathrm{i}^2) \tag{4.6}$$

$$p(\Phi_t(\Theta_\mathrm{i})) \sim \mathcal{N}(\phi_t^\mathrm{i}, \sigma_\mathrm{i}^2) \tag{4.7}$$

$$c_\mathrm{i}, r_\mathrm{i}, \beta_\mathrm{i}, w_\mathrm{i}, b_\mathrm{i}, q_\mathrm{i}, \sigma_\mathrm{i} \sim Half-Cauchy(0, 2.5) \tag{4.8}$$

$$\Omega_0^\mathrm{i}, \Phi_0^\mathrm{i} \sim Uniform(0,1) \tag{4.9}$$

To allow flexibility, half-Cauchy priors with scale of 2.5 are assigned to the model parameters, including the standard deviation σ of the likelihood function. The HMC sampler for this MAP estimation is constructed using `stan`, a Bayesian computational framework. The sampler drew 5000 samples for each model parameter, and was made sure that the sampler had good mixing by observing that $\hat{R}$ was equal to 1.0. The MAP estimate of the model parameters were obtained by taking the mode of the posterior distribution, using Kernel density estimation.

To evaluate the model fit, the Pearson correlation between the simulated and observed system dynamics was computed. Given two time series vectors x and y, the Pearson correlation coefficient ρ_{xy} is computed by the following equation:

$$\rho_{xy} = \frac{cov(x,y)}{\sigma(x)\sigma(y)} \tag{4.10}$$

where, $cov(x,y)$ is the covariance between x and y, and $\sigma(x)$ denotes the standard deviation of x.

Furthermore, to interpret the model parameters, multivariate regression was performed on the model parameters using the socio-economic variables listed in Table 4.1. We investigate which socio-economic variable explains the heterogeneity in the estimated model parameters by selecting

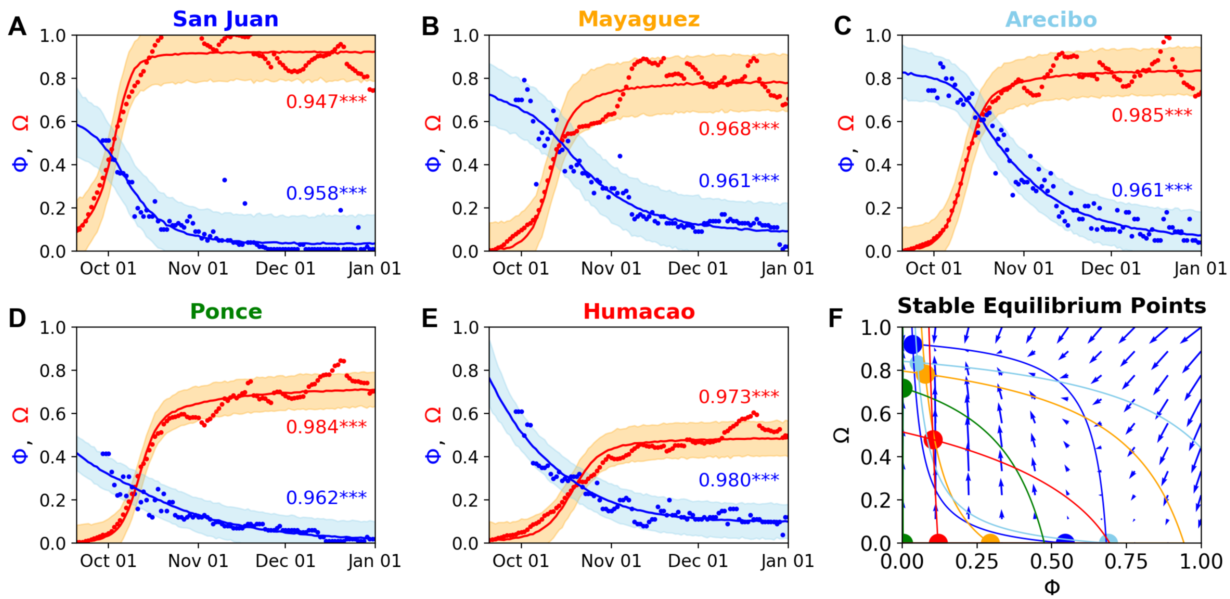

Figure 4.2. Estimation of regional socio-physical recovery dynamics. **A-E.** Observed (dotted) and estimated (solid curves) social (orange) and physical (skyblue) recovery dynamics in each region, using the calibrated socio-physical system dynamics model. The shaded ranges around the simulated dynamics show the 95% Bayesian credible interval. In addition to the strong and significant correlation shown in Table S4, the plots qualitatively show that the system dynamics model is able to replicate the observed dynamics. **F.** Equilibrium analysis of the five regions. Each region has 2 stable equilibrium points (color filled circles: desirable (high Ω, low Φ) and undesirable ($\Omega = 0$)). Direction field for San Juan are shown (arrows).

the variable with the highest statistical significance in the regression analysis. All of the model parameters as well as the socio-economic variables were log transformed prior to the multivariate regression to assure positivity.

These empirical observations on the dynamic states of social and physical systems are useful in identifying the disparities across the five regions in disaster recovery [316]. Although such observations could be informative for monitoring system states, analyzing them in isolation neglects the functional interdependent relationships that exist between the urban social and physical systems. Examples of functional interdependencies include: dependence of water networks' (physical systems) recovery on local and federal agencies (social systems), operation of local businesses (social systems) depending on power-grid infrastructure (physical systems), and communities depending on recovery of critical services. In order to quantitatively capture the functional coupling between the social and physical systems, the empirical observations are integrated with a dynamic model of coupled socio-physical systems.

The coupled dynamics model of socio-physical systems, originally proposed by Klammler et al. [31], is composed of two coupled differential equations. This model is applied due to its high similarity with empirical observations, especially the logistic recovery curve of social systems (Figure 4.1C) and exponential recovery curve of physical systems (Figure 4.1D). In this study, we revised the model by including an additional parameter q in Equation (1) to relax the assumption that the recovery of physical systems deterministically depend on social systems recovery; the second term $-(w\Omega+q)\Phi$ is the general form of the original $-w\Phi\Omega$ term. Among the model parameters $\Theta = \{\Omega_0, \Phi_0, c, r, \beta, w, b, q\}$, c and w dictate the coupling strength among the socio-physical systems, and completely decoupled urban systems can be characterized with $c = w = 0$. Descriptions of the model parameters are listed in Table S3. The model parameters were calibrated to the data in the five regions using Hamiltonian Monte Carlo (HMC) sampling methodology and maximum a posteriori (MAP) estimation. Figure 4.2 A-E show the observed social and physical recovery dynamics (in dotted lines) against the calibrated social and physical simulation dynamics (in solid lines), colored in orange and blue, respectively, for each region in Puerto Rico. The plots show the high reproducibility of the socio-physical recovery dynamics model, with high Pearson correlation (all higher than $R = 0.9$) between the data and the model. The estimated model parameter values (mean and 95% credible intervals) for the five regions as well as for different point-of-interest categories are shown in Table S4. The generalizability of the socio-physical dynamics model was evaluated via testing on recovery data of different point-of-interest (POI) categories (Figure 4.3), including education, medical, construction, automotive, grocery, and other stores. The fitting results in Figure 4.4 show that the socio-physical dynamics model is capable of evaluating industry level recovery. The stability of the socio-physical systems in the five regions was analyzed. Figure 4.2F shows the phase plane of the socio-physical systems. The stable equilibrium points (filled circles), null-clines (solid lines), and direction field (arrows; only for San Juan is shown) are shown in the diagram.

The socio-physical systems in the five regions each have 2 stable equilibrium points, 1 being a desirable equilibrium (high social recovery Ω, low physical service deficit Φ), and 1 being an

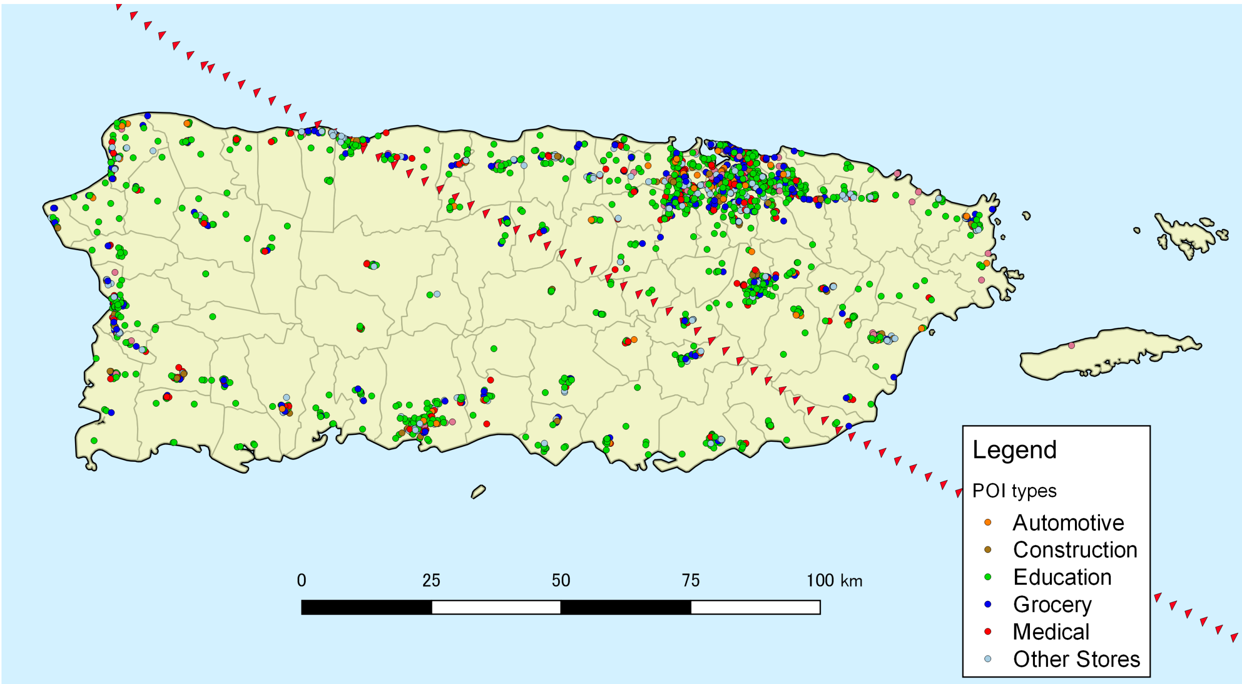

Figure 4.3. Location and categories of POIs in Puerto Rico used in the analysis.

undesirable equilibrium ($\Omega = 0$). The desirable equilibrium state of Humacao (red) in particular, is $\Omega \sim 0.5$ and $\Phi \sim 0.13$, which highlights the long-term chronic deficit compared to other regions.

4.1.3 Urban Scale and Socio-Physical Interdependencies

The coupled urban socio-physical model and the estimated parameters allow us to further understand the regional heterogeneity of characteristics in Puerto Rico. Among the model parameters shown in Figure 4.5A, c and w govern the strength of interdependencies that exist across the social and physical systems (i.e. "coupling parameters"). Parameter c ("***dependence***") controls to what extent physical service deficit slows down the recovery of social systems. Larger *dependence* indicates that social systems are highly dependent on the recovery of physical systems, lacking self-reliance. Parameter w ("***efficiency***") controls how efficiently the social systems are able to restore damaged physical systems. Larger *efficiency* indicates higher recovery capacity of social systems. Figure 4.5B shows the parameters c, w of the five regions. The estimated parameters suggest a trade-off relationship between efficiency w and dependence c, where San Juan (blue) (most populated, higher average income) have high recovery efficiency but the social systems have

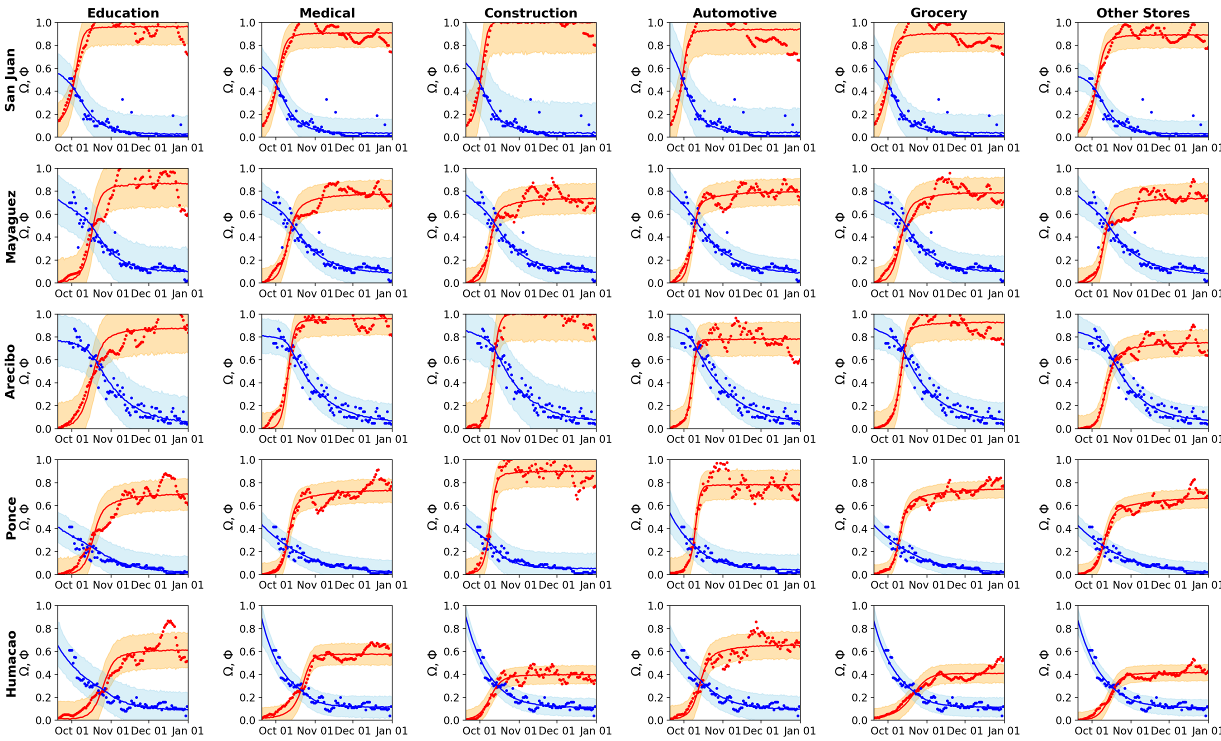

Figure 4.4. Observed (dotted) and estimated (solid curves) social (orange) and physical (skyblue) recovery dynamics in each region for different POI types, using the calibrated socio-physical system dynamics model. The shaded ranges around the simulated dynamics show the 95% Bayesian credible interval.

high dependence on the physical systems, and on the other hand, Humacao (red) (less populated) has less recovery efficiency but are more self-reliant. Arecibo (skyblue) and Mayaguez (orange) (intermediate population density) are placed in between San Juan and Arecibo regions. Although Ponce (green) had less recovery efficiency, its social systems had high dependence on physical systems. The implications of these coupling parameters on the resilience of the regions are further investigated and discussed in the following section (Figure 4.6).

To further interpret the estimated model parameters, multivariate analysis was conducted on the model parameters of the POI types in the five regions Θ using socio-economic variables, including the total number of housing damage rates, mean income, and gross regional income (GRI) of each region, shown in Table 4.1. As a result, it was found that $\log_{10}$(GRI) had relatively weak but statistically significant correlation with model parameters (c, r, w), Panels C-F in Figure 4.5 show the significant correlation (weak scaling) between the model parameters $c, r, w, \frac{q}{w}$ and GRI.

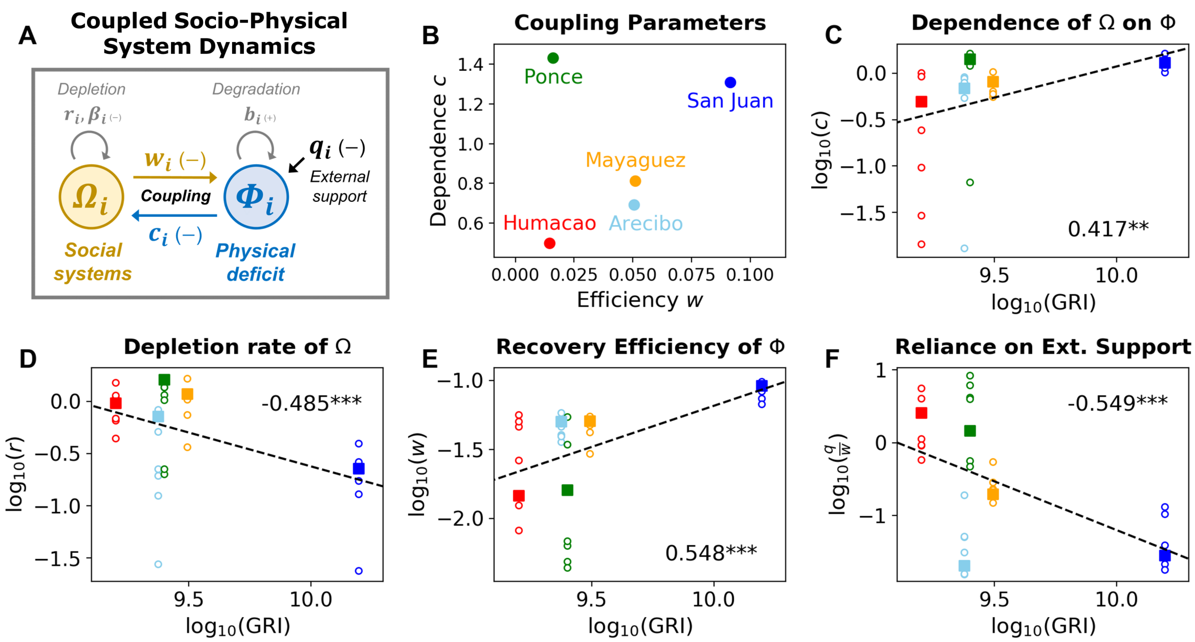

Figure 4.5. Regional differences in system dynamics model parameters. **A.** Setup of the coupled socio-physical system dynamics model and the model parameters. **B.** Estimated coupling parameter values for the five regions suggest a trade-off relationship between efficiency in recovery (w), and dependence on physical infrastructure systems (c). **C-F.** Correlation between the estimated model parameters ($c, r, w, \frac{q}{w}$) and the gross regional income (GRI) in log-log plot. Colors correspond to the five regions in Figure 4.1B, and the dotted black line shows the linear regression of the logged variables. The Pearson correlation coefficient is shown in the bottom corner of each plot, with stars indicating its statistical significance (***: $p < 0.01$, **:$p < 0.05$, *:$p < 0.1$). Significant correlation was observed, indicating that regions experience different recovery dynamics based on their GRI.

The color-filled square plots show the parameters for the aggregated regional dynamics, and open circles show the estimated parameters for each POI category. The strong positive correlation between GRI and c, and between GNI and w indicate that regions with more population and income are more efficient in recovery, but also more dependent on physical systems. This shows that the bi-directional dependencies between social and physical systems grow stronger as cities become larger and wealthier. This supports our hypothesis that larger urban systems are embedded within more complex interdependencies between social and physical systems. This also agrees with the analysis in Padowski et al. [317] on water systems in several cities in US and Africa, which showed how managers of larger cities need to overcome the lack of local resources by constructing more complex social and physical frameworks. Such wealthier regions also are affected by lower depletion rates of social systems (r), which suggest better maintenance capacities. Moreover, these regions require less external support for physical recovery, in relative terms with respect to their internal recovery efficiency ($\frac{q}{w}$).

4.2 Interdependencies and Resilience

To measure the resilience of the coupled urban socio-physical systems defined by the systems dynamics model and estimated model parameters, we simulate the longitudinal dynamics under various disaster scenarios. Based on the literature, we assume that hurricane occurrence follow a Poisson process with rate of λ [318]. Moreover, we assume that the intensity of hurricanes follow an exponential distribution with mean α, as assumed in previous modeling literature [31]. According to the Tropical Meteorology Project at Colorado State University and the GeoGraphics Laboratory at Bridgewater State University, Puerto Rico is predicted to have a 8% probability of 1 or more major (Category 3-4-5 on the Saffir-Simpson scale) hurricanes tracking within 50 miles of the island in a given year [319]. We convert this value to parameters λ and α using the following logic. Parameter λ is calibrated based on the frequency of hurricane occurrence. The cumulative probability function of an exponential distribution with mean α is given by $F(x;\alpha) = 1 - \mathrm{e}^{\alpha x}$ when $x > 0$. Thus, the probability of the shock exceeding x is given by $p = 1 - F(x;\alpha) = \mathrm{e}^{-\alpha x}$. Thus, if we assume that a major hurricane has an intensity of 1, in order to have probability p, we set $\alpha = -\log p$. We assume that hurricanes only occur during the hurricane season (June 1st $\sim$ November 30th), and 500 simulations (each simulating over a 10 year time horizon) were run for each region.

Using this simulation framework, we investigate whether by reforming the strengths of interdependencies between the social and physical systems (model parameters c, w), the resilience of these regions in Puerto Rico could be improved. To address this question, regional model parameters on efficiency w and dependence c are varied within a range of parameters ($0 \leq w \leq 0.1$, $0 \leq c \leq 1.5$), while keeping all of the other model parameters (i.e., r, β, q, b) the same for each region. In each simulation run, the collapse time (timestep when $\Omega = 0$) was recorded to represent the resilience

(= ability to build back after shocks) of the region. Similar to the aforementioned framework, the impacts of reforming coupling parameters on the regional resilience (this time, using mean collapse time) are simulated. Panels B-F in Figure 4.6 show the resilience of the five regions under different strengths of socio-physical interdependencies. The black crosses indicate the current situation of socio-physical interdependencies in the regions. Warmer colors indicate longer collapse times (more resilient), while colder colors indicate quicker collapse times (less resilient). In all of the regions, we observe that improving recovery efficiency w and lowering the dependence on physical systems c lead to resilient urban systems. However, note that the marginal improvements of the two levers vary for different regions. While San Juan, Mayaguez, and Arecibo could gain more resilience by shifting in both directions (right-wards and down-wards), Humacao may yield little marginal gain by strengthening its physical efficiency (right-wards). Rather, Humacao should further decrease its dependence on physical infrastructure and strive towards a self-sustainable and decentralized system to improve its resilience to future shocks. Reforming the socio-physical interdependencies is one policy lever that can be implemented to enhance resilience. Other policies include improving the robustness of physical infrastructure, which can be also simulated with our model by applying a buffer that reduces the magnitude of shocks when they are below a certain threshold. Improving the robustness of infrastructure is also shown to be effective in improving the resilience of these regions (Figure 4.7), which agrees with current practices (e.g., building structures such as sea walls, water drainage systems). To enhance the resilience of urban systems to future shocks, it is crucial to not only focus on the structural improvements but also to maintain self-reliance of social systems, especially in urban areas.

In many OECD countries, reliable critical services (e.g., water, sewage, power, transport) are available on demand, provided by robust connectivity to efficiently (and often centrally) managed critical infrastructure systems. On the other hand, cities in less developed regions and countries have less reliable provision of such services, thus, citizens often utilize a wide array of adaptive strategies to cope and to overcome service deficits of critical infrastructure systems [314], [320]. For example, household interviews have found that citizens in the Humacao region, which were most heavily affected by Hurricane Maria, supported eachother in the absence of critical physical infrastructure services (e.g., "... Her neighbors and the community bakery allow her to store cold food in their refrigerators.") [321]. In such regions, households use reserves (e.g., pre-positioning

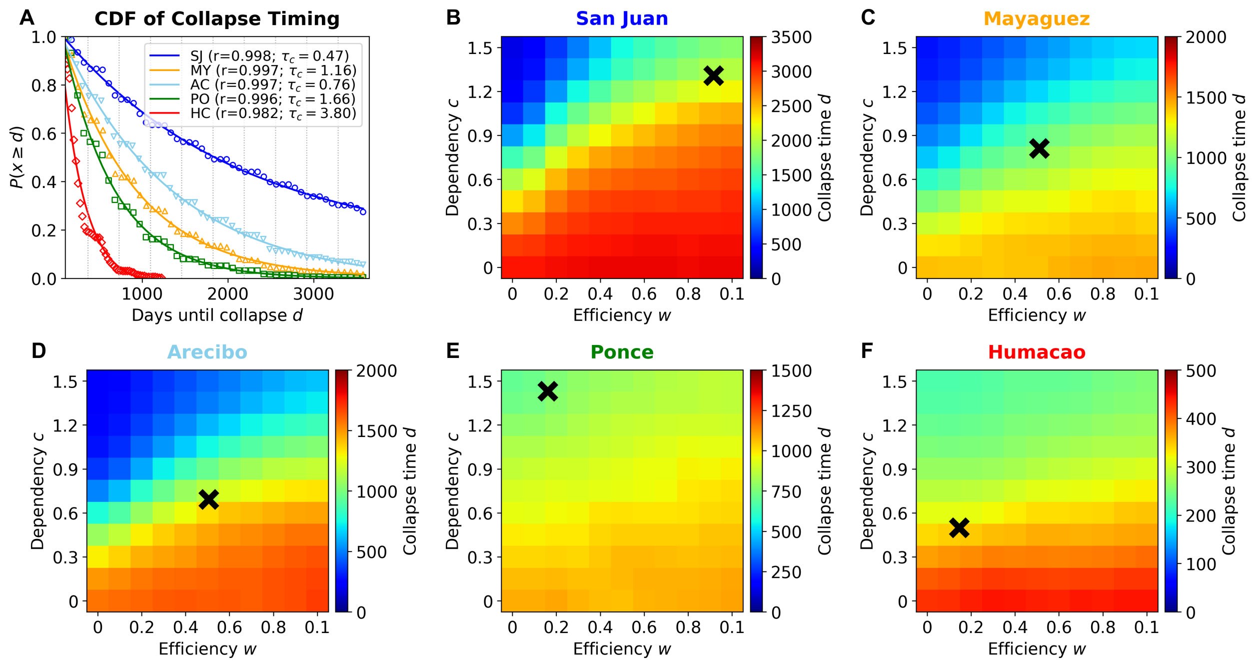

Figure 4.6. Resilience implications of socio-physical interdependencies. **A.** Cumulative density functions of collapse timing across the shock sequence simulations in the five regions. San Juan and Humacao are shown to be the most and least resilient, respectively. **B-F.** Resilience implications of reforming the interdependencies (efficiency *w* and dependence *c*) between the social and physical systems. In all regions, increasing efficiency and lowering the dependence on physical systems benefit regional resilience, although the marginal effects vary across regions. Note that the color bar scales vary across panels.

critical supplies or boarding homes) or seek assistance from alternate providers (sharing generators; purchasing bottled water) [315]. As more cities face urbanization and robust physical infrastructure are built, the dependence of social entities (e.g., households, businesses) on such physical systems will increase. As suggested in San Juan's case in this study, high robustness and efficiency of physical infrastructure could lead to changes in people's behavioral patterns, putting higher dependence on physical infrastructure, similar to the citizens in OECD countries. The exception seems to be Ponce, which had both high dependence and low efficiency (Figure 4.5A). This was because Ponce was not in the direct path of the hurricane, and the region was given more financial support from federal agencies such as FEMA [322]. However, with increasing frequency and intensity of climate related hazards, recent disasters have shown the risk of over-reliance on physical systems, as no engineered system is fail-proof [98]. The simulation results obtained in this study reinforce this point, based on empirical data and modeling, that increasing dependency on physical systems decreases the resilience of communities. Therefore, the proposition of this study – the importance of maintaining self-reliance of social systems – will become key as cities simultaneously face rapid urbanization and climate change.

Enhancing community-level resilience requires trade offs at multiple spatial and temporal scales [323], [324] between security at household scales to sustainability at larger scales. Similarly, trade offs need to be made between increasing robustness of the physical (engineered) infrastructures or decentralizing their management. Adaptive capacity required to cope with chronic disturbances and major shocks requires balancing diverse ”capitals” (see [315]), which are unequally distributed within and among urban communities in a region. Thus, optimizing interdependencies and resource flows among affected communities is another path to enhancing regional resilience.

Another challenge in building community resilience is that persistent inequalities exist in adaptive capacity within and between urban communities [315]. Poorest and marginalized communities suffer the most during disasters, and lacking adaptive capacity or access to external subsidies, recover the last , or may not recover at all. Thus, regional community resilience must ensure equitable access to reliable critical services [325].

The insights presented in this study could be applied in policy making to provide more resilient urban systems and favorable recovery outcomes after disasters [326]. Together with detailed estimations of costs to implement various policy levers (e.g., decreasing household dependence by installing power generators in rural areas, improving connectivity of social networks enabling more social capital in urban areas), policy makers will be able to perform cost-benefit analysis for enhancing regional resilience. One important next step in this line of research is to operationalize the policy levers by quantitatively connecting them with changes to the model parameters. This could be achieved by further downscaling the model and using survey data that asks households and communities on their level of social bonding and reliance on centralized infrastructure during diaster events. As discussed in this paper, the extent of self-reliance should be carefully weighed based on the type of community (urban versus rural), the starting points of the physical and social networks, the socio-demographics and the local institutional rules that govern the recovery. The marginal benefit from an improvement in social networks versus physical networks vary across urban and rural areas. For instance in Humacao, we observe that if the physical networks are not improved from their current situation, improvements in social networks can only result in small improvements in the collapse time (Figure 4.6F). A key finding is that rural communities need to have a base level of physical network efficiency for them to be resilient.

By taking into account deep uncertainties in future climate conditions, macroeconomic trends, and demographic changes, a robust decision making framework can be applied to the coupled socio-physical dynamics model to make robust policy decisions [327]. Although the model was evaluated on data collected from Puerto Rico after Hurricane Maria, the model is generalizable to any type of disaster in any given region or city. Recently, data collected from mobile devices have been increasingly used for post-disaster assessment of population dynamics, which can be used to capture the recovery of social systems [45], [155], [313]. Applying the coupled socio-physical dynamics model to other regions of various characteristics could generate insights on its resilience in future climate scenarios.

Several limitations in the proposed approach and results open up various research opportunities. First, investigation at a finer-spatial resolution, for example on a county or census tract scale, could provide more detailed results and estimations that could be utilized by decision makers in municipal governments. However, down-scaling the analysis could bias the estimations with data sparsity. A more robust model parameter estimation method could be a topic worthy of investigation for future studies. A finer grained analysis could allow a more detail analysis on socio-demographic inequalities and equitable resilience to disasters [179], [328], [329]. On the other hand, previous studies have focused on larger cities, often with several million households [314]. Extending this data-model approach towards both microscopic and macroscopic directions would be an interesting next step. Moreover, the resilience simulations assumed that changing the coupling parameters do not affect the other model parameters of social and physical systems. Further investigation relaxing this assumption is needed to obtain a full picture of the resilience implications. Second, the data on the recovery of physical systems on the regional scale used to calibrate the model was limited to just water service deficit, due to the lack of available data in Puerto Rico after Hurricane Maria for the other types of infrastructure systems. Collection of data for other physical infrastructure including power, gas, transportation systems, more specifically a regionally disaggregated time series data on the service deficit could allow us to extend the analysis to a multi-layer physical network. Third, a scaling relationship between the estimated model parameters and regional gross income can be found in Figure 4.5. Bettencourt et al. [330] have shown that the generalizability of scaling patterns by testing various urban metrics including total wages, total electricity consumption, and total road length. Similarly, the results should be examined further by using datasets of recovery after other events in different cities, regions, and across different disaster types.

The complexity of cities are increasing due to rapid urbanization around the world. Such interdependencies between social and physical systems could amplify the impact of disruptions caused by natural hazards, posing a threat to cities within an impacted region as we face climate change. In this study, we proposed a data-driven modeling framework to infer the socio-physical interdependencies in urban systems and their effects on regional-scale disaster recovery and resilience. Large-scale mobility data collected from mobile phone users in Puerto Rico during Hurricane Maria were used to calibrate the model across five regions within the island. Estimation results indicated that as cities grow in scale and expand their centralized infrastructure systems, the recovery efficiency of critical services improves, however, curtails the self-reliance of socio-economic systems during crises, posing a trade-off in urban management. Further longitudinal simulation results using hypothetical future climate scenarios showed that maintaining self-reliance among social systems could be key in developing resilient urban socio-physical systems for cities facing rapid urban growth. Economic expansion and population growth in larger cities increase community demands for critical services based on resources drawn from increasing regional scales. Migration from smaller cities to larger cities adversely impacts the socioeconomic well being of smaller communities, while overwhelming the existing critical infrastructure, a problem most evident in growth of informal settlements in mega-cities in Asia, Africa, and South America. Thus, evaluating and managing community resilience at regional scales is of increasing importance. These results encourage a paradigm shift in urban planning – to carefully assess the complex interdependencies between social and physical systems – to improve regional resilience of urban systems to future shocks.

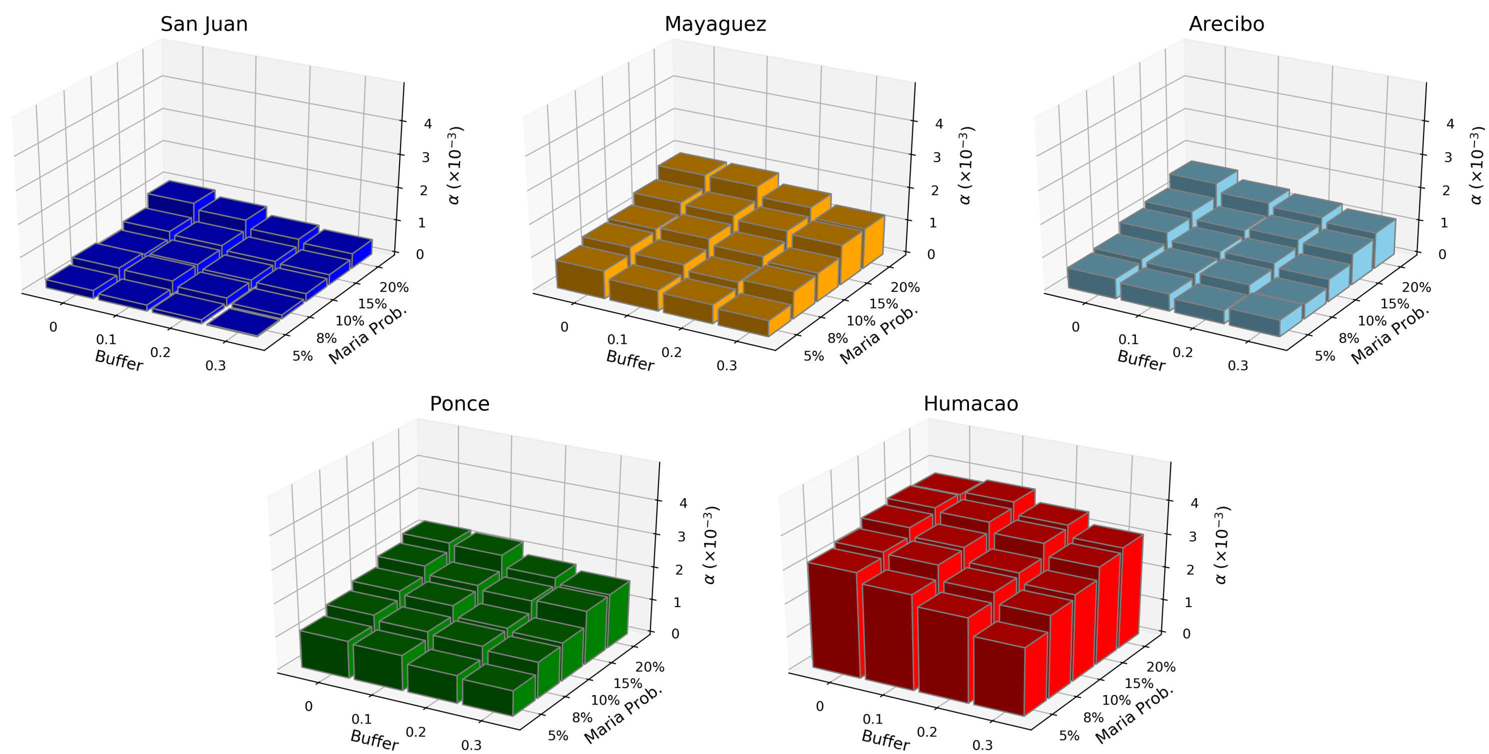

Figure 4.7. Effects of physical robustness on the resilience of the regions.

5. TOWARDS INTER-REGIONAL TRANSFERABILITY

The previous sections have used large-scale novel datasets to measure and model the post-disaster recovery dynamics of urban socio-physical systems, revealing significant heterogeneity in recovery trajectories across different regions due to their diverse socio-demographic and -economic characteristics. Such modeling techniques are shown to be successful in regions and disaster events where large amounts of human behavior data could be collected from mobile devices. One critical drawback of such data-driven modeling techniques lie in their inability to model scenarios where data are sparse or not available, which is common in disaster events in low-income regions or developing countries where mobile phone (or smartphone) penetration rates are relatively low. To overcome this challenge, in this Section, we develop supplemental methods to transfer model-derived predictions and insights across different regions.

5.1 Inter-Regional Translation of Places

In the urban computing field, large mobility datasets collected from mobile devices such as GPS trajectory data have allowed us to observe the dynamics of cities at an unprecedented spatio-temporal resolution and scale [331], [332]. Combined with recurrent neural network (RNN) models, recent studies have made significant progress in quantifying the functions of places in an analogical manner to word embeddings in the natural language processing field (e.g. [333]–[337]). Such high dimensional representations of places ("*place embeddings*") have been shown to effectively capture the complex functions of places within cities [338], and have been applied in various downstream tasks in urban planning, such as identifying spatial clusters with respect to functionality [339], choosing sites for opening new stores [340], and predicting where users will go to in future timesteps [341].

However, such studies have been limited to understanding the place representations of cities in an individual manner, and has lacked an inter-city perspective. Because the representations of different cities were not generated in a common vector space, it has been difficult to transfer insights based on place representations from one city to another, let alone transferring various phenomena (e.g. evacuation after disasters) across cities. If we could map place representations learned in one city to another, in the same way we translate words to words across different languages, we would be able to utilize knowledge accumulated in other cities to perform better analyses and predictions. For example, we may be able to predict locations that could become evacuation shelters in future disasters in city ψ, by translating the representations of places that became evacuation shelters in a past disaster in city ϕ to city ψ.

In this study, we attempt to bridge these gaps by treating *cities* and *languages* analogously, which extends the analogies made by previous studies ("places and words" and "trip sequences and sentences"). More specifically, our goal is to develop methods that can map places from different cities with similar meanings closely on a common vector space via an operation analogous to *translation*. We propose models that extend the methods developed in the natural language processing field for unsupervised machine language translation tasks [342]–[344]. Figure 5.1 shows an illustration of our problem setting and approach. Given representations of places X_ϕ, X_ψ in cities ϕ and ψ, directly overlaying X_ϕ on X_ψ would be uninformative, since the vector spaces are not aligned with eachother. Using methods to translate representations, we obtain $\tilde{X}_\phi = f(X_\phi)$ which is aligned to the space of city ψ, allowing us to compare representations of places in different cities for further analyses and predictions.

The model performances are tested using real world data collected from mobile phones in 2 cities in Japan, and are validated using landuse data. Results show that our methods are able to accurately translate place representations from one city to another.

The main contributions of this section are as follows:

- We propose and test methods to translate place representations across cities, which can map places from different cities with similar functions closely together.
- We verify that our method can successfully translate place representations, using real mobility world data from 2 cities.
- We make the translated place representations publicly available for researchers and practitioners.

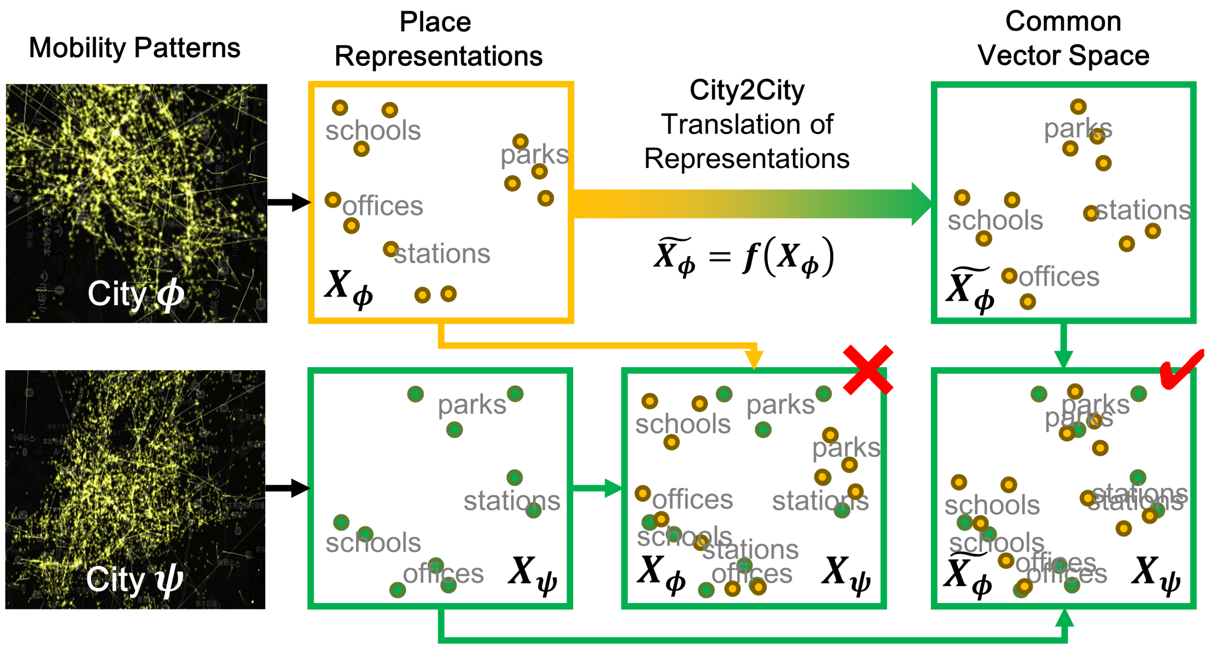

Figure 5.1. Illustration of our problem setting. Given representations of places in 2 cities (ϕ, ψ) generated from the observed mobility patterns, our problem is to translate the place representations of city ϕ to the vector space of city ψ, so that similar places from the two cities become mapped closely in the common vector space, as shown in the bottom right panel.

Definition 1 (Human Mobility Patterns)

Sequences of users' staypoint locations with timestamps are extracted from mobility data using methods explained in Section 3.1. The usual human mobility patterns of a city c is the set of all staypoint sequences of individuals whose home location belongs to city c.

Definition 2 (Place Representations)

A city c is divided into disjoint cells by grid sizes of r meters. We will call each cell as a place i, and denote its representation as $\mathbf{x}_\mathrm{i}^c$, which is a d-dimensional vector. Place representations $\mathbf{x}_\mathrm{i}^c$ are learned from the human mobility patterns observed in city c, using methods explained in Section 3.2. Representations of all places are stacked as a $(d \times n_c)$ matrix $\mathbf{X}_c$, where n_c is the number of places in city c.

Problem Definition (Translation of Place Representations)

Place representations $\mathbf{X}_c$ are learned for each city c from the observed mobility patterns. Thus, for different cities, the vector spaces are not shared. Translating place representations from city ϕ to city ψ is equivalent to finding a mapping function f that aligns the two vector spaces, i.e., $\mathbf{X}_\psi \approx \tilde{\mathbf{X}_\phi} = f(\mathbf{X}_\phi)$. Methods used to translate place representations are explained in Section 3.3.

5.1.1 Methodology: Unsupervised machine translation of places

Extracting Human Mobility Patterns

We first extract human mobility pattern datasets for each city, from the location data observed from mobile phones. Each observation of the location data contains the user ID, timestamp, longitude and latitude. More details of the mobile phone data that we use in this study are explained in Section 4.1.1. Our goal is to extract users' sequences of staypoint locations from the observations. We achieve this by setting two threshold parameters; one spatial threshold and one temporal threshold. To cope with noisy location observations (e.g. spatial errors in GPS data), we perform mean shift clustering to estimate the true location for each observation, as described in previous studies (e.g. [226], [227]). For each user, we read their location data in time order, and search for locations where the user has stayed within the distance defined by the spatial threshold parameter for a duration longer than the time defined by the temporal threshold parameter. We use 1000 meters as the spatial threshold, and 30 minutes as the temporal threshold in this study. As a result, we are able to obtain sequences of staypoint locations for each user, which will be used to generate place representations using methods explained in the following section.

Generating Place Representations

To obtain the representations of places in a city, we solve a self-supervised task in which an LSTM RNN model is trained to predict the next staypoint of a user using mobility data, which is analogous to language models which are trained to predict the next word in a sentence. After training an LSTM RNN model using staypoint sequences of a city c, we extract and stack the embedding layer's parameters of the size $n_c \times d$, and define it as the matrix of place representations

$\mathbf{X}_c$. We refer to this place representation learning architecture as "`MobLSTM`" in the following sections. Specific model hyperparameter settings are explained in Section 4.2.1.

Translating Place Representations

Three approaches for translating place representations across cities are tested. The first approach is to jointly learn the place representations of places in both cities using a common `MobLSTM` architecture (Section 3.3.1). The second and third approaches learn place representations using `MobLSTM` separately for different cities, and then attempt to align them using an optimization method (Section 3.3.2), or adversarial training (Section 3.3.3).

Joint Learning Approach

In the first approach, we apply the `MobLSTM` model to the two cities together on the self-supervised next staypoint prediction task. We merge the mobility datasets of two cities into one, train the model over the merged data, and use the transposed embedding layer matrix of the size $d \times (n_\phi + n_\psi)$ as the representation matrix. The rationale behind this approach is that, representations of places with similar functions will be visited in a similar manner (e.g. time of day, day of week, after and before certain places) regardless of the city the places belong to. To let the model treat places of cities ϕ and ψ as equally as possible, we mask the candidates of ψ at the output when the next staypoint belongs to ϕ and vice versa, releasing the model from the burden of distinguishing between two cities. A previous study shows that this approach is effective in translating embeddings of one language to another in an unsupervised manner [345]. We refer to this translation method as "`Joint-MobLSTM`".

Procrustes Transformation Approach

The second approach applies the Procrustes transformation method, which is originally used in the supervised problem setting. Given place representations $\mathbf{X}_\psi$ and $\mathbf{X}_\phi$, and a dictionary of pairs of places which are ranked by their popularity (indicated by the superscript (i)), orthogonal Procrustes is applied to align them together into a common vector space by optimizing the following function:

$$R^* = \underset{R^T R = I}{\operatorname{argmin}} \sum_{\mathrm{i}=1}^{N} \left\| R X_{\phi}^{(\mathrm{i})} - X_{\psi}^{(\mathrm{i})} \right\|_F \tag{5.1}$$

where $\mathbf{R} \in \mathbb{R}^{d \times d}$, and $\left\| \cdot \right\|_F$ is the Frobenius norm. The solution gives the best rotational alignment of the two vector spaces. Although our original problem is in the unsupervised setting, we generate synthetic representation pairs by pairing up the top N visited places from both cities. We use $N = 500$ as the default number of place pairs, however we test its effect on translation performance in Section 4.4.4. We refer to this translation method as "`MobLSTM-P`".

Adversarial Training Approach

The Procrustes method requires a dictionary of pairs of places from the two cities that are expected to be mapped closely together, however, a fully unsupervised approach is shown to work better in some settings [343], [346]. The third approach uses adversarial training to learn the transition matrix R, which is then used for translating the representations learned via `MobLSTM` between the two cities. A similar approach as Conneau et al. [343] is taken here, where a model is trained the discriminate between representations randomly selected from $R\mathbf{X}_{\phi}$ and $\mathbf{X}_{\psi}$. R is then trained to prevent the discriminator from making accurate predictions [347]. The standard training procedure of deep adversarial networks is used for train the adversarial model [348]. We refer to this translation method as "`MobLSTM-Adv`".

5.1.2 Experimental Validation

In our experiments, we define the sizes of the places as $r = 1000m \times 1000m$ grid cells. Through the qualitative analysis of the place representations in Section 4.3.3, we confirm that this spatial scale is granular enough to be able to identify specific places. Moreover, the evacuation shelter analysis in Section 5 shows that the scale is informative enough to assist disaster relief officers in practice. We generated and translated representations of places (grid cells) instead of specific place of interests (POIs) that are specified in maps, because there are cases where places with no particular POI could have significant meanings to the people.

Table 5.1. Data statistics for the two cities

	Kumamoto	Okayama
# Users	94,053	119,349
# GPS staypoints	2,832,329	2,382,861
Data period	2016/2/1∼2/29	2018/6/1∼6/30
# places n_c	2565	2163

Mobile Phone Data

Yahoo Japan Corporation[1] collects location information of mobile phone app users in order to send relevant notifications and information to the users. The users in this study have accepted to provide their location information. The data are anonymized so that individuals cannot be specified, and personal information such as gender, age and occupation are unknown. Each GPS record consists of a user's unique ID (random character string), timestamp, longitude, and latitude. The data acquisition frequency of GPS locations changes according to the movement speed of the user to minimize the burden on the user's smartphone battery. If it is determined that the user is staying in a certain place for a long time, data is acquired at a relatively low frequency, and if it is determined that the user is moving, the data is acquired more frequently. The data has a sample rate of approximately 2% of the population, and past studies suggest that this sample rate is enough to grasp the macroscopic urban dynamics [160], [349]. Table 5.1 shows the statistics of the dataset collected for two cities (Kumamoto and Okayama), which are the cities that we focus on in this study. There are around 100,000 unique active users from both areas, and their location data were analyzed to extract their home locations and staypoint locations using methods in Section 3.1.

Landuse Data

To validate whether the generated and translated place representations correctly reflect the functionality of the places, we use the Urban Area Land Use Mesh Data[2] in the National Land Numerical Information Database[3] provided by the Ministry of Infrastructure, Land, and Transport

[1] ↑https://about.yahoo.co.jp/info/en/company/
[2] ↑http://nlftp.mlit.go.jp/ksj/gml/datalist/KsjTmplt-L03-b-u.html
[3] ↑http://nlftp.mlit.go.jp/ksj/

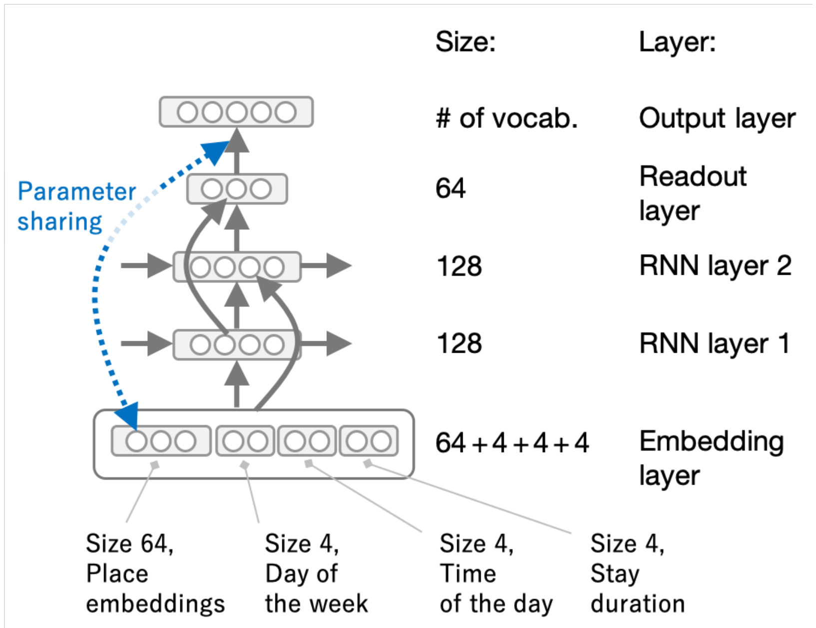

Figure 5.2. The overview of the LSTM RNN decoder/autoencoder

and Tourism of Japan. The dataset divides all urban areas of the entire country into $100m \times 100m$ grid cells, and assigns one category to each grid cell out of 17 options. The 17 options include farmland, residential area, business district, parks, forests, factories, public facilities, water body, open spaces, roads, railways, golf courses, etc. We aggregate these data into our spatial scale ($1000m \times 1000m$), thus for each place, we have a 17 dimensional vector where each element shows how many pixels of a specific land type exists in that place.

Model Hyperparameter Settings

To conduct the representation learning of places described in Section 3.2, we setup the model and input data as follows (Figure 5.2). The model consists of the embedding layer, LSTM RNN block, readout layer, and the output layer. While the main input of the model is a sequence of staypoints representing a user's movement, we added two supplementary values, which are the timestamp of when the user had entered that place and the duration time of the stay, to incorporate time-dependency of the users' behavior. The embeddings of staypoints were set to 96-dimensional vectors.

The timestamp and stay duration were converted to 8-dimensional and 4-dimensional vectors respectively, and the three vectors at each step were concatenated into a 108-dimensional vector. The LSTM RNN block scanning over the embedding sequence consists of two layers of the size 128, and the hidden vectors of both layers were fed into the readout layer of the size 96, which were then read by the output layer producing the probability distribution over staypoints for the next place prediction. The parameter matrix of the staypoint embedding was reused as the output layer's matrix to reduce the total number of parameters and make the training data usage more efficient. We applied dropout with the keep probability 0.7 to three points of the model: the embedding layer, readout layer, and output layer. We continued the training for 20 epochs, evaluated performance on the validation data at the end of each epoch, and used the embedding matrix of the best model for subsequent processing.

Comparative Methods

We first assess the quality of place representations generated by `MobLSTM` and `Joint-MobLSTM` in Section 5.1.3. Then, after clarifying that the generated representations accurately embed the functions of places in each city individually, we validate the performances of translation models `MobLSTM`, `Joint-MobLSTM`, `MobLSTM-Adv`, and `MobLSTM-P` in Section 5.1.3.

Evaluation Metrics

Two metrics are used to evaluate the performances of the translation methods. Given two sets of places, we measure the average mutual norm distance and average mutual cosine similarity of the place representations of those places.

`Average Mutual Norm Distance` (AMND). Given 2 place representations $x_{\mathrm{i}}, x_{\mathrm{j}} \in \mathbb{R}^d$, norm distance is defined as $\text{Norm-Dist}(\mathrm{i},\mathrm{j}) = \left\| x_{\mathrm{i}} - x_{\mathrm{j}} \right\|$. The average mutual norm distance between sets of places I and J is defined by the following:

$$s_{nd}(I,J) = \frac{1}{Z(I,J)} \sum_{\mathrm{i}\in I} \sum_{\mathrm{j}\in J;\mathrm{j}\neq\mathrm{i}} \text{Norm-Dist}(\mathrm{i},\mathrm{j}) \tag{5.2}$$

where $Z(I,J)$ is the number of unique combinations between the places in sets I and J.

`Average Mutual Cosine Similarity` (AMCS). Cosine similarity is a commonly used metric to measure the similarity between 2 place representations $x_{\rm i}$,$x_{\rm j} \in \mathbb{R}^d$, and is defined as:

$$\text{cos-sim}(\mathrm{i},\mathrm{j}) = \frac{x_{\rm i} \cdot x_{\rm j}}{||x_{\rm i}||\,||x_{\rm j}||} \tag{5.3}$$

We use the average mutual cosine similarity to measure the similarity between representations of two sets of places. Similar to the average mutual norm distance, average mutual cosine similarity between sets of places I and J is defined by the following:

$$s_{cs}(I,J) = \frac{1}{Z(I,J)} \sum_{\mathrm{i}\in I} \sum_{\mathrm{j}\in J;\mathrm{j}\neq \mathrm{i}} \text{cos-sim}(\mathrm{i},\mathrm{j}) \tag{5.4}$$

In both experiments (Sections 4.3.1 and 4.3.2), we show whether the results are statistically significant by comparing the performance metrics to random pairs of places generated by the same model. For example, to assess the quality of place representations of `MobLSTM` for business places in Kumamoto in Section 4.3.1, we compare the AMND between representations of pairs of business places in Kumamoto generated by `MobLSTM`, against the AMND between representations of pairs of business places and randomly selected non-business places in Kumamoto generated by `MobLSTM`. Similarly, for example, to validate the translation performance of `MobLSTM-P` for business places in Section 4.3.2, we compare the AMND between representations of pairs of business places in Kumamoto and Okayama translated by `MobLSTM-P`, against the AMND between representations of pairs of business places in Kumamoto and randomly selected non-business places in Okayama translated by `MobLSTM-P`. Similarity between random pairs are shown in Figures 5.3 and 5.4 as gray crosses (vertical line indicate error bars).

5.1.3 Results

Intra-city Validation of Place Representations

To validate whether the place representations were correctly generated (i.e. representations of places with the same functionality are mapped closely), we measured the AMND and AMCS

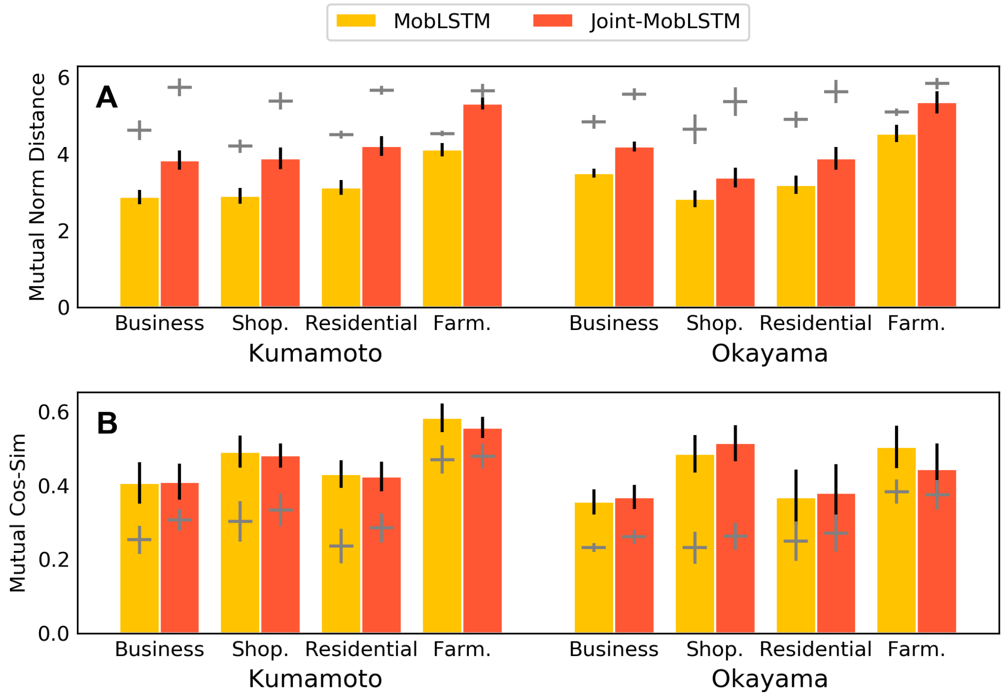

Figure 5.3. Intra-city validation results of business, shopping, residential and farmland areas in Kumamoto and Okayama with (A) AMND and (B) AMCS metrics. For both models, generated representations of all landuse types showed statistically significant intra-city similarity.

between places with the same landuse labels (business districts, shopping malls, residential areas, and farmland areas). We refer to this validation scheme as "intra-city validation". Figure 5.3 shows the validation results for both cities. Note that for norm distance (A), lower is better, and for cosine similarity (B), higher is better. All error bars (vertical lines) show the standard deviation of the results of 10 iterations. Results show that both models were able to generate accurate representations, and embedded places with same landuse labels closer to eachother than randomly selected pairs of places. `MobLSTM` and `Joint-MobLSTM` had comparable performances for generating place representations, however we see that `MobLSTM` had slightly better performances (lower norm distances and higher cosine similarity) for many of the landuse types. This result agrees with our intuition, because `MobLSTM` is able to allocate more dimensions in the parameter space to encode information related to places in their own city, whereas `Joint-MobLSTM` shares the parameter space across different cities, having less dimensions to encode the representations for each city.

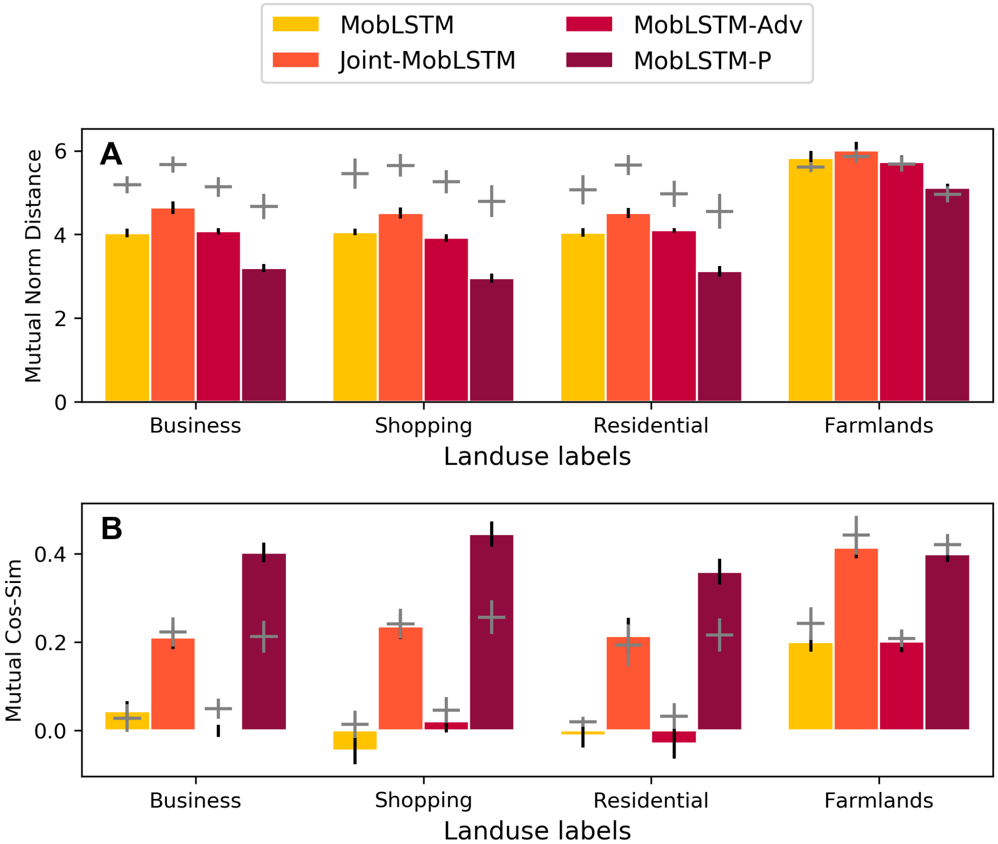

Figure 5.4. Inter-city translation results from Kumamoto to Okayama of business, shopping, residential and farmland areas with (A) AMND and (B) AMCS metrics. `MobLSTM-P` is able to translate place representations across Kumamoto and Okayama for business, shopping, and residential areas, but not for farmland areas where little human mobility patterns are observed.

Inter-city Translation of Place Representations

To quantitatively validate the performance of translating place representations across cities, we measured the AMND and AMCS between places with same landuse types across different cities (e.g. similarity between representations of places with shopping malls in Kumamoto and representations of places with shopping malls in Okayama). We refer to this validation scheme as "inter-city translation". Figure 5.4 shows the translation accuracy of all tested methods. Out of the four models, `MobLSTM` has had no translation operation, and in all landuse types the AMCS performance is worse than random, which confirms the negative example illustrated in Figure 5.1

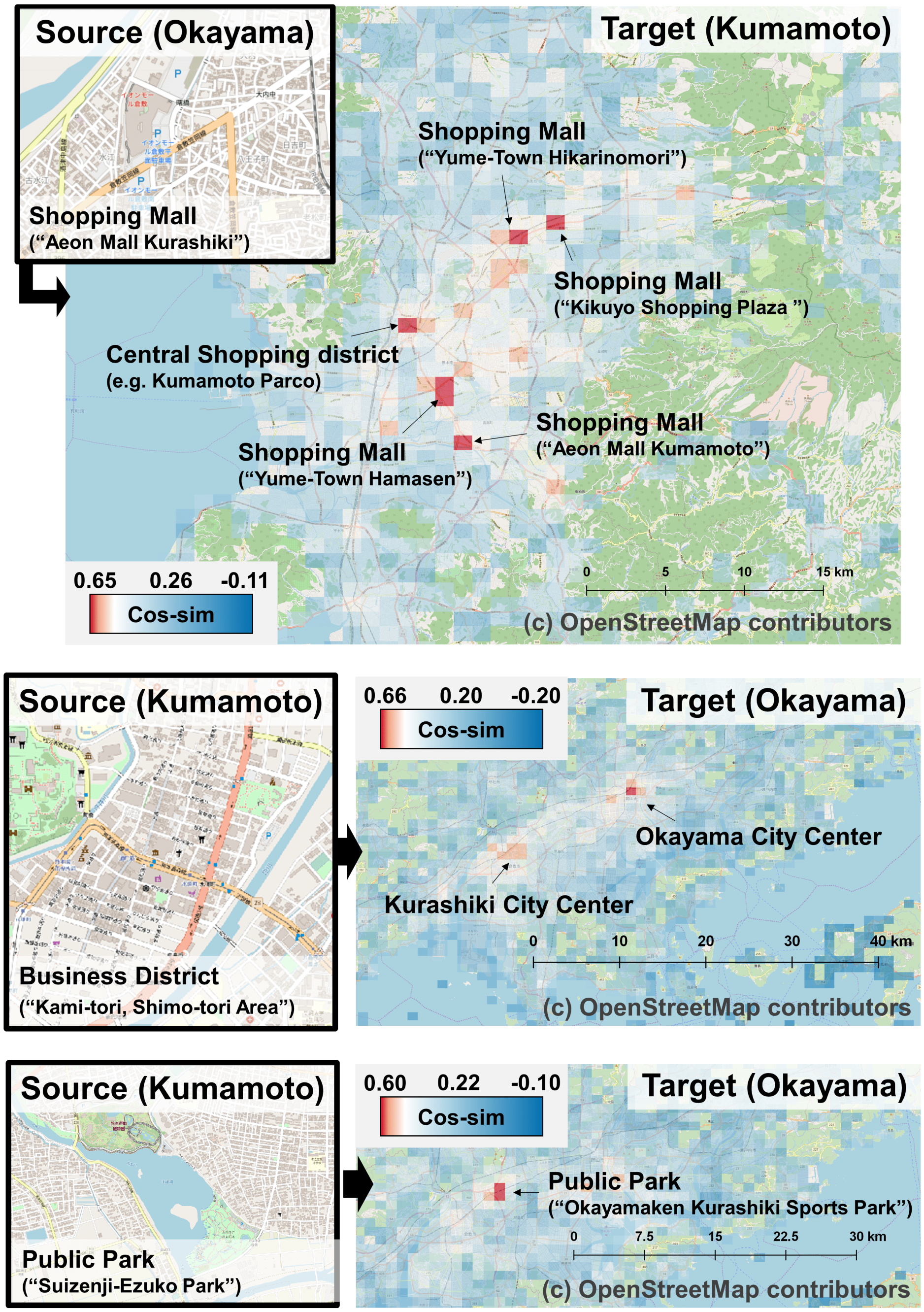

Figure 5.5. Qualitative analysis and inspection of the translated place representations across cities using `MobLSTM-P`. The three panels show that for both directions (Kumamoto $\rightarrow$ Okayama and vice-versa), places such as shopping malls, business districts, and public parks were successfully translated so that places with similar functions from different cities were mapped closely together in the common vector space.

does occur, and that a translation operation is indeed needed to compare place representations from different cities.

The rest of the models compare the performances of different translation methods. For business, shopping, and residential areas, the AMND seems to be lower than random for all methods, which implies that all of these types of places are clustered together in the vector space, away from the farmland areas. The AMCS metric allows us to measure more specific differences in the place representations, by normalizing the vectors by their lengths. AMCS results show that `MobLSTM-P` is able to translate representations of business, shopping and residential places successfully (statistically significantly). Even though `Joint-MobLSTM` and `MobLSTM-Adv` approaches are shown to succeed in language translation tasks, they fail to do so in place translation tasks. The failure of `Joint-MobLSTM` implies that the model was complex enough to completely distinguish places between Kumamoto and Okayama, and to embed them separately in the common vector space, contrary to our intuition. For `Joint-MobLSTM` to perform better, further searching for the appropriate model architecture may be effective, however is not cost effective considering the vast model space. `MobLSTM-Adv` failing to align the two vector spaces indicates that the probability distribution of the place representations of two cities are completely different, in contrary to word vector spaces. Even with `MobLSTM-P`, representations of farmlands were not successfully translated across cities. This is because we are not using many farmland areas as anchor points in our dictionary for solving the optimization problem (Section 3.3.2), due to the lack of observed human mobility patterns in such areas. Overall, results in Figure 5.4 confirm that `MobLSTM-P` is successful in translating representations of places visited by people (business, shopping, and residential) across cities.

Qualitative Inspection of Translated Representations

In addition to the quantitative evaluation, we inspected whether the place representations translated by `MobLSTM-P` were actually mapped close to similar places in the target city. Figure 5.5 shows successful cases where the place of the source city is mapped closely with similar locations in the target city. In each of the three panels, the original place in the source city is shown in the left black box (e.g. Shopping Mall “Aeon Mall Kurashiki” of Okayama), and the cosine-similarity

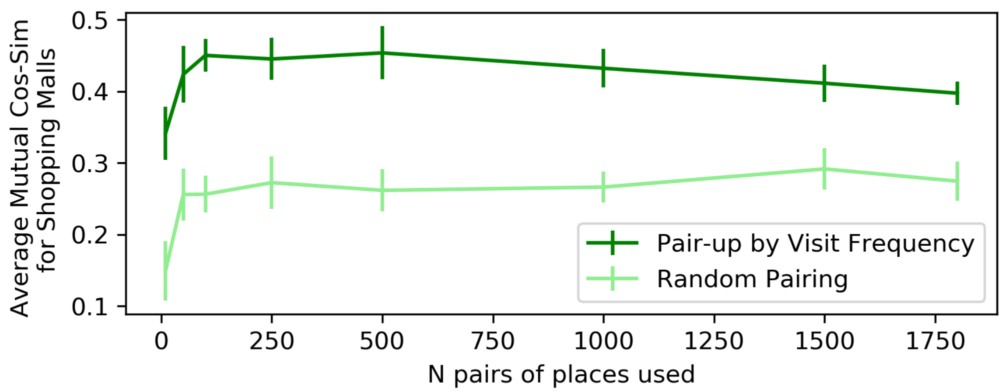

Figure 5.6. Translation performance of shopping malls from Kumamoto to Okayama using `MobLSTM-P`, using different number of anchor places for translation (x-axis), chosen by 2 different criteria (most frequently visited or random).

values between the representations of all places in the target city and the translated representation of the original place is shown in color on the map. Red and blue colors show high and low similarity, respectively. The color bar is adjusted so that only the places with top 5 percentile cosine similarity are shown in red. For places with high similarity (red places), POIs within each place are annotated on the map.

The left panel shows how a shopping mall in Okayama, when translated to the Kumamoto vector space, becomes mapped close to major shopping malls in Kumamoto, including the central shopping district, Aeon Mall Kumamoto, and several other shopping facilities. The two panels on the right side show how translation of places in the opposite direction (Kumamoto $\rightarrow$ Okayama) also produced intuitive and accurate results. The top right panel shows that the business districts of Kumamoto (the Kami-tori and Shimo-tori area), when translated to the Okayama vector space, were similar to the two major city center districts (Okayama city center and Kurashiki city center), implying that urban functionality can also be translated successfully, reinforcing our results in Figure 5.4. The bottom right panel shows an instance where even a major public park in Kumamoto ("Suizenji-Ezuko Park") was successfully translated so that it became mapped close to a major park in Okayama ("Okayamaken Kurashiki Sports Park"). Although public parks were not included in our quantitative evaluation, this result implies that `MobLSTM-P` can translate more specific places of interest to other cities. Overall, Figure 5.5 shows promising results that `MobLSTM-P` successfully maps similar places together onto the common vector space.

Sensitivity to Number of Place Pairs

The `MobLSTM-P` model requires a synthetic dictionary (a dataset with pairs of places) used to solve the optimization task. In the previous sections, we used $N = 500$ as the number of anchor places (i.e. pairs of places used for the optimization task). Here we show a sensitivity analysis of this parameter, by looking at the average mutual cosine similarity of shopping places in Kumamoto and Okayama using `MobLSTM-P` with different values of N. We observe from Figure 5.6 that the performance initially increases as we increase the number of pairs. However we see a plateau in performance after $N = 100$, and a decrease after $N = 500$, implying that choosing too many places as anchors adds too much irrelevant information for choosing the optimal rotation. Even though our method beats random pairing (light green color) for all N values, this result indicates that selecting the appropriate number of anchor places is important for the performance of our method. Further investigation using data from more cities is needed to determine whether there is a universal rule in determining the appropriate parameter value for N.

In this paper, we proposed and tested methods to translate place representations across cities. Experimental results using real world mobility data from two cities in Japan clarified that we are indeed able to translate representations of places across cities accurately using `MobLSTM-P`, which finds the best rotational alignment between vector spaces using anchor places based on visit frequencies through optimization. We clarified both quantitatively and qualitatively that places from different cities with similar landuse types became mapped closely in the common vector space after translation. Moreover, although the task of translating place representations across cities is analogous to word translation across languages, we observed several differences in the problem setting through failures of methods that were successful in the language translation domain, namely the joint learning (`Joint-MobLSTM`) and adversarial learning (`MobLSTM-Adv`) approaches. In addition to evaluating the translation performances, we showcased a case study of an important urban challenge that may be better approached using our inter-city translation method, which was to use the representations of evacuation shelter locations from a disaster in the past to predict evacuation shelters in a future disaster in another city.

Now, we discuss future research opportunities that this study enables. The first direction of research is on improving the accuracy of the translation task. In this study, we tested several methods that extended the state of the art methods for unsupervised machine language translation developed in the natural language processing field. However, we believe that we are able to improve the accuracy by further integrating characteristics specific to geographical locations, that are different from words and sentences. For example, words have stronger interchangeability characteristics, since words can often be interchanged with very little or even no cost at all (*I have a **cat*** $\leftrightarrow$ *I have a **dog***). However, that is much less likely in sequence of places and it is much rare to have two or more places with exact interchangeability in the routines for human beings. Integrating insights from the human behavioral sciences into building the representation learning and translation model would be an interesting topic for future studies.

The second direction of research is to increase the diversity of cities for testing. Although the finding that we are able to translate place representations across different cities (Kumamoto and Okayama) was insightful and promising, we are motivated in further investigating whether this method works between a more diverse set of cities, such as Tokyo, Japan and Indianapolis, USA, where various aspects (e.g. social norms, peoples' mobility patterns, city structures) are more different than between Kumamoto and Okayama. Should the method fail in such diverse pairs of cities, developing new models that consider exogenous contexts via fusion with other data sources would be an important and interesting problem. We hope to utilize a larger mobility dataset to investigate this topic in future studies.

We would also like to look into potential problems where we can apply this technique. Selection of appropriate locations to open new stores has been a popular problem in urban planning [340]. Testing whether translating successful/unsuccessful locations across cities could predict success/failure of new stores, is of future research interest.

5.2 Overcoming City Size Imbalance via Hierarchical Anchoring

A recent study adopted unsupervised language translation methods into the urban computing field to share knowledge and insights among different cities [350]. Several unsupervised neural machine translation methods developed in the natural language processing field were tested to perform translation of places across cities. However, due to the rather straightforward adoption of the translation methods, further validation showed that the translation method perform poorly across cities with different scales (e.g. Tokyo with 30M residents and Niigata with 0.8M). One possible reason of this failure was the significant imbalance in the scales of the source and target domains, since the scales of cities have much larger variance than that of vocabulary sizes across languages [351]. This *domain imbalance problem* is a key issue that needs to be solved to translate place embeddings across cities (Figure 5.7). Solving this issue could also potentially benefit unsupervised translation tasks in various fields of research in addition to languages and cities, where the source and target domains could have significantly different scales.

Analysis of mobility patterns within cities around the globe using novel mobility datasets have revealed various interesting properties of urban structures [352], including fractal properties [353], scaling laws [330], and hierarchical organization [354]. In particular, a recent study revealed positive connections between the hierarchical properties of cities and key urban indicators including higher use of public transport, higher levels of walkability, lower pollutant emissions per capita and better health indicators [355].

In this study, we attempt to overcome the aforementioned *domain imbalance problem* that exist in unsupervised translation tasks with an innovative method that utilizes the hierarchical structures that are common across domains of different sizes. We demonstrate our approach and its effectiveness through the example of unsupervised translation of place embeddings across cities with varying scales. We propose a translation model that aligns the vector spaces of the source and target domains using the hierarchical structure common across both domains. The model performances are tested using real world mobility data collected from mobile phones in 6 cities of varying scales in Japan, and are validated using landuse data. Results show that our methods are able to accurately translate place embeddings across cities, especially under the domain imbalance problem setting, where the urban scales are significantly different.

The key contributions of this section are as follows:

- To the best of our knowledge, this study is the first to address the *domain imbalance problem* in unsupervised embedding translation tasks, and to present a method to overcome the problem.

- We propose a novel unsupervised translation method that leverages the common hierarchical structures across domains to generate effective anchor points.

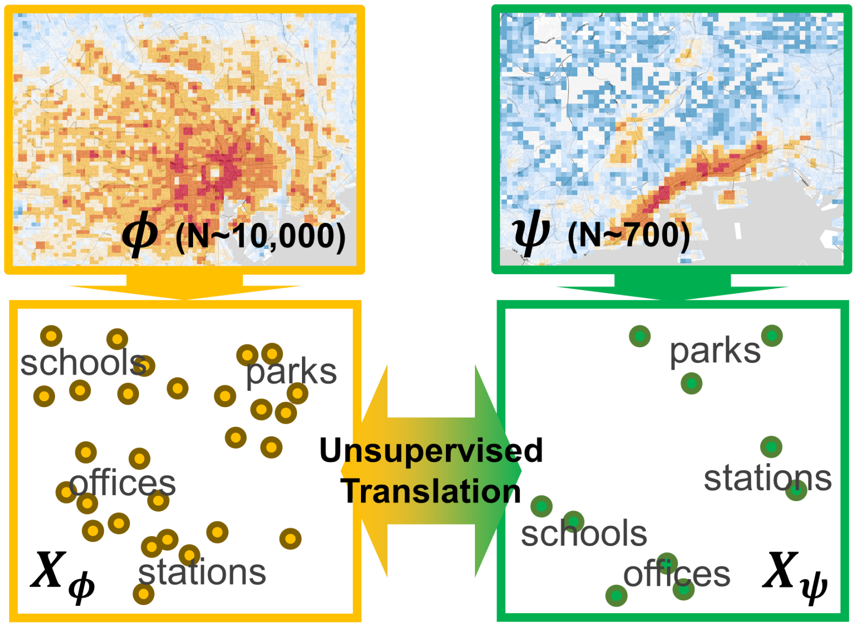

Figure 5.7. Illustration of the *domain imbalance problem* setting, where our objective is to translate embeddings across domains with significant imbalance in vocabulary sizes in an unsupervised manner.

- We verify that our method can successfully improve the unsupervised translation accuracy of place embeddings across cities with varying sizes, using real world mobility data from 6 heterogeneous cities.

5.2.1 Methodology: Hierarchical Anchoring

Generating Place Embeddings from Human Mobility Trajectories

We first extract human mobility patterns in each city from the location data observed from mobile phones. Each observation of the location data contains the user ID, timestamp, longitude and latitude. More details of the mobile phone data that we use in this study are explained in Section 4.1.1. Our goal is to extract users' sequences of staypoint locations from the observations. We achieve this by setting two threshold parameters; one spatial threshold and one temporal threshold. To cope with noisy location observations (e.g. spatial errors in GPS data), we perform mean shift clustering to estimate the true location for each observation, as described in previous studies (e.g. [226]). For each user, we read their location data in time order, and search for locations where the

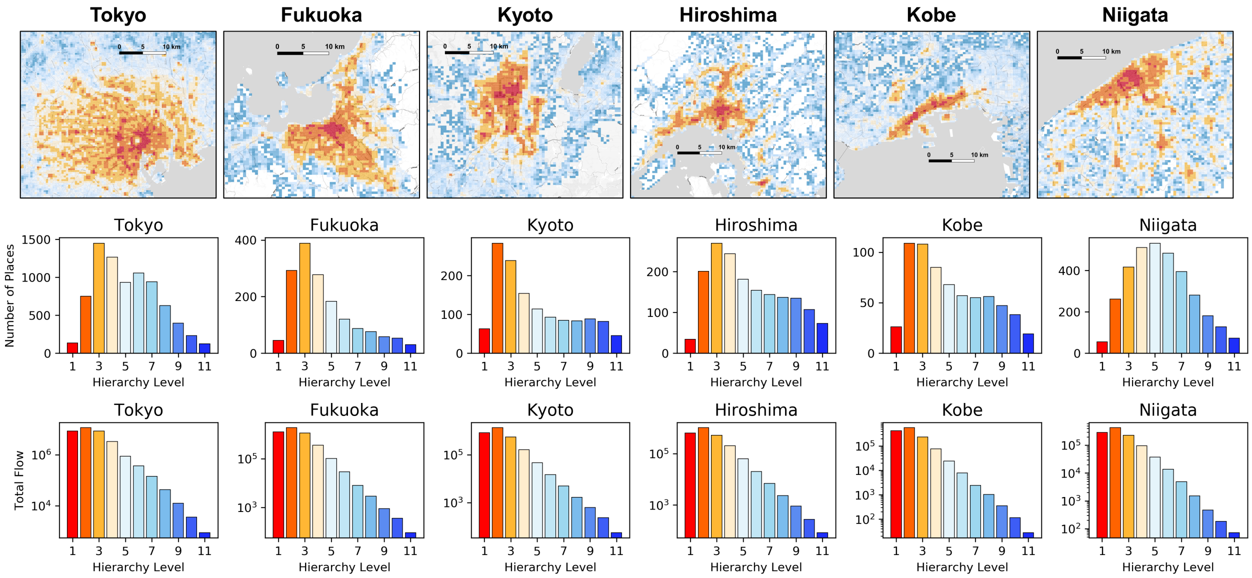

Figure 5.8. Universal hierarchical structure of cities used in our study.

user has stayed within the distance defined by the spatial threshold parameter for a duration longer than the time defined by the temporal threshold parameter. We use 1000 meters as the spatial threshold, and 30 minutes as the temporal threshold in this study. As a result, we are able to obtain sequences of staypoint locations for each user, which will be used to generate place embeddings using methods explained in the following section.

To obtain the embeddings of places in a city, we solve a self-supervised task in which an Long Short-Term Memory (LSTM) RNN model is trained to predict the next staypoint of a user using mobility data, which is analogous to language models which are trained to predict the next word in a sentence. After training an LSTM RNN model using staypoint sequences of a city c, we extract and stack the embedding layer's parameters of the size $n_c \times d$, and define it as the matrix of place embeddings X_c. We refer to this place embedding learning model as "`IndivLSTM`" in the following sections. Specific model hyperparameter settings are explained in Section 4.2.1.

Analysis of Hierarchical Structure

One popular method of determining the hierarchical structures in cities is to iteratively apply the Loubar method proposed in [352], which uses the Lorentz curve of the number of visits to each location [355]. The Lorentz curve, which is a standard notion in the economics domain, is a cumulative distribution function of a distribution of datapoints. Given the average daily visit count values for all places in a city, we first sort the datapoints by ascending order and denote them as $(n_1 < \cdots < n_\mathrm{i} < \cdots < n_{N_c})$, where n_k is the daily visit count in the k-th popular place in city c, and N_c is the total number of places in city c. The Lorentz curve is constructed by plotting the proportion of the places $F = \frac{\mathrm{i}}{N_c}$ on the horizontal axis and the cumulative proportion of the covered visit counts L, which is calculated by the following equation. An example of the Lorentz curve is shown in the Supplementary Material (Figure A1)

$$f(\mathrm{i}) = \frac{\sum_{\mathrm{j}=1}^{\mathrm{i}} n_\mathrm{j}}{\sum_{\mathrm{j}=1}^{N_c} n_\mathrm{j}} \tag{5.5}$$

If the visit counts of all places were equal, the Lorentz curve would be a linear diagonal function.

The minimum threshold value of the first hierarchical level is computed by taking the intersection between the tangent of $f(F)$ at point $F = 1$ (i.e. the maximum value of the Lorentz curve) and the horizontal axis ($f(F) = 0$). In Louail et al., [352], the computed minimum threshold value was used to classify places in a city into "hotspots" and other places. Bassolas et al. [355] extended this method in an iterative manner to find multiple minimum thresholds for different hierarchical layers. After extracting the places in hierarchical level l, those places are excluded from the data distribution, and the minimum threshold value is recalculated using the new distribution to extract the places in hierarchical level $l+1$. This procedure is iterated until all of the places in the city are assigned to a hierarchical level. For a more detailed explanation on the methods of urban hierarchical structure analysis, readers should refer to the Supplementary Material and Bassolas et al. [355].

Figure 5.8 shows the estimated urban hierarchical structures in each city used in this study. The first row shows the colored maps of each city, where the colors indicate the hierarchical level each place belongs to (red: hierarchical level 1, blue: hierarchical level 11). The second row shows the histogram of the number of places belonging to each of the hierarchical levels in each city. The third row shows the total number of visits observed in the places belonging to each layer, which is calculated as $\sum_{\mathrm{j}:l(\mathrm{j})=L} n_\mathrm{j}$ for hierarchical level L where $l(\mathrm{j})$ denotes the hierarchical level of place j. While the second row highlights the different distributions of the number of places in

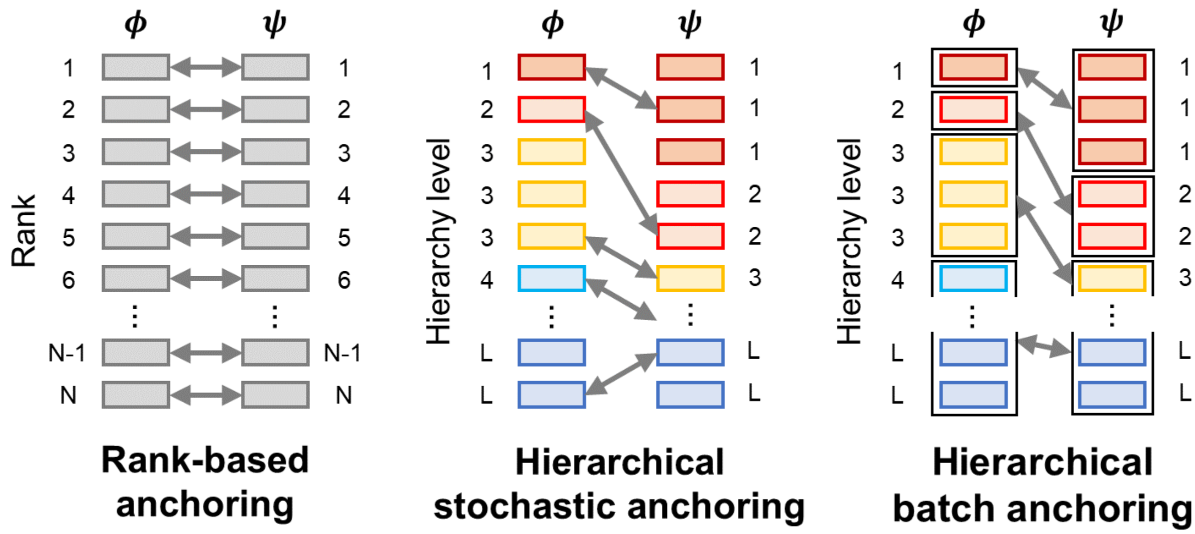

Figure 5.9. Illustrative explanation of how the embeddings across the pair of cities are aligned in different methods.

each hierarchy (i.e. Tokyo and Fukuoka are more shifted to the left with more high-level places compared to Niigata), the distribution of the total number of visits in each hierarchical level are strikingly similar across all cities, where the majority of the visits are concentrated in the first couple of hierarchical levels in all cities. This common hierarchical characteristic across cities motivates us to exploit the urban hierarchical structures. In the next section, we explain how we take advantage of this common hierarchical structure in our method for translating embeddings across imbalanced domains.

Translation via Hierarchical Anchoring

In previous studies in the natural language processing field, various methods have been proposed to obtain the best rotation matrix $R \in \mathbb{R}^{d \times d}$ that maps 2 embedding matrices $X_\psi, X_\phi \in \mathbb{R}^{d \times N}$ in an unsupervised manner. A previous study on unsupervised translation of place embeddings showed that a rank-based Procrustes alignment performed best out of the various methods [350]. Although this method was shown to be successful in cases where the source and target domains were of similar scales, a straightforward application to domain imbalanced settings could be problematic (and we show in the experiments that this is indeed the case). To overcome the difficulty in translation of embeddings under domain size imbalance (e.g. cities with different sizes), we propose a hierarchical alignment strategy to map the two domains. The main idea is to generate anchoring points based on hierarchical levels.

To perform translation, we first create anchoring embedding matrices, which serve as reference points to compute the optimal alignment operators. Figure 5.9 illustrates the different methods to create anchoring embedding matrices across cities. The left panel shows the **rank-based anchoring** method, which generates a one-to-one matching based on the sorted rank of places to generate anchoring pairs to align the embeddings. The center panel shows the **hierarchical stochastic anchoring** approach, where anchoring pairs of embeddings are selected within each hierarchical level in a stochastic manner with a predefined probability p, and are stacked together to obtain the anchoring embedding matrices for the two domains. The right panel shows the **hierarchical batch anchoring** approach, which instead of randomly selecting the embedding pairs, the mean vectors of the embeddings in each hierarchical level are computed and stacked to generate the anchoring embedding matrices, which are used to find the best alignment operator.

To find the optimal alignment operator using the anchoring embedding matrices, we test the Orthogonal Procrustes alignment and Affine alignment methods. Given the anchoring embedding matrices X^*_ϕ and X^*_ϕ for cities ϕ and ψ, respectively, Orthogonal Procrustes alignment computes the rotational matrix that optimizes the following equation:

$$R^* = \underset{R^T R = I}{\operatorname{argmin}} \left\| R X^*_\phi - X^*_\psi \right\|_F \tag{5.6}$$

where, $R \in \mathbb{R}^{d \times d}$ is the optimal rotational matrix, and $\|\cdot\|_F$ is the Frobenius norm. Affine alignment introduces an extra transformation vector that increases the model complexity, and solves the following problem:

$$A^*, b^* = \underset{A,b}{\operatorname{argmin}} \left\| (A X^*_\phi + b) - X^*_\psi \right\|_F \tag{5.7}$$

where, $A^* \in \mathbb{R}^{d \times d}$ is the optimal rotational matrix and $b^* \in \mathbb{R}^d$ is the optimal transformation vector. The optimization can be performed using standard solvers using least squares method. In the experiments, we test the effectiveness of different combinations of anchor embedding matrix

Table 5.2. Statistics showing the varying scales of the cities

Scale	City	# Users	# Steps.	# Places (Urban)
Large	Tokyo	308,140	43,498,760	8020 (589)
Medium	Fukuoka	41,111	7,288,330	1636 (84)
	Kyoto	29,920	4,867,294	1363 (30)
	Hiroshima	21,868	3,876,699	1741 (25)
	Kobe	17,172	2,704,310	676 (63)
Small	Niigata	10,619	2,156,353	3312 (8)

generation methods (rank-based, hierarchical stochastic, and hierarchical batch), and alignment methods (Orthogonal Procrustes and Affine alignment).

5.2.2 Experiment Settings

Mobile Phone Location Data

Yahoo Japan Corporation[4] collects location information of mobile phone app users in order to send relevant notifications and information to the users. The users in this study have accepted to provide their location information. The data are anonymized so that individuals cannot be specified, and personal information such as gender, age and occupation are unknown. Each GPS record consists of a user's unique ID (random character string), timestamp, longitude, and latitude. The data acquisition frequency of GPS locations changes according to the movement speed of the user to minimize the burden on the user's smartphone battery. The data has a sample rate of approximately 2% of the population, and past studies suggest that this sample rate is enough to grasp the macroscopic urban dynamics. Table 5.2 shows the statistics of the dataset collected for 6 cities that we focus on in this study. We observe that the cities are significantly imbalanced in terms of the number of mobile phone users, total step sizes, and the number of places classified as urban areas.

[4] ↑https://about.yahoo.co.jp/info/en/company/

Land Use Data

To validate whether the translated place embeddings correctly capture the functionality of the places, we use the Urban Area Land Use Mesh Data[5] in the National Land Numerical Information Database[6] provided by the Ministry of Infrastructure, Land, and Transport and Tourism of Japan. The dataset divides all urban areas of the country into $100m \times 100m$ grid cells, and assigns one category to each grid cell out of 17 options. The 17 options include farmland, residential area, business district, parks, forests, factories, public facilities, water body, open spaces, roads, railways, golf courses, etc. Because the categories are very detailed, we categorize these landuse categories into 7 label types: high-rise buildings, low-rise dense residential areas, low-rise sparse residential areas, industrial areas, agricultural areas, public facilities and parks, and water bodies. We aggregate these data into our spatial scale ($500m \times 500m$), and label each place with the landuse label which has the majority number of pixels in that $500m \times 500m$ place.

Model Hyperparameters

To learn the place embeddings described in Section 3.1, we setup the model and input data with the following procedure. The model consists of the embedding layer, LSTM RNN block, readout layer, and the output layer. While the main input of the model is a sequence of staypoints representing a user's movement, we added two supplementary values, which are the timestamp of when the user had entered that place and the duration time of the stay, to incorporate time-dependency of the users' behavior. The embeddings of staypoints were set to 64-dimensional vectors. The timestamp and stay duration were converted to 8-dimensional and 4-dimensional vectors respectively, and the three vectors at each step were concatenated into a 76-dimensional vector. The LSTM RNN block scanning over the embedding sequence consists of two layers of the size 128, and the hidden vectors of both layers were fed into the readout layer of the size 64, which were then read by the output layer producing the probability distribution over staypoints for the next place prediction. The parameter matrix of the staypoint embedding was reused as the output layer's matrix to reduce the total number of parameters and make the training data usage

[5]↑http://nlftp.mlit.go.jp/ksj/gml/datalist/KsjTmplt-L03-b-u.html
[6]↑http://nlftp.mlit.go.jp/ksj/

more efficient. We applied dropout with the keep probability 0.8 to three points of the model: the embedding layer, readout layer, and output layer. We continued the training for 20 epochs, evaluated performance on the validation data at the end of each epoch, and used the embedding matrix of the best model for subsequent processing.

Comparative Methods

We compare the translation performances of the methods described in Section 3.3, as well as a state-of-the-art method used in language translation tasks. The combinations of the anchor embeddings matrix generation and alignment methods are as follows: rank based + Procrustes (`RP`), rank based + Affine (`RA`), hierarchical stochastic anchoring + Procrustes (`HSP`), hierarchical stochastic anchoring + Affine (`HSA`), hierarchical batch anchoring + Procrustes (`HBP`), and hierarchical batch anchoring + Affine (`HBA`). For the stochastic anchoring methods, results using $p = 0.5$ are reported since this probability had the best performance out of all 0.1 incremental values of p. In addition, we test **`JointLSTM`**, which applies the `IndivLSTM` model to all of the 6 cities together on the self-supervised next staypoint prediction task. We merge the mobility datasets of the cities into one and train the model over the merged data to obtain the place embeddings of all cities. To allow the model to treat places of the two cities as equally as possible, we mask the candidates of ψ at the output when the next staypoint belongs to ϕ and vice versa, releasing the model from the burden of distinguishing between two cities. The rationale behind this approach is that, places with similar functions will be visited in a similar manner (e.g. time of day, day of week, after and before certain places) regardless of the city, and that the mobility patterns of people are common across different cities. A previous study shows that this approach is effective in translating word embeddings of one language to another in an unsupervised manner [345].

Evaluation Metrics

To evaluate the performance of the translation methods, we test the prediction accuracy of landuse classification using the translated place embeddings. Embeddings and landuse labels from the source city are used as training data, and the embeddings and landuse data from the target city are used as test data. We denote the place embeddings of the source (ϕ) and target (ψ) cities as

Table 5.3. Quality of generated place embeddings measured by land use classification accuracy.

Method	Cities					
	Tokyo	Fukuoka	Kyoto	Hiroshima	Kobe	Niigata
`IndivLSTM`	0.691	0.809	0.794	0.827	0.675	0.748
`JointLSTM`	0.679	0.780	0.724	0.710	0.639	0.735
Random	0.341	0.383	0.353	0.437	0.315	0.507

X_ϕ and X_ψ. Similarly, we denote the landuse labels of each place in the source and target cities as y_ϕ and y_ψ. We also denote the translated place embeddings of city ϕ as $f(X_\phi) := \tilde{X_\phi}$ using the translation function $f(\cdot)$. We first train the landuse label classifier using the labels (y_ϕ) and translated place embeddings from the source city ($\tilde{X_\phi}$). Then, we test the predictive accuracy of landuse labels (y_ψ) using the trained classifier and the place embeddings from the target city (X_ψ). If the embeddings are perfectly translated and mapped into the target city, the classifier would be able to classify the landuse labels using the test data similarly as the training data. We use logistic regression as the classifier, and since the problem is a multi-class classification task, we use accuracy and F1-score as the evaluation metrics. The default hyper-parameter of the logistic regression model was set to $C = 1$, but we clarify that the ranking of the performances of the various translation methods do not depend on the choice of the classifier or the hyper-parameter.

5.2.3 Results of Domain Imbalance Urban Translation

Quality of Generated Place Embeddings

Before performing any translation task, we check that the place embeddings produced by the two LSTM models described in Section 3.1 are of high quality. Table 5.3 shows the land use classification accuracy using the produced place embeddings in each city. As previously explained, logistic regression was used to classify the land use labels using only the place embeddings as features. Training and test data were randomly shuffled and split into 80% and 20% of the data, and the reported accuracy results are the mean values of 10 trials. Details of the experiment settings are noted in Section 2.6 of the Supplementary Material. We observe that for all cities, despite some differences across cities, both the place embeddings generated by `IndivLSTM` and `JointLSTM` are

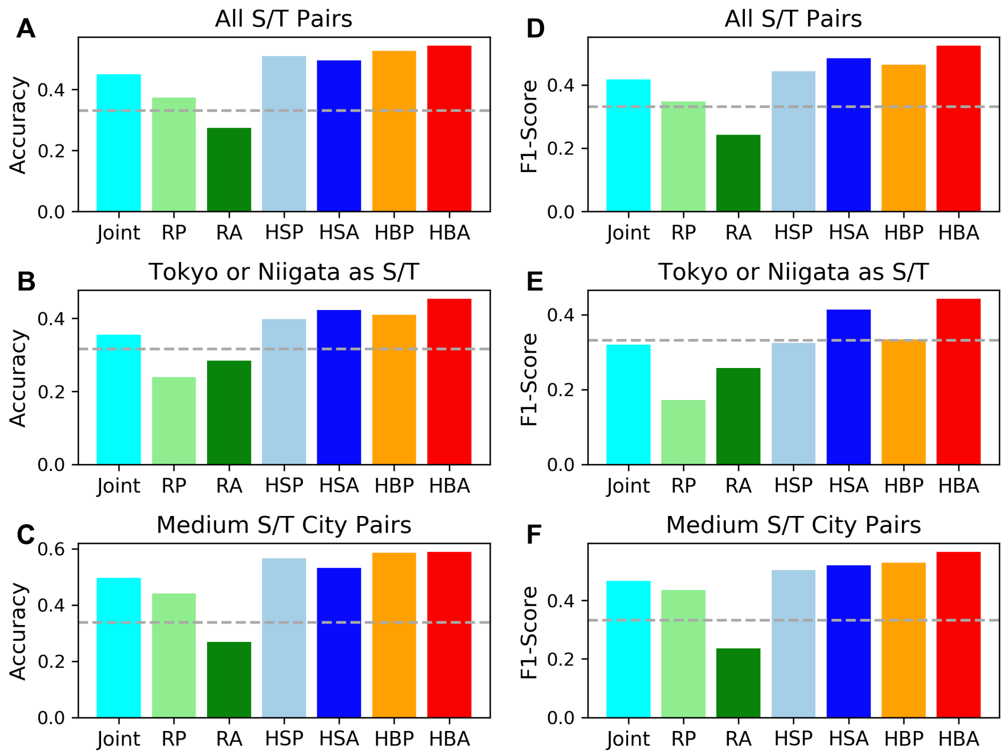

Figure 5.10. Translation performance of methods, measured by mean accuracy (A-C) and mean F1-score (D-F) of landuse prediction. (A) and (D) show results across all city pairs. (B) and (E) show results of translation when source or target city is either Tokyo or Niigata. (C) and (F) show performances when source and target cities are both medium sized.

able to encode landuse information well, as previously shown by various studies (e.g. [338]). The results also show that the quality of place embeddings drop using the `JointLSTM` model compared to the `IndivLSTM` model, since the `JointLSTM` model shares model parameters across all cities. We note that the unsupervised translation methods are agnostic of the place embedding generation methods. In the unsupervised translation experiments, we use the place embeddings produced by these LSTM-based models.

Translation Accuracy

In this study, we quantitatively evaluate the translation accuracy of each method using the predictive performance of the landuse labels, which is a multi-class classification task. Figure 5.10 shows the translation performances of the proposed method (red) and the comparative methods

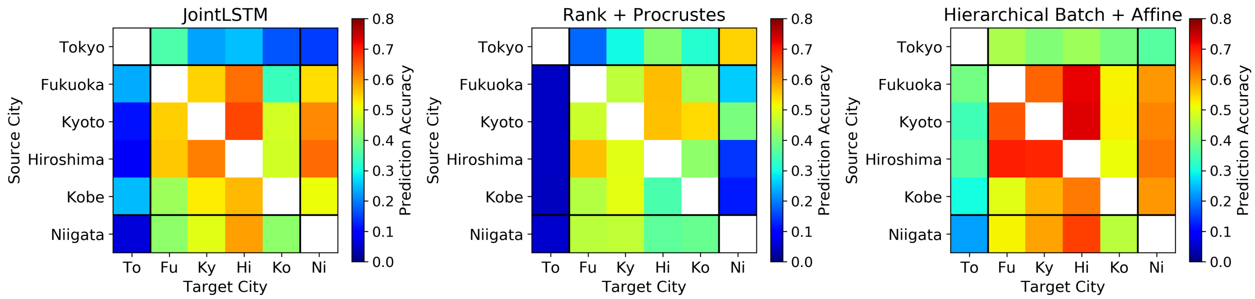

Figure 5.11. Mean pairwise translation accuracy across all source and target cities with different scales. Left: Accuracy using the `JointLSTM` method. Center: Accuracy using rank-based anchoring and Procrustes alignment method [350]. Right: Accuracy using hierarchical batch anchoring Affine alignment method (Proposed method).

(Table 5.2). In all panels, the horizontal dashed gray line shows the accuracy when we use randomized labels. The left column presents the performances using accuracy, and the right column uses the weighted F1-score. The top row shows the mean performance metrics of place embedding translation across all city pairs, whereas the panels in the center row and the bottom row show the performances when Tokyo or Niigata (large or small cities) are either or both the source or the target city, and when both the source and target cities are medium sized cities (Fukuoka, Kyoto, Hiroshima, or Kobe), respectively. Most importantly, we observe that our proposed translation method that performs Affine alignment using hierarchical batch anchoring ("HBA") performs best in all of the cases. Using the hierarchical structures for anchoring performs better than using rank based anchoring ("RP" and "RA") in all of its variants ("HBP", "HSP" and "HSA"). The joint learning approach ("Joint") performs better than the random baseline in most cases, however its performances are limited compared to the hierarchical approaches. The rank-based Procrustes approach ("RP"), which was shown to perform well in a previous study across cities with similar sizes [350], performs well across medium source and target city pairs in this study as well (panels C and F), however is inferior to the hierarchical anchoring approaches under domain imbalance.

To obtain a more detailed understanding of the translation accuracy across the cities with different scales, we plot the pairwise translation performances of the three main methods (JointLSTM, rank-based anchoring + Procrustes alignment, and hierarhical-batch anchoring + Affine) in Figure 5.11. The matrices show the predictive F1-scores from the source city (vertical axis) to the target city (horizontal axis), where warmer colors (red, orange) show higher predictive performances. The diagonal elements are colored white because there are no translation operations involved in predicting landuse labels of the same city. The matrices are divided into sections with black border lines, showing the boundaries between large, medium, and small cities. We can immediately observe a significant difference in predicting the target landuse labels in Tokyo (large city), where the RP (Rank-based Orthogonal Procrustes) method performs particularly poorly. Translation from medium cities to Niigata (small city) works better using our proposed method compared to the two other methods. One exception was the predictive accuracy from Tokyo to Niigata, where the RP method performed better compared to the hierarchical batch anchored Affine mapping. This phenomenon can be explained by looking at the sensitivity analysis conducted in the next subsection, where we point out the effects of selecting which hierarchical layers to use for translation on the performances.

Which Hierarchical Levels should we use?

So far, we have clarified the effectiveness of our unsupervised translation approach that uses hierarchical anchoring. Here, we further conduct sensitivity analysis on the number of hierarchical layers used in our translation method. Figure 5.12A shows the relationship between the number of hierarchy levels used and the prediction accuracy in landuse classification task using HBA method for each source-target city pair. The red, blue, black, and green plots show the translation tasks with Tokyo as the source ("From Tokyo"), Tokyo as the target ("To Tokyo"), from Tokyo to Niigata, and tasks with other cities as source and target, respectively. We observe intuitive trends in translation across the source-target groups. The increasing trend in the red plots (Tokyo as source city) indicate that increasing the number of hierarchical levels and including more rural areas increases the translation accuracy to cities smaller than itself, whereas the decreasing trend in the blue plots (Tokyo as target city) indicate that increasing the number of hierarchical levels and including information from more rural areas in the more rural source city decreases the translation accuracy. In contrast to these dependencies of translation accuracy from and to Tokyo on the number of hierarchical levels, the translation accuracy stays consistent with respect to the number of hierarchical levels across source and target cities of similar scales.

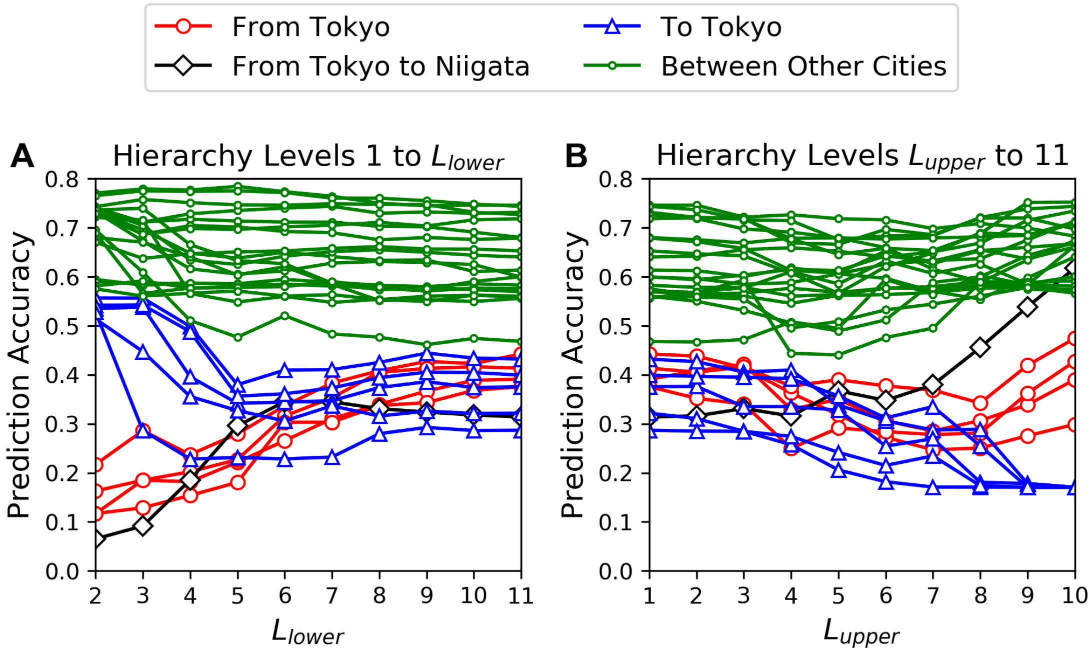

Figure 5.12. Sensitivity of translation accuracy with respect to the hierarchical levels used for translation using HBA. (A) Using hierarchical levels from the highest level $L = 1$ to L_{lower}. (B) Using hierarchical levels starting from L_{upper} to the lowest level $L = 11$. $L_{lower} = 11$ in panel A and $L_{upper} = 1$ in panel B correspond to the same case, where all hierarchical levels from $L = 1$ to $L = 11$ are used.

Figure 5.12B shows the inverse setting of Figure 5.12A, where we select only a subset of the lower hierarchical layers for translation. We observe that once again, the translation accuracy stays consistent with respect to the number of hierarchical levels across medium source and target cities. However, we observe that when using Tokyo as the source, the accuracy increases when we limit the hierarchical layers to lower layers (e.g. $L = 8, 9, 10$). In fact, although we observed a low translation accuracy for Tokyo $\rightarrow$ Niigata in Figure 5.11, we clarify that this was because we used the upper-level hierarchical information from Tokyo which was less relevant to Niigata. When we use Tokyo as the target, the translation accuracy drops as we throw away upper-level hierarchical information from the medium and smaller sized cities.

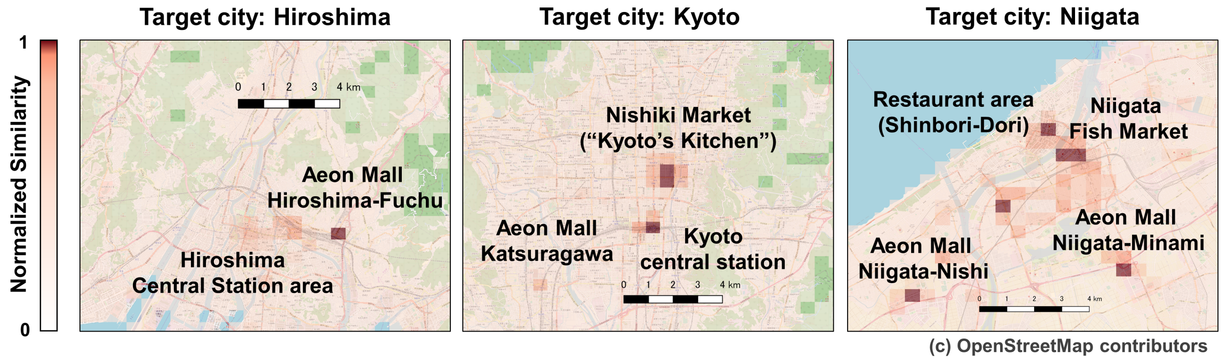

Figure 5.13. Case study showing the results of translating Tsukiji Fish Market (Tokyo) to Hiroshima, Kyoto, and Niigata via hierarchical batch anchoring and Affine alignment. We were able to translate the fish market in Tokyo into large scale shopping malls and local markets across cities of different scales.

Case Study: Translating *Tsukiji Fish Market*

Finally, we qualitatively assess the translation performance through a case study of translating a point-of-interest (POI). Figure 5.13 shows the translation results of "Tsukiji Fish Market" from Tokyo to Hiroshima, Kyoto, and Niigata. Tsukiji Fish Market[7], one of the largest fish markets in Tokyo, is a very popular tourist spot for visitors and also for local residents. Each of the panels in Figure 5.13 show the similarity of each place to the translated Tsukiji Fish Market embedding $\tilde{x}_{Tsuki\mathrm{ji}}$. Given the norm distance of place i, denoted as $d(x_\mathrm{i}) = \left\|x_\mathrm{i} - \tilde{x}_{Tsuki\mathrm{ji}}\right\|_2$, the similarity is computed by normalizing the norm distances with respect to all the places in the city. Normalized similarity is computed as $S(\mathrm{i}) = \frac{\max d(x_\mathrm{i}) - d(x_\mathrm{i})}{\max d(x_\mathrm{i}) - \min d(x_\mathrm{i})}$. Places colored in bold red color indicate high proximity close to $S(\mathrm{i}) = 1$ with minimum norm distance, and the POIs inside those places are annotated in the maps. We can observe that for all the cities, we are able to detect large scale shopping malls (e.g. Aeon Malls in all cities) and even the Nishiki market[8] in Kyoto and Niigata Fish Market, which are popular markets for purchasing local products, via translation of places.

[7] ↑
[8] ↑

Discussions

In this study, we proposed a novel unsupervised translation method that exploits the hierarchical structure that exist across different domains to enable translation of embeddings across domains of imbalanced sizes. The effectiveness of our method was shown through experiments using real data collected from 6 Japanese cities with varying sizes. It was interesting to observe that hierarchical batch anchoring worked better than hierarchical stochastic anchoring in all experiment settings. This implies that the hierarchical anchoring works best with fewer but less noisy anchor points. Although the joint learning method is considered to be one of the state-of-the-art methods in unsupervised translation tasks in the language domain, our analysis showed that the method using hierarchical structures worked better under domain imbalance settings. The key assumption of the joint learning method is that the mobility patterns (or sentences in the language domain) have similar structures across different cities. However, as we can see from Table 5.2, the average length of staypoints per user differed significantly across cities of different sizes (e.g. Tokyo: 141 steps/user, Niigata: 203 steps/user), indicating that such assumptions do not hold in cities.

In addition to the improvement in landuse label prediction tasks using the translated place embeddings, further analysis on using different combinations of hierarchical levels for translation in Section 5.2.3 provided interesting insights and possible reasoning on the translation performances of the proposed method. Figure 5.12 shows the strong dependence of translation accuracy on the hierarchical layers we use for translation. In general, it was found that when translating from a large city (e.g. Tokyo) to smaller cities, using the full set of hierarchical levels is optimal. In the extreme domain imbalance case (from Tokyo to Niigata), it was found that limiting information to only the bottom 2 hierarchical levels produced best translation accuracy. On the other hand, when we translate from smaller cities to larger cities, using information from only the higher hierarchical levels was often sufficient and better than using information from all of the layers in the smaller cities. Although these findings match our intuition, further investigation needs to be done in finding rules and methods in choosing the optimal ranges of hierarchical levels that we should use for translation, given the sizes of the source and target domains.

We believe this study leads to many research questions worthy of investigation. Representation (or embedding) learning has become a large branch of machine learning in recent years [356], and its techniques have been applied to various data types, including graphs [357] and images [358]. A natural extension of this study would be to apply our method to unsupervised translation tasks using embeddings generated from other types of data, such as language translation where vocabulary sizes significant vary across the languages. Since hierarchical structure analysis is agnostic to data, it can be easily extended to other problem settings. For example in the language setting, vocabulary can be grouped into hierarchical levels based on their appearance frequencies. Applying the translated place embeddings to solve various downstream urban problems would be another broad research direction. For example, selection of appropriate locations to open new stores has been a popular problem in urban computing [340]. Applying the translation results of place embeddings, such as the example shown in Figure 5.13 on the Tsukiji Fish Market, may assist planning of new store locations.

Despite the rising interest in unsupervised translation tasks, how to overcome the *domain imbalance problem* has been understudied. Using place embeddings and cities as an example problem setting, we propose and test a novel unsupervised translation method that exploits the hierarchical structures that are common across different domains despite scale differences. Experiments using data collected from 6 Japanese cities of different sizes clarified that our hierarchical anchoring approach improves the translation performance compared to previously proposed methods. Our method is agnostic to the type of input data, thus could be applied to unsupervised translation tasks in various fields in addition to linguistics and urban computing.

The next step is to utilize the methods developed in this chapter for disaster resilience applications, such as evacuation and return movement prediction tasks. An experimental setup would be to train an evacuation destination model using place embedding and human mobility data from one city, translate the embeddings to the target city and simulate/test the evacuees' destinations using the trained model and translated place embeddings. Several experiments need to be conducted to validate the effectiveness of the framework. For example, a thorough investigation is needed to unravel the types of region pairs that the inter-city translation of places are successful, and when they fail, to effectively operationalize this technique. Secondly, how to combine the translated place embeddings with variables that cannot be captured using POI information, such as government capacity and decision making during disaster response, and effects of social network influence and social norms that are crucial for evacuation decision making. A natural methodological next step of this work would be to develop a model that can translate human mobility trajectories (not places) across cities, similar to document translation methods in NLP, such as Seq2Seq models.

6. KNOWLEDGE SYNTHESIS

With rapid urbanization progressing in cities around the world and climate change increasing the intensity and frequency of natural hazards, improving the resilience of urban systems has never been more important, as emphasized in Section 1.1. In the meanwhile, novel, high-frequency, high-granular, and large-scale datasets, which were comprehensively summarized in Section 1.2, have become more and more available for academic and research activities. In this dissertation, I synthesized the vast body of work and my novel scientific contributions that utilize such big data for disaster recovery and urban resilience, from four interconnected aspects – recovery trajectories of communities after disasters (Chapter 2), socio-economic inequality that exist in recovery among communities (Chapter 3), understanding the interdependencies between socio-physical systems among communities and how they govern the recovery trajectories (Chapter 4), and methods for inter-regional transfer of insights (Chapter 5). Here, I will synthesize the knowledge obtained from Chapters 2-5 to present a holistic understanding of urban disaster resilience, and then proceed to show 2 key steps that are currently needed to translate the technical contributions to real-world impacts on improving the resilience of cities.

6.1 Summary of Contributions on Urban Resilience Research

In this dissertation, we started off in Chapter 2 by investigating whether generalizable patterns exist in disaster recovery trajectories across different regions and disaster events, similar to how universal patterns were found in typical human behavior [124]. Using large-scale mobility datasets collected from over 1 million mobile phone users across five major disaster events that occurred in the US and Japan, we discovered that population displacement and recovery follow a universal exponential pattern, irrespective of the type of disaster or the region that they occur in. Further investigation explained this exponential pattern through the positive relationships between displacement distance and time until return. While universal patterns were observed on the macroscopic scale, substantial heterogeneity was also observed across communities, even with similar levels of disaster damage. The heterogeneity was explained by a set of factors including social and physical networks, and guided us to look more deeper into intra-regional inequalities in recovery. Chapter 3 was dedicated to quantifying the intra-regional inequality in recovery among households and business firms, using a causal inference framework. Data from Hurricane Irma in Florida and Hurricane Maria in Puerto Rico revealed significant inequality in both post-disaster evacuation mobility with respect to household income, and economic recovery of business firms with respect to the located regions and business category. Taken together, such data-driven insights in recovery patterns (both universality and heterogeneity/inequality) can be used to develop policy decisions for achieving a better, quicker, and inclusive recovery after disasters.

The vast literature on the complexity of cities and the insights on the importance of social and physical networks on disaster recovery obtained in Chapter 2 motivated us to investigate the interdependencies between social and physical systems during disaster recovery. We proposed a data-driven dynamical systems modeling approach, where large-scale observations of social and physical recovery were used to calibrate a dynamical model of coupled systems. Using Puerto Rico as a case study, it was revealed that indeed, social and physical systems are interdependent during the disaster recovery phase, and the degree of such interdependencies varied across regions. More specifically, we discovered the trade-off relationship between infrastructure recovery efficiency and socio-economic self-reliance, and that as cities grow in scale, infrastructure efficiency improves but results in loss of self-reliance, which erode the resilience of communities. This lays a scientific foundation to further investigate the interdependencies between social and physical systems in cities, and how to improve resilience of the overall urban system. The future research questions that this study motivates us to pursue are discussed in Section 6.4. Finally, we propose an artificial intelligence approach to transfer the data-driven knowledge obtained in Chapters 2, 3, and 4 across different cities. We showed that by applying techniques from the unsupervised machine translation literature in natural language processing field and tailoring it for the urban settings, we are able to identify places with similar functionality across different cities by just using large-scale mobility data, with no prior knowledge. This final chapter opens up several interesting avenues of research on the inter-city learning of disaster recovery dynamics to prepare for unprecedented disasters (also known as "black swan events"), or under scenarios where data are sparse, such as in developing countries and rural regions.

In summary, this dissertation discussed computational approaches to understanding urban resilience from various perspectives. Given these theoretical, empirical, and methodological advances, now I will indicate two future steps that the urban resilience research community needs to follow to further maximize the impacts on policy making for building resilient and inclusive communities.

6.2 From "Data-Driven Modeling" to "Data-Driven Dynamical Systems Modeling"

Data-Driven Modeling

Throughout chapters 2 and 3, I have summarized various efforts that utilize or develop applied statistical models to unravel correlations between variables and outcomes in large-scale datasets. Examples of this practice, which I refer to as "*Data-Driven Modeling*", include long short term (LSTM) memory neural networks to predict evacuation mobility using web search text as input (Section 2.3), generalized linear regression to understand factors that contribute to communities' quicker population recovery after disasters (Section 3.1), and Bayesian structural time series models to predict the non-disaster trends of foot traffic to businesses (Section 4.2). Despite the stark differences in the complexity of the models (i.e., number of model parameters, non-linearity of model structure), the common denominator of these models are that they exploit correlations between features and the objective variable(s). With models with simple structures (e.g., linear models), we are able to obtain coefficients, or some form of weight, that quantifies the contributions of each variable, which can provide interpretability of the model to some extent. However, one key criticism of these data-driven models is the lack of understanding in the (often dynamical) generative processes of the observed phenomena. This is especially an issue in our problem context, since disaster recovery is a dynamic process, which is affected by various other dynamic factors (e.g., interdependencies with physical infrastructure recovery, social and physical network effects) over the time horizon. In order to develop effective policies and apply them in the right timing, we need a structured and interpretable understanding of the disaster recovery process. Therefore, although data-driven modeling could provide useful insights in monitoring and quantifying the states of systems, the field needs to move beyond "*Data-Driven Modeling*", towards a more physics-based "*Systems Modeling*" approach, powered by the available big data sources.

Systems Modeling

To address the limitations of the "*Data Driven Modeling*" approaches, in Chapter 5 of this dissertation, I present a synthesis of an alternative approach that uses physics-based dynamical modeling techniques, which I refer to as "*Systems Modeling*". Systems modeling aims to capture complex feedbacks, cascading effects, and interdependencies across various heterogeneous components that constitute the system through mathematical and computational tools (cite). Often, the complex (and non-linear) interactions between components result in outcomes that cannot be derived from summation of individual behavior, such as critical transitions, tipping points, and bifurcations [62]. Examples of such phenomena include critical transitions in ecological systems such as shallow lakes exposed to accumulation of phosphorus and organic matter [359], shifts in climate scenarios [66], and percolation in social systems [360]. Systems modeling approaches can be implemented in various granularity of detail, ranging from a parsimonious model composed by a set of differential equations (DE), to high fidelity agent based model simulations (ABM), both with complementing pros and cons. The biggest advantage of a DE approach is that it allows researchers to obtain an understanding of the essential processes that govern the system, laying a scientific foundation for more detailed investigation. Moreover, DEs enable analytical tractability on the stability of the system, identification of equilibrium points, and significant interpretability of the model parameters. However, they are often limited to an aggregated understanding of the system due to its parsimonious nature, and lacks the ability to deliver specific policy recommendations in the context of disaster recovery and resilience. Chapter 5 shows examples of such parsimonious modeling approaches, using differential equations to capture socio-physical interdependencies. On the other hand, ABMs enable a more detailed, often spatially explicit understanding of the dynamic process, with the cost of analytical tractability and parsimony. ABMs are often more suitable for evaluating the effects of concrete policies on disaster recovery outcomes.

Data-Driven Systems Modeling

Compared with "Data-Driven Modeling" approaches, "Systems Modeling" has three main advantages. Systems modeling enables 1) better understanding and transparency of the underlying process that generates the observed data; 2) simulation of non-linear (e.g., feedbacks, cascades, in-

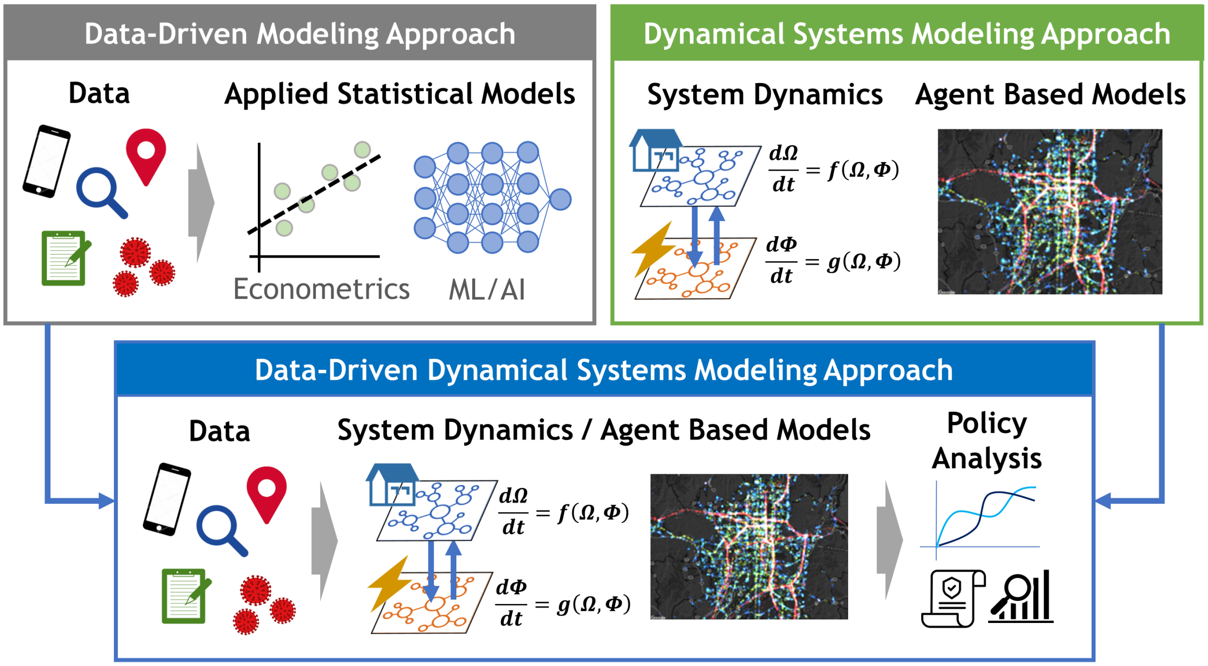

Figure 6.1. Illustration of differences between the Data-driven modeling, dynamical systems modeling, and data-driven dynamical systems modeling (D3S) approaches.

terdependencies) effects outside observed domain in data; and 3) counterfactual scenario analyses using various input parameters and synthetic data. Such characteristics are essential for informing policy decision making, since accountability and interpretability of the models are critical for the decision making process, and evaluating counterfactual scenarios is also essential for running cost-benefit analysis between multiple policy levers. To leverage the advantages of systems modeling approaches and also the availability of novel datasets, a "*Data-driven Systems Modeling*" approach is proposed and tested in this dissertation. The coupled urban socio-physical dynamics model presented in Section 5.1 demonstrates an example of the Data-driven Systems Modeling approach. The study presents a parsimonious model that characterizes the interdependencies between social and physical systems in urban systems, and calibrates the model parameters using a Markov Chain Monte Carlo approach. As a result, the model was able to: 1) unravel the interdependent and non-linear dynamics between social and physical systems during disaster recovery, 2) quantify the intra-regional variability in socio-physical coupling and recovery inequality, and 3) evaluate the resilience of urban systems to hypothetical recursive shocks under various socio-physical coupling parameter settings.

While the presented model was designed to be parsimonious, there are countless directions in which the systems model can be extended, to account for more detailed urban characteristics. For example, we may account for interdependencies with different urban systems, including cyber systems that consider various wireless sensor networks and power grids that connect households and vehicles during disaster recovery ("cyber-social-physical systems"). Social and physical systems, which were regionally aggregated components in the presented study, may be more disaggregated to account for heterogeneity within the systems. Social systems can be decomposed into various entities, including household networks, public agency networks, and non-profit organization networks, which in aggregate characterize the social capital of the communities [57]. Physical systems can also be disaggregated into various types of networks, including road networks, power grids, water and sewage pipelines, and natural resources such as rivers. Such physical systems could be interconnected through various types of interdependencies, including physical, cyber, geographic, and logical interdependencies [100]. As I will discuss in Section 6.2, such detailed systems models could be useful in identifying effective and concrete policies to improve the resilience of the entire system. Such disaggregation of the system models come in hand with new challenges, including the need to overcome the lack of data for model calibration. Such new research challenges that arise due to model disaggregation, and recent new ideas to overcome such challenges, will be further discussed in the following Sections.

6.3 Linking "Data-Driven Systems Modeling" and "Management"

Given the enormous size of economic damage inflicted by natural hazards on communities (more than US$ 2 trillion over the past 20 years globally), federal and local government agencies are the major source of funding for disaster response, recovery, and resilience (cite). Therefore, naturally one of the primary goals of developed models of disaster recovery and resilience becomes informing decision making agencies on most effective policies for improving resilience. However, practices of using novel high-frequency datasets (e.g., mobile phone location data) for public policy decision making is still in its infancy.

6.3.1 Opportunities

Increasing Availability of Data Products

As reviewed in Chapter 1, many studies have already utilized the various kinds of mobile phone location data for disaster management. However, these were often enabled by direct partnerships or collaborations between researchers and private companies who own the data, making the data extremely difficult to access for researchers outside the agreement. Due to the increased attention and interest on mobile phone location data during the COVID-19 pandemic, there has been several notable efforts where mobile phone location data, in their anonymized forms, are being made openly available for the public use. For example, the PlaceKey community (https://www.placekey.io/) have contributed to this effort by providing a semi-open platform where researchers can freely access aggregated mobile phone location data for analysis. The data are spatially and temporally aggregated to point-of-interests, and also made sure that a substantial small number of visit counts are masked, so that the individual users are unidentifiable. There are cases where researchers have led the efforts in anonymizing the data and making the mobility data open source. The team of researchers from The Robert Koch Institute and Humboldt University of Berlin have developed a dataset which contains mobility data collected from mobile phones in Germany during the first half of 2020 (January-July), and mobility data from March 2019, which can be used to study changes in mobility during the COVID-19 pandemic in 2020 (https://www.covid-19-mobility.org/).

In addition to these efforts, various organizations including major tech firms have made significant contributions in publishing aggregate statistics of mobility (e.g., social distancing, travel distance) during the COVID-19 for various regions around the world. The Google COVID-19 Community Mobility Reports, which contained the time series data of travelled distance in various cities around the world, was used by practitioners to monitor the effects of non-pharmaceutical policies on mobility restrictions [361]. A similar report on mobility patterns was also issued by Apple [362]. Camber Systems developed the county-level social distancing tracker based on aggregated and anonymous location data to understand how populations are engaging in social distancing over time (https://covid19.cambersystems.com/). The COVID-19 Mobility Data Network (CMDN) is a network of infectious disease epidemiologists at universities working with technology companies to use aggregated mobility data to support the COVID-19 response. The CMDN developed the Facebook Data for Good Mobility Dashboard, which visualizes the aggregate mobility trends, computed from Facebook mobility data, at the regional levels for various countries around the world (https://visualization.covid19mobility.org/).

Data for Development

With the availability of various types of novel datasets including social media data, mobile phone location data (call detail records, GPS), web search query data, and satellite imagery data, there has been significant efforts to utilize big data analytics for tackling challenges in development [363]. Several open data challenges have been initiated by collaborations between academia and industry data providers, such as the *Data4Development Challenge* held by Orange, which provided mobile phone data from Ivory Coast for analysis [364]. Large tech firms, including Google, Facebook, Apple, and Microsoft, have all boosted their efforts in utilizing the enormous amount of collected data for development and disaster management. Google.org, the is the charitable arm of Google, has committed roughly US$100 million in investments and grants to nonprofits annually to tackle various issues including disaster response, improving accessibility to education, and more recently, recovering from COVID-19 impacts (https://www.google.org/). International agencies have also accelerated their engagement in utilizing such big data sources for development projects. The World Bank has initiated the Development Data Partnership (https://datapartnership.org/), which is a partnership between international organizations and companies, created to facilitate the use of third-party data in research and international development. The Partnership includes more than 20 private companies, including location intelligence companies such as Google, Cuebiq, Safegraph, and CARTO, and social media companies including Twitter and Facebook. To assist the utilization of these datasets, recently, the Global Facility for Disaster Reduction and Recovery (GFDRR) - a partnership hosted within the World Bank - has undertaken efforts on using GPS location data collected from smartphones to analyze post-disaster population displacement for disaster relief and urban planning policy making. GFDRR has published working papers and publications on several case studies using smartphone location data accessed through the Development Data Partnership initiative, including the population displacement patterns and income inequality

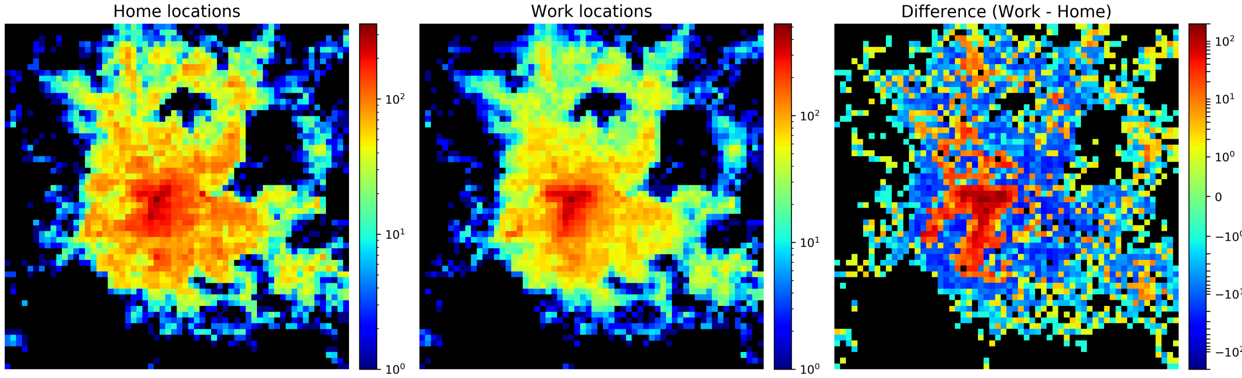

Figure 6.2. Pre-disaster density maps (∼ 2017/9/16) of estimated home locations, office locations, and difference in density. Hotspots during the day and night are visualized in Mexico City and peripheral regions [157]

in Mexico City after the Puebla Earthquake [157] and socioeconomic gaps in mobility reduction during the COVID-19 pandemic in Colombia, Mexico, and Indonesia [365].

Open Source Toolkits for Mobility Analytics

To assist policy makers and non-data experts to leverage the increasing availability of mobile phone location datasets, there has also been several efforts to develop open source toolkits for mobility data analytics. `scikit-mobility` is a Python-based library that enables various operations and analyses on large-scale mobility data [366]. Compared to previous Python based mobility analysis libraries such as `Bandicoot` [367] and `movingpandas` [368], `scikit-mobility` is most comprehensive, containing functions for pre-processing, stop detection, computation of mobility metrics (e.g., displacements, characteristic distance, origin-destination matrix), trajectory synthesis, visualizations, and privacy risk quantification. There exists several libraries to conduct trajectory analysis in the R ecosystem, however, none of the libraries are optimized for human mobility data, thus lacks functions for generating synthetic trajectories and producing advanced visualizations (for a review, see [369]). `OSMnx` is a powerful library for acquiring, constructing, analyzing, and visualizing complex street networks from OpenStreetMap [370]. In combination with human mobility data, `OSMnx` enables users to perform various spatial analysis including route estimation and point-of-interest visit estimation. More recently, the GFDRR developed an open-source location data analytics toolkit in Python, `MobilKit`, in collaboration with Purdue University

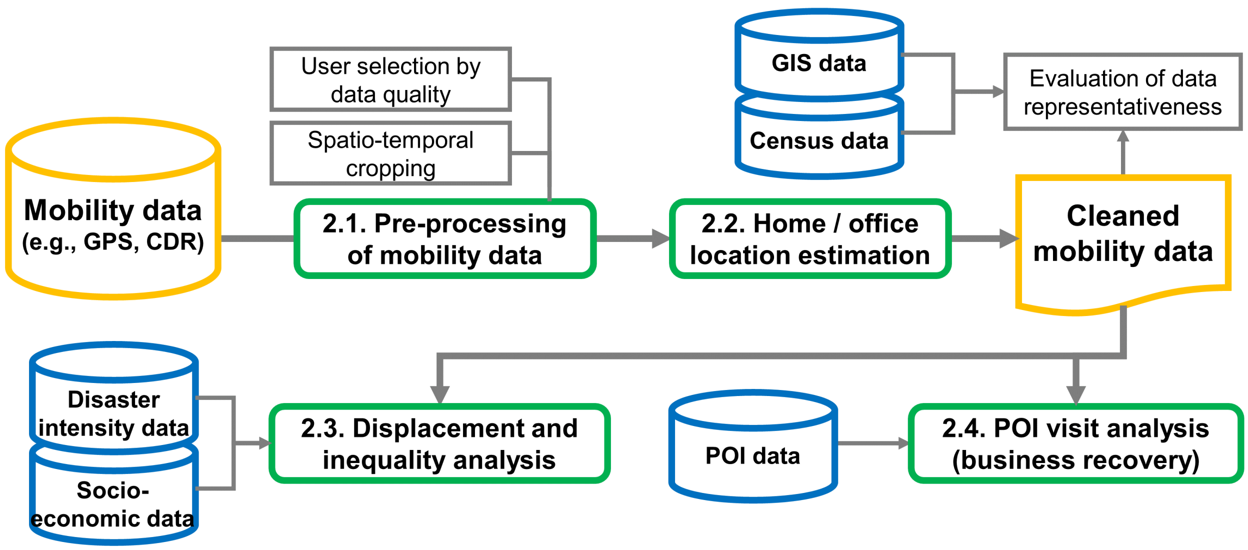

Figure 6.3. Flowchart of the disaster mobility analytics toolkit that we developed in collaboration with The World bank [371].

and MindEarth (a non-profit based in Switzerland; https://www.mindearth.org/), which extends the functions in `scikit-mobility` to conduct post-disaster mobility analysis (https://github.com/GFDRR/mobilkit) [371]. To enable non-experts to use the softwares, the codes are optimized using Dask [372] for parallel computing, so that analysis on massive mobility datasets can be conducted under constrained resources, on local laptop or desktop computers. Figure 6.3 shows the flowchart of the disaster mobility analytics toolkit that we developed. Using the toolkit, we analyzed data collected from the Puebla Earthquake in Mexico, and revealed income inequality effects in displacement patterns, as well as differences in urban catchment patterns of various points-of-interest [157]. Figure 6.2 shows the pre-earthquake home locations, office locations, and difference in density estimated from mobile phone location data. Hotspots during the day and night are visualized in Mexico City and peripheral regions.

6.3.2 Challenges in Linking Data, Systems Modeling, and Policy

Despite such efforts, we still lack strong pipelines connecting data-driven modeling, data-driven systems modeling, and policy evaluation and analysis. While there needs to be further collaboration between academics and practitioners to establish such information pipelines, there are specific challenges that need to be addressed.

Understanding the Data Generative Process

One of the key drawbacks of using the more recently available smartphone GPS location data is the lack of our understanding in how these data are collected and processed. Several studies have conducted investigations on the representativeness of these datasets (e.g., [242]) using raw data, by quantifying the correlation between the number of mobile phone users estimated to be living in each geographical region, and the census population information. This metric, however, is far from comprehensive, and we have pressing demand for a more thorough investigation on various aspects of socio-demographic and socio-economic characteristics, and to ensure that the observation samples in the data are not biased towards a specific population group of wealth, region, ethnicity, gender, etc. This procedure becomes even more difficult when only aggregate information, such as the total number of daily users in a specific region or the daily number of visitors to a specific point-of-interest, are provided by the data providers. In addition to the uncertainties in the sample representativeness, the data collection procedure is not transparent. For example, some softwares and applications collect location data when the device detects substantial movement, therefore, only a very small number of points would be observed if the user stays at one location (e.g., home) during the entire day. Other algorithms collect location information in extremely high frequency (e.g., every minute), irrespective of the amount of movement. This is partly the reason why we observe such a large variance (i.e. truncated power law) in the number of observation points per user [242]. In the absence of methods and algorithms for correcting the bias in the data, the trustworthiness of the data products and analysis will be undermined. A more open discussion between data users – researchers and practitioners – and data providers to further understand the process of dataset generation, and a standardized way of quantifying and reporting the representativeness biases and the potential errors present within the dataset are essential for more inclusive, fair, and trustworthy data products for disaster response.

Data Governance

As we experience an increase and universal accessibility to large scale mobile phone location data, the protection of personal privacy has never been more important [373]. Previous studies have revealed that a very few number of data points could reveal the identity of the user with high accuracy, highlighting the importance of anonymization techniques [374]. Following such public concerns, data providers have started to provide processed data, aggregated by space and time. For example, the Disaster Maps data in the Facebook Data for Good program aggregates population density and flow into each day, into 6 kilometer size grid cells, and further applies spatial smoothing algorithms to anonymize the data. This process, although effective in anonymizing the data and protecting the users' privacy, comes with a price in the data granularity and uncertainties in the data quality, as explained in the previous Section. To address this issue and to balance out the data quality with privacy protection, the concept and techniques of differential privacy are gaining attention. Differential privacy is a criterion, which tools are devised to satisfy. It enables the collection, analysis, and sharing of statistical estimates using personal data while protecting the privacy of the individuals in the dataset [375]. Techniques such as differential privacy may serve as one baseline to ensure the safety of personal privacy, but we are still amidst the search for a holistic framework that integrates technical solutions, ethical guidelines, and regulations on the use of mobile phone location data.

Tailoring Model Outputs with Policy Needs

As discussed in the previous Section, the Data-Driven Dynamical Systems Modeling approach can be implemented in a wide range of spatial and temporal granularity, as well as system component details and scale. In order to link model outputs with policy needs, there needs to be sufficient input from the policy maker side to specify the model details. More specifically, the following questions should be asked to build the systems model: What are the specific policy levers that the policy makers have as options, and what are their spatial and temporal scale of interest? What variables and evaluation metrics consist the objective function of the decision maker? How much uncertainty do the policy makers want to consider when simulating the likely future outcomes? Extensive communication between researchers and practitioners is key to effectively linking models to development policy support tools.

Preparing for Unprecedented Events

The Tohoku Tsunami, which struck the Tohoku coast in Japan in 2011 following a Magnitude 9.0 earthquake, caused over 15,000 deaths and over $360 billion in economic damage. Despite the large number of earthquakes hitting Japan each year, the previous tsunamis that hit the Tohoku coast were in 1896 (over 20,000 deaths), 1933 (over 3,000 deaths), and a minor event in 1960 (142 deaths). This makes the 2011 Tohoku Tsunami the most catastrophic disaster event in over 100 years (since the 1896 tsunami). Similarly, Hurricane Maria (Category 5) was the largest hurricane to make landfall in Puerto Rico. This rarity, even though such climate shocks are increasing year by year, increases the difficulty in preparing for severe natural hazards, since many cities do not have prior data to predict future disaster scenarios. Spatially explicit simulation models perform poorly when applied to different cities, because of varying urban properties (e.g. socio-economic, geographic characteristics). One approach to overcome this challenge is to develop computational techniques that allows us to transfer insights, dynamics, and simulation models across regions so that cities can learn from each others' experiences. This could lead to better preparation for unprecedented, black swan events (e.g. "What if a 2011 Tohoku-level Tsunami hit Los Angeles?").

Various analogical problem settings have been worked on in the computer science field. For example, transfer learning [376] and reinforcement learning [377] are computational frameworks that can be applied in these settings. Recent works have attempted to learn human behavior from one city and use the learned behavioral model to predict human mobility dynamics in counterfactual scenarios in a different city using inverse reinforcement learning [378]. Our studies described in Chapter 5, based on unsupervised machine translation approaches, are also attempts to bridge this research gap. Despite such methodological advances, we still lack extensive empirical testing that validates the performance of these algorithms, and the limits of inter-regional transfer. For example, understanding the pairings of cities where knowledge transfer and translation works well, and those where they fail, are still under-studied.

Effective Communication of Findings

To effectively communicate the prediction results from various simulation models to different stakeholders, and to obtain feedback to further improve the models, the measures and indices of recovery and resilience need to be tailored for different stakeholders. For instance, for city agencies, the effects of various policies on household and business recovery at the aggregate level, and any inequalities that may emerge in recovery, should be emphasized. On the contrary, when presenting results to local community members, metrics of recovery should focus more on the individual and household levels to enhance engagement. When communicating the results to policy makers, it is important to quantify the sources of uncertainties and to what degree they can affect the outcomes of the simulation predictions. Recently, various visualization tools including dashboards and web-based GIS platforms have been developed for this purpose. Such tools would enable us to communicate the sensitivity of recovery predictions under various policy scenarios using toggle bars and have a sustainable, bi-directional dialogue with community stakeholders at various workshops. For example, the "MyCityForecast" tool, developed by researchers at The University of Tokyo, is a successful example of such visualization tool [379]. Other dashboards have been developed to tackle the COVID-19 pandemic (e.g., [380]), however, we currently lack effective interfaces to communicate disaster resilience simulation results to policy makers.

6.4 Future Research Directions

To address the aforementioned two recommended trajectories of the research field, I propose various exciting research directions left for future research endeavours, ranging from technical innovations in data-driven dynamical systems modeling, to establishing an open-source platform where scientists and practitioners can share data, models, and insights for a more united approach to tackling resilience challenges.

1) Disaggregation of Social and Physical System Components

The data-driven systems model explained in Section 5.1 was a parsimonious model, composed of aggregate "social" and "physical" systems. While this modeling approach laid out a scientific foundation for further understanding the resilience of coupled urban systems to shocks by revealing socio-physical interdependencies and their effects on resilience, such aggregation comes with a drawback of not being able to capture the specific dynamics that occur within various systems. For example, aggregation of social systems results in neglecting the structures of social networks among households and local organizations, which are understood to be crucial in building up social capital and community resilience [57]. Physical infrastructure systems are also inter-connected and interdependent with each other in many ways [100] (for example, traffic lights that control transportation infrastructure depend on functioning power networks). Enhancing the details of the coupled model by disaggregating social and physical system components is a computationally challenging but important research direction.

2) Spatially Explicit Modeling for Decision Making

The presented models in Chapter 4 were agnostic in the location; that is, it could be applied to any location of interest with availability of data. However, to further apply the model results for decision making, the models need to take into consideration various spatial and local contexts. One example of such context is the spatial configuration of the social and physical networks. More specifically, many specific urban characteristics such as the spatial distributions of population groups, spatial segregation of income groups, locations with high risks of flooding, the spatial layout of the power grid in urban areas, all affect how the disaster effects play out in cities. In addition to disaggregating the social and physical system components (Future research direction 1), there is a need to model the dynamics in a more spatially explicit manner. Agent based simulations of urban dynamics is a useful approach that is used in various disciplines and problem settings (e.g., [114], [115], [120]). Efforts to integrate insights that were revealed by system dynamics models into agent based simulation frameworks is a promising direction for urban disaster resilience.

3) Application to Resilience of Specific Infrastructure Systems

Many urban infrastructure systems are functionally coupled with social systems. One example of such infrastructure are transportation networks. So far in the literature, transportation resilience has been studied from an engineering resilience perspective (e.g., [95], [96], [381]), neglecting the complex feedback dynamics that occur between physical systems service deficit (traffic congestion), and human travel behavior. By applying the theoretical framework of socio-physical coupling posed in this dissertation, we may be able to better understand the resilience of specific infrastructure systems. Fusion with domain expertise (e.g., transport modeling, electrical engineering) could further increase the reality and usefulness of the developed models.

4) Feedbacks Across Spatial Scales

In many of our studies, we have collected various data from individuals (e.g., mobile phone users) and analyzed/modeled them to extract insights about the urban social and physical systems in a spatially aggregated scale (i.e., county-level). Such analysis of collective individual patterns have revealed interesting emergent patterns, such as universal population recovery patterns (Section 2.1) and logistic recovery of business firms (Section 3.3). Insights at the aggregated level are useful for decision makers on the municipal and regional government levels. However, to build community resilience from the bottom up, there needs to be more efforts on giving back such knowledge to stakeholders at the community and household levels. With the ubiquitousness of smartphones and online social networking platforms, the cost of reaching local communities has substantially decreased. How to translate the insights obtained from aggregate models into the local stakeholders' scale is a challenging but important research direction for the future.

5) Cross-City Learning for Unprecedented Shocks

As addressed as one of the challenges in linking systems modeling to development, despite the increasing number of various shocks to cities due to climate change and rapid urbanization (see Section 1.1), from each city's point of view, (fortunately) there are not enough disaster events that they experience to fully learn from. In order to prepare for future unprecedented shocks, it is necessary to synthesize insights from various past disaster events across the world. Therefore, the million dollar question becomes; how can cities learn from eachother for better preparation? Although this has been implemented in the operational knowledge sharing perspectives through various inter-city organizations such as the Rockefeller Foundation's 100 Resilient Cities Initiative (https://www.rockefellerfoundation.org/100-resilient-cities/), on the more computational and predictive levels, transfering insights of post-disaster dynamics across cities is a challenging task. Utilizing novel approaches such as transfer learning [376] and reinforcement learning [377], as well as unsupervised machine translation approaches [343], [346], [382] as shown in Chapter 5, could provide solutions for this problem.

6) Fusion of Multiple Data Sources

While we have seen a rapid increase of the usage of mobile phone location data, there are several other types of data that have been used frequently in disaster management, including satellite imagery (for a review article, see [383]) and social media data (for review articles, see [188], [384]). Satellite imagery, despite its low frequency of data collection, enables the observation of damages to the natural and built environments in a detailed spatial scale. On the other hand, social media data contains rich information on the peoples' opinions, ideas, and sentiments at a high temporal granularity. Moreover, combining mobile phone location data with household surveys could allow us to analyze both the post-disaster mobility patterns as well as the motivations behind such behavior. More recently, credit card transaction data has become more available for research purposes (e.g., [385]). Using credit card data, we are able to understand the economic impacts of disasters and epidemics at a spatially and temporally granular level. Combining these datasets with mobile phone location data and human mobility analytics (e.g., application in poverty estimation [386]) could enable a more holistic understanding of the social, physical, and economic dimensions of the disaster response and recovery dynamics.

7) Open-Source Platform For Data, Models, and Insights

As discussed in the challenges in linking systems modeling to development, in order to enhance knowledge sharing for cities across the globe and between researchers and practitioners, we need a unifying scheme to share data, models, and insights. We developed an open-source Github repository with the Global Facility for Disaster Recovery and Reduction (GFDRR) of The World Bank (https://github.com/GFDRR/mobility-analysis/), which enables non-experts to analyze mobile phone location data for disaster resilience and urban planning applications on their local laptop computer environments. As introduced in the previous sections, with the increase in popularity for using mobility data during the COVID-19 pandemic has led to more data sharing platforms and communities, with careful considerations of differential privacy [387], [388]. However, there is still little effort in information sharing between academics and industry stakeholders, who have more access to disaggregate datasets. Further collaborations need to be facilitated to have a better understanding of how such data are collected from users, data representativeness, and various socio-economic biases that exist in the sample populations, which could significantly skew analysis results and lead to inequitable policy decisions.

REFERENCES

[1] F. E. Otto, S. Philip, S. Kew, S. Li, A. King, and H. Cullen, "Attributing high-impact extreme events across timescales—a case study of four different types of events," *Climatic change*, vol. 149, no. 3-4, pp. 399–412, 2018.

[2] C. B. Field, *Managing the risks of extreme events and disasters to advance climate change adaptation: special report of the intergovernmental panel on climate change*. Cambridge University Press, 2012.

[3] M. K. Van Aalst, "The impacts of climate change on the risk of natural disasters," *Disasters*, vol. 30, no. 1, pp. 5–18, 2006.

[4] P. Wallemacq, *Economic losses, poverty & disasters: 1998-2017*. Centre for Research on the Epidemiology of Disasters, CRED, 2018.

[5] M. Coronese, F. Lamperti, K. Keller, F. Chiaromonte, and A. Roventini, "Evidence for sharp increase in the economic damages of extreme natural disasters," *Proceedings of the National Academy of Sciences*, vol. 116, no. 43, pp. 21 450–21 455, 2019.

[6] S. Schmidt, C. Kemfert, and P. Höppe, "Tropical cyclone losses in the usa and the impact of climate change—a trend analysis based on data from a new approach to adjusting storm losses," *Environmental Impact Assessment Review*, vol. 29, no. 6, pp. 359–369, 2009.

[7] The World Bank, *Resilient cities*, https://www.worldbank.org/en/topic/urbandevelopment/brief/resilient-cities-program, Accessed: 2020-04-07.

[8] S. Hallegatte, A. Vogt-Schilb, M. Bangalore, and J. Rozenberg, *Unbreakable: building the resilience of the poor in the face of natural disasters*. World Bank Publications, 2016.

[9] S. Hallegatte, J. Rentschler, and B. Walsh, *Building back better: achieving resilience through stronger, faster, and more inclusive post-disaster reconstruction*. World Bank, 2018.

[10] L. A. Johnson and R. B. Olshansky, *After great disasters: How six countries managed community recovery*. Lincoln Institute of Land Policy Cambridge, MA, 2016.

[11] I. Roefs, B. Meulman, J. H. Vreeburg, and M. Spiller, "Centralised, decentralised or hybrid sanitation systems? economic evaluation under urban development uncertainty and phased expansion," *Water research*, vol. 109, pp. 274–286, 2017.

[12] E. Wilkinson, J. Twigg, and R. Few, "Building back better: A resilience caribbean after the 2017 hurricanes," *London: Overseas Development Institute (ODI)*, 2018.

[13] A. D. Roque, D. Pijawka, and A. Wutich, "The role of social capital in resiliency: Disaster recovery in puerto rico," *Risk, Hazards & Crisis in Public Policy*, vol. 11, no. 2, pp. 204–235, 2020.

[14] L. Pyles, J. Svistova, S. Ahn, and T. Birkland, "Citizen participation in disaster recovery projects and programmes in rural communities: A comparison of the haiti earthquake and hurricane katrina," *Disasters*, vol. 42, no. 3, pp. 498–518, 2018.

[15] J. Collodi, M. Pelling, A. Fraser, M. Borie, and S. Di Vicenz, "How do you build back better so no one is left behind? lessons from sint maarten, dutch caribbean, following hurricane irma," *Disasters*, 2019.

[16] S. Hallegatte, A. Vogt-Schilb, J. Rozenberg, M. Bangalore, and C. Beaudet, "From poverty to disaster and back: A review of the literature," *Economics of Disasters and Climate Change*, vol. 4, no. 1, pp. 223–247, 2020.

[17] M. N. Burton-Chellew, R. M. May, and S. A. West, "Combined inequality in wealth and risk leads to disaster in the climate change game," *Climatic change*, vol. 120, no. 4, pp. 815–830, 2013.

[18] Y. Sakai, J. P. Estudillo, N. Fuwa, Y. Higuchi, and Y. Sawada, "Do natural disasters affect the poor disproportionately? price change and welfare impact in the aftermath of typhoon milenyo in the rural philippines," *World Development*, vol. 94, pp. 16–26, 2017.

[19] C. A. Felima, "Haiti's disproportionate casualties after environmental disasters: Analyzing human vulnerabilities and the impacts of natural hazards," *Journal of Haitian Studies*, pp. 6–28, 2009.

[20] P. Warr and L. L. Aung, "Poverty and inequality impact of a natural disaster: Myanmar's 2008 cyclone nargis," *World Development*, vol. 122, pp. 446–461, 2019.

[21] H.-A. H. Dang, P. F. Lanjouw, and R. Swinkels, "Who remained in poverty, who moved up, and who fell down?" *Poverty reduction in the course of African development*, pp. 183–217, 2017.

[22] M. Masozera, M. Bailey, and C. Kerchner, "Distribution of impacts of natural disasters across income groups: A case study of new orleans," *Ecological economics*, vol. 63, no. 2-3, pp. 299–306, 2007.

[23] E. Enarson, A. Fothergill, and L. Peek, "Gender and disaster: Foundations and directions," in *Handbook of disaster research*, Springer, 2007, pp. 130–146.

[24] L. Hemingway and M. Priestley, "Natural hazards, human vulnerability and disabling societies: A disaster for disabled people?," 2006.

[25] S. V. Ukkusuri, T. Yabe, and K. Seetharam, "Non-pharmaceutical interventions for covid-19: Evidence from large-scale mobility data in tokyo," *Asian Development Bank Institute Policy Brief Series*, vol. 10, no. 6, 2020.

[26] C. Bambra, R. Riordan, J. Ford, and F. Matthews, "The covid-19 pandemic and health inequalities," *J Epidemiol Community Health*, vol. 74, no. 11, pp. 964–968, 2020.

[27] J. A. Weill, M. Stigler, O. Deschenes, and M. R. Springborn, "Social distancing responses to covid-19 emergency declarations strongly differentiated by income," *Proceedings of the National Academy of Sciences*, vol. 117, no. 33, pp. 19 658–19 660, 2020.

[28] R. Verma, T. Yabe, and S. V. Ukkusuri, "Mobility-based contact exposure explains the disparity of spread of covid-19 in urban neighborhoods," *arXiv preprint arXiv:2102.03698*, 2021.

[29] World Bank, *Poverty and shared prosperity 2016: Taking on inequality*, 2016.

[30] A. Fahlberg, T. J. Vicino, R. Fernandes, and V. Potiguara, "Confronting chronic shocks: Social resilience in rio de janeiro's poor neighborhoods," *Cities*, vol. 99, p. 102 623, 2020.

[31] H. Klammler, P. Rao, and K. Hatfield, "Modeling dynamic resilience in coupled technological-social systems subjected to stochastic disturbance regimes," *Environment Systems and Decisions*, vol. 38, no. 1, pp. 140–159, 2018.

[32] The World Bank, *Urban development*, https://www.worldbank.org/en/topic/urbandevelopment/overview, Accessed: 2020-04-07.

[33] P.-A. Balland, C. Jara-Figueroa, S. G. Petralia, M. P. Steijn, D. L. Rigby, and C. A. Hidalgo, "Complex economic activities concentrate in large cities," *Nature Human Behaviour*, vol. 4, no. 3, pp. 248–254, 2020.

[34] X. Li, Y. Zhou, M. zhao, and X. Zhao, *Harmonization of dmsp and viirs nighttime light data from 1992-2018 at the global scale*, Jan. 2020. DOI: 10.6084/m9.figshare.9828827.v3. [Online]. Available: https://figshare.com/articles/dataset/Harmonization-of-DMSP-and-VIIRS-nighttime-light-data-from-1992-2018-at-the-global-scale/9828827/3.

[35] G. M. de Espindola, E. L. N. da Costa Carneiro, and A. C. Façanha, "Four decades of urban sprawl and population growth in teresina, brazil," *Applied Geography*, vol. 79, pp. 73–83, 2017.

[36] Z. Kovacic, S. Smit, J. K. Musango, A. C. Brent, and M. Giampietro, "Probing uncertainty levels of electrification in informal urban settlements: A case from south africa," *Habitat International*, vol. 56, pp. 212–221, 2016.

[37] E. A. Adams, "Intra-urban inequalities in water access among households in malawi's informal settlements: Toward pro-poor urban water policies in africa," *Environmental Development*, vol. 26, pp. 34–42, 2018.

[38] L. A. Guzman, D. Oviedo, and C. Rivera, "Assessing equity in transport accessibility to work and study: The bogotá region," *Journal of Transport Geography*, vol. 58, pp. 236–246, 2017.

[39] D. Hernandez, "Uneven mobilities, uneven opportunities: Social distribution of public transport accessibility to jobs and education in montevideo," *Journal of Transport Geography*, vol. 67, pp. 119–125, 2018.

[40] D. M. Nassar and H. G. Elsayed, "From informal settlements to sustainable communities," *Alexandria engineering journal*, vol. 57, no. 4, pp. 2367–2376, 2018.

[41] S. Hallegatte, C. Green, R. J. Nicholls, and J. Corfee-Morlot, "Future flood losses in major coastal cities," *Nature climate change*, vol. 3, no. 9, pp. 802–806, 2013.

[42] D. S. Williams, M. Manez Costa, C. Sutherland, L. Celliers, and J. Scheffran, "Vulnerability of informal settlements in the context of rapid urbanization and climate change," *Environment and Urbanization*, vol. 31, no. 1, pp. 157–176, 2019.

[43] A. Zerbo, R. C. Delgado, and P. A. González, "Vulnerability and everyday health risks of urban informal settlements in sub-saharan africa," *Global Health Journal*, 2020.

[44] P. Murray-Tuite and B. Wolshon, "Evacuation transportation modeling: An overview of research, development, and practice," *Transportation Research Part C: Emerging Technologies*, vol. 27, pp. 25–45, 2013.

[45] X. Lu, L. Bengtsson, and P. Holme, "Predictability of population displacement after the 2010 haiti earthquake," *Proceedings of the National Academy of Sciences*, vol. 109, no. 29, pp. 11 576–11 581, 2012.

[46] E. Fussell, K. J. Curtis, and J. DeWaard, "Recovery migration to the city of new orleans after hurricane katrina: A migration systems approach," *Population and environment*, vol. 35, no. 3, pp. 305–322, 2014.

[47] L. K. Siebeneck, M. K. Lindell, C. S. Prater, H.-C. Wu, and S.-K. Huang, "Evacuees' reentry concerns and experiences in the aftermath of hurricane ike," *Natural Hazards*, vol. 65, no. 3, pp. 2267–2286, 2013.

[48] J. P. Cangialosi, A. S. Latto, and R. Berg, "National hurricane center tropical cyclone report: Hurricane irma," *National Hurricane Center*, vol. 30, 2018.

[49] M. Batty, “Cities as complex systems: Scaling, interaction, networks, dynamics and urban morphologies.,” 2009.

[50] L. M. Bettencourt, “Cities as complex systems,” *Modeling complex systems for public policies*, pp. 217–236, 2015.

[51] L. M. Bettencourt, “The origins of scaling in cities,” *science*, vol. 340, no. 6139, pp. 1438–1441, 2013.

[52] E. Krueger, C. Klinkhamer, C. Urich, X. Zhan, and P. S. C. Rao, “Generic patterns in the evolution of urban water networks: Evidence from a large asian city,” *Physical Review E*, vol. 95, no. 3, p. 032 312, 2017.

[53] X. Zhan, S. V. Ukkusuri, and P. S. C. Rao, “Dynamics of functional failures and recovery in complex road networks,” *Physical Review E*, vol. 96, no. 5, p. 052 301, 2017.

[54] S. Yang, O. Büttner, J. W. Jawitz, R. Kumar, P. S. C. Rao, and D. Borchardt, “Spatial organization of human population and wastewater treatment plants in urbanized river basins,” *Water Resources Research*, vol. 55, no. 7, pp. 6138–6152, 2019.

[55] A. Shreevastava, P. S. C. Rao, and G. S. McGrath, “Emergent self-similarity and scaling properties of fractal intra-urban heat islets for diverse global cities,” *Physical Review E*, vol. 100, no. 3, p. 032 142, 2019.

[56] C. Finch, C. T. Emrich, and S. L. Cutter, “Disaster disparities and differential recovery in new orleans,” *Population and Environment*, vol. 31, no. 4, pp. 179–202, 2010.

[57] D. P. Aldrich, *Building resilience: Social capital in post-disaster recovery*. University of Chicago Press, 2012.

[58] J. W. McCaughey, P. Daly, I. Mundir, S. Mahdi, and A. Patt, “Socio-economic consequences of post-disaster reconstruction in hazard-exposed areas,” *Nature Sustainability*, vol. 1, no. 1, p. 38, 2018.

[59] J. Aerts, W. Botzen, K. Clarke, S. Cutter, J. W. Hall, B. Merz, E. Michel-Kerjan, J. Mysiak, S. Surminski, and H. Kunreuther, “Integrating human behaviour dynamics into flood disaster risk assessment,” *Nature Climate Change*, p. 1, 2018.

[60] C. Holling, “Principles of insect predation,” *Annual review of entomology*, vol. 6, no. 1, pp. 163–182, 1961.

[61] C. S. Holling, “Resilience and stability of ecological systems,” *Annual review of ecology and systematics*, vol. 4, no. 1, pp. 1–23, 1973.

[62] M. Scheffer, *Critical transitions in nature and society*. Princeton University Press, 2020, vol. 16.

[63] M. Scheffer, S. Carpenter, J. A. Foley, C. Folke, and B. Walker, "Catastrophic shifts in ecosystems," *Nature*, vol. 413, no. 6856, p. 591, 2001.

[64] C. Folke, S. Carpenter, B. Walker, M. Scheffer, T. Elmqvist, L. Gunderson, and C. S. Holling, "Regime shifts, resilience, and biodiversity in ecosystem management," *Annu. Rev. Ecol. Evol. Syst.*, vol. 35, pp. 557–581, 2004.

[65] S. H. Strogatz, *Nonlinear dynamics and chaos with student solutions manual: With applications to physics, biology, chemistry, and engineering*. CRC press, 2018.

[66] M. Scheffer, S. R. Carpenter, T. M. Lenton, J. Bascompte, W. Brock, V. Dakos, J. Van de Koppel, I. A. Van de Leemput, S. A. Levin, E. H. Van Nes, *et al.*, "Anticipating critical transitions," *science*, vol. 338, no. 6105, pp. 344–348, 2012.

[67] T. M. Lenton, "Early warning of climate tipping points," *Nature climate change*, vol. 1, no. 4, pp. 201–209, 2011.

[68] M. Scheffer, J. Bascompte, W. A. Brock, V. Brovkin, S. R. Carpenter, V. Dakos, H. Held, E. H. Van Nes, M. Rietkerk, and G. Sugihara, "Early-warning signals for critical transitions," *Nature*, vol. 461, no. 7260, pp. 53–59, 2009.

[69] S. R. Carpenter and W. A. Brock, "Rising variance: A leading indicator of ecological transition," *Ecology letters*, vol. 9, no. 3, pp. 311–318, 2006.

[70] V. Guttal and C. Jayaprakash, "Changing skewness: An early warning signal of regime shifts in ecosystems," *Ecology letters*, vol. 11, no. 5, pp. 450–460, 2008.

[71] L. Dai, D. Vorselen, K. S. Korolev, and J. Gore, "Generic indicators for loss of resilience before a tipping point leading to population collapse," *Science*, vol. 336, no. 6085, pp. 1175–1177, 2012.

[72] L. H. Gunderson, *Panarchy: understanding transformations in human and natural systems*. Island press, 2001.

[73] C. Folke, "Resilience: The emergence of a perspective for social–ecological systems analyses," *Global environmental change*, vol. 16, no. 3, pp. 253–267, 2006.

[74] M. A. Janssen, T. A. Kohler, and M. Scheffer, "Sunk-cost effects and vulnerability to collapse in ancient societies," *Current anthropology*, vol. 44, no. 5, pp. 722–728, 2003.

[75] M. Scheffer, F. Westley, and W. Brock, "Slow response of societies to new problems: Causes and costs," *Ecosystems*, vol. 6, no. 5, pp. 493–502, 2003.

[76] R. Biggs, M. Schlüter, D. Biggs, E. L. Bohensky, S. BurnSilver, G. Cundill, V. Dakos, T. M. Daw, L. S. Evans, K. Kotschy, *et al.*, "Toward principles for enhancing the resilience of ecosystem services," *Annual review of environment and resources*, vol. 37, pp. 421–448, 2012.

[77] C. Folke, J. Colding, and F. Berkes, "Synthesis: Building resilience and adaptive capacity in social-ecological systems," *Navigating social-ecological systems: Building resilience for complexity and change*, vol. 9, no. 1, pp. 352–387, 2003.

[78] P. Olsson, V. Galaz, and W. J. Boonstra, "Sustainability transformations: A resilience perspective," *Ecology and Society*, vol. 19, no. 4, 2014.

[79] M. E. Newman, A.-L. E. Barabási, and D. J. Watts, *The structure and dynamics of networks.* Princeton university press, 2006.

[80] A.-L. Barabási, "Network science," *Philosophical Transactions of the Royal Society A: Mathematical, Physical and Engineering Sciences*, vol. 371, no. 1987, p. 20 120 375, 2013.

[81] A.-L. Barabási and R. Albert, "Emergence of scaling in random networks," *science*, vol. 286, no. 5439, pp. 509–512, 1999.

[82] R. Cohen, K. Erez, D. Ben-Avraham, and S. Havlin, "Resilience of the internet to random breakdowns," *Physical review letters*, vol. 85, no. 21, p. 4626, 2000.

[83] R. Cohen, K. Erez, D. Ben-Avraham, and S. Havlin, "Breakdown of the internet under intentional attack," *Physical review letters*, vol. 86, no. 16, p. 3682, 2001.

[84] C. M. Schneider, A. A. Moreira, J. S. Andrade, S. Havlin, and H. J. Herrmann, "Mitigation of malicious attacks on networks," *Proceedings of the National Academy of Sciences*, vol. 108, no. 10, pp. 3838–3841, 2011.

[85] J. Gao, B. Barzel, and A.-L. Barabási, "Universal resilience patterns in complex networks," *Nature*, vol. 530, no. 7590, p. 307, 2016.

[86] J. Gao, X. Liu, D. Li, and S. Havlin, "Recent progress on the resilience of complex networks," *Energies*, vol. 8, no. 10, pp. 12 187–12 210, 2015.

[87] X. Huang, J. Gao, S. V. Buldyrev, S. Havlin, and H. E. Stanley, "Robustness of interdependent networks under targeted attack," *Physical Review E*, vol. 83, no. 6, p. 065 101, 2011.

[88] S. V. Buldyrev, R. Parshani, G. Paul, H. E. Stanley, and S. Havlin, "Catastrophic cascade of failures in interdependent networks," *Nature*, vol. 464, no. 7291, pp. 1025–1028, 2010.

[89] R. Parshani, S. V. Buldyrev, and S. Havlin, "Interdependent networks: Reducing the coupling strength leads to a change from a first to second order percolation transition," *Physical review letters*, vol. 105, no. 4, p. 048 701, 2010.

[90] C. E. La Rocca, H. E. Stanley, and L. A. Braunstein, "Strategy for stopping failure cascades in interdependent networks," *Physica A: Statistical Mechanics and its Applications*, vol. 508, pp. 577–583, 2018.

[91] J. Gao, S. V. Buldyrev, H. E. Stanley, and S. Havlin, "Networks formed from interdependent networks," *Nature physics*, vol. 8, no. 1, pp. 40–48, 2012.

[92] J. Gao, S. V. Buldyrev, S. Havlin, and H. E. Stanley, "Robustness of a network of networks," *Physical Review Letters*, vol. 107, no. 19, p. 195 701, 2011.

[93] S. Havlin, D. Y. Kenett, E. Ben-Jacob, A. Bunde, R. Cohen, H. Hermann, J. Kantelhardt, J. Kertész, S. Kirkpatrick, J. Kurths, *et al.*, "Challenges in network science: Applications to infrastructures, climate, social systems and economics," *The European Physical Journal Special Topics*, vol. 214, no. 1, pp. 273–293, 2012.

[94] L. H. Gunderson, "Ecological resilience—in theory and application," *Annual review of ecology and systematics*, vol. 31, no. 1, pp. 425–439, 2000.

[95] C. Wan, Z. Yang, D. Zhang, X. Yan, and S. Fan, "Resilience in transportation systems: A systematic review and future directions," *Transport reviews*, vol. 38, no. 4, pp. 479–498, 2018.

[96] A. A. Ganin, M. Kitsak, D. Marchese, J. M. Keisler, T. Seager, and I. Linkov, "Resilience and efficiency in transportation networks," *Science advances*, vol. 3, no. 12, e1701079, 2017.

[97] J. Park, T. P. Seager, P. S. C. Rao, M. Convertino, and I. Linkov, "Integrating risk and resilience approaches to catastrophe management in engineering systems," *Risk Analysis*, vol. 33, no. 3, pp. 356–367, 2013.

[98] D. J. Yu, M. L. Schoon, J. K. Hawes, S. Lee, J. Park, P. S. C. Rao, L. K. Siebeneck, and S. V. Ukkusuri, "Toward general principles for resilience engineering," *Risk Analysis*, vol. 40, no. 8, pp. 1509–1537, 2020.

[99] P. S. C. Rao, E. Krueger, and C. J. Klinkhamer, "Resilient urban infrastructure?" *Decision Analysis Today*, vol. 36, no. 3, pp. 25–30, 2017.

[100] S. M. Rinaldi, J. P. Peerenboom, and T. K. Kelly, "Identifying, understanding, and analyzing critical infrastructure interdependencies," *IEEE Control Systems*, vol. 21, no. 6, pp. 11–25, 2001.

[101] S. L. Cutter, L. Barnes, M. Berry, C. Burton, E. Evans, E. Tate, and J. Webb, "A place-based model for understanding community resilience to natural disasters," *Global environmental change*, vol. 18, no. 4, pp. 598–606, 2008.

[102] S. K. Aksha and C. T. Emrich, "Benchmarking community disaster resilience in nepal," *International journal of environmental research and public health*, vol. 17, no. 6, p. 1985, 2020.

[103] S. L. Cutter, "The landscape of disaster resilience indicators in the usa," *Natural hazards*, vol. 80, no. 2, pp. 741–758, 2016.

[104] M. Ouyang, "Review on modeling and simulation of interdependent critical infrastructure systems," *Reliability engineering & System safety*, vol. 121, pp. 43–60, 2014.

[105] E. J. Baker, "Hurricane evacuation behavior," *International journal of mass emergencies and disasters*, vol. 9, no. 2, pp. 287–310, 1991.

[106] N. Dash and H. Gladwin, "Evacuation decision making and behavioral responses: Individual and household," *Natural Hazards Review*, vol. 8, no. 3, pp. 69–77, 2007.

[107] W. G. Peacock, H. Gladwin, and B. H. Morrow, *Hurricane Andrew: Ethnicity, gender and the sociology of disasters*. Routledge, 2012.

[108] J. C. Whitehead, B. Edwards, M. Van Willigen, J. R. Maiolo, K. Wilson, and K. T. Smith, "Heading for higher ground: Factors affecting real and hypothetical hurricane evacuation behavior," *Global Environmental Change Part B: Environmental Hazards*, vol. 2, no. 4, pp. 133–142, 2000.

[109] J. K. Riad, F. H. Norris, and R. B. Ruback, "Predicting evacuation in two major disasters: Risk perception, social influence, and access to resources 1," *Journal of Applied Social Psychology*, vol. 29, no. 5, pp. 918–934, 1999.

[110] M. K. Lindell, J.-C. Lu, and C. S. Prater, "Household decision making and evacuation in response to hurricane lili," *Natural Hazards Review*, vol. 6, no. 4, pp. 171–179, 2005.

[111] J. L. Demuth, R. E. Morss, J. K. Lazo, and C. Trumbo, "The effects of past hurricane experiences on evacuation intentions through risk perception and efficacy beliefs: A mediation analysis," *Weather, Climate, and Society*, vol. 8, no. 4, pp. 327–344, 2016.

[112] A. M. Sadri, S. V. Ukkusuri, and H. Gladwin, "The role of social networks and information sources on hurricane evacuation decision making," *Natural Hazards Review*, vol. 18, no. 3, p. 04 017 005, 2017.

[113] A. M. Sadri, S. V. Ukkusuri, S. Lee, R. Clawson, D. Aldrich, M. S. Nelson, J. Seipel, and D. Kelly, "The role of social capital, personal networks, and emergency responders in post-disaster recovery and resilience: A study of rural communities in indiana," *Natural Hazards*, vol. 90, no. 3, pp. 1377–1406, 2018.

[114] S. V. Ukkusuri, S. Hasan, B. Luong, K. Doan, X. Zhan, P. Murray-Tuite, and W. Yin, "A-rescue: An agent based regional evacuation simulator coupled with user enriched behavior," *Networks and Spatial Economics*, vol. 17, no. 1, pp. 197–223, 2017.

[115] S. Dong, A. Esmalian, H. Farahmand, and A. Mostafavi, "An integrated physical-social analysis of disrupted access to critical facilities and community service-loss tolerance in urban flooding," *Computers, Environment and Urban Systems*, vol. 80, p. 101 443, 2020.

[116] A. Y. Grinberger and D. Felsenstein, "Dynamic agent based simulation of welfare effects of urban disasters," *Computers, Environment and Urban Systems*, vol. 59, pp. 129–141, 2016.

[117] J. M. Links, B. S. Schwartz, S. Lin, N. Kanarek, J. Mitrani-Reiser, T. K. Sell, C. R. Watson, D. Ward, C. Slemp, R. Burhans, *et al.*, "Copewell: A conceptual framework and system dynamics model for predicting community functioning and resilience after disasters," *Disaster medicine and public health preparedness*, vol. 12, no. 1, pp. 127–137, 2018.

[118] E. J. Sutley and S. Hamideh, "An interdisciplinary system dynamics model for post-disaster housing recovery," *Sustainable and Resilient Infrastructure*, vol. 3, no. 3, pp. 109–127, 2018.

[119] E. J. Sutley, S. Hamideh, M. K. Dillard, D. Gu, K. Seong, and J. W. van de Lindt, "Integrative modeling of housing recovery as a physical, economic, and social process," 2019.

[120] T. Kanno, S. Koike, T. Suzuki, and K. Furuta, "Human-centered modeling framework of multiple interdependency in urban systems for simulation of post-disaster recovery processes," *Cognition, Technology & Work*, vol. 21, no. 2, pp. 301–316, 2019.

[121] V. D. Blondel, A. Decuyper, and G. Krings, "A survey of results on mobile phone datasets analysis," *EPJ data science*, vol. 4, no. 1, p. 10, 2015.

[122] S. Jiang, G. A. Fiore, Y. Yang, J. Ferreira Jr, E. Frazzoli, and M. C. González, "A review of urban computing for mobile phone traces: Current methods, challenges and opportunities," in *Proceedings of the 2nd ACM SIGKDD international workshop on Urban Computing*, 2013, pp. 1–9.

[123] F. Calabrese, G. Di Lorenzo, L. Liu, and C. Ratti, “Estimating origin-destination flows using opportunistically collected mobile phone location data from one million users in boston metropolitan area,” *IEEE Pervasive Computing*, vol. 10, no. 4, pp. 36–44, 2011.

[124] M. C. Gonzalez, C. A. Hidalgo, and A.-L. Barabasi, “Understanding individual human mobility patterns,” *nature*, vol. 453, no. 7196, p. 779, 2008.

[125] S. Hasan, C. M. Schneider, S. V. Ukkusuri, and M. C. González, “Spatiotemporal patterns of urban human mobility,” *Journal of Statistical Physics*, vol. 151, no. 1-2, pp. 304–318, 2013.

[126] C. Song, Z. Qu, N. Blumm, and A.-L. Barabási, “Limits of predictability in human mobility,” *Science*, vol. 327, no. 5968, pp. 1018–1021, 2010.

[127] T. Pei, S. Sobolevsky, C. Ratti, S.-L. Shaw, T. Li, and C. Zhou, “A new insight into land use classification based on aggregated mobile phone data,” *International Journal of Geographical Information Science*, vol. 28, no. 9, pp. 1988–2007, 2014.

[128] P. Deville, C. Linard, S. Martin, M. Gilbert, F. R. Stevens, A. E. Gaughan, V. D. Blondel, and A. J. Tatem, “Dynamic population mapping using mobile phone data,” *Proceedings of the National Academy of Sciences*, vol. 111, no. 45, pp. 15 888–15 893, 2014.

[129] N. E. Phillips, B. L. Levy, R. J. Sampson, M. L. Small, and R. Q. Wang, “The social integration of american cities: Network measures of connectedness based on everyday mobility across neighborhoods,” *Sociological Methods & Research*, p. 0 049 124 119 852 386, 2019.

[130] J. E. Blumenstock, “Inferring patterns of internal migration from mobile phone call records: Evidence from rwanda,” *Information Technology for Development*, vol. 18, no. 2, pp. 107–125, 2012.

[131] F. Finger, T. Genolet, L. Mari, G. C. de Magny, N. M. Manga, A. Rinaldo, and E. Bertuzzo, “Mobile phone data highlights the role of mass gatherings in the spreading of cholera outbreaks,” *Proceedings of the National Academy of Sciences*, vol. 113, no. 23, pp. 6421–6426, 2016.

[132] A. Wesolowski, N. Eagle, A. J. Tatem, D. L. Smith, A. M. Noor, R. W. Snow, and C. O. Buckee, “Quantifying the impact of human mobility on malaria,” *Science*, vol. 338, no. 6104, pp. 267–270, 2012.

[133] L. Bengtsson, J. Gaudart, X. Lu, S. Moore, E. Wetter, K. Sallah, S. Rebaudet, and R. Piarroux, “Using mobile phone data to predict the spatial spread of cholera,” *Scientific reports*, vol. 5, p. 8923, 2015.

[134] M. S. Iqbal, C. F. Choudhury, P. Wang, and M. C. González, "Development of origin–destination matrices using mobile phone call data," *Transportation Research Part C: Emerging Technologies*, vol. 40, pp. 63–74, 2014.

[135] L. Alexander, S. Jiang, M. Murga, and M. C. González, "Origin–destination trips by purpose and time of day inferred from mobile phone data," *Transportation research part c: emerging technologies*, vol. 58, pp. 240–250, 2015.

[136] Y. Xu, A. Belyi, I. Bojic, and C. Ratti, "Human mobility and socioeconomic status: Analysis of singapore and boston," *Computers, Environment and Urban Systems*, vol. 72, pp. 51–67, 2018.

[137] J. L. Toole, Y.-R. Lin, E. Muehlegger, D. Shoag, M. C. González, and D. Lazer, "Tracking employment shocks using mobile phone data," *Journal of The Royal Society Interface*, vol. 12, no. 107, p. 20 150 185, 2015.

[138] X. Qian and S. V. Ukkusuri, "Spatial variation of the urban taxi ridership using gps data," *Applied Geography*, vol. 59, pp. 31–42, 2015.

[139] P. Maas, S. Iyer, A. Gros, W. Park, L. McGorman, C. Nayak, and P. A. Dow, "Facebook disaster maps: Aggregate insights for crisis response & recovery.," in *KDD*, vol. 19, 2019, p. 3173.

[140] S. Jia, S. H. Kim, S. V. Nghiem, P. Doherty, and M. C. Kafatos, "Patterns of population displacement during mega-fires in california detected using facebook disaster maps," *Environmental Research Letters*, vol. 15, no. 7, p. 074 029, 2020.

[141] B. Klein, T. LaRocky, S. McCabey, L. Torresy, F. Privitera, B. Lake, M. U. Kraemer, J. S. Brownstein, D. Lazer, T. Eliassi-Rad, S. V. Scarpino, M. Chinazzi, and A. Vespignani, *Assessing changes in commuting and individual mobility in major metropolitan areas in the united states during the covid-19 outbreak*, https://www.networkscienceinstitute.org/publications/assessing-changes-in-commuting-and-individual-mobility-in-major-metropolitan-areas-in-the-united-states-during-the-covid-19-outbreak (accessed June 26, 2020), 2020.

[142] M. U. Kraemer, C.-H. Yang, B. Gutierrez, C.-H. Wu, B. Klein, D. M. Pigott, L. du Plessis, N. R. Faria, R. Li, W. P. Hanage, *et al.*, "The effect of human mobility and control measures on the covid-19 epidemic in china," *Science*, vol. 368, no. 6490, pp. 493–497, 2020.

[143] S. Lai, N. W. Ruktanonchai, L. Zhou, O. Prosper, W. Luo, J. R. Floyd, A. Wesolowski, M. Santillana, C. Zhang, X. Du, H. Yu, and A. J. Tatem, "Effect of non-pharmaceutical interventions for containing the covid-19 outbreak in china," *medRxiv*, 2020. DOI: 10.1101/2020.03.03.20029843.

[144] E. Pepe, P. Bajardi, L. Gauvin, F. Privitera, B. Lake, C. Cattuto, and M. Tizzoni, "Covid-19 outbreak response: A first assessment of mobility changes in italy following national lockdown," *medRxiv*, 2020. DOI: 10.1101/2020.03.22.20039933.

[145] P. Bonato, P. Cintia, F. Fabbri, D. Fadda, F. Giannotti, P. L. Lopalco, S. Mazzilli, M. Nanni, L. Pappalardo, D. Pedreschi, *et al.*, "Mobile phone data analytics against the covid-19 epidemics in italy: Flow diversity and local job markets during the national lockdown," *arXiv preprint arXiv:2004.11278*, 2020.

[146] G. A. Wellenius, S. Vispute, V. Espinosa, A. Fabrikant, T. C. Tsai, J. Hennessy, B. Williams, K. Gadepalli, A. Boulange, A. Pearce, *et al.*, "Impacts of state-level policies on social distancing in the united states using aggregated mobility data during the covid-19 pandemic," *arXiv preprint arXiv:2004.10172*, 2020.

[147] S. Gao, J. Rao, Y. Kang, Y. Liang, and J. Kruse, "Mapping county-level mobility pattern changes in the united states in response to covid-19," *Available at SSRN 3570145*, 2020.

[148] M. Dahlberg, P.-A. Edin, E. Grönqvist, J. Lyhagen, J. Östh, A. Siretskiy, and M. Toger, "Effects of the covid-19 pandemic on population mobility under mild policies: Causal evidence from sweden," *arXiv preprint arXiv:2004.09087*, 2020.

[149] C. Santana, F. Botta, H. Barbosa, F. Privitera, R. Menezes, and R. Di Clemente, *Analysis of human mobility in the uk during the covid-19 pandemic*, https://covid19-uk-mobility.github.io/ (published April 8, 2020; accessed June 26, 2020), 2020.

[150] P. Cintia, D. Fadda, F. Giannotti, L. Pappalardo, G. Rossetti, D. Pedreschi, S. Rinzivillo, P. Bonato, F. Fabbri, F. Penone, *et al.*, "The relationship between human mobility and viral transmissibility during the covid-19 epidemics in italy," *arXiv preprint arXiv:2006.03141*, 2020.

[151] F. Schlosser, B. F. Maier, D. Hinrichs, A. Zachariae, and D. Brockmann, "Covid-19 lockdown induces structural changes in mobility networks – implication for mitigating disease dynamics," *arXiv preprint arXiv: 2007.01583*, 2020.

[152] T. Yabe, K. Tsubouchi, N. Fujiwara, T. Wada, Y. Sekimoto, and S. V. Ukkusuri, "Non-compulsory measures sufficiently reduced human mobility in tokyo during the covid-19 epidemic," *Scientific reports*, vol. 10, no. 1, pp. 1–9, 2020.

[153] W. F. Yushimito, M. Jaller, and S. Ukkusuri, "A voronoi-based heuristic algorithm for locating distribution centers in disasters," *Networks and Spatial Economics*, vol. 12, no. 1, pp. 21–39, 2012.

[154] J. S. Kargel, G. J. Leonard, D. H. Shugar, U. K. Haritashya, A. Bevington, E. Fielding, K. Fujita, M. Geertsema, E. Miles, J. Steiner, *et al.*, "Geomorphic and geologic controls of geohazards induced by nepal's 2015 gorkha earthquake," *Science*, vol. 351, no. 6269, 2016.

[155] R. Wilson, E. zu Erbach-Schoenberg, M. Albert, D. Power, S. Tudge, M. Gonzalez, S. Guthrie, H. Chamberlain, C. Brooks, C. Hughes, *et al.*, "Rapid and near real-time assessments of population displacement using mobile phone data following disasters: The 2015 nepal earthquake," *PLoS currents*, vol. 8, 2016.

[156] Flowminder.org, *Monitoring population movements post disaster: 2015 nepal earthquake*, https://www.flowminder.org/what-we-do/data-applications/disaster-management/monitoring-population-movements-post-disaster-2015-nepal-earthquake/, Accessed: 2021-03-22, 2015.

[157] T. Yabe, N. K. Jones., N. L. Gracia, M. Khan, S. V. Ukkusuri, S. Fraiberger, and A. Montford, "Post disaster analytics using mobile phone data: A case study of puebla earthquake," *World Bank Working Papers*, 2021.

[158] A. Dobra, N. E. Williams, and N. Eagle, "Spatiotemporal detection of unusual human population behavior using mobile phone data," *PloS one*, vol. 10, no. 3, e0120449, 2015.

[159] T. Yabe, Y. Sekimoto, K. Tsubouchi, and S. Ikemoto, "Cross-comparative analysis of evacuation behavior after earthquakes using mobile phone data," *PLOS ONE*, vol. 14, no. 2, pp. 1–12, Feb. 2019. DOI: 10.1371/journal.pone.0211375. [Online]. Available: https://doi.org/10.1371/journal.pone.0211375.

[160] T. Yabe, K. Tsubouchi, A. Sudo, and Y. Sekimoto, "A framework for evacuation hotspot detection after large scale disasters using location data from smartphones: Case study of kumamoto earthquake," in *Proceedings of the 24th ACM SIGSPATIAL International Conference on Advances in Geographic Information Systems*, ACM, 2016, p. 44.

[161] Yahoo Japan Corporation, *Big data report: Estimating evacuation hotspots after disasters using location data*, https://about.yahoo.co.jp/info/blog/20160714/bigdata-report.html, Accessed: 2021-03-22, 2016.

[162] Z. Duan, Z. Lei, M. Zhang, W. Li, J. Fang, and J. Li, "Understanding evacuation and impact of a metro collision on ridership using large-scale mobile phone data," *IET Intelligent Transport Systems*, vol. 11, no. 8, pp. 511–520, 2017.

[163] J. Ghurye, G. Krings, and V. Frias-Martinez, "A framework to model human behavior at large scale during natural disasters," in *2016 17th IEEE International Conference on Mobile Data Management (MDM)*, IEEE, vol. 1, 2016, pp. 18–27.

[164] L. Yin, J. Chen, H. Zhang, Z. Yang, Q. Wan, L. Ning, J. Hu, and Q. Yu, “Improving emergency evacuation planning with mobile phone location data,” *Environment and Planning B: Urban Analytics and City Science*, vol. 47, no. 6, pp. 964–980, 2020.

[165] X. Song, Q. Zhang, Y. Sekimoto, and R. Shibasaki, “Prediction of human emergency behavior and their mobility following large-scale disaster,” in *Proceedings of the 20th ACM SIGKDD international conference on Knowledge discovery and data mining*, ACM, 2014, pp. 5–14.

[166] A. Sudo, T. Kashiyama, T. Yabe, H. Kanasugi, X. Song, T. Higuchi, S. Nakano, M. Saito, and Y. Sekimoto, “Particle filter for real-time human mobility prediction following unprecedented disaster,” in *Proceedings of the 24th ACM SIGSPATIAL International Conference on Advances in Geographic Information Systems*, ACM, 2016, p. 5.

[167] Y. Sekimoto, A. Sudo, T. Kashiyama, T. Seto, H. Hayashi, A. Asahara, H. Ishizuka, and S. Nishiyama, “Real-time people movement estimation in large disasters from several kinds of mobile phone data,” in *Proceedings of the 2016 ACM International Joint Conference on Pervasive and Ubiquitous Computing: Adjunct*, 2016, pp. 1426–1434.

[168] Z. Fan, X. Song, R. Shibasaki, and R. Adachi, “Citymomentum: An online approach for crowd behavior prediction at a citywide level,” in *Proceedings of the 2015 ACM International Joint Conference on Pervasive and Ubiquitous Computing*, ACM, 2015, pp. 559–569.

[169] Z. Fan, X. Song, R. Shibasaki, T. Li, and H. Kaneda, “Citycoupling: Bridging intercity human mobility,” in *Proceedings of the 2016 ACM International Joint Conference on Pervasive and Ubiquitous Computing*, ACM, 2016, pp. 718–728.

[170] Y. Pang, K. Tsubouchi, T. Yabe, and Y. Sekimoto, “Replicating urban dynamics by generating human-like agents from smartphone gps data,” in *Proceedings of the 26th ACM SIGSPATIAL International Conference on Advances in Geographic Information Systems*, ACM, 2018, pp. 440–443.

[171] Y. Pang, K. Tsubouchi, T. Yabe, and Y. Sekimoto, “Intercity simulation of human mobility at rare events via reinforcement learning,” in *Proceedings of the 28th International Conference on Advances in Geographic Information Systems*, 2020, pp. 293–302.

[172] S. Hankaew, S. Phithakkitnukoon, M. G. Demissie, L. Kattan, Z. Smoreda, and C. Ratti, “Inferring and modeling migration flows using mobile phone network data,” *IEEE Access*, vol. 7, pp. 164 746–164 758, 2019.

[173] S. Lai, E. zu Erbach-Schoenberg, C. Pezzulo, N. W. Ruktanonchai, A. Sorichetta, J. Steele, T. Li, C. A. Dooley, and A. J. Tatem, “Exploring the use of mobile phone data for national migration statistics,” *Palgrave Communications*, vol. 5, no. 1, p. 34, 2019.

[174] X. Lu, D. J. Wrathall, P. R. Sundsøy, M. Nadiruzzaman, E. Wetter, A. Iqbal, T. Qureshi, A. Tatem, G. Canright, K. Engø-Monsen, *et al.*, "Unveiling hidden migration and mobility patterns in climate stressed regions: A longitudinal study of six million anonymous mobile phone users in bangladesh," *Global Environmental Change*, vol. 38, pp. 1–7, 2016.

[175] R. J. Acosta, N. Kishore, R. A. Irizarry, and C. O. Buckee, "Quantifying the dynamics of migration after hurricane maria in puerto rico," *Proceedings of the National Academy of Sciences*, vol. 117, no. 51, pp. 32 772–32 778, 2020.

[176] A. Marzuoli and F. Liu, "A data-driven impact evaluation of hurricane harvey from mobile phone data," in *2018 IEEE International Conference on Big Data (Big Data)*, IEEE, 2018, pp. 3442–3451.

[177] T. Yabe, S. V. Ukkusuri, and P. S. C. Rao, "Mobile phone data reveals the importance of pre-disaster inter-city social ties for recovery after hurricane maria," *Applied Network Science*, vol. 4, no. 1, p. 98, 2019.

[178] J. S. Jia, J. Jia, C. K. Hsee, and B. Shiv, "The role of hedonic behavior in reducing perceived risk: Evidence from postearthquake mobile-app data," *Psychological science*, vol. 28, no. 1, pp. 23–35, 2017.

[179] T. Yabe and S. V. Ukkusuri, "Effects of income inequality on evacuation, reentry and segregation after disasters," *Transportation Research Part D: Transport and Environment*, pp. 102–260, 2020.

[180] J. W. Baker, "Efficient analytical fragility function fitting using dynamic structural analysis," *Earthquake Spectra*, vol. 31, no. 1, pp. 579–599, 2015.

[181] X. Andrade, F. Layedra, C. Vaca, and E. Cruz, "Risc: Quantifying change after natural disasters to estimate infrastructure damage with mobile phone data," in *2018 IEEE International Conference on Big Data (Big Data)*, IEEE, 2018, pp. 3383–3391.

[182] D. Pastor-Escuredo, A. Morales-Guzmán, Y. Torres-Fernández, J.-M. Bauer, A. Wadhwa, C. Castro-Correa, L. Romanoff, J. G. Lee, A. Rutherford, V. Frias-Martinez, *et al.*, "Flooding through the lens of mobile phone activity," in *IEEE Global Humanitarian Technology Conference (GHTC 2014)*, IEEE, 2014, pp. 279–286.

[183] T. Yabe, K. Tsubouchi, and Y. Sekimoto, "Fusion of terrain information and mobile phone location data for flood area detection in rural areas," in *2018 IEEE International Conference on Big Data (Big Data)*, IEEE, 2018, pp. 881–890.

[184] L. Sinnenberg, A. M. Buttenheim, K. Padrez, C. Mancheno, L. Ungar, and R. M. Merchant, "Twitter as a tool for health research: A systematic review," *American journal of public health*, vol. 107, no. 1, e1–e8, 2017.

[185] S. E. Jordan, S. E. Hovet, I. C.-H. Fung, H. Liang, K.-W. Fu, and Z. T. H. Tse, “Using twitter for public health surveillance from monitoring and prediction to public response,” *Data*, vol. 4, no. 1, p. 6, 2019.

[186] A. Tumasjan, T. Sprenger, P. Sandner, and I. Welpe, “Predicting elections with twitter: What 140 characters reveal about political sentiment,” in *Proceedings of the International AAAI Conference on Web and Social Media*, vol. 4, 2010.

[187] R. Buettner and K. Buettner, “A systematic literature review of twitter research from a socio-political revolution perspective,” in *2016 49th Hawaii International Conference on System Sciences (HICSS)*, IEEE, 2016, pp. 2206–2215.

[188] M. Martinez-Rojas, M. del Carmen Pardo-Ferreira, and J. C. Rubio-Romero, “Twitter as a tool for the management and analysis of emergency situations: A systematic literature review,” *International Journal of Information Management*, vol. 43, pp. 196–208, 2018.

[189] A. M. Sadri, S. Hasan, S. V. Ukkusuri, and J. E. S. Lopez, “Analysis of social interaction network properties and growth on twitter,” *Social Network Analysis and Mining*, vol. 8, no. 1, p. 56, 2018.

[190] A. M. Sadri, S. Hasan, S. V. Ukkusuri, and M. Cebrian, “Crisis communication patterns in social media during hurricane sandy,” *Transportation research record*, vol. 2672, no. 1, pp. 125–137, 2018.

[191] Y. Kryvasheyeu, H. Chen, E. Moro, P. Van Hentenryck, and M. Cebrian, “Performance of social network sensors during hurricane sandy,” *PLoS one*, vol. 10, no. 2, e0117288, 2015.

[192] Q. Wang and J. E. Taylor, “Quantifying human mobility perturbation and resilience in hurricane sandy,” *PLoS one*, vol. 9, no. 11, e112608, 2014.

[193] Q. Wang and J. E. Taylor, “Patterns and limitations of urban human mobility resilience under the influence of multiple types of natural disaster,” *PLoS one*, vol. 11, no. 1, e0147299, 2016.

[194] T. Sakaki, M. Okazaki, and Y. Matsuo, “Earthquake shakes twitter users: Real-time event detection by social sensors,” in *Proceedings of the 19th international conference on World wide web*, ACM, 2010, pp. 851–860.

[195] Y. Kryvasheyeu, H. Chen, N. Obradovich, E. Moro, P. Van Hentenryck, J. Fowler, and M. Cebrian, “Rapid assessment of disaster damage using social media activity,” *Science advances*, vol. 2, no. 3, e1500779, 2016.

[196] D. Kumar, T. Yabe, and S. V. Ukkusuri, "Social-media aided hyperlocal help-network matching & routing during emergencies," in *2018 IEEE International Conference on Big Data (Big Data)*, IEEE, 2018, pp. 1606–1611.

[197] T. Yabe and S. V. Ukkusuri, "Integrating information from heterogeneous networks on social media to predict post-disaster returning behavior," *Journal of Computational Science*, vol. 32, pp. 12–20, 2019.

[198] D. Kumar and S. V. Ukkusuri, "Enhancing demographic coverage of hurricane evacuation behavior modeling using social media," *Journal of Computational Science*, vol. 45, p. 101 184, 2020.

[199] C. Silverstein, H. Marais, M. Henzinger, and M. Moricz, "Analysis of a very large web search engine query log," in *ACm SIGIR Forum*, ACM New York, NY, USA, vol. 33, 1999, pp. 6–12.

[200] J. Ginsberg, M. H. Mohebbi, R. S. Patel, L. Brammer, M. S. Smolinski, and L. Brilliant, "Detecting influenza epidemics using search engine query data," *Nature*, vol. 457, no. 7232, pp. 1012–1014, 2009.

[201] E. H. Chan, V. Sahai, C. Conrad, and J. S. Brownstein, "Using web search query data to monitor dengue epidemics: A new model for neglected tropical disease surveillance," *PLoS neglected tropical diseases*, vol. 5, no. 5, e1206, 2011.

[202] C. Wu, F. Wu, J. Liu, S. He, Y. Huang, and X. Xie, "Neural demographic prediction using search query," in *Proceedings of the Twelfth ACM International Conference on Web Search and Data Mining*, 2019, pp. 654–662.

[203] S. Goel, J. M. Hofman, S. Lahaie, D. M. Pennock, and D. J. Watts, "Predicting consumer behavior with web search," *Proceedings of the National academy of sciences*, vol. 107, no. 41, pp. 17 486–17 490, 2010.

[204] G.-R. Xue, H.-J. Zeng, Z. Chen, Y. Yu, W.-Y. Ma, W. Xi, and W. Fan, "Optimizing web search using web click-through data," in *Proceedings of the thirteenth ACM international conference on Information and knowledge management*, 2004, pp. 118–126.

[205] T. Mikolov, I. Sutskever, K. Chen, G. S. Corrado, and J. Dean, "Distributed representations of words and phrases and their compositionality," in *Advances in neural information processing systems*, 2013, pp. 3111–3119.

[206] A. Joulin, E. Grave, P. Bojanowski, M. Douze, H. Jégou, and T. Mikolov, "Fasttext.zip: Compressing text classification models," *arXiv preprint arXiv:1612.03651*, 2016.

[207] J. Pennington, R. Socher, and C. D. Manning, "Glove: Global vectors for word representation," in *In EMNLP*, 2014.

[208] D. Kang and I. Kang, "Query2vec: Learning deep intentions from heterogeneous search logs," Technical report, Naver Labs, Tech. Rep., 2015.

[209] T. Yabe, K. Tsubouchi, T. Shimizu, Y. Sekimoto, and S. V. Ukkusuri, "Predicting evacuation decisions using representations of individuals' pre-disaster web search behavior," in *Proceedings of the 25th ACM SIGKDD International Conference on Knowledge Discovery & Data Mining*, ACM, 2019, pp. 2707–2717.

[210] T. Yabe, K. Tsubouchi, and S. V. Ukkusuri, "Early warning of covid-19 hotspots using mobility of high risk users from web search queries," *arXiv preprint arXiv:2010.13254*, 2020.

[211] A. Rovetta and A. S. Bhagavathula, "Covid-19-related web search behaviors and infodemic attitudes in italy: Infodemiological study," *JMIR public health and surveillance*, vol. 6, no. 2, e19374, 2020.

[212] A. I. Bento, T. Nguyen, C. Wing, F. Lozano-Rojas, Y.-Y. Ahn, and K. Simon, "Evidence from internet search data shows information-seeking responses to news of local covid-19 cases," *Proceedings of the National Academy of Sciences*, vol. 117, no. 21, pp. 11 220–11 222, 2020.

[213] A. Mavragani, "Tracking covid-19 in europe: Infodemiology approach," *JMIR public health and surveillance*, vol. 6, no. 2, e18941, 2020.

[214] A. Walker, C. Hopkins, and P. Surda, "The use of google trends to investigate the loss of smell related searches during covid-19 outbreak," in *International Forum of Allergy & Rhinology*, Wiley Online Library, 2020.

[215] A. Rajan, R. Sharaf, R. S. Brown, R. Z. Sharaiha, B. Lebwohl, and S. Mahadev, "Association of search query interest in gastrointestinal symptoms with covid-19 diagnosis in the united states: Infodemiology study," *JMIR public health and surveillance*, vol. 6, no. 3, e19354, 2020.

[216] C. Li, L. J. Chen, X. Chen, M. Zhang, C. P. Pang, and H. Chen, "Retrospective analysis of the possibility of predicting the covid-19 outbreak from internet searches and social media data, china, 2020," *Eurosurveillance*, vol. 25, no. 10, p. 2 000 199, 2020.

[217] S. Hisada, T. Murayama, K. Tsubouchi, S. Fujita, S. Yada, S. Wakamiya, and E. Aramaki, "Surveillance of early stage covid-19 clusters using search query logs and mobile device-based location information," *Scientific Reports*, vol. 10, no. 1, pp. 1–8, 2020.

[218] B. Xu, B. Gutierrez, S. Mekaru, K. Sewalk, L. Goodwin, A. Loskill, E. L. Cohn, Y. Hswen, S. C. Hill, M. M. Cobo, *et al.*, "Epidemiological data from the covid-19 outbreak, real-time case information," *Scientific data*, vol. 7, no. 1, pp. 1–6, 2020.

[219] H. W. Fischer, G. F. Stine, B. L. Stoker, M. L. Trowbridge, and E. M. Drain, "Evacuation behaviour: Why do some evacuate, while others do not? a case study of the ephrata, pennsylvania (usa) evacuation," *Disaster prevention and management: an international journal*, vol. 4, no. 4, pp. 30–36, 1995.

[220] R. Lovreglio, E. Ronchi, and D. Nilsson, "An evacuation decision model based on perceived risk, social influence and behavioural uncertainty," *Simulation Modelling Practice and Theory*, vol. 66, pp. 226–242, 2016.

[221] N. Golshani, R. Shabanpour, A. Mohammadian, J. Auld, and H. Ley, "Evacuation decision behavior for no-notice emergency events," *Transportation Research Part D: Transport and Environment*, 2019.

[222] J. Collins, R. Ersing, A. Polen, M. Saunders, and J. Senkbeil, "The effects of social connections on evacuation decision making during hurricane irma," *Weather, climate, and society*, vol. 10, no. 3, pp. 459–469, 2018.

[223] S. Wong, S. Shaheen, and J. Walker, "Understanding evacuee behavior: A case study of hurricane irma," 2018.

[224] Federal Emergency Management Agency, *Fema housing assistance data*, https://www.fema.gov/media-library/assets/documents/34758, Accessed: 2019-12-14.

[225] COJ, *Disaster reports for disasters in japan (japanese)*, http://www.bousai.go.jp/, Accessed: 2018-09-07, 2018.

[226] D. Ashbrook and T. Starner, "Using gps to learn significant locations and predict movement across multiple users," *Personal and Ubiquitous computing*, vol. 7, no. 5, pp. 275–286, 2003.

[227] H. Kanasugi, Y. Sekimoto, M. Kurokawa, T. Watanabe, S. Muramatsu, and R. Shibasaki, "Spatiotemporal route estimation consistent with human mobility using cellular network data," in *Pervasive Computing and Communications Workshops (PERCOM Workshops), 2013 IEEE International Conference on*, IEEE, 2013, pp. 267–272.

[228] C. E. Rasmussen and C. K. Williams, "Gaussian processes for machine learning. 2006," *The MIT Press, Cambridge, MA, USA*, vol. 38, pp. 715–719, 2006.

[229] C. A. Myers, T. Slack, and J. Singelmann, “Social vulnerability and migration in the wake of disaster: The case of hurricanes katrina and rita,” *Population and Environment*, vol. 29, no. 6, pp. 271–291, 2008.

[230] F. Simini, M. C. González, A. Maritan, and A.-L. Barabási, “A universal model for mobility and migration patterns,” *Nature*, vol. 484, no. 7392, p. 96, 2012.

[231] M. Shimizu, “Resilience in disaster management and public policy: A case study of the tohoku disaster,” *Risk, Hazards & Crisis in Public Policy*, vol. 3, no. 4, pp. 40–59, 2012.

[232] M. Barthélemy, “Spatial networks,” *Physics Reports*, vol. 499, no. 1-3, pp. 1–101, 2011.

[233] A. Barrat, M. Barthélemy, and A. Vespignani, “The effects of spatial constraints on the evolution of weighted complex networks,” *Journal of Statistical Mechanics: Theory and Experiment*, vol. 2005, no. 05, P05003, 2005.

[234] A. Barrat, M. Barthelemy, R. Pastor-Satorras, and A. Vespignani, “The architecture of complex weighted networks,” *Proceedings of the national academy of sciences*, vol. 101, no. 11, pp. 3747–3752, 2004.

[235] T. Opsahl, F. Agneessens, and J. Skvoretz, “Node centrality in weighted networks: Generalizing degree and shortest paths,” *Social networks*, vol. 32, no. 3, pp. 245–251, 2010.

[236] G. Fagiolo, “Clustering in complex directed networks,” *Physical Review E*, vol. 76, no. 2, p. 026 107, 2007.

[237] C. Zhong, S. M. Arisona, X. Huang, M. Batty, and G. Schmitt, “Detecting the dynamics of urban structure through spatial network analysis,” *International Journal of Geographical Information Science*, vol. 28, no. 11, pp. 2178–2199, 2014.

[238] A. De Montis, M. Barthélemy, A. Chessa, and A. Vespignani, “The structure of interurban traffic: A weighted network analysis,” *Environment and Planning B: Planning and Design*, vol. 34, no. 5, pp. 905–924, 2007.

[239] W. Li and X. Cai, “Statistical analysis of airport network of china,” *Physical Review E*, vol. 69, no. 4, p. 046 106, 2004.

[240] E. Almaas, B. Kovacs, T. Vicsek, Z. Oltvai, and A.-L. Barabási, “Global organization of metabolic fluxes in the bacterium escherichia coli,” *Nature*, vol. 427, no. 6977, p. 839, 2004.

[241] M. D. Ward and K. S. Gleditsch, *Spatial regression models*. Sage Publications, 2018, vol. 155.

[242] T. Yabe, K. Tsubouchi, N. Fujiwara, Y. Sekimoto, and S. V. Ukkusuri, “Understanding post-disaster population recovery patterns,” *Journal of the Royal Society Interface*, vol. 17, no. 163, p. 20 190 532, 2020.

[243] M. E. Guy and S. A. McCandless, “Social equity: Its legacy, its promise,” *Public Administration Review*, vol. 72, no. s1, S5–S13, 2012.

[244] C. Burton and S. L. Cutter, “Levee failures and social vulnerability in the sacramento-san joaquin delta area, california,” *Natural Hazards Review*, vol. 9, no. 3, pp. 136–149, 2008.

[245] C. T. Emrich, E. Tate, S. E. Larson, and Y. Zhou, “Measuring social equity in flood recovery funding,” *Environmental Hazards*, pp. 1–23, 2019.

[246] N. Doorn, P. Gardoni, and C. Murphy, “A multidisciplinary definition and evaluation of resilience: The role of social justice in defining resilience,” *Sustainable and Resilient Infrastructure*, vol. 4, no. 3, pp. 112–123, 2019.

[247] D. J. Kettl, *On risk and disaster: Lessons from Hurricane Katrina*. University of Pennsylvania Press, 2006.

[248] A. Alesina, A. Devleeschauwer, W. Easterly, S. Kurlat, and R. Wacziarg, “Fractionalization,” *Journal of Economic growth*, vol. 8, no. 2, pp. 155–194, 2003.

[249] E. Moro, D. Calacci, X. Dong, and A. Pentland, *Economical segregation of encounter networks in cities*, Main conference on the scientific analysis of mobile phone datasets (NetMob), Oxford, United Kingdom, 2019.

[250] T. M. Shaughnessy, M. L. White, and M. D. Brendler, “The income distribution effect of natural disasters: An analysis of hurricane katrina,” *Journal of Regional Analysis and Policy*, vol. 40, no. 1100-2016-89674, 2010.

[251] M. E. Kahn, “The death toll from natural disasters: The role of income, geography, and institutions,” *Review of economics and statistics*, vol. 87, no. 2, pp. 271–284, 2005.

[252] M. J. Gibson and M. Hayunga, “We can do better: Lessons learned for protecting older persons in disasters,” 2006.

[253] J. L. Renne, T. W. Sanchez, and T. Litman, “Carless and special needs evacuation planning: A literature review,” *Journal of Planning Literature*, vol. 26, no. 4, pp. 420–431, 2011.

[254] J. L. Renne and E. Mayorga, “What has america learned since hurricane katrina? evaluating evacuation plans for carless and vulnerable populations in 50 large cities across the united states,” Tech. Rep., 2018.

[255] D. R. Bish, “Planning for a bus-based evacuation,” *OR spectrum*, vol. 33, no. 3, pp. 629–654, 2011.

[256] T. Litman, “Lessons from katrina and rita: What major disasters can teach transportation planners,” *Journal of transportation engineering*, vol. 132, no. 1, pp. 11–18, 2006.

[257] A. Analytics, *Hurricane irma event recap report*, http://thoughtleadership.aonbenfield.com/Documents/20180328-ab-if-hurricane-irma-recap.pdf, Online; accessed 17 September 2018, 2018.

[258] Miami-Dade County Open Data Hub, *Fema flood zone map*, https://gis-mdc.opendata.arcgis.com/datasets/cb44c8fd35474a9d8b8ec35eda9ee40f-0, Accessed: 2019-12-14.

[259] A. Sen and J. E. Foster, *On economic inequality*. Oxford University Press, 1997.

[260] U. S. C. Bureau, *American community survey*, https://www.census.gov/programs-surveys/acs, Accessed: 2019-12-14.

[261] United States Census Bureau, *Media household income for counties in the united states: 2013-2017*, https://www.census.gov/library/visualizations/2018/comm/acs-5yr-income-all-counties.html, Accessed: 2019-12-14.

[262] United States Census Bureau, *United states census bureau geography files*, https://www.census.gov/geographies/mapping-files/time-series/geo/tiger-line-file.html, Accessed: 2019-12-14.

[263] F. Clementi and M. Gallegati, “Pareto’s law of income distribution: Evidence for germany, the united kingdom, and the united states,” in *Econophysics of wealth distributions*, Springer, 2005, pp. 3–14.

[264] M. I. Marshall, L. S. Niehm, S. B. Sydnor, and H. L. Schrank, “Predicting small business demise after a natural disaster: An analysis of pre-existing conditions,” *Natural Hazards*, vol. 79, no. 1, pp. 331–354, 2015.

[265] S. Sydnor, L. Niehm, Y. Lee, M. Marshall, and H. Schrank, “Analysis of post-disaster damage and disruptive impacts on the operating status of small businesses after hurricane katrina,” *Natural Hazards*, vol. 85, no. 3, pp. 1637–1663, 2017.

[266] G. R. Webb, K. J. Tierney, and J. M. Dahlhamer, “Predicting long-term business recovery from disaster: A comparison of the loma prieta earthquake and hurricane andrew,” *Global Environmental Change Part B: Environmental Hazards*, vol. 4, no. 2, pp. 45–58, 2002.

[267] J. Lee, “Business recovery from hurricane harvey,” *International journal of disaster risk reduction*, vol. 34, pp. 305–315, 2019.

[268] M. Batty, “Big data, smart cities and city planning,” *Dialogues in Human Geography*, vol. 3, no. 3, pp. 274–279, 2013.

[269] U. Gurun and D. Solomon, *The perils of private provision of public goods*, 2019.

[270] A. Harvey and S. Koopman, “Structural time series models,” *Wiley StatsRef: Statistics Reference Online*, 2014.

[271] R. E. Bellman and K. L. Cooke, “Differential-difference equations,” 1963.

[272] K. H. Brodersen, F. Gallusser, J. Koehler, N. Remy, S. L. Scott, *et al.*, “Inferring causal impact using bayesian structural time-series models,” *The Annals of Applied Statistics*, vol. 9, no. 1, pp. 247–274, 2015.

[273] A. Goodman-Bacon, “Difference-in-differences with variation in treatment timing,” National Bureau of Economic Research, Tech. Rep., 2018.

[274] A. C. Harvey, *Forecasting, structural time series models and the Kalman filter*. Cambridge university press, 1990.

[275] P. S. Leeflang, T. H. Bijmolt, J. Van Doorn, D. M. Hanssens, H. J. Van Heerde, P. C. Verhoef, and J. E. Wieringa, “Creating lift versus building the base: Current trends in marketing dynamics,” *International Journal of Research in Marketing*, vol. 26, no. 1, pp. 13–20, 2009.

[276] S. L. Scott and H. R. Varian, “Predicting the present with bayesian structural time series,” *Available at SSRN 2304426*, 2013.

[277] S. L. Scott and H. R. Varian, “Bayesian variable selection for nowcasting economic time series,” National Bureau of Economic Research, Tech. Rep., 2013.

[278] J. Nakajima and M. West, “Bayesian analysis of latent threshold dynamic models,” *Journal of Business & Economic Statistics*, vol. 31, no. 2, pp. 151–164, 2013.

[279] G. W. Imbens and D. B. Rubin, “Rubin causal model,” *The new palgrave dictionary of economics*, pp. 1–10, 2017.

[280] A. C. Harvey, T. M. Trimbur, and H. K. Van Dijk, “Trends and cycles in economic time series: A bayesian approach,” *Journal of Econometrics*, vol. 140, no. 2, pp. 618–649, 2007.

[281] O. Poyser, “Exploring the dynamics of bitcoin’s price: A bayesian structural time series approach,” *Eurasian Economic Review*, vol. 9, no. 1, pp. 29–60, 2019.

[282] P. T. Brandt and J. R. Freeman, "Advances in bayesian time series modeling and the study of politics: Theory testing, forecasting, and policy analysis," *Political Analysis*, vol. 14, no. 1, pp. 1–36, 2006.

[283] P. T. Brandt, J. R. Freeman, and P. A. Schrodt, "Real time, time series forecasting of inter- and intra-state political conflict," *Conflict Management and Peace Science*, vol. 28, no. 1, pp. 41–64, 2011.

[284] Y. Jiang, Z. Song, and A. Kusiak, "Very short-term wind speed forecasting with bayesian structural break model," *Renewable energy*, vol. 50, pp. 637–647, 2013.

[285] F. de Vocht, "Inferring the 1985–2014 impact of mobile phone use on selected brain cancer subtypes using bayesian structural time series and synthetic controls," *Environment international*, vol. 97, pp. 100–107, 2016.

[286] A. Gelman, J. B. Carlin, H. S. Stern, D. B. Dunson, A. Vehtari, and D. B. Rubin, *Bayesian data analysis*. Chapman and Hall/CRC, 2013.

[287] P. Wright, *Logistics nightmare drives fuel panic in puerto rico*, https://weather.com/storms/hurricane/news/puerto-rico-fuel-gas-shortages-hurricane-maria, Online; accessed 30 December 2019, 2017.

[288] M. Williams, *Six months after hurricane maria, puerto ricans who evacuated island remain stranded in hotels*,
, Online; accessed 30 December 2019, 2018.

[289] A. Taylor, *University of puerto rico closed after hurricane maria*, https://www.the-scientist.com/news-opinion/university-of-puerto-rico-closed-after-hurricane-maria-30845, Online; accessed 30 December 2019, 2017.

[290] B. Fox, B. Finley, M. Daly, L. Kellman, D. Superville, C. Gillette, J. Wagner, and M. D. Shear, *Puerto rico's stores reopen with little to sell*, https://www.arkansasonline.com/news/2017/sep/27/island-stores-reopening-with-little-to-/, Online; accessed 30 December 2019, 2017.

[291] S. Fortunato and D. Hric, "Community detection in networks: A user guide," *Physics reports*, vol. 659, pp. 1–44, 2016.

[292] M. Rosvall, D. Axelsson, and C. T. Bergstrom, "The map equation," *The European Physical Journal Special Topics*, vol. 178, no. 1, pp. 13–23, 2009.

[293] J. P. Bagrow and Y.-R. Lin, "Mesoscopic structure and social aspects of human mobility," *PloS one*, vol. 7, no. 5, 2012.

[294] W. Yin, P. Murray-Tuite, S. V. Ukkusuri, and H. Gladwin, “An agent-based modeling system for travel demand simulation for hurricane evacuation,” *Transportation research part C: emerging technologies*, vol. 42, pp. 44–59, 2014.

[295] T. Yabe, Y. Zhang, and S. V. Ukkusuri, “Quantifying the economic impact of disasters on businesses using human mobility data: A bayesian causal inference approach,” *EPJ Data Science*, vol. 9, no. 1, p. 36, 2020.

[296] World Bank, *Systems of cities: Harnessing urbanization for growth and poverty alleviation*, 2009.

[297] UNISDR, “Disaster risk and resilience,” *Thematic Think Piece, UN System Task Force on the Post-2015 UN Development Agenda*, 2012.

[298] T. Elmqvist, E. Andersson, N. Frantzeskaki, T. McPhearson, P. Olsson, O. Gaffney, K. Takeuchi, and C. Folke, “Sustainability and resilience for transformation in the urban century,” *Nature sustainability*, vol. 2, no. 4, pp. 267–273, 2019.

[299] M. Moglia, S. J. Cork, F. Boschetti, S. Cook, E. Bohensky, T. Muster, and D. Page, “Urban transformation stories for the 21st century: Insights from strategic conversations,” *Global Environmental Change*, vol. 50, pp. 222–237, 2018.

[300] D. P. Aldrich and M. A. Meyer, “Social capital and community resilience,” *American Behavioral Scientist*, vol. 59, no. 2, pp. 254–269, 2015.

[301] J. Waters and W. N. Adger, “Spatial, network and temporal dimensions of the determinants of adaptive capacity in poor urban areas,” *Global Environmental Change*, vol. 46, pp. 42–49, 2017.

[302] T. Yabe, P. S. C. Rao, and S. V. Ukkusuri, “Regional differences in resilience of social and physical systems: Case study of puerto rico after hurricane maria,” *Environment and Planning B: Urban Analytics and City Science*, p. 2 399 808 320 980 744, 2020.

[303] S. L. Cutter, K. D. Ash, and C. T. Emrich, “The geographies of community disaster resilience,” *Global environmental change*, vol. 29, pp. 65–77, 2014.

[304] K. de Koning, T. Filatova, A. Need, and O. Bin, “Avoiding or mitigating flooding: Bottom-up drivers of urban resilience to climate change in the usa,” *Global environmental change*, vol. 59, p. 101 981, 2019.

[305] P. Cui and D. Li, “A sna-based methodology for measuring the community resilience from the perspective of social capitals: Take nanjing, china as an example,” *Sustainable Cities and Society*, vol. 53, p. 101 880, 2020.

[306] Y. Yang, S. T. Ng, S. Zhou, F. J. Xu, and H. Li, "A physics-based framework for analyzing the resilience of interdependent civil infrastructure systems: A climatic extreme event case in hong kong," *Sustainable Cities and Society*, vol. 47, p. 101 485, 2019.

[307] S. Mohebbi, Q. Zhang, E. C. Wells, T. Zhao, H. Nguyen, M. Li, N. Abdel-Mottaleb, S. Uddin, Q. Lu, M. Wakhungu, *et al.*, "Cyber-physical-social interdependencies and organizational resilience: A review of water, transportation, and cyber infrastructure systems and processes," *Sustainable Cities and Society*, p. 102 327, 2020.

[308] M. Modica and A. Reggiani, "Spatial economic resilience: Overview and perspectives," *Networks and Spatial Economics*, vol. 15, no. 2, pp. 211–233, 2015.

[309] C. Klinkhamer, E. Krueger, X. Zhan, F. Blumensaat, S. Ukkusuri, and P. S. C. Rao, *Functionally fractal urban networks: Geospatial co-location and homogeneity of infrastructure*, 2017.

[310] E. Schubert, J. Sander, M. Ester, H. P. Kriegel, and X. Xu, "Dbscan revisited, revisited: Why and how you should (still) use dbscan," *ACM Transactions on Database Systems (TODS)*, vol. 42, no. 3, pp. 1–21, 2017.

[311] Federal Emergency Management Agency, *Fema housing assistance program data*, https://www.fema.gov/media-library/assets/documents/34758, Accessed: 2018-09-07, 2018.

[312] J. Padilla, *Tracking status.pr*, https://statuspr.jpadilla.com/, Online; accessed June 30 2020, 2017.

[313] T. Yabe, K. Tsubouchi, N. Fujiwara, Y. Sekimoto, and S. V. Ukkusuri, "Understanding post-disaster population recovery patterns," *Journal of the Royal Society Interface*, vol. 17, no. 163, p. 20 190 532, 2020.

[314] E. Krueger, D. Borchardt, J. W. Jawitz, H. Klammler, S. Yang, J. Zischg, and P. Rao, "Resilience dynamics of urban water supply security and potential of tipping points," *Earth's Future*, vol. 7, no. 10, pp. 1167–1191, 2019.

[315] E. Krueger, P. S. C. Rao, and D. Borchardt, "Quantifying urban water supply security under global change," *Global Environmental Change*, vol. 56, pp. 66–74, 2019.

[316] S. L. Cutter, K. D. Ash, and C. T. Emrich, "Urban–rural differences in disaster resilience," *Annals of the American Association of Geographers*, vol. 106, no. 6, pp. 1236–1252, 2016.

[317] J. C. Padowski, L. Carrera, and J. W. Jawitz, "Overcoming urban water insecurity with infrastructure and institutions," *Water Resources Management*, vol. 30, no. 13, pp. 4913–4926, 2016.

[318] S. Rose, P. Jaramillo, M. J. Small, I. Grossmann, and J. Apt, “Quantifying the hurricane risk to offshore wind turbines,” *Proceedings of the National Academy of Sciences*, vol. 109, no. 9, pp. 3247–3252, 2012.

[319] Landfalling Hurricane Probability Project, *Caribbean-central america landfall probabilities*, http://hurricanepredictor.com/, 2020 (accessed September 1, 2020).

[320] P. Klingel, “Technical causes and impacts of intermittent water distribution,” *Water Science and Technology: Water Supply*, vol. 12, no. 4, pp. 504–512, 2012.

[321] Internews, *Humacao: Photo camp puerto rico*, https://internews.org/PR-photo-camp/humacao-photo-camp-puerto-rico, Online; accessed 17 January 2021, 2018.

[322] Federal Emergency Management Agency, *Three years after hurricane mar*, https://www.fema.gov/pre release/20200916/three-years-after-hurricane-maria-fema-obligations-reach-73-billion, Online; accessed 2 November 2020, 2020.

[323] L. Chelleri, J. J. Waters, M. Olazabal, and G. Minucci, “Resilience trade-offs: Addressing multiple scales and temporal aspects of urban resilience,” *Environment and Urbanization*, vol. 27, no. 1, pp. 181–198, 2015.

[324] E. H. Krueger, D. Borchardt, J. W. Jawitz, and P. S. C. Rao, “Balancing security, resilience, and sustainability of urban water supply systems in a desirable operating space,” *Environmental Research Letters*, vol. 15, no. 3, p. 035 007, 2020.

[325] T. M. Logan and S. D. Guikema, “Reframing resilience: Equitable access to essential services,” *Risk Analysis*, 2020.

[326] R. Q. Grafton, L. Doyen, C. Béné, E. Borgomeo, K. Brooks, L. Chu, G. S. Cumming, J. Dixon, S. Dovers, D. Garrick, *et al.*, “Realizing resilience for decision-making,” *Nature Sustainability*, vol. 2, no. 10, pp. 907–913, 2019.

[327] S. Hallegatte, A. Shah, R. Lempert, C. Brown, and S. Gill, *Investment decision making under deep uncertainty-application to climate change*. The World Bank, 2012.

[328] V. Hewawasam and K. Matsui, “Equitable resilience in flood prone urban areas in sri lanka: A case study in colombo divisional secretariat division,” *Global Environmental Change*, vol. 62, p. 102 091, 2020.

[329] J. Verschuur, E. Koks, A. Haque, and J. Hall, “Prioritising resilience policies to reduce welfare losses from natural disasters: A case study for coastal bangladesh,” *Global Environmental Change*, vol. 65, p. 102 179, 2020.

[330] L. M. Bettencourt, J. Lobo, D. Helbing, C. Kühnert, and G. B. West, "Growth, innovation, scaling, and the pace of life in cities," *Proceedings of the national academy of sciences*, vol. 104, no. 17, pp. 7301–7306, 2007.

[331] M. Batty, K. W. Axhausen, F. Giannotti, A. Pozdnoukhov, A. Bazzani, M. Wachowicz, G. Ouzounis, and Y. Portugali, "Smart cities of the future," *The European Physical Journal Special Topics*, vol. 214, no. 1, pp. 481–518, 2012.

[332] C. Ratti, D. Frenchman, R. M. Pulselli, and S. Williams, "Mobile landscapes: Using location data from cell phones for urban analysis," *Environment and Planning B: Planning and Design*, vol. 33, no. 5, pp. 727–748, 2006.

[333] S. Feng, G. Cong, B. An, and Y. M. Chee, "Poi2vec: Geographical latent representation for predicting future visitors," in *Thirty-First AAAI Conference on Artificial Intelligence*, 2017.

[334] X. Liu, Y. Liu, and X. Li, "Exploring the context of locations for personalized location recommendations.," in *IJCAI*, 2016, pp. 1188–1194.

[335] B. Yan, K. Janowicz, G. Mai, and S. Gao, "From itdl to place2vec: Reasoning about place type similarity and relatedness by learning embeddings from augmented spatial contexts," in *Proceedings of the 25th ACM SIGSPATIAL International Conference on Advances in Geographic Information Systems*, ACM, 2017, p. 35.

[336] S. Zhao, T. Zhao, I. King, and M. R. Lyu, "Geo-teaser: Geo-temporal sequential embedding rank for point-of-interest recommendation," in *Proceedings of the 26th international conference on world wide web companion*, International World Wide Web Conferences Steering Committee, 2017, pp. 153–162.

[337] H. Wang and Z. Li, "Region representation learning via mobility flow," in *Proceedings of the 2017 ACM on Conference on Information and Knowledge Management*, ACM, 2017, pp. 237–246.

[338] Y. Zhang, Q. Li, W. Tu, K. Mai, Y. Yao, and Y. Chen, "Functional urban land use recognition integrating multi-source geospatial data and cross-correlations," *Computers, Environment and Urban Systems*, vol. 78, p. 101 374, 2019.

[339] Z. Yao, Y. Fu, B. Liu, W. Hu, and H. Xiong, "Representing urban functions through zone embedding with human mobility patterns.," in *IJCAI*, 2018, pp. 3919–3925.

[340] M. Xu, T. Wang, Z. Wu, J. Zhou, J. Li, and H. Wu, "Demand driven store site selection via multiple spatial-temporal data," in *Proceedings of the 24th ACM SIGSPATIAL International Conference on Advances in Geographic Information Systems*, ser. SIGSPACIAL '16, Burlingame, California: ACM, 2016, 40:1–40:10, ISBN: 978-1-4503-4589-7. DOI: 10.1145/2996913.2996996. [Online]. Available: http://doi.acm.org/10.1145/2996913.2996996.

[341] B. Chang, Y. Park, D. Park, S. Kim, and J. Kang, "Content-aware hierarchical point-of-interest embedding model for successive poi recommendation.," in *IJCAI*, 2018, pp. 3301–3307.

[342] M. Zhang, Y. Liu, H. Luan, and M. Sun, "Adversarial training for unsupervised bilingual lexicon induction," in *Proceedings of the 55th Annual Meeting of the Association for Computational Linguistics (Volume 1: Long Papers)*, 2017, pp. 1959–1970.

[343] A. Conneau, G. Lample, M. Ranzato, L. Denoyer, and H. Jégou, "Word translation without parallel data," *arXiv preprint arXiv:1710.04087*, 2017.

[344] M. Artetxe, G. Labaka, and E. Agirre, "A robust self-learning method for fully unsupervised cross-lingual mappings of word embeddings," *arXiv preprint arXiv:1805.06297*, 2018.

[345] T. Wada and T. Iwata, "Unsupervised cross-lingual word embedding by multilingual neural language models," *arXiv preprint arXiv:1809.02306*, 2018.

[346] M. Artetxe, G. Labaka, E. Agirre, and K. Cho, "Unsupervised neural machine translation," *arXiv preprint arXiv:1710.11041*, 2017.

[347] Y. Ganin, E. Ustinova, H. Ajakan, P. Germain, H. Larochelle, F. Laviolette, M. Marchand, and V. Lempitsky, "Domain-adversarial training of neural networks," *The Journal of Machine Learning Research*, vol. 17, no. 1, pp. 2096–2030, 2016.

[348] I. Goodfellow, J. Pouget-Abadie, M. Mirza, B. Xu, D. Warde-Farley, S. Ozair, A. Courville, and Y. Bengio, "Generative adversarial nets," in *Advances in neural information processing systems*, 2014, pp. 2672–2680.

[349] K. Nishi, K. Tsubouchi, and M. Shimosaka, "Hourly pedestrian population trends estimation using location data from smartphones dealing with temporal and spatial sparsity," in *Proceedings of the 22nd ACM SIGSPATIAL International Conference on Advances in Geographic Information Systems*, ACM, 2014, pp. 281–290.

[350] T. Yabe, K. Tsubouchi, T. Shimizu, Y. Sekimoto, and S. V. Ukkusuri, “City2city: Translating place representations across cities,” in *Proceedings of the 27th ACM SIGSPATIAL International Conference on Advances in Geographic Information Systems*, 2019, pp. 412–415.

[351] T. Mikolov, Q. V. Le, and I. Sutskever, “Exploiting similarities among languages for machine translation,” *arXiv preprint arXiv:1309.4168*, 2013.

[352] T. Louail, M. Lenormand, O. G. C. Ros, M. Picornell, R. Herranz, E. Frias-Martinez, J. J. Ramasco, and M. Barthelemy, “From mobile phone data to the spatial structure of cities,” *Scientific reports*, vol. 4, p. 5276, 2014.

[353] M. Batty, *Cities and complexity: understanding cities with cellular automata, agent-based models, and fractals*. The MIT press, 2007.

[354] S. Grauwin, M. Szell, S. Sobolevsky, P. Hövel, F. Simini, M. Vanhoof, Z. Smoreda, A.-L. Barabási, and C. Ratti, “Identifying and modeling the structural discontinuities of human interactions,” *Scientific reports*, vol. 7, p. 46 677, 2017.

[355] A. Bassolas, H. Barbosa-Filho, B. Dickinson, X. Dotiwalla, P. Eastham, R. Gallotti, G. Ghoshal, B. Gipson, S. A. Hazarie, H. Kautz, *et al.*, “Hierarchical organization of urban mobility and its connection with city livability,” *Nature communications*, vol. 10, no. 1, pp. 1–10, 2019.

[356] Y. Bengio, A. Courville, and P. Vincent, “Representation learning: A review and new perspectives,” *IEEE transactions on pattern analysis and machine intelligence*, vol. 35, no. 8, pp. 1798–1828, 2013.

[357] W. L. Hamilton, R. Ying, and J. Leskovec, “Representation learning on graphs: Methods and applications,” *arXiv preprint arXiv:1709.05584*, 2017.

[358] X. Lu, X. Zheng, and Y. Yuan, “Remote sensing scene classification by unsupervised representation learning,” *IEEE Transactions on Geoscience and Remote Sensing*, vol. 55, no. 9, pp. 5148–5157, 2017.

[359] M. Scheffer and E. Jeppesen, “Regime shifts in shallow lakes,” *Ecosystems*, vol. 10, no. 1, pp. 1–3, 2007.

[360] S. Solomon, G. Weisbuch, L. de Arcangelis, N. Jan, and D. Stauffer, “Social percolation models,” *Physica A: Statistical Mechanics and its Applications*, vol. 277, no. 1-2, pp. 239–247, 2000.

[361] A. Aktay, S. Bavadekar, G. Cossoul, J. Davis, D. Desfontaines, A. Fabrikant, E. Gabrilovich, K. Gadepalli, B. Gipson, M. Guevara, *et al.*, "Google covid-19 community mobility reports: Anonymization process description (version 1.0)," *arXiv preprint arXiv:2004.04145*, 2020.

[362] C. Cot, G. Cacciapaglia, and F. Sannino, "Mining google and apple mobility data: Temporal anatomy for covid-19 social distancing," *Scientific reports*, vol. 11, no. 1, pp. 1–8, 2021.

[363] M. Hilbert, "Big data for development: A review of promises and challenges," *Development Policy Review*, vol. 34, no. 1, pp. 135–174, 2016.

[364] V. D. Blondel, M. Esch, C. Chan, F. Clérot, P. Deville, E. Huens, F. Morlot, Z. Smoreda, and C. Ziemlicki, "Data for development: The d4d challenge on mobile phone data," *arXiv preprint arXiv:1210.0137*, 2012.

[365] S. P. Fraiberger, P. Astudillo, L. Candeago, A. Chunet, N. K. Jones, M. F. Khan, B. Lepri, N. L. Gracia, L. Lucchini, E. Massaro, *et al.*, "Uncovering socioeconomic gaps in mobility reduction during the covid-19 pandemic using location data," *arXiv preprint arXiv:2006.15195*, 2020.

[366] L. Pappalardo, F. Simini, G. Barlacchi, and R. Pellungrini, *Scikit-mobility: A python library for the analysis, generation and risk assessment of mobility data*, 2019. arXiv: 1907.07062 [physics.soc-ph].

[367] Y.-A. De Montjoye, L. Rocher, and A. S. Pentland, "Bandicoot: A python toolbox for mobile phone metadata," *The Journal of Machine Learning Research*, vol. 17, no. 1, pp. 6100–6104, 2016.

[368] A. Graser, "Movingpandas: Efficient structures for movement data in python," *GIForum*, vol. 1, pp. 54–68, 2019.

[369] R. Joo, M. E. Boone, T. A. Clay, S. C. Patrick, S. Clusella-Trullas, and M. Basille, "Navigating through the r packages for movement," *Journal of Animal Ecology*, vol. 89, no. 1, pp. 248–267, 2020.

[370] G. Boeing, "Osmnx: New methods for acquiring, constructing, analyzing, and visualizing complex street networks," *Computers, Environment and Urban Systems*, vol. 65, pp. 126–139, 2017.

[371] T. Yabe, N. K. Jones., N. L. Gracia, M. Khan, S. V. Ukkusuri, S. Fraiberger, and A. Montford, "Python toolkit for post-disaster assessment using large-scale mobility data," *World Bank Working Papers*, 2021.

[372] M. Rocklin, "Dask: Parallel computation with blocked algorithms and task scheduling," in *Proceedings of the 14th python in science conference*, Citeseer, vol. 126, 2015.

[373] New York Times, *Opinion: Twelve million phones, one dataset, zero privacy*, https://www.nytimes.com/interactive/2019/12/19/opinion/location-tracking-cell-phone.html, Accessed: 2020-04-07.

[374] Y.-A. De Montjoye, C. A. Hidalgo, M. Verleysen, and V. D. Blondel, "Unique in the crowd: The privacy bounds of human mobility," *Scientific reports*, vol. 3, p. 1376, 2013.

[375] A. Wood, M. Altman, A. Bembenek, M. Bun, M. Gaboardi, J. Honaker, K. Nissim, D. R. O'Brien, T. Steinke, and S. Vadhan, "Differential privacy: A primer for a non-technical audience," *Vand. J. Ent. & Tech. L.*, vol. 21, p. 209, 2018.

[376] S. J. Pan and Q. Yang, "A survey on transfer learning," *IEEE Transactions on knowledge and data engineering*, vol. 22, no. 10, pp. 1345–1359, 2009.

[377] R. S. Sutton and A. G. Barto, *Reinforcement learning: An introduction*. MIT press, 2018.

[378] Y. Pang, T. Kashiyama, T. Yabe, K. Tsubouchi, and Y. Sekimoto, "Development of people mass movement simulation framework based on reinforcement learning," *Transportation research part C: emerging technologies*, vol. 117, p. 102 706, 2020.

[379] Y. Hasegawa, Y. Sekimoto, T. Seto, Y. Fukushima, and M. Maeda, "My city forecast: Urban planning communication tool for citizen with national open data," *Comput. Environ. Urban Syst*, vol. 77, 2019.

[380] E. Dong, H. Du, and L. Gardner, "An interactive web-based dashboard to track covid-19 in real time," *The Lancet infectious diseases*, vol. 20, no. 5, pp. 533–534, 2020.

[381] S. A. Markolf, C. Hoehne, A. Fraser, M. V. Chester, and B. S. Underwood, "Transportation resilience to climate change and extreme weather events–beyond risk and robustness," *Transport policy*, vol. 74, pp. 174–186, 2019.

[382] M. Artetxe, G. Labaka, and E. Agirre, "Unsupervised statistical machine translation," *arXiv preprint arXiv:1809.01272*, 2018.

[383] K. E. Joyce, S. E. Belliss, S. V. Samsonov, S. J. McNeill, and P. J. Glassey, "A review of the status of satellite remote sensing and image processing techniques for mapping natural hazards and disasters," *Progress in physical geography*, vol. 33, no. 2, pp. 183–207, 2009.

[384] K. Muniz-Rodriguez, S. K. Ofori, L. C. Bayliss, J. S. Schwind, K. Diallo, M. Liu, J. Yin, G. Chowell, and I. C.-H. Fung, "Social media use in emergency response to natural disasters: A systematic review with a public health perspective," *Disaster medicine and public health preparedness*, vol. 14, no. 1, pp. 139–149, 2020.

[385] R. Di Clemente, M. Luengo-Oroz, M. Travizano, S. Xu, B. Vaitla, and M. C. González, "Sequences of purchases in credit card data reveal lifestyles in urban populations," *Nature communications*, vol. 9, no. 1, pp. 1–8, 2018.

[386] J. E. Steele, P. R. Sundsøy, C. Pezzulo, V. A. Alegana, T. J. Bird, J. Blumenstock, J. Bjelland, K. Engø-Monsen, Y.-A. de Montjoye, A. M. Iqbal, *et al.*, "Mapping poverty using mobile phone and satellite data," *Journal of The Royal Society Interface*, vol. 14, no. 127, p. 20 160 690, 2017.

[387] C. Dwork, "Differential privacy: A survey of results," in *International conference on theory and applications of models of computation*, Springer, 2008, pp. 1–19.

[388] N. Kishore, M. V. Kiang, K. Engø-Monsen, N. Vembar, S. Balsari, and C. Buckee, "Mobile phone data analysis guidelines: Applications to monitoring physical distancing and modeling covid-19," 2020.

PUBLICATIONS

Published Papers during PhD

- **Yabe, T.**, Rao, P. S. C., & Ukkusuri, S. V. (2021). Modeling the Influence of Online Social Media Information on Post-Disaster Mobility Decisions. *Sustainability, 13(9)*, 5254.

- **Yabe, T.**, Jones, N. K., Lozano-Gracia, N., Khan, M. F., Ukkusuri, S. V., Fraiberger, S., Montfort, A. (2021). Location Data Reveals Disproportionate Disaster Impact Amongst the Poor: A Case Study of the 2017 Puebla Earthquake Using *Mobilkit KDD Workshop on Data Driven Humanitarian Mapping.*

- Ubaldi, E., **Yabe, T.**, Jones, N. K., Khan, M. F., Ukkusuri, S. V., Strano, E. (2021). *Mobilkit*: A Python Toolkit for Urban Resilience and Disaster Risk Management Analytics using High Frequency Human Mobility Data. *KDD Workshop on Data Driven Humanitarian Mapping.*

- **Yabe, T.**, & Ukkusuri, S. V. (2020). Effects of income inequality on evacuation, reentry and segregation after disasters. *Transportation Research Part D: Transport and Environment, 82,* 102260.

- **Yabe, T.**, Tsubouchi, K., Fujiwara, N., Wada, T., Sekimoto, Y., & Ukkusuri, S. V. (2020). Non-compulsory measures sufficiently reduced human mobility in Tokyo during the COVID-19 epidemic. *Scientific Reports, 10*(1), 1-9.

- **Yabe, T.**, Tsubouchi, K., Fujiwara, N., Sekimoto, Y., & Ukkusuri, S. V. (2020). Understanding post-disaster population recovery patterns. *Journal of the Royal Society Interface, 17*(163), 20190532.

- **Yabe, T.**, Tsubouchi, K., Shimizu, T., Sekimoto, Y., & Ukkusuri, S. V. (2020). Unsupervised Translation via Hierarchical Anchoring: Functional Mapping of Places across Cities. *In Proceedings of the 26th ACM SIGKDD International Conference on Knowledge Discovery & Data Mining* (pp. 2841-2851).

- **Yabe, T.**, Zhang, Y., & Ukkusuri, S. V. (2020). Quantifying the economic impact of disasters on businesses using human mobility data: a Bayesian causal inference approach. *EPJ Data Science, 9*(1), 36.

- **Yabe, T.**, Rao, P. S. C., & Ukkusuri, S. V. (2020). Regional differences in resilience of social and physical systems: Case study of Puerto Rico after Hurricane Maria. *Environment and Planning B: Urban Analytics and City Science, 48 (5)*, 1042-1057.

- Ukkusuri, S. V., **Yabe, T.**, & Seetharam, K. E. (2020). Non-Pharmaceutical Interventions for COVID-19: Evidence from Large-Scale Mobility Data in Tokyo. *Asian Development Bank Institute Policy Briefs 10*(1).

- **Yabe, T.**, Tsubouchi, K., Shimizu, T., Sekimoto, Y., & Ukkusuri, S. V. (2019). Predicting Evacuation Decisions using Representations of Individuals' Pre-Disaster Web Search Behavior. *In Proceedings of the 25th ACM SIGKDD International Conference on Knowledge Discovery & Data Mining* (pp. 2707-2717).

- **Yabe, T.**, & Ukkusuri, S. V. (2019). Integrating information from heterogeneous networks on social media to predict post-disaster returning behavior. *Journal of Computational Science, 32*, 12-20.

- **Yabe, T.**, Ukkusuri, S. V., & Rao, P. S. C. (2019). Mobile phone data reveals the importance of pre-disaster inter-city social ties for recovery after hurricane maria. *Applied Network Science, 4*(1), 1-18.

- **Yabe, T.**, Tsubouchi, K., Shimizu, T., Sekimoto, Y., & Ukkusuri, S. V. (2019). City2city: Translating place representations across cities. *In Proceedings of the 27th ACM SIGSPATIAL International Conference on Advances in Geographic Information Systems* (pp. 412-415).

- Kumar, D., **Yabe, T.**, & Ukkusuri, S. V. (2018). Social-Media aided Hyperlocal Help-Network Matching & Routing during Emergencies. *In 2018 IEEE International Conference on Big Data (Big Data)* (pp. 1606-1611). IEEE.

- Verma, R., **Yabe, T.**, & Ukkusuri, S. V. (2021). Spatiotemporal contact density explains the disparity of COVID-19 spread in urban neighborhoods. *Scientific Reports, 11(1)*, 1-11.

Papers Under Review

- **Yabe, T.**, Rao, P. S. C., Ukkusuri, S. V., & Cutter, S. L. Towards Data-Driven, Dynamical Complex Systems Approaches to Disaster Resilience. Under review in *Proceedings of the National Academy of Sciences*.
- **Yabe, T.**, Jones, N. K. W., Rao, P. S. C., Gonzalez, M. C., & Ukkusuri, S. V. Mobile Phone Location Data for Disasters: A Review from Natural Hazards and Epidemics. Under review in *Science Advances*.
- **Yabe, T.**, Tsubouchi, K., Sekimoto, Y., & Ukkusuri, S. V. Early Warning of COVID-19 Hotspots using Mobility of High-Risk Users from Web Search Queries. Under review in *Computers, Environment, and Urban Systems*.
- **Yabe, T.**, Jones., N. K., Khan, M., Ukkusuri, S. V., & Fraiberger, S. Post Disaster Analytics using Mobile Phone Data: A case study of Puebla Earthquake. Under review in *World Bank Working Papers*.
- **Yabe, T.**, Rao, P. S. C., & Ukkusuri, S. V. Resilience of Interdependent Urban Socio-Physical Systems using Large-Scale Mobility Data: Modeling Recovery Dynamics. Under review in *Sustainable Cities and Society*.
- Mittal, S., **Yabe, T.**, & Ukkusuri, S. V. Cross-sectoral relationships in business entry dynamics around a highway corridor. Under review in *Transportmetrica A: Transport Science*.
- Lee, S., Benedict, B., Jarvis, C., **Yabe, T.**, Siebeneck, L., & Ukkusuri, S. V. Trajectories of social support, household recovery and return timing after Hurricane Sandy. Under review in *Natural Hazards Review*.

VITA

Takahiro Yabe was born in Chiba, Japan on May 5th, 1992. After living in London, U.K. (4 years) and Calgary, Canada (3 years) during his childhood and graduating from Shibuya Makuhari High School in Chiba, he entered The University of Tokyo in April 2011. He received his Bachelor and Master's degrees from The University of Tokyo in 2015 and 2017, respectively, and headed to Purdue University to pursue his Ph.D. in Civil Engineering. During the 4 years, he conducted research on the intersection of disaster resilience, big mobility data analytics, and urban computing under the guidance of Professor Satish V. Ukkusuri, as a member of the UMNI Lab. During his Ph.D., he also worked as a Data Science Consultant for the Global Facility for Disaster Reduction and Recovery, The World Bank, on using smartphone location data for disaster resilience projects in Mexico City and Chennai, India. After his Ph.D., Dr. Yabe will move to Boston, Massachusetts to join the MIT Media Lab Human Dynamics Group as a Postdoctoral Associate.